Development of Immunotherapeutic Approach for Effective Elimination of Ovarian Cancer Cells by Inducing Immunogenic Cell Death

Inaugural Dissertation
submitted to the
Faculty of Biology and Chemistry
in partial fulfilment of the requirements
for the degree of
Doctor of Natural Sciences (Dr. rer. nat.) of the
Faculty of Biology and Chemistry of
Justus Liebig University Giessen

by T M Mohiuddin
of
Bagerhat, Bangladesh

Giessen, 2024

This research was conducted in the Department of Gynecology and Obstetrics

Director: Prof. Dr. med. Ivo Meinhold Heerlein of the Faculty of Medicine of the Justus Liebig University Giessen

This research was partially supported by a research grant from the university medical center Giessen and Marburg (UKGM) (8/2021 GI)

First Supervisor and first Reviewer: Prof. Dr. Andreas Krueger

Second Supervisor and second Reviewer: Prof. Dr. med. Ivo Meinhold-Heerlein

Chair: Prof. Dr. rer. nat. Sandra B. Hake

Examiner: Prof. Dr. Reinhard Dammann

Date of Doctoral Defense:

01.09.2025

Abstract

Ovarian cancer represents one of the most common forms of female gynecological cancer. The existing treatment modalities include surgery and chemotherapy, which are unable to treat local and long-distant micro-metastases. Near infrared photoimmunotherapy (NIR-PIT) is a newly developed treatment strategy that can selectively kill the cancer cells and induce immunogenic cell death and thereby stimulate anti-tumor immune responses. In this study, we developed five NIR-PIT agents by conjugating scFv-SNAP tag fusion proteins with BG-modified IRdye700 to target ovarian cancer cells, which expressed cell surface antigens EGFR, Her2, FOLR1, TROP2 and TF. The flow cytometry and microscopic studies confirmed the specificity of all the investigated NIR-PIT agents binding to corresponding overexpressed cancer cells. We demonstrated that all five NIR-PIT agents decreased the cell viability in a concentration dependent manner with IC_{50} values of ~42-283 nM. Moreover, all the examined NIR-PIT agents induced cell death by ~80-92% among them the most representing cell death occurred by irreversible necrosis or regulated necrosis. The NIR-PIT agents triggered major hallmarks of immunogenic cell death, cell surface expression of calreticulin, HSP70, HSP90 and the extracellular release of ATP and HMGB1. Furthermore, co-culturing immature dendritic cells with EGFR and TF targeting NIR-PIT agents mediated dying cancer cells enhanced dendritic cell maturation, as indicated by increased expression of CD80, CD86, CD40 and HLADR. Taken together, our results suggested that all five investigated NIR-PIT agents have great potential to be applied for ovarian cancer treatment.

Zusammenfassung

Das Ovarialkarzinom ist eine der häufigsten Formen von gynäkologischen Krebserkrankungen bei Frauen. Die bestehenden Behandlungsmethoden umfassen operative Verfahren und Systemtherapien im Sinne von Chemotherapien, Antiangiogenese und PARP-Inhibition. Diese sind jedoch vielfach nicht in der Lage, lokale und distante Mikrometastasen zu eliminieren. Die Nahinfrarot-Photoimmuntherapie (NIR-PIT) ist eine neu entwickelte Behandlungsstrategie, die selektiv Krebszellen abtöten und immunogenen Zelltod induzieren kann, wodurch anti-tumorale Immunantworten stimuliert werden. In dieser Studie entwickelten wir fünf NIR-PIT-Reagentien, indem wir scFv-SNAP-Tag-Fusionsproteine mit BG-modifiziertem IRdye700 konjugierten, um Ovarialkarzinomzellen zu targetieren, die die Zelloberflächenantigene EGFR, Her2, FOLR1, TROP2 und TF exprimierten. Die Durchflusszytometrie- und mikroskopischen Untersuchungen bestätigten die Spezifität aller untersuchten NIR-PIT-Agenten bei der Bindung an die entsprechenden/korrespondierenden überexprimierten Oberflächenantigene der Krebszellen. Wir konntenzeigen, dass alle fünf NIR-PIT-Reagenten die Zellviabilität konzentrationsabhängig mit IC_{50}-Werten von etwa 42-283 nM verringerten. Zudem induzierten alle untersuchten NIR-PIT-Agenten eine Zelltodrate von etwa 80-92%, wobei der Großteil des Zellsterbens durch irreversible Nekrose oder regulierte Nekrose erfolgte. Die NIR-PIT-Agenten lösten wesentliche Merkmale der immunwirsame Zellzerstörung aus, wie die Zelloberflächenexpression von Calreticulin, HSP70, HSP90 und die extrazelluläre Freisetzung von ATP und HMGB1. Außerdem förderte die Co-Kultur unreifer dendritischer Zellen mit EGFR- und TF-targetierten NIR-PIT-Agenten, die sterbende Krebszellen vermittelten, die Reifung dendritischer Zellen, was durch die erhöhte Expression von CD80, CD86, CD40 und HLADR angezeigt wurde. Zusammenfassend deuten unsere Ergebnisse darauf hin, dass alle fünf untersuchten NIR-PIT-Reagenzien ein großes Potenzial für die Anwendung bei der Behandlung des Ovarialkarzinoms haben.

Table of contents

1 Introduction

Cancer is a complex disease involved in the development of abnormal cell growth. It is caused by genetic, chemical, or environmental factors for instance gene mutations, radiation, chronic inflammation, viral infection and hormonal imbalances (Barot *et al* 2023). Cancer is one of the most prevalent diseases and the second leading cause of death worldwide (Bray *et al* 2021). In 2022, the most common diagnosed cancers are lung cancer (12.4%), female breast cancer (11.6%), colorectal cancer (9.6 %), prostate cancer (7.3%) and stomach cancer (4.9%) (Bray *et al* 2024). Besides these, gynecological cancers including cervical, ovarian and endometrial cancer have a serious impact on women´s health worldwide (Siegel *et al* 2019; Siegel *et al* 2023; Siegel *et al* 2024). Cancer treatment is challenging because of the complexity and diversity of the disease, resistance to treatment and toxicity of the therapies (Barot *et al* 2023; Phi *et al* 2018). Next-generation sequencing, artificial intelligence, machine learning, biopsy and digital pathology are utilized in patient-specific cancer treatment (Barot *et al* 2023).

1.1 Ovarian cancer

Ovarian cancer (OvCa) is the most fatal female gynecological cancer (Stewart *et al* 2019). In USA, OvCa is the fifth leading cause of cancer-related deaths among women. In 2024, approximately 12,740 women of OvCa are projected to die in USA and the estimated number of new cases will be 19,680 (Siegel *et al* 2024). In 2022, the estimated new cases of OvCa were 324,398 worldwide among them 206,839 patients died (Bray *et al* 2024).

OvCa can develop from three kind of cells: epithelial cell, germ cell, and sex-cord-stromal cell. Epithelial OvCa is the most common which is approximately 85-95% and the second most common cause of death among all the gynecological cancers. There are four primary histological subtypes of epithelial OvCa: serous, endometrioid, mucinous, and clear cell. Serous tumors are categorized into two classifications: high-grade serous carcinomas (70-80% of all subtypes of epithelial cancer) and low-grade serous carcinomas (Stewart *et al* 2019).

Many known risk factors may increase the development of OvCa including genetic factors, age, obesity, hormone therapy, infertility treatment and others (Momenimovahed *et al* 2019). Germline mutations in *BRCA genes* are the most known genetic risk factors which is also associated with most subtypes of epithelial OvCa (Zhang *et al* 2011). Besides *BRCA genes*, other germline mutations in DNA repair genes, such as *PALB, BRIP1, MSH2, MLH1*, *PMS2, RAD51C* and *RAD51D* can increase the risk of developing OvCa (Norquist *et al* 2016; Walsh

et al 2011). Moreover, inherited mutations in other DNA repair genes, *CHEK2*, *MRE11A*, *RAD50*, *ATM* and *TP53* might also cause OvCa (Matulonis *et al* 2016).

Currently available clinical approaches for screening OvCa include the clinical investigation with the use of a transvaginal ultrasonography for physical assessment by clinicians and measurements of protein biomarker cancer antigen 125 (CA125) in serum level or use in combination. Although these screening modalities are unable to increase the survival rate, they can help to detect early-stage cancers (Liberto *et al* 2022). After diagnosis of OvCa, the physicians need to determine the staging that describes the abundance of cancer cells in the body (Figure 1).

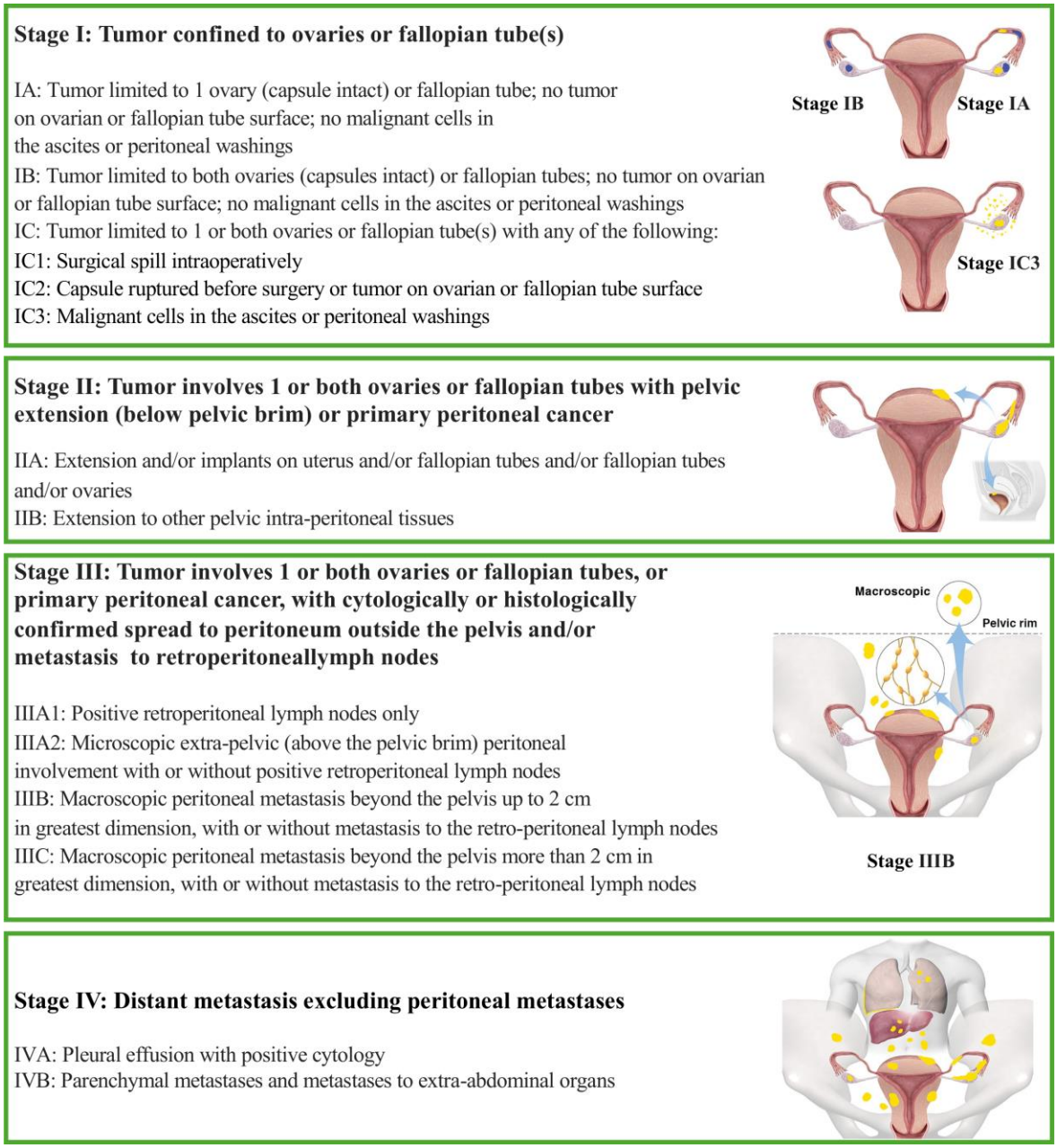

Figure 1: FIGO staging of OvCa (Javadi *et al* 2016; Meinhold-Heerlein *et al* 2015; Zeppernick *et al* 2014).

Moreover, staging helps to determine the best treatment strategy (Oliveira *et al* 2021). OvCa treatment is difficult because almost 75% of cases are diagnosed in stage III or IV (Doubeni *et al* 2016; Sambasivan 2022). The clinical relevant FIGO (International Federation of Gynecology and Obstetrics) stage is determined during the primary operation ("surgical staging"). The FIGO stage is the basis for the stage-dependent further treatment (Meinhold-Heerlein *et al* 2015; Zeppernick *et al* 2014). Rapid disease development (local to distance metastasis), resistance to therapies and relapse after treatment are also responsible for the high mortality rate of OvCa (Lheureux *et al* 2019).

1.1.1 Ovarian cancer treatment

Despite the advancement in treatment modalities such as extensive surgical cytoreduction and newer adjuvant treatment, the overall survival rate remains lower than 40% for stage III and 20% for stage IV OvCa patients (Sambasivan 2022; Torre *et al* 2018). The treatment strategies for OvCa depend on its pathological stages. Current therapeutic choices for OvCa treatment are combining debulking surgery and drug treatment (Stewart *et al* 2019). In addition, treatments with cytotoxic T cell infiltration in ovarian tumors and tumor-specific antibodies increased the overall survival rate (Hwang *et al* 2012; Zhang *et al* 2003).

1.1.1.1 Surgery

Debulking surgery is the most commonly used treatment for OvCa patients by which maximal reduction of tumor and precise intra-abdominal staging can be possible (Hishida *et al* 2021). For stage III-IV OvCa, primary debulking surgery followed by platinum-based chemotherapy has become standard treatment (Armstrong *et al* 2022, Sambasivan 2022). The TRUST trial evaluates the value of a neoadjuvant systemic treatment before debulking surgery (Mahner *et al* 2017; Reuss *et al* 2019). The DESKTOP trial series have defined the AGO score which helps to identify relapsed cases who benefit from surgery. Furthermore, they evaluated the value of debulking surgery for relapsed cases showing an improved overall survival for platin-sensitive cases with positive AGO score In contrast, patients with platin-resistant tumors e.g. with relapse after less than one year, do not benefit from secondary surgery (Harter *et al* 2021).

1.1.1.3 Chemotherapy

Chemotherapy is widely used in OvCa treatment depending on the stage of the cancer. Carboplatin in combination with paclitaxel represents the gold standard for primary systemic treatment. Since about 15 years, the angiogenesis inhibitor bevacizumab has been added due

to its improvement of the progressive free survival in advanced stages of high-grade serous cancers (Oza *et al* 2015; Pfisterer *et al* 2006; Tewari *et al* 2019). Recently, the PARP inhibitors such as olaparib and niraparib in combination with carboplatin and paclitaxel have improved not only the progressive-free, but also the overall survival in patients with most subgroups of ovarian cancer. In general, 80 % of ovarian cancers show sensitivity to platinum-based chemotherapy (Yang *et al* 2022). Additional cytostatic drugs such as anthracyclines and others can be used. In addition, various sequences and combinations utilizing bevacizumab and PARP inhibitors are also utilized when a relapse occurs. Chemotherapeutic agents have short- and long-term side effects and toxicity and loose their effectivity over time (Nurgül *et al* 2018). Therefore, there is an important need to develop new therapeutic strategies that are effective even in highly pre-treated cancer cases and show little side-effects at the same time (Konstantinopoulos and Matulonis 2023).

1.1.1.3 Molecular targeted therapy

Molecular targeted therapies are emerging as ground-breaking and promising cancer treatment strategies that inhibit cancer growth and metastasis by interfering with specific molecules. Ideal target identification is important to develop successful molecular targeted therapies in cancer. The therapeutic agents can act as a cell surface antigen, can bind receptors or influence growth factors and signal transduction pathways which regulate the cell cycle progression, metastasis and cell death (Lee *et al* 2018). Drugs used in molecular targeted therapy can interfere with the regulation of the cell cycle, induce cancer cell death and inhibit the signals for the promotion of cancer cell growth. Several molecular targeted therapeutic agents also trigger antitumor immune response by inducing immunogenic cell death (ICD), recruiting $CD8^+$ T-cell and inhibiting the progression immunosuppressive myeloid cells (Min and Lee 2022). Agents used in molecular targeted therapy can be small molecules, therapeutic monoclonal antibodies (mAb) or their fragments, small peptides or gene therapy approaches (Lee *et al* 2018; Zhong *et al* 2021). As already mentioned, potential targeted therapeutic agents include poly ADP-ribose polymerase (PARP) inhibitors, angiogenesis inhibitors, inhibitors for DNA repair mechanisms, tumor-intrinsic signaling pathway inhibitors and selective estrogen receptor down-regulators, (Shigetomi *et al* 2012; Wang *et al* 2020). Other potential therapeutic targets include folate receptor α (FOLR1), RAS/RAF/MER pathway, PI3K/AKT pathway and immune checkpoints (Guan and Lu 2018). Drugs targeting angiogenesis such as anti-VEGF antibody (Bevacizumab) have been used in OvCa treatment in combination with chemotherapy and as maintenance treatment post chemotherapy (Figure 2) (Haunschild and Tewari 2020).

Moreover, some PARP inhibitors (Olaparib, Rucaparib, Niraparib) have been approved by US Food and Drug Administration (FDA) for the treatment of advanced or recurrent OvCa (Wang *et al* 2020).

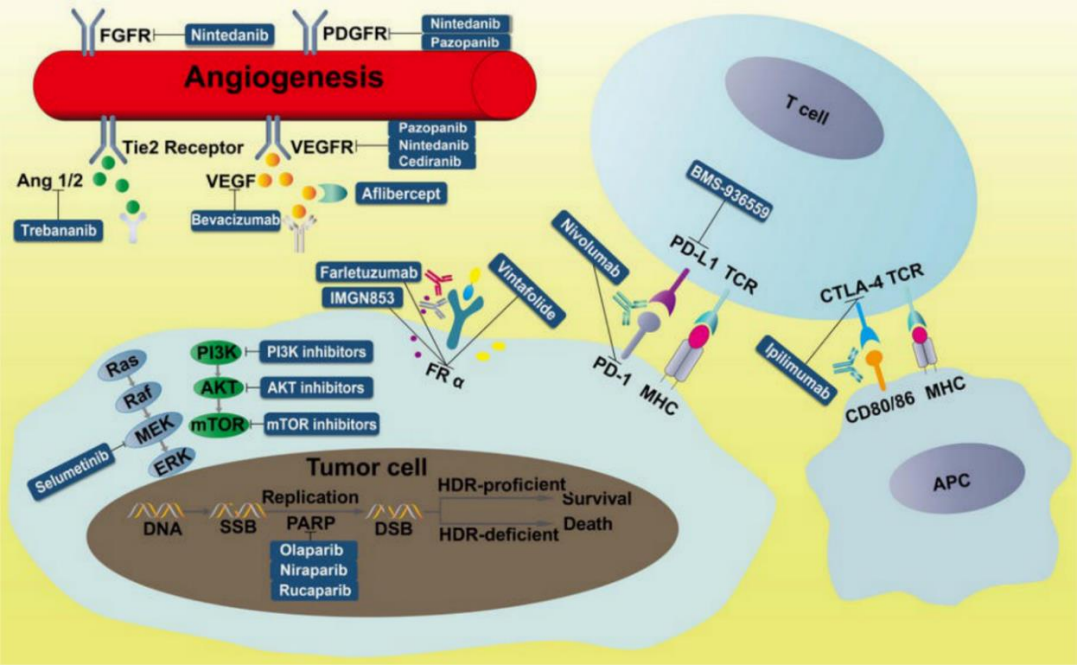

Figure 2: Key therapeutic targets of OvCa. PDGFR, platelet-derived growth factor receptor; TCR, T-cell receptor; VEGF, vascular endothelial growth factor; VEGFR, VEGF receptor; APC, antigen-presenting cell; FGFR, fibroblast growth factor receptor; MHC, major histocompatibility complex; PARP, poly (adenosine diphosphate-ribose) polymerase; PD-1, programmed cell death protein 1; PD-L1, programmed death-ligand 1 (Reprinted with permission from Guan and Lu 2018, Copyright 2024 Discovery Medicine under an open access Creative Common CC BY license).

1.1.1.4 Antibody drug conjugate

Antibody-drug conjugate (ADC) is a promising type of targeted treatment (Calo and O'Malley 2021). ADC comprises of mAb to target cancer cell specific antigens conjugated with a potent cytotoxic agent using a linker which is stable and ensures the delivery of cytotoxic payload that induce cell death (Karpel *et al* 2023). Cancer cells differentially express cancer-specific antigens, which can be used to target ADCs while minimizing systemic toxicity compared to classical chemotherapeutic agents. After administration of ADCs intravenously, the antibody part of ADC recognizes and attaches to its target followed by internalization into the cell via receptor-mediated endocytosis (Figure 3). The linker of ADCs can be either cleavable or non-cleavable (Chau *et al* 2019). The free cytotoxic warheads are released into the cytoplasm by hydrolysis, proteolysis or reductive cleavage of disulphide bonds, where they interfere with the

cellular mechanisms, induce apoptosis, and ultimately cause cell death (Khongorzul *et al* 2020).

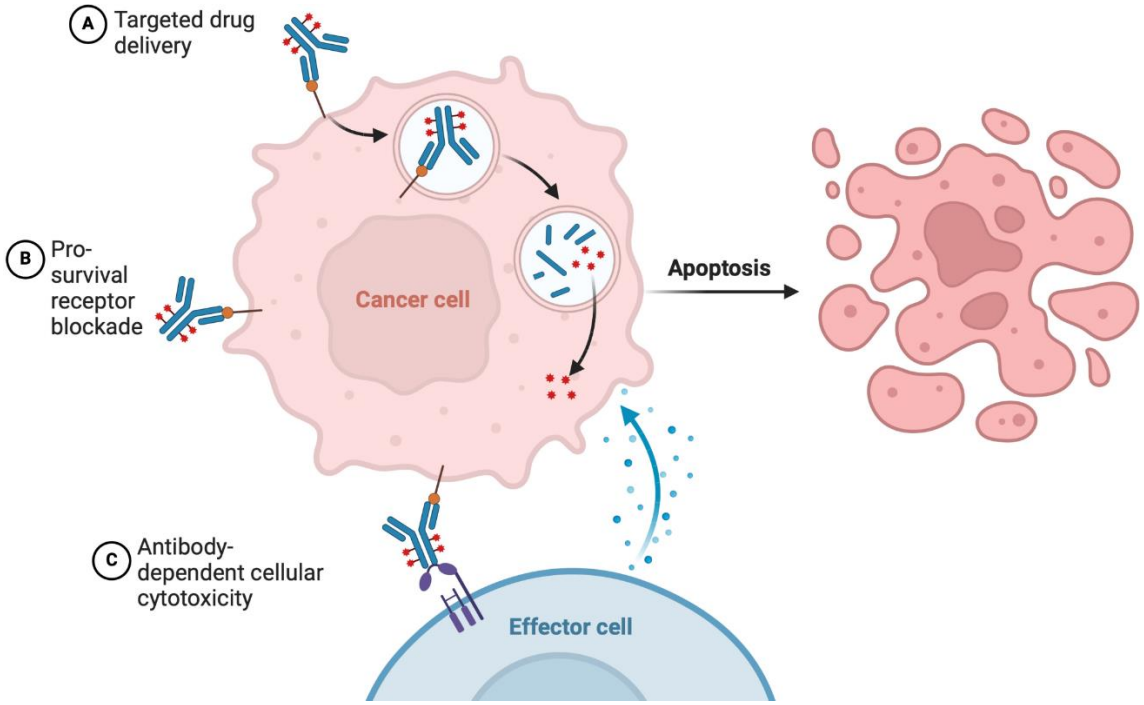

Figure 3: Mechanism of action of ADC (Created with Biorender.com).

More than 15 ADCs are under preclinical investigation in OvCa. Some of the ADCs have promising results in early-phase clinical trials (Manzano and Ocaña 2020). Many cytotoxic agents have been used as ADC payload and most promising ADCs utilize microtubule-targeting and DNA-damaging agents (Marmé 2022). In human epidermal growth factor receptor 2 (Her2)-positive breast cancer, Trastuzumab-deruxtecan was approved targeting Her2 (Keam 2020). Mirvetuximab soravtansine is a FOLR1 targeting ADC that received FDA accelerated approval for treating FOLR1 positive and platinum-resistance epithelial OvCa (Dilawari *et al* 2023, Heo 2023).

1.1.1.5 Photodynamic therapy

Photodynamic therapy (PDT) is a targeted treatment mostly depending on the generation of cytotoxic singlet oxygen and other reactive oxygen species that can directly destroy tumor cells via the activation of a photosensitizer (PS) by exposing to light at a corresponding wavelength (Figure 4) (Gunaydin *et al* 2021; Liu *et al* 2021; Wang *et al* 2021).

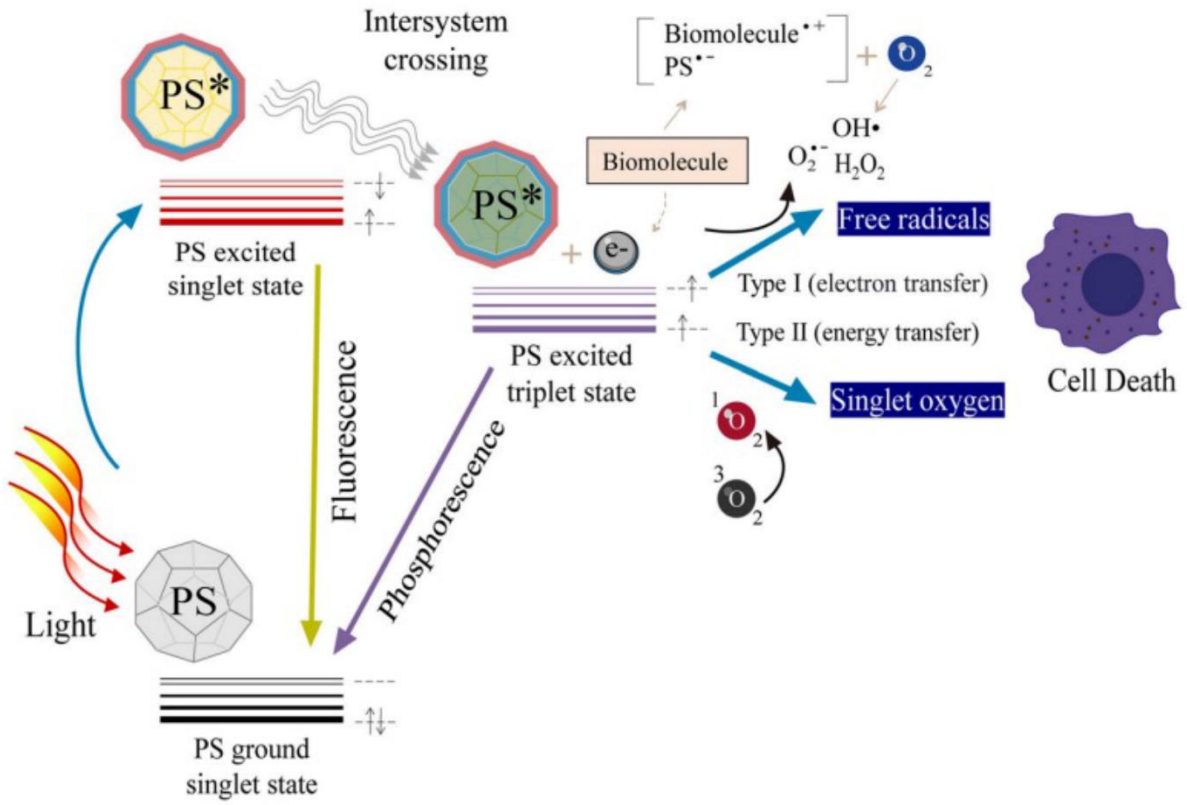

Figure 4: Schematic illustration of photodynamic reactions of PDT. PS absorbs energy from light that generate reactive oxygen species by either type I or type II and kill tumor cells (Reprinted with permission from Sai *et al* 2021, Copyright 2021 Springer Nature under a Creative Commons Attribution 4.0 International License).

mAb targeting CA125 antigen, which is expressed in 80% of non-mucinous OvCa, is conjugated with a chlorin-based PS (chlorin e6 monoethylendiamine monoamide) that shows selective phototoxicity to OvCa cells (Goff *et al* 1996). Moreover, FOLR1 targeted PDT was developed by conjugating folic acid to pyropheophorbide a-polyethylene glycol for intraperitoneal OvCa (Baydoun *et al* 2023). Over 40 years, PDT has been used to treat cancer. PDT is associated to induce antitumor immune response but not powerful enough to treat metastatic tumor because immunosuppression of tumor microenvironment could limit the antitumor immunity (Li *et al* 2020; Shen *et al* 2020). To solve this problem, a combination of PDT with immune checkpoint inhibitor and immuno-adjuvant is applied for synergistic treatment of tumors (Shen *et al* 2020). Most of the PDTs are unable to destroy deep tumors which can be overcome by using fiber optics inserted under interstitial photodynamic therapy (Shafirstein *et al* 2017). Moreover, nano-targeted photodynamic immunotherapy can be able of better tumor targeting and generating less side effects to the surrounding cells as compared to conventional PDT (Liu *et al* 2021). The PDT and ADC treatment have some side effects that highlighting the need to develop new therapeutic modalities.

1.2 Near-infrared photoimmunotherapy

Near-infrared photoimmunotherapy (NIR-PIT) is a newly developed, fastest growing photoimmunotherapeutic approach for cancer treatment that utilizes a mAb or their fragments conjugated with a photo-activable phthalocyanine-derivative dye, IRDye700DX (IR700) (Kobayashi and Choyke 2019; Kobayashi *et al* 2021; Mitsunaga *et al* 2011). Firstly, the antibody IR700 conjugates is introduced into the patient to bind with the cancer cells. After local exposure of NIR light to the tumor, rapid and selective cancer cell death occurs by activating the antibody IR700 conjugates. This approach induces the ICD by releasing damage-associated molecular patterns (DAMPs), tumor-associated antigens (TAAs) and triggering an antitumor immune response (Maruoka *et al* 2021; Mohiuddin *et al* 2023; Nakajima and Ogawa 2024). However, this antitumor immune response is not sufficient to treat the metastatic tumor because of the rapid development of immune suppressive cells in the tumor microenvironment (Li *et al* 2020; Shen *et al* 2020). Therefore, immune regulatory cells targeting NIR-PIT is used in combination with cancer cells targeting NIR-PIT to induce robust antitumor immune response. In addition, a combination of NIR-PIT with immune checkpoint inhibitors and immunoadjuvants can be applied as a synergistic treatment against tumor cells (Shen *et al* 2020). NIR-PIT demonstrates promising success both in preclinical and clinical applications for treating different cancers for more than a decade (Paraboschi *et al* 2021). To enhance the tumor immunogenicity, targeting capability, stability, and flexibility of NIR-PIT agents, different cancer cells and regulatory cells targeting moieties are used in NIR-PIT (Peng *et al* 2022; Xu *et al* 2020; Zou *et al* 2021).

1.2.1 Antibody and antibody mimetic-based NIR-PIT

Tumor growth and their progression might be associated with an increased expression of receptors involved in the regulation of certain signaling pathways. Therefore, targeting these receptors using specific ligands such as antibodies, their fragments, and mimetics can enhance tumor cell selectivity and the surrounding tissue remain unaffected (Even-Desrumeaux *et al* 2011). In NIR-PIT, mAb and antibody derivatives such as fragment antigen-binding (Fab), single chain antibody fragment (scFv), diabody, minibody, nanobody, as well as antibody mimetics, were used to conjugate IR700 for producing photo-immunoconjugates (Figure 5) (von Felbert *et al* 2016; Fernandes *et al* 2019; Mitsunaga *et al* 2011; Wollschlaeger *et al* 2018). Most clinical and preclinical studies involve cetuximab and panitumumab conjugated with IR700 for targeting the membrane receptor epidermal growth factor receptor (EGFR)

overexpressing cancer cells (Mussini *et al* 2022; Okada *et al* 2022). Furthermore, pertuzumab-IR700 and trastuzumab-IR700 showed antitumor effects of Her2-expressing cancer cells (Hirata *et al* 2021; Mitsunaga *et al* 2011; Nishimura *et al* 2020; Sato *et al* 2015a; Sato *et al* 2015b). Besides targeting the EGFR and Her2, several antibodies targeting different TAAs are used to generate NIR-PIT reagents for example, anti-CD44 antibody (Maruoka *et al* 2020), anti-prostate-specific membrane antigen (PMSA) antibody (Nagaya *et al* 2017), anti-CD47 antibody (Kiss *et al* 2019; Yang *et al* 2022), anti-epithelial cell adhesion molecule (EpCAM) antibody (Isoda *et al* 2018), and anti-tumor-associated calcium signal transducer 2 (TROP2) antibody (Nishimura *et al* 2019).

Besides the full-length mAb, their fragments such as scFv and Fab, lacking the antibody Fc region, are also used to develop NIR-PIT reagents. These fragments have efficient tumor penetration, and faster tissue clearance because of their smaller molecular size. For example, scFv against EGFR (Bauerschlag *et al* 2017; Mitsunaga *et al* 2011), EpCAM, and chondroitin sulphate proteoglycan (CSPG4) (Amoury *et al* 2016) are used to generate NIR-PIT agents for treating skin, breast and OvCa. Furthermore, F(ab′)2-IR700 targeting CD25 demonstrated selective elimination of tumor-infiltrating regulatory T cells (T_{regs}) only within the tumor microenvironment, resulting in upregulation of the anti-tumor immune responses (Maruoka *et al* 2021; Sato *et al* 2016).

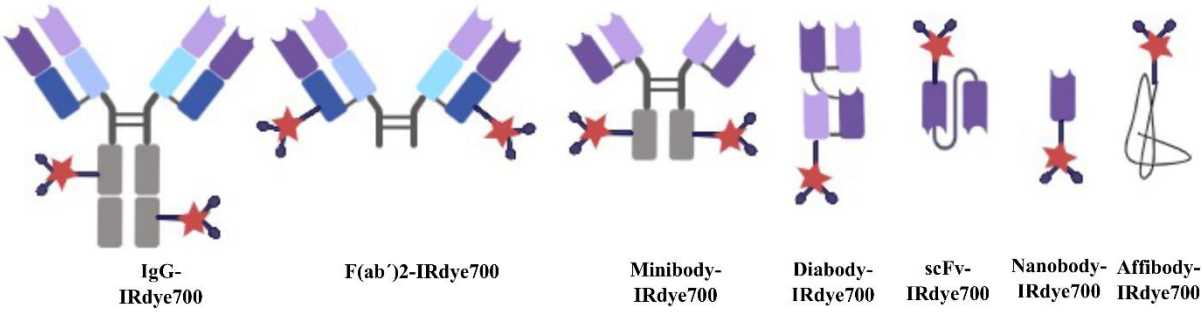

Figure 5: Schematic diagram depicting structure of an IgG molecule and a variety of engineered antibody formats conjugated with IR700 which are used in NIR-PIT (Reprinted and adopted with permission from Fu *et al* 2018, Copyright 2018 Wiley under an open access Creative Commons Attribution 4.0 International License).

Moreover, affibody molecules are small (6.5 kDa) affinity proteins which are used to generate NIR-PIT. It can bind protein targets with a high affinity and selectivity (Frejd and Kim 2017; Ståhl *et al* 2017). Affibody has the abilities of good tumor penetration, rapid clearance, and can even pass the blood-brain barrier due to its small size (Tolmachev *et al* 2007). Recently, Her2 affibody ($Z_{Her2:2395}$)-IR700 is developed that triggers ICD of the targeted cells, resulting in

maturation of dendritic cell (DC) and induction of anticancer immunity (Mączyńska *et al* 2020; Yamaguchi *et al* 2021). In addition, EGFR affibody ($Z_{EGFR:03115}$)-IR700 exhibits brain tumor destruction by inducing ICD and altering an immunosuppressive tumor into an immune-sensitive one (Burley *et al* 2018; Mączyńska *et al* 2022). In addition, a dimeric platelet-derived growth factor receptor β (PDGFRβ) affibody ($Z_{PDGFRβ}$)-IR700 showed PDGFRβ overexpressed pericytes cell death, resulting in damage of the tumor blood vessels, thereby inducing tumor destruction (Shi *et al* 2017). Therefore, affibody molecule could be an attractive alternative to mAb for designing the NIR-PIT.

Moreover, diabody and minibody targeting PSMA are used in NIR-PIT, for instance PSMA-diabody-IR700 and PSMA-minibody-IR700 that showed significant inhibition of tumor growth and enhance survival rate (Watanabe *et al* 2015). In addition, nanobodies are also used in NIR-PIT which are highly soluble and physically stable (Jovčevska and Muyldermans 2020). G protein-coupled receptor nanobody-IR700 demonstrated selective cell death of US28-expressing glioblastoma cells (De Groof *et al* 2019).

1.2.2 Peptide and small ligand-based NIR-PIT

Besides antibodies and their fragments, short peptide targeting TAAs of the target cells can be used in NIR-PIT by conjugating with IR700. For instance, a nanoconjugate is developed by binding IR700 with arginine-glycine-aspartic acid (RGD) peptide linked with human serum albumin. This RGD peptide nanoconjugate shows effective cancer-specific delivery and massive cancer cell killing properties by targeting the integrins, which are highly expressed in several cancers (Li *et al* 2017). Moreover, multiple cyclic RGD peptides can be used to obtain better accumulation into the target sites and significant inhibition of the tumor growth (Dou *et al* 2018). In addition, Low-molecular-weight (LMW) ligands are also used in NIR-PIT for targeting cancer antigens due to their efficient tumor penetration and reduced immunogenicity (Liu *et al* 2019; Sasikumar *et al* 2017). Recently, a study showed that IR700 conjugated LMW ligand targeting PSMA induces cancer cell death (Nakajima *et al* 2021).

1.2.3 Therapeutic mechanism of NIR-PIT

The NIR-PIT enhances tumor specificity over PDT by engaging the selective target using highly specific mAb. The mechanisms of NIR-PIT induced cell death remain unclear. The current evidence of the mechanisms of NIR-PIT are discussed in the following section.

1.2.3.1 Physicochemical reaction after NIR light exposure

Cancer targeting moiety of antibody IR700 conjugates binds specifically to the tumor after intravenous injection the conjugates. After NIR light exposure, a photochemical ligand reaction occurs that releases the hydrophilic side chains of IR700 which in turn makes the remaining molecule hydrophobic. Unbound antibody IR700 can be easily removed by urinal excretion system. Moreover, it is reported that the photochemical reaction changes antibody IR700 conjugates bound cell membrane to water insoluble aggregates which causes cells swelling and subsequently releases the intracellular materials and leads to necrotic cell death (Kobayashi *et al* 2021; Kobayashi and Choyke 2019; Kobayashi *et al* 2020; Monaco *et al* 2022; Sato *et al* 2018). Internalized NIR-PIT agents also have cytotoxic effects and can induce necrotic cell death, which causes significant leakage of the lysosomal contents into the cytosol (Figure 6). Nevertheless, cytotoxicity by NIR-PIT is weaker in lysosomes than in the plasma membranes (Nakajima and Ogawa 2020).

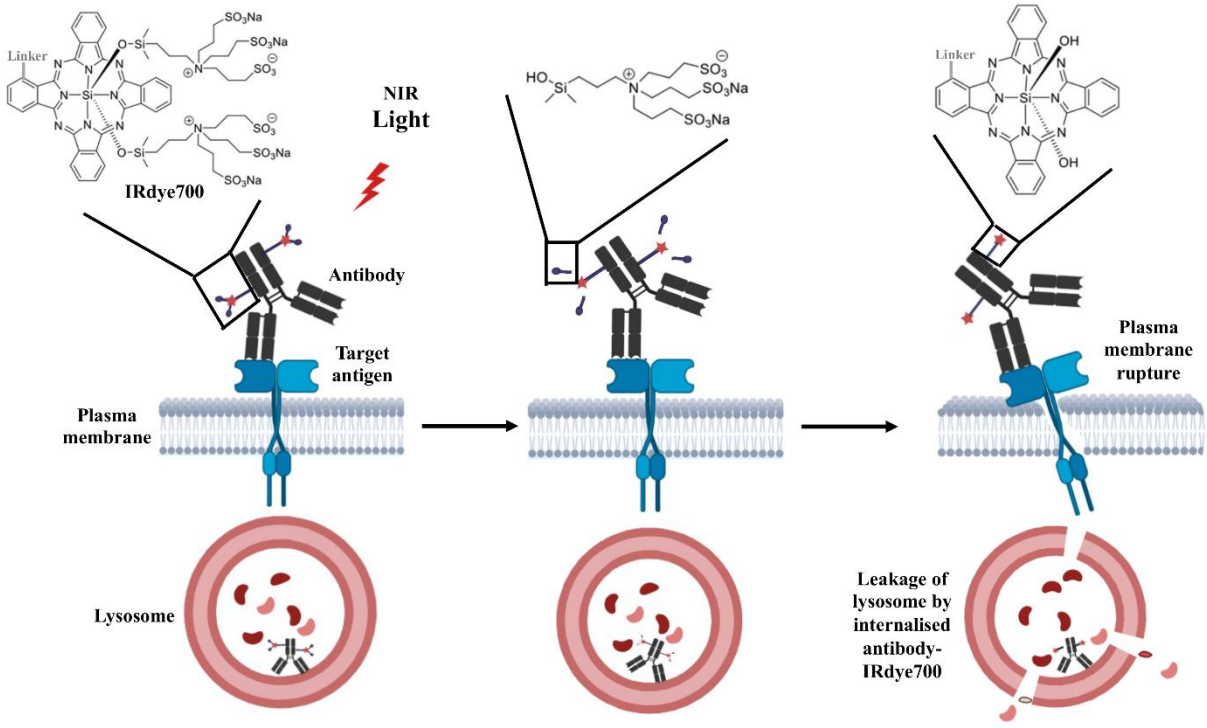

Figure 6: Physicochemical changes in antibody IR700 conjugates. An antibody IR700–antigen complex is formed on the antigen on the cell membrane and internalised antibody IR700 is localized in lysosomes after endocytosis (left). Upon NIR light exposure, axial ligands are released from the IR700 molecule (middle). The photochemical reaction changes antibody IR700 conjugates to water insoluble aggregates which causes cells swelling, rupture of cell membrane and breaking the lysosomal compartments that leads to necrotic cell death (right) (Reprinted and modified with permission from Maruoka *et al* 2021 and Mohiuddin *et al* 2023, Copyright 2024 Elsevier and MDPI under an open access Creative Common CC BY license).

1.2.3.2 ICD and anti-tumor immune augmentation

NIR-PIT induces the consequent cell swelling and bursting that represents an uncontrolled and rapid cell death. This rapid cell lysis leads to the release of cytoplasmic antigens and DAMPs such as calreticulin, high-mobility group box 1 (HMGB1), adenosine triphosphate (ATP), heat shock protein (HSP) 70, and HSP90 in the extracellular space, which is a characteristic feature of ICD (Garg *et al* 2010; Kobayashi and Choyke 2019; Mitsunaga *et al* 2011; Nagaya *et al* 2019a; Ogawa *et al* 2017). These DAMP markers are responsible for the maturation of DCs, which prime the naive $CD8^+$ T cells which is then proliferated due to the rapid release of multiple neoantigens and can attack the residual cancer cells (Figure 7). The induced immune cells can enhance systemic anticancer immune response via their migration throughout the body and by attacking distant metastatic sites (Maruoka *et al* 2021).

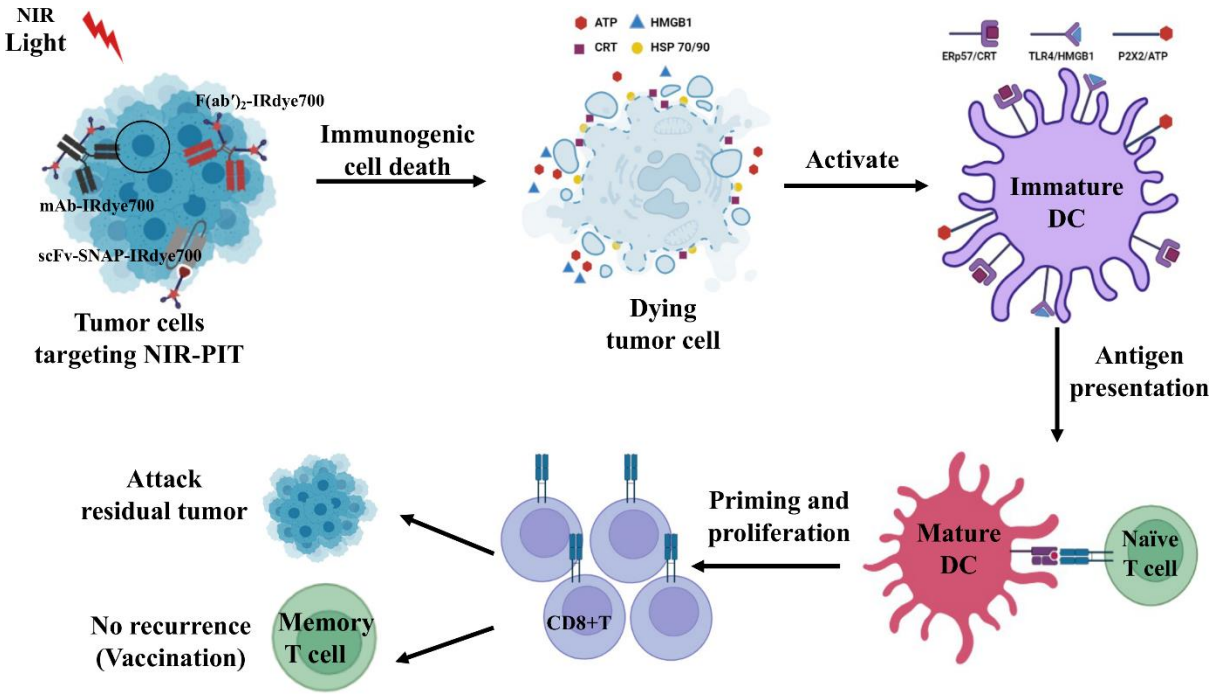

Figure 7: Biological mechanism of NIR-PIT induced ICD. This ICD triggers the antitumor host immunity against treated cancer cells (Reprinted and modified with permission from Mohiuddin *et al* 2023, Copyright MDPI under an open access Creative Common CC BY license).

However, successful NIR-PIT therapy can be hindered by expanding tumor induced T_{regs} cells which induces immunosuppression via different molecular mechanisms (Wan 2010). Therefore, host immunity can be enhanced by NIR-PIT targeting immune suppressor cells, resulting in the selective depletion of inhibitory immune cells. Several studies reported that NIR-PIT selectively diminishes the T_{regs} within the TME without removing the local effector

T cells, resulting in rapid activation and migration of $CD8^+$ T and NK cells that can kill the local and long-distance cancer cells (Figure 8) (Maruoka *et al* 2021).

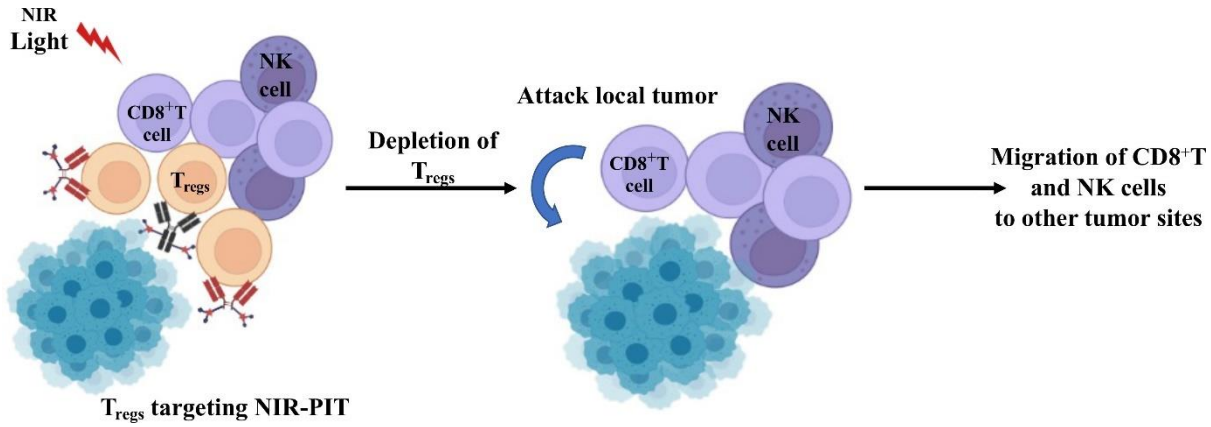

Figure 8: Enhancement of systemic antitumor host immunity induced through selective depletion of T_{regs} by NIR-PIT (Reprinted and modified with permission from Mohiuddin *et al* 2023, Copyright MDPI under an open access Creative Common CC BY license).

1.2.4 Super-enhanced permeability and retention (SUPR)

NIR-PIT selectively kills the tumor cells without affecting the surrounding normal cells by targeting the overexpressed antigen on the target cells (Mitsunaga *et al* 2011). NIR-PIT can be applied repeatedly to suppress residual cancer cells and recurrence cancer attacks (Mitsunaga *et al* 2012). NIR-PIT has distinct features related to its effect on tumor vascularity. After NIR light exposure, the NIR-PIT bound perivascular cells undergo necrosis, generating a space between the vessels and the remaining tumor mass wall, increase in blood volume, and decrease in blood velocity which enhances the vascular permeability of the nanosized drug in the treated tumor bed (Figure 9). This nanodrugs can remain for several days in the tumor bed. This SUPR of NIR-PIT enhances the delivery of nanodrugs into the tumor bed (Kobayashi and Choyke 2019; Kobayashi *et al* 2020). A combination of NIR-PIT and anticancer nanodrugs has more efficient therapeutic effects compared to individual therapy (Nishimura *et al* 2020; Okada *et al* 2021).

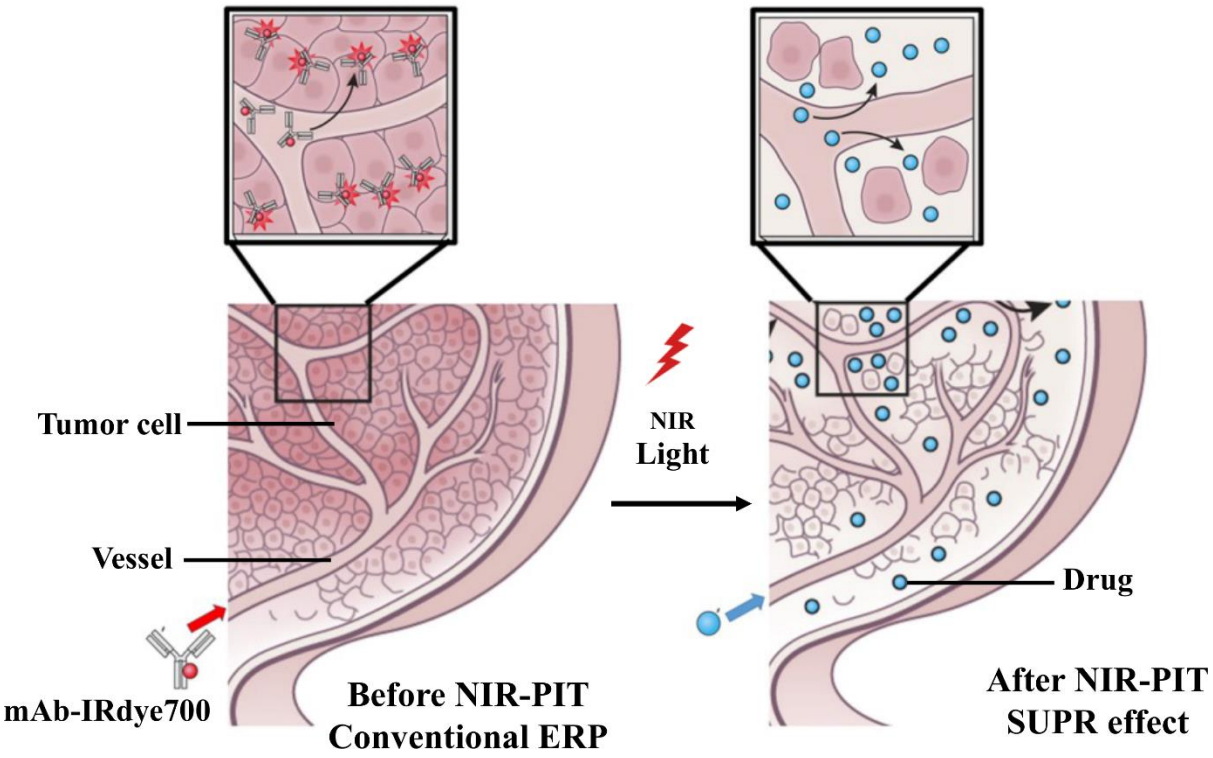

Figure 9: The mechanism of SUPR effects induced by NIR-PIT (Reprinted with permission from Kobayashi and Choyke 2019, Copyright 2024 Royal Society of Chemistry under an open access Creative Commons Attribution 4.0 International License).

1.2.5 NIR light delivery method for NIR-PIT

To attain effective therapeutic activities, the delivery of NIR light to the target site is very crucial. NIR light can enter approximately 2 cm into the tissue from the surface of the exposure **(**Maruoka *et al* 2021). NIR light can be administered to the tumor sites for instance in the mouth and skin with a conventional extracorporeal apparatus that has a frontal diffuser (Henderson and Morries 2015). A fiber optic diffuser under endoscopic guidance is developed to deliver NIR light into the deeply located tumor, such as peritoneum and thorax tumor (Figure 10A) (Nagaya *et al* 2018; Nagaya *et al* 2019b). To overcome the limitations of conventional external irradiation devices and endoscope diffusers, a novel catheter mounted with light emitting diodes is developed which has the ability to reach deep tissue and irradiation, non-kinking properties and resistance to thermal burn (Hirata *et al* 2021). Recently, an endovascular-therapy-based light illumination technology (ET-BLIT) was developed using a single lumen catheter system containing a partial transparent catheter with a transparent distal end connected to the thermocouple head and a lateral light irradiation specific optical light diffuser (Figure 10). ET-BLIT helps to provide deep light irradiation within the organs of the body such as liver and kidneys without damaging the blood vessel or other side effects (Tsukamoto *et al* 2022).

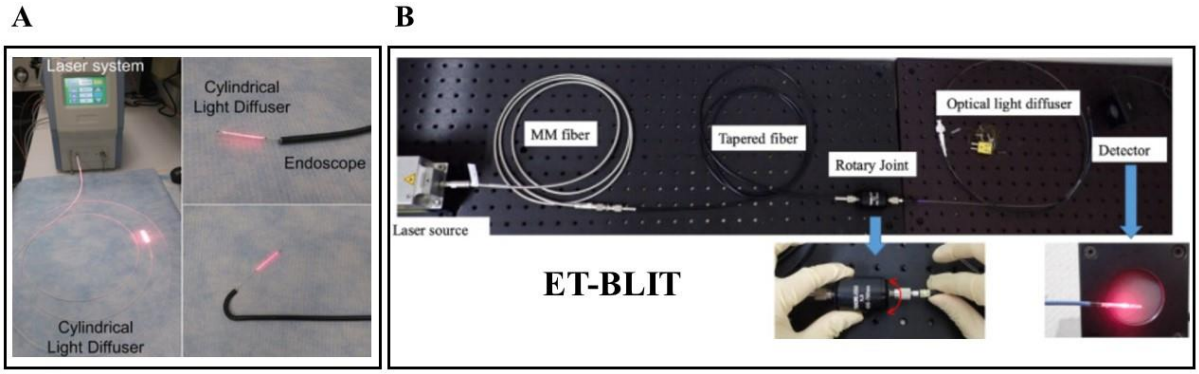

Figure 10: Different NIR light delivery devices. **A**. Cylindrical light diffuser through the endoscope with a NIR laser system (Reprinted with permission from Nagaya *et al* 2018, Copyright 2018 Wiley under an open access Creative Common CC BY license). **B**. ET-BLIT. A tapered fiber is used to connect the multimode fiber (MM fiber) and rotary joint to prevent light leakage. A rotary joint is used to rotate the optical light diffuser (Reprinted with permission from Tsukamoto *et al* 2022, Copyright 2022 Elsevier under an open Creative Commons Attribution-Non-Commercial License).

1.2.6 Monitoring the therapeutic effects of NIR-PIT

Real-time observation of tumor accumulation, therapeutic effect, and suitable NIR light irradiation in NIR-PIT are important for precise treatment (Maruoka *et al* 2021; Zhang *et al* 2022). Several imaging modalities are used to measure the efficacy of NIR-PIT directly after treatment. Bioluminescence imaging can be used preclinically to monitor the effectiveness of NIR-PIT (Nakajima *et al* 2014). During NIR-PIT, IR700 fluorescence imaging is used to confirm the accumulation of NIR-PIT agents in tumor tissues and the fluorescence signal disappears after NIR light irradiation at 690 nm (Kobayashi and Choyke 2019; Sato *et al* 2018; Zhang *et al* 2022). Another imaging modality is 18F-fluorodeoxyglucose positron emission tomography imaging which provides early metabolic changes in the tumors. It can be used to evaluate the immediate treatment success in NIR-PIT-treated tumors (Sano *et al* 2013).

Besides fluorescence imaging, optical coherence tomography (OCT) can be used to reveal dramatic hemodynamic changes in tumor vessels during NIR-PIT. OCT shows the difference in treated tumors compared to the untreated tumors (Liang *et al* 2014). Moreover, a two-channel fluorescence fibre imaging system and two-photon microscopy with and without a microprism are used to monitor the therapeutic effects and the micro-distribution of the NIR-PIT agent from the tumor surface to the deep tumor during and after treatment (Tang *et al* 2017). In addition, early therapeutic effects, tumoricidal effects and hemodynamic changes induced by NIR-PIT can be monitored by ^{13}C MRI, BOLD MRI and photoacoustic imaging (Kishimoto *et al* 2018; Zhang *et al* 2022). Recently, a customized camera system

(LIGHTVISION) is designed to monitor the effect of NIR-PIT in real-time at wavelengths of 830 nm, which is far from the intense laser excitation light at 690 nm. This camera system can detect indocyanine green and the fluorescence arising from IR700 during NIR-PIT (Inagaki *et al* 2021).

1.2.7 Targeting molecules for NIR-PIT for cancer treatment

Many NIR-PIT agents were developed for targeting different types of cancers in the last twelve years. At the beginning, EGFR and Her2 targeted NIR-PIT agents are developed and then expanded to target diverse cancer cell surface antigens (such as EpCAM, CD44, CD47, TROP2, PMSA, CD133, CAFs, CEA, CD20, CD146, Cadherin-17, VEGFR-2, CD25, CD29, CD206, PD-L1 and CTLA4) by using the mAb, antibody fragment, and nanobody (Mohiuddin *et al* 2023). However, NIR-PIT can be applied to any cancer if the available tumor antigens are overexpressed (Maruoka *et al* 2021). In last few years, regulatory T cells and myeloid derived suppressor cells targeting (CTLA4, CD25, Ly6G, VISTA, Gr1) NIR-PIT agents are used to deplete the intra tumoral immunosuppressive cells. Moreover, NIR-PIT agents are generated targeting tumor-associated macrophages (targeting CD209), cancer associated fibroblast (targeting FAP) and cancer neo-vasculature (targeting VEGFR2) (Figure 11) (Kato *et al* 2021b).

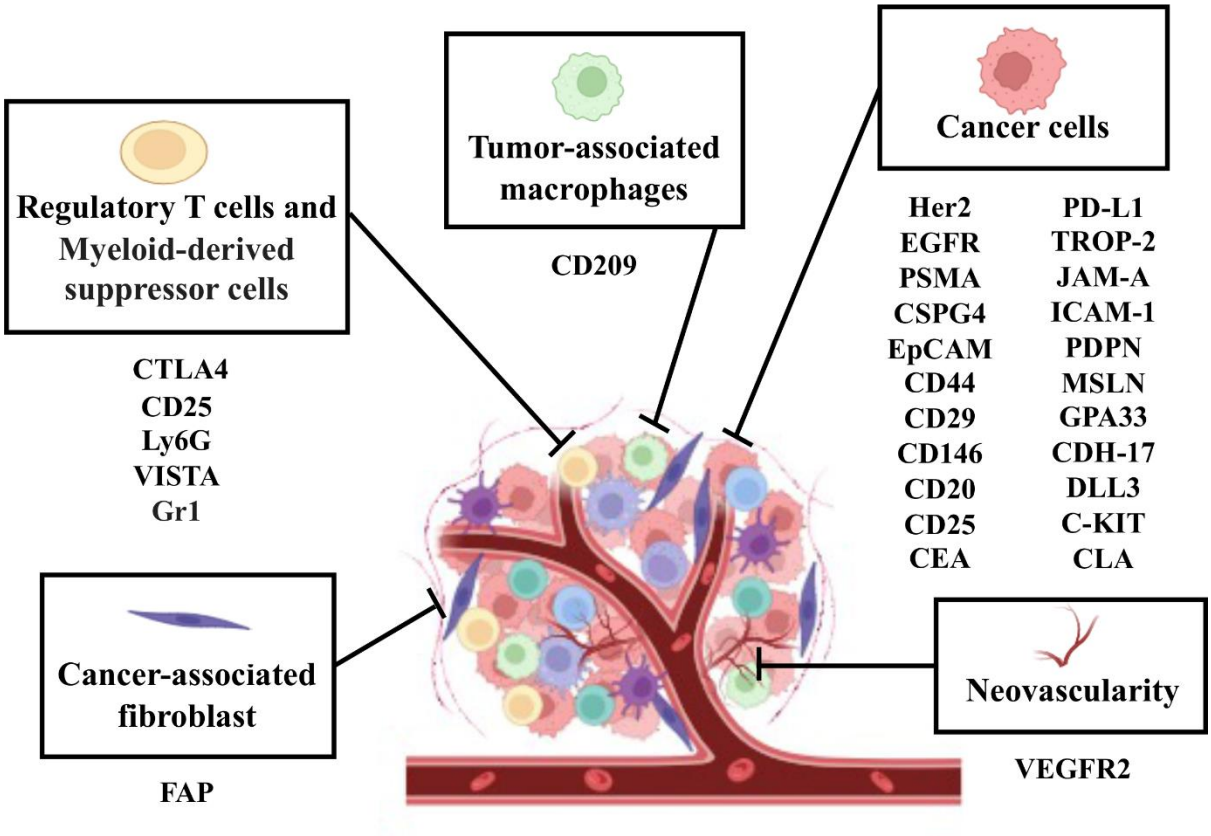

Figure 11: Target molecules of NIR-PIT developed for cancer therapy. NIR-PIT can target surface molecules expressing cancer cells, regulatory T cells, cancer-associated fibroblasts, tumor-associated macrophages and neovascularity. FAP, fibroblast activation protein; CEA, carcinoembryonic antigen; MSLN, mesothelin; CDH-17, Cadherin-17; TROP2, tumor-associated calcium signal transducer 2; GPA33, glycoprotein A33 antigen; DLL3, delta-like protein 3; PDPN, podoplanin; ICAM-1, intercellular adhesion molecule-1; JAM-A, junctional adhesion molecule-A; CLA, cutaneous lymphocyte antigen; VEGFR-2, vascular endothelial growth factor receptor 2; PD-L1, programmed death-ligand 1; CTLA4, cytotoxic T-lymphocyte-associated protein 4; VISTA, V-domain immunoglobulin suppressor of T cell activation; GR-1, granulocyte receptor-1 antigen; Ly6G, lymphocyte antigen 6 complex locus G6D. (Reprinted and modified with permission from Kato *et al* 2021b, Copyright MDPI under an open access Creative Common CC BY license).

1.3 Regulated cell death

Regulated cell death (RCD) is triggered by the formation of signal amplification complexes which is controlled by a variety of biomacromolecules. It is a ubiquitous process in living organisms which is also known as programmed cell death when it occurs in physiological conditions. In the last few decades, different forms of RCD are reported including apoptosis, ferroptosis, necroptosis, pyroptosis, autophagy-dependent cell death, entosis, NETosis, lysosome-dependent cell death and alkaliptosis (Peng *et al* 2022; Tang *et al* 2019). This study is mainly focused on apoptosis, ferroptosis and necroptosis.

1.3.1 Apoptosis

Apoptosis is a form of regulated cell death (RCD) mediated by proteases of the caspase family which are caspase 3 (CASP3), CASP6 and CASP7, and initiated by CASP8 and CASP9 (Galluzzi *et al* 2018; Kumar *et al* 2022; Vitale *et al* 2023). It is characterized by cell shrinkage, increases of cytoplasmic density, disappears the mitochondrial membrane, membrane blebbing, DNA condensation and fragmentation (Figure 12) (Elmore 2007; Saraste and Pulkki 2000). Apoptosis can be occurred through the death receptor apoptotic pathway (extrinsic) or mitochondrial apoptotic pathway (intrinsic) (Galluzzi *et al* 2018). Apoptosis can be inhibited by altering expression and structure of the caspase-family of genes (Wong 2011).

1.3.2 Necroptosis

Necroptosis is a caspase-independent death program which is different from apoptosis and pyroptosis. It is caused by phosphorylation and activation of the necroptotic kinase RIPK3 (receptor-interacting serine-threonine kinase 3) which also requires RIPK1 activity (Bedoui *et al* 2020). RIPK3 phosphorylate the pseudo kinase MLKL (mixed lineage kinase domain like), resulting in substantial conformational changes and translocation of MLKL to the plasma membrane that induces membrane permeabilization, loss of membrane integrity and cytosolic osmolarity and eventual necroptotic cell death (Figure 12) (Gong *et al* 2017; Khan *et al* 2014; Newton 2015). Necroptosis is a characteristic feature of releasing intracellular contents, resulting in induction of effective anti-tumor immune responses (Yatim *et al* 2015).

1.3.3 Ferroptosis

Ferroptosis is an iron-dependent type of RCD (Dixon *et al* 2012). Ferroptosis is initiated by inhibiting the xc-cystine/glutamate antiporter or glutathione peroxidase 4 (GPX4), leading to lethal levels lipid peroxidation (Stockwell *et al* 2017). GPx4 is known for its unique function to convert lipid hydroperoxides (L-OOH) to non-toxic lipid alcohols (L-OH) in the cell membrane. Inactivation of Gpx4 leads to overwhelming lipid peroxidation of polyunsaturated fatty acids (PUFAs), leading to consecutive depletion of PUFAs from plasma membrane, thereby increasing membrane permeability and altering integrity and eventual cell death (Figure 12) (Stockwell *et al* 2017; Yang *et al* 2014). Damages resulting from lipid peroxidation in mitochondria can cause shrinkage and reduction in mitochondrial cristae (Neitemeier *et al* 2017). Lipophilic antioxidants and iron chelators can inhibit the ferroptosis (Stockwell *et al* 2017).

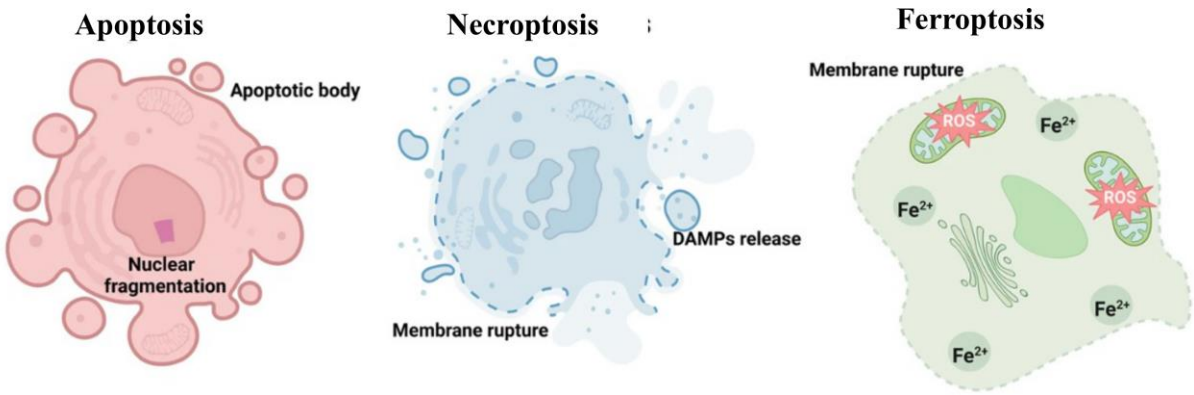

Figure 12. Morphological characteristics of apoptosis, necroptosis and ferroptosis. (Reprinted with permission from Chen *et al* 2023, Copyright 2023 Springer Nature under a Creative Commons Attribution 4.0 International License).

1.4 Potential biomarkers for OvCa treatment

The target selection for the development of NIR-PIT depends on the overexpression of certain receptors on the cell surface of cancer cells. Several cell surface receptors are identified in OvCa based on expression profile analysis, which leads to develop NIR-PIT (Hiss 2012; Schröfelbauer *et al* 2023).

1.4.1 EGFR

EGFR is a transmembrane protein that contains a single α-helix transmembrane domain, an extracellular domain, an intracellular domain and a C-terminal phosphorylation domain. The extracellular domain can bind the ligand and the intracellular domain has the tyrosine kinase properties. EGFR is a member of the tyrosine kinases ErbB family (Burgess *et al* 2003, Lee *et al* 2006; Schlessinger 2002). EGFR plays a key role in epithelial malignancies, and its activity enhances tumor growth, invasion, and metastasis (Normanno *et al* 2006). The EGFR remains in auto-inhibited state at the plasma membrane (PM) under unstimulated condition. Upon ligand binding to EGFR, autophosphorylation occurs and induces the receptor dimerization (Ono and Kuwano 2006). Ligand-dependent EGFR activation triggers the multiple signaling cascade which are essential for cell survival, proliferation and differentiation (Sigismund *et al* 2018).

EGFR is overexpressed in several cancers like head-and-neck, prostate (Di Lorenzo *et al* 2002), ovarian (Wang *et al* 2016), breast (Maennling *et al* 2019), renal (Minner *et al* 2012), colon (Pabla *et al* 2015), lung (Wang *et al* 2018), pancreas (Grapa *et al* 2019) and skin (Cañueto *et al* 2017) cancers that makes EGFR is an attractive target for diagnosis and therapy of different

cancers. Several anti EGFR mAbs are already approved, and some are ongoing clinical trials for different cancer treatment (Cai *et al* 2020; Kasi *et al* 2023). Cetuximab and panitumab are FDA approved anti EGFR mAbs treatment of metastatic colorectal cancer and head and neck cancer. These antibodies specifically bind to the extracellular domain III of EGFR and thus inhibiting ligand binding and receptor activation (Cai *et al* 2020; Hynes and Lane 2005). However, cetuximab and panitumumab conjugated with IR700 are used for most clinical and preclinical studies in NIR-PIT (Mohiuddin *et al* 2023). In 2020, cetuximab-IR700 is conditionally approved as the first NIR-PIT drug in Japan (Maruoka *et al* 2021). In addition, several EGFR tyrosine kinase inhibitors such as gefitinib, afatinib and erlotinib are used to treat lung and pancreatic cancer. These molecules inhibit the EGFR autophosphorylation by specifically binding to the catalytic tyrosine kinase domain of EGFR (Zubair and Bandyopadhyay 2023).

1.4.2 Her2

Her2 is a transmembrane glycoprotein that belongs to the ErbB family and having tyrosine kinase activity. Her2 plays a pivotal role in cell proliferation and tumor cell metastasis. Her2 overexpression is detected in various cancer types, including OvCa (Luo *et al* 2018), breast cancers (Ménard *et al* 2000), pancreatic carcinomas (Han *et al* 2021), endometrial carcinoma (Rolitsky *et al* 1999), small cell lung cancer (Potti *et al* 2002). The FDA approved Her2 targeting ADC (fam-trastuzumab deruxtecan-nxki) for the treatment of Her2-low metastatic breast cancer (Narayan *et al* 2023). The Her2-targeting NIR-PIT using trastuzumab induced Her2-expressing small cell lung cancer cells death with high efficacy *in vitro* and *in vivo* (Takahashi *et al* 2021).

1.4.3 FOLR1

FOLR1 is a glycosylphosphatidylinositol-anchored cell surface glycoprotein binds to folic acid and its derivatives with high affinity (Luhrs *et al* 1989) and mediates cellular processes, including cell division, proliferation, and tissue growth by signaling cascades and folate cycle components (Cheung *et al* 2016). FOLR1 is an attractive therapeutic target for different cancer treatment as FOLR1 is overexpressed in tumors such as breast cancer (Norton *et al* 2020), lung cancer (O'Shannessy *et al* 2012), cervical cancer (Yazaki *et al* 2022), Endometrioid-type endometrial carcinoma (Senol *et al* 2015), brain cancer (McCord *et al* 2021) and OvCa (Bax *et al* 2023). FOLR1 targeted PDT are developed to conjugate a folate moiety to the Si-rhodamine derivative for the treatment of FR-overexpressing tumors (Aung *et al* 2022).

1.4.4 TROP2

TROP2 is a transmembrane glycoprotein that has a pivotal role in tumor growth, apoptosis and invasion (Goldenberg *et al* 2018, Wen *et al* 2022). *TROP2* is composed of a hydrophobic signal peptide, a long extracellular domain, a short transmembrane domain and a cytoplasmic tail (Lenárt *et al* 2020). TROP2 was initially identified in trophoblast cell surface marker and overexpressed in many solid cancers (Zeng *et al* 2016). The normal epithelial cells show baseline expression of TROP2 (Trerotola *et al* 2013).

The overexpression of TROP2 correlates with a poor prognosis in various cancers including gastric cancer (Zhao *et al* 2016), cervical cancer (Liu *et al* 2013), lung cancer (Inamura *et al* 2017), oral squamous cell carcinoma (Zhang *et al* 2020), colorectal cancer (Ohmachi *et al* 2006), pancreatic cancer (Mas *et al* 2023), endometrioid endometrial carcinoma (Bignotti *et al* 2011), ovarian carcinoma (Dum *et al* 2022; Wu *et al* 2017; Xu *et al* 2016). TROP2 targeted first ADC (Sacituzumab govitecan) was clinically approved by the FDA for refractory metastatic triple negative breast cancer in April 2020 (Bardia *et al* 2019; Jin *et al* 2022; Syed 2020). NIR-PIT targeting TROP2 is effective for TROP2-expressing human pancreatic carcinoma and cholangiocarcinoma cell lines *in vitro* and *in vivo* (Nishimura *et al* 2019).

1.4.5 Tissue factor (TF)

Tissue factor (TF) is a transmembrane glycoprotein. It is composed of three domains: an extracellular domain, a transmembrane domain, and a cytoplasmic COOH-terminal domain which is involved in signal transduction (Butenas 2012). TF expression is found to be upregulated in many types of cancer cells (Ahmadi *et al* 2023). It is suggested that TF might contribute to cancer progression and metastasis through several signaling pathways (Hisada *et al* 2019).

TF is aberrantly increased on the surface of tumor cells and vascular endothelial cells in various malignancies, such as pancreatic cancer (Gerotziafas *et al* 2012, Nitori *et al* 2005), OvCa (Cocco *et al* 2011), triple-negative breast cancer (Ueno *et al* 2000), gastric cancer (Lo *et al* 2012), cervical cancer (Zhao *et al* 2018), lung cancer (Goldin-Lang *et al* 2008). TF targeted ADC (Tivdak) was granted accelerated FDA approval for the treatment of adult recurrent or metastatic cervical cancer patients (Tong *et al* 2021). TF-cascade-targeted PDT is used in different cancer treatment for instance breast cancer (Hu *et al* 2010), lung cancer (Cheng *et al* 2011), malignant lymphoma (Li *et al* 2020).

1.5 scFv

The scFv consists of variable regions of light (V_L) and heavy (V_H) chains, which are joined together by a flexible peptide linker to produce a single polypeptide. To enhance stability and binding affinity of scFv, protein engineering can be used by changing the amino acid sequence (Ahmad *et al* 2012; Pirkalkhoran *et al* 2023). The *E. coli*-derived scFv have some limitations because of their misfolding. The misfolded state binds antigen in a heterogeneous fashion including non-specific binding that makes challenging of scFv functional characterization (Vendel *et al* 2012). Transient expression in HEK293-6E combined with optimized expression vectors and fed batch processes provides robust and versatile production of scFv antibodies (Jäger *et al* 2013).

The scFv can be used especially for drug delivery in cancer treatment as it retains the complete antigen-binding capability (Chester *et al* 2004). The scFv has better tumor penetration due to its small size, reduced immunogenicity, lower retention times in nontarget tissue and more rapid blood clearance in compared to the whole antibody molecule (Ahmad *et al* 2012; Colcher *et al* 1998; Yokota *et al* 1992). In 2021, scFv of brolicizumab received FDA approval for age macular degeneration treatment (Nguyen *et al* 2020). The scFv is extensively used to develop several molecular targeted therapies including targeted photodynamic therapy, ADC or photoimmunotherapy.

1.6 SNAP-tag technology for site-specific antibody-PS conjugation

Site-specific conjugation methods are applied to generate homogeneous NIR-PIT agents. SNAP-tag is a simple and robust site-specific conjugation method. SNAP-tag is a recombinant variant of the human DNA repair enzyme O6-alkylguanine-DNA alkyl transferase (AGT) that reacts with benzylguanine (BG) derivatives via irreversible transfer of an alkyl group to a cysteine residue (Gautier *et al* 2008; Keppler *et al* 2003). Several mutations are introduced to improve the wild type AGT properties such as reducing its size and the DNA binding activity, improving the folding by removing two non-essential cysteines residues (Gronemeyer *et al* 2006).

SNAP tag provides the flexible way of labelling proteins with various BG-modified molecules *in vitro* and *in vivo*, thus overcoming the problems of nonspecific targeting and heterogeneity (Chouman *et al* 2017). It is used in cancer diagnosis and treatment by conjugating BG-modified effector molecules for instance PSs, drugs, or fluorophores (Hussain *et al* 2011, Kampmeier *et*

al 2010). By targeting TAAs, SNAP-tag antibody-labelling technology with different fluorophores, tumors can be screened prior to therapy (Gong *et al* 2012; Keppler *et al* 2004). In ADC, SNAP-tag-based antibody fusion protein is used to couple benzylguanine modified auristatin F in an irreversible 1:1 stoichiometric reaction (Huysamen *et al* 2023; Mungra *et al* 2023; Zhang *et al* 2022). In NIR-PIT, SNAP-tag technology has promising potential to conjugate BG modified IR700 to tumor cell-specific scFv and generates highly homogenous NIR-PIT agents (Figure 13) (Amoury *et al* 2016; Bauerschlag *et al* 2017; Von Felbert *et al* 2016).

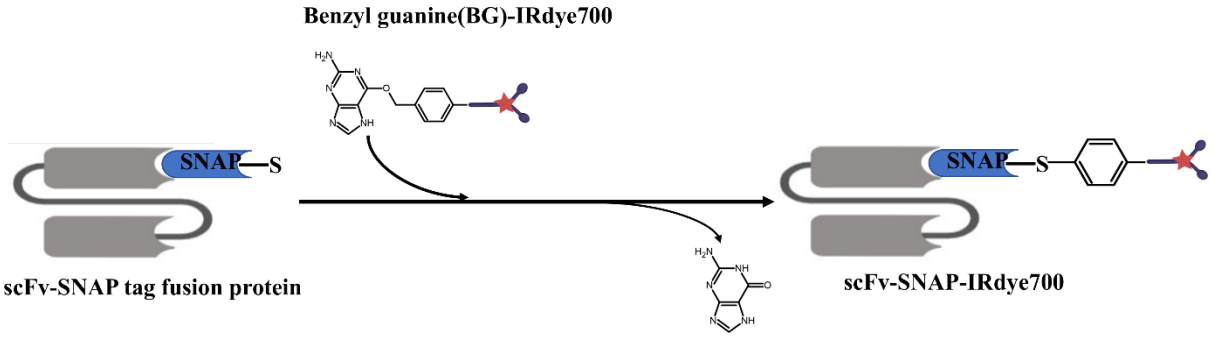

Figure 13: SNAP tag technology to generate site specific conjugation of scFv with IR700. (Reprinted with permission from Hussain *er al* 2019, Copyright 2019 Springer Nature under a Creative Commons Attribution 4.0 International License).

1.7 Aims and objectives

Surgery, chemotherapy or targeted therapy are used to treat primary OvCa and its metastases with relatively large and clear-vascularized patterns. However, these existing treatment modalities are failed to treat local and long-distant micro-metastases that usually cause tumor relapse. Therefore, there is a high unmet medical need to develop treatment strategies that can eliminate both primary OvCa and metastatic lesions effectively. NIR-PIT is an alternative treatment strategy that uses IR700, which can be activated locally and on-demand using nontoxic light to generate cytotoxic pathways which kill the targeted cancer cells. Furthermore, NIR-PIT induces ICD pathways that eventually stimulate host immune system against dead cancer cell antigens. In addition, dying cancer cells help to develop memory cells that stimulates a tumor-specific immune response to recognize and systemically eliminate residual tumor cells. The aims of this project are-

1. Development of NIR-PIT approach by conjugating IR700 to the scFv targeting EGFR, Her2, FOLR1, TROP2 and TF using the SNAP tag technology.

2. *In vitro* NIR-PIT agents validation by investigating their targeting specificity using flow cytometry and fluorescence microscopy.
3. Determining the cell death induced by NIR-PIT agents in dose dependent manner using XTT cell viability assay. Quantifying the NIR-PIT agents toxicity by discriminating the viable, necrotic and apoptotic cells using Annexin assay.
4. Determining the type of NIR-PIT induced cell death by using different cell death inhibitors that specifically block apoptosis, necroptosis and ferroptosis.
5. Evaluating immunological responses triggered by NIR-PIT-killed tumor cells by analyzing the ICD hallmark (calreticulin, HSP70, HSP90, ATP and HMGB1).
6. Analyzing the expression of DC surface markers CD80, CD86, CD40 and HLADR using flow cytometry to determine DC maturation induced by NIR-PIT-killed tumor cells.

2 Materials and Methods

All materials and methods used in this study are described in the following chapter.

2.1 Cell culture

OvCa cell lines SKOV3, OVCAR3, IGROV1, A2780, Hey and human embryonic kidney cell line HEK293T were purchased from American Type Culture Collection. These cell lines were cultured in RPMI 1640 complete culture medium. The scFv-SNAP containing HEK293T cells were cultured in RPMI 1640 complete culture medium supplemented with 0.1% zeocin for selection. All cells were cultured in an incubator at 37°C in a humidified atmosphere containing 5% CO_2 for no more than 30 passages.

2.2 Expression of scFv-SNAP fusion proteins

The scFv-SNAP containing HEK293T cells were cultured in RPMI 1640 complete medium supplemented with 0.1% (v/v) zeocin to keep the transfected cells selection. Cells were grown in triple-layer flasks containing 150 mL culture medium. Culture supernatant was collected and used for protein enrichment.

2.2.1 scFv-SNAP tag fusion proteins enrichment

The culture supernatant was centrifuged at 5000 rpm for 10 min at 4°C and then filtered through 0.45 µm Corning® Vacuum Filter to get cell-free culture supernatant. Äkta FLPC system and Ni-NTA super flow (Qiagen, Hilden, Germany) cartridge were used to purify the C-terminal 6X His-tagged fusion proteins from cell-free supernatants. Firstly, the culture supernatant was adjusted by mixing with 4X Ni-NTA binding buffer (50 mM NaH_2PO4, 300 mM NaCl, 10 mM imidazole, pH 8) in a 1:4 ratio which was then run through Ni-NTA super flow cartridge at a 0.5–1 mL/min flow rate after equilibrating the cartridge with 10 column volumes of 1X Ni-NTA binding buffer. Then, Ni-NTA washing buffer (50 mM NaH_2PO4, 300 mM NaCl, 40 mM imidazole, pH 8) was applied until the UV absorbance value reached the baseline to wash away the non-specifically bound proteins. Finally, Ni-NTA elution buffer (50 mM NaH_2PO4, 300 mM NaCl, 250 mM imidazole, pH 8) was applied to elute the SNAP tag fusion proteins. The Ni-NTA Cartridge was washed by NaOH (0.5 M) to remove residual proteins from the resin. To strip the nickel ions from the column, stripping buffer (20 mM NaH_2PO4, 500 mM NaCl, 50 mM EDTA, pH 7.4) was applied to the column which was then recharged by $NiCl_2$ solution for further purification. During purification, all the eluted fractions were collected. After that,

the buffer of the protein in elution fraction was exchanged to PBS by using HiTrap desalting column (Cytiva) using the manufacturer protocol. The column was washed with 5-column volumes of PBS. The elution fraction was applied to column at 2 mL/min flow rate and collected the elution fraction. The column was washed with 5-column volumes of water, followed by 5-column volumes of ethanol. All the PBS buffer exchanged proteins were stored at -20°C.

2.2.2 Detection of purified protein and concentration measurement

All the eluted fractions were collected which was then incubation with SNAP-Surface® Alexa Fluor® 488 for 20 min in the dark at room temperature. All the samples were mixed with 5 × Protein Loading Buffer and loaded in 10% SDS gel along with blue pre-stained protein standard broad range (New England Biolabs) at 160 V for 60 min. After separation, labelled proteins were visualized either with a UV transilluminator Gel Doc XR gel documentation system or Odyssey DLx Imager to confirm the activity of SNAP tag by visualizing Alexa Fluor® 488 signals and the presence of proteins followed by Coomassie brilliant blue staining. The protein concentration was determined by bovine serum albumin (BSA) standards (New England Biolabs, 20 mg/mL). BSA was diluted with PBS to prepare four BSA concentrations (0.2, 0.1, 0.05, 0.025 µg/µL). Samples and each concentration of BSA standard solutions were run in 10% SDS gel. Using standard curve, protein concentration was determined by Image Lab software.

2.2.3 Modification of IR700 with BG

IR700 and BG-PEG-NHS were dissolved to 1.0 nM and 10 nM in DMSO respectively, followed by incubating at a 1:2 molar ratio at room temperature for 2 h. Conjugated IR700 and BG-PEG-NHS (BG-IR700) was analyzed and purified by high-performance liquid chromatography (HPLC) according to Hussain *et al* 2019 (Hussain *et al* 2019). The mass of BG-IR700 was confirmed using a Bruker MicroTOF LC mass spectrometer with an electrospray ion source. All HPLC and mass spectrometry analysis were done by the HPLC facility, Institute of Organic Chemistry, Justus-Liebig-University Giessen.

2.2.4 Conjugation of SNAP tag fusion proteins with BG-modified molecules

SNAP-Surface® Alexa Fluor® 488, SNAP-Surface® Alexa Fluor® 647 or BG-IR700 were conjugated to SNAP tag fusion proteins by incubating them at a 2:1 molar ratio at room temperature in dark for 2 h. The residual dyes were removed by 40K MWCO Zeba™ Spin

Desalting Columns according to manufacturer's protocol. Protein labeling was visualized with a UV transilluminator Gel Doc XR gel documentation system or Odyssey DLX Imager after separation by SDS-PAGE and the concentration was determined as described in 2.2.5.

2.2.5 Protein separation by electrophoresis

Sodium dodecyl-sulfate polyacrylamide gel electrophoresis (SDS-PAGE) is a commonly used method for protein separation and analysis. Protein samples were mixed with 5X Protein Loading Buffer and run in 10% SDS gel along with protein standard at 160 V for 60 min. Gel was visualized using ChemiDoc XRS+ System or Odyssey DLx Imager.

2.3 Expression level analysis of cell surface antigens in OvCa cells

Cell surface expression of EGFR, Her2, FOLR1, Trop2 and TF was analyzed by flow cytometry. OvCa cells (4 x 10^5) were incubated with anti-EGFR (EGFR mAb, clone H11, 0.5 µg), anti FOLR1 (FOLR1 mAb, clone 548908, 0.5 µg) and anti-Trop2 (Trop2 mAb, clone MR54, 1 µg), anti TF (CD142 mAb, clone HTF-1, 10 µL) (130-098-741) antibodies 200 µL of PBS for 30 min on ice. For Her2 expression analysis, cells were fixed by 4% formaldehyde solution for 10 min followed by permeabilization with 0.1% Triton X-100 in TBS at room temperature for 5 min. Followed by adding blocking buffer (10% FBS and 1% BSA in PBS) on ice for 30 min. The cells were incubated with anti-Her2 (ErbB2 mAb, 3B5) antibody for 30 min on ice. After washing twice with PBS, the cells were incubated with goat anti-mouse IgG (H+L) Highly Cross-Adsorbed Secondary Antibody conjugated with Alexa Fluor™ Plus 647 (0.25 µg) for 30 min on ice. After washing twice, cells were resuspended in 200 µL of PBS and analyzed by CytoFLEX S Flow Cytometers. Data was analyzed in FlowJo 10.7.1. from three independent experiments. The delta mean fluorescence intensity (ΔMFI) was calculated from the MFI of the cells expressing the marker of interest divided by the MFI of the unstained cells.

2.4 Determining the binding property of NIR-PIT agents

Flow cytometry and fluorescence microscopy were used to analyze the binding specificity of NIR-PIT agents to OvCa cell lines.

2.4.1 Binding property determination by flow cytometry

The binding efficiency of the NIR-PIT agents was determined by flow cytometry. OvCa cell lines (SKOV3, OVCAR3, IGROV1, A2780, OVCAR4 and Hey) were used to analyze the binding efficiency of 647 conjugated scFv-Erbitux-SNAP, scFv-Hereceptin-SNAP, scFv-

Farletuzumab-SNAP, scFv-Tisotuzumab-SNAP and scFv-Sacituzumab-SNAP. Cells (4 x 10^5) were washed with 1 mL PBS twice, followed by incubation with 1 µg of scFv-SNAP-647 with PBS for 30 min on ice. Cells were washed with 1 mL PBS twice and resuspended in 200 µL of PBS and analyzed by CytoFLEX S Flow Cytometers. Data was analyzed in FlowJo 10.7.1. from three independent experiments. The ΔMFI was calculated from the MFI of the cells expressing the marker of interest divided by the MFI of the unstained cells. In addition, IR700 conjugated scFv-Hereceptin-SNAP, scFv-Farletuzumab-SNAP, scFv-Tisotuzumab-SNAP and scFv-Sacituzumab-SNAP were used to confirm the specific binding using same flow cytometry setup and analyzed by CytoFLEX LX Flow Cytometers.

2.4.2 Binding property analysis by fluorescence microscopy

Fluorescence microscopy was used to confirm the binding of IR700 conjugated fusion proteins to OvCa cell lines. Cells were seeded in black 96-well plate with a clear bottom to a density of 40,000 cells/well and incubated overnight at 37°C. Cells were washed with PBS twice, and then incubated with 1 µg of each scFv-SNAP-IR700 on ice for 30 min. Then the cells were washed with PBS twice, followed by incubating with Hoechst 33,342 fluorescent nuclear counterstain (Thermo Fisher Scientific) (1:500 in PBS) for 10 min at room temperature. Cells were washed with PBS three times and incubated in 50 µL of PBS. The bindings were visualized with a DMi8 S Live-cell microscope using a 100X oil objective.

2.5 Photocytotoxicity of NIR-PIT agents

The photocytotoxicity of immunotherapeutic agents were evaluated using a Cell Proliferation (XTT) Kit II. SKOV3, OVCAR3, IGROV1, A2780, OVCAR4 and Hey cells were seeded in 96-well plates at a density of 5000 cells/well in 50 µL of culture medium and incubated at 37°C overnight. The cells were washed with serum-free medium twice, followed by incubation with serially diluted (12.5, 25, 50, 100, 200, 400, 800, 1600 nM) IR700 conjugated antibodies (scFv-Erbitux-SNAP-IR700, scFv-Herceptin-SNAP-IR700, scFv-Farletuzumab-SNAP-IR700, scFv-Tisotumab-SNAP-IR700 and scFv-Sacituzumab-SNAP-IR700 and unconjugated antibodies (scFv-Erbitux-SNAP, scFv-Herceptin-SNAP, scFv-Farletuzumab-SNAP, scFv-Tisotumab-SNAP and scFv-Sacituzumab-SNAP) at 37°C for 4 h in the dark. Cells incubated with media or zeocin were set as negative or positive control, respectively. Cells were washed with serum-free medium media three times. A red light-emitting diode (LED), which emits light at 670 to 710 nm wavelength (L690-66-60; Marubeni America Co., New York, NY) was used to irradiate the cells with LED power density 20 µW/cm^2 at 400 mA CW (measured with an

optical power meter, PM 100; Thorlabs, Newton, NJ). After NIR-light irradiation (2 J/cm^2), the cells were cultured in complete medium for 24 h at 37°C and 5% CO_2 in the dark. Cell viability was determined by incubating the cells with a 50 µL XTT labeling mixture at 37°C for 4 h. Reduction of XTT to formazan by viable tumor cells was monitored at a 450 nm absorbance wavelength and 650 nm reference wavelength using an Infinite® MPlex microplate reader (Figure 14). The data were analyzed in GraphPad software using dose response curve from triplicate of two independent experiments.

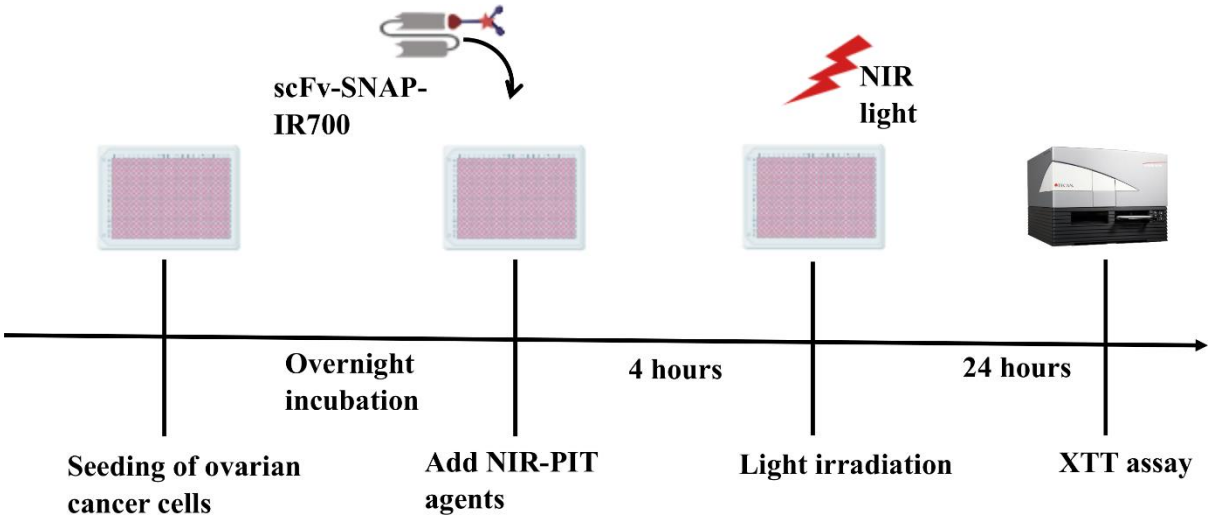

Figure 14: Schematic diagram of photocytotoxic experiments using XTT assay.

2.6 Induction of cell death by NIR-PIT agents

After the treatment with NIR-PIT agents, cell death induction was determined using SNAP-Surface® Alexa Fluor® 647 conjugated Annexin-SNAP fusion protein and propidium iodide (PI) according to Zhang *et al* 2022 (Zhang *et al* 2022). SKOV3, OVCAR3, IGROV1, A2780, OVCAR4 and Hey cells were seeded in 24-well plates at a density of 50,000 cells/well in triplicates and incubated at 37°C overnight. The cells were washed with serum-free medium twice, followed by incubation with serially diluted IR700 conjugated antibodies (scFv-Erbitux-SNAP-IR700, scFv-Herceptin-SNAP-IR700, scFv-Farletuzumab-SNAP-IR700, scFv-Tisotumab-SNAP-IR700 and scFv-Sacituzumab-SNAP-IR700 in 1600 nM and unconjugated antibodies (scFv-Erbitux-SNAP, scFv-Herceptin-SNAP, scFv-Farletuzumab-SNAP, scFv-Tisotumab-SNAP and scFv-Sacituzumab-SNAP in 1600 nM at 37°C for 4 h in the dark. Cells incubated with media or zeocin were set as negative or positive control, respectively. The cells were washed with serum-free medium three times. After NIR-light irradiation (2 J/cm^2), the cells were cultured in complete medium for 24 h at 37°C and 5% CO_2 in the dark. After 24 h, floating cells were collected, and adherent cells were harvested by trypsinization. Cells were

washed with 1 mL of Annexin binding buffer at 500 g for 5 min for twice. Then the cells were incubated with 0.5 µg of AnnexinV-SNAP-647 in 100 µL of Annexin binding buffer at room temperature for 30 min. Cells were washed with 1 mL of Annexin binding buffer once and resuspended in 100 µL of Annexin binding buffer, followed by incubation with 0.1 µg of propidium iodide (Thermo Fisher Scientific) at room temperature for 10 min. The necrotic, early apoptotic and late apoptotic cells were detected on Cytoflex S Flow Cytometer (Figure 15). The data were analyzed in FlowJo and GraphPad software from triplicate of two independent experiments.

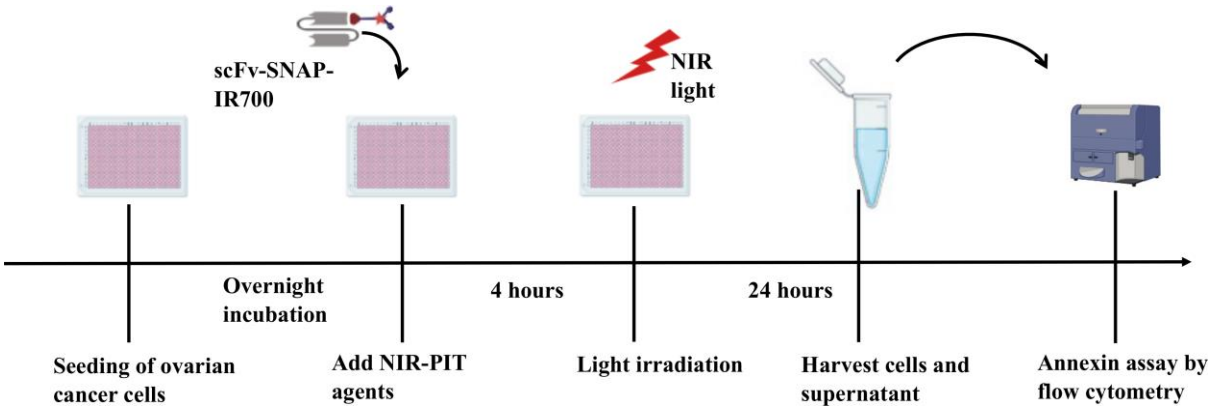

Figure 15: Schematic diagram of Annexin assay experiments for determining cell death.

2.7 Determining the type of cell death induced by NIR-PIT agents

To determine the type of cell death induced by NIR-PIT reagents in OvCa cells, we used three different cell death inhibitors that specifically block: apoptosis (zVAD-fmk, 25 µM, Invivogen), necroptosis (Necrostatin-1, 20 µM, AdipoGen life Sciences) and ferroptosis (Ferrostatin-1, 1 µM, Cayman Chemical Company). In this experiment we used one cell line for each NIR-PIT agent (OVCAR4 cells for scFv-Erbitux-SNAP-IR700, OVCAR3 for scFv-Herceptin-SNAP-IR700, IGROV1 for scFv-Farletuzumab-SNAP-IR700, Hey for scFv-Sacituzumab-SNAP-IR700, SKOV3 for scFv-Tisotumab-SNAP-IR700). Cells were incubated with 1600 nM NIR-PIT agent for 4 h at 37°C in the dark. After three washing steps with PBS, fresh phenol red-free culture medium containing respective cell death inhibitor was added to the cells and incubated for 30 min at 37°C. The cells were treated with NIR-light as described in section 2.2. XTT assay was performed to determine the cell scavenging ability by cell death inhibitor (Figure 16). The percentage of cell death inhibition was calculated by subtracting the percentage of cell viability of respective inhibitor with the percentage of cell viability of without the inhibitor. The data were analyzed in GraphPad software from triplicate of two independent experiments.

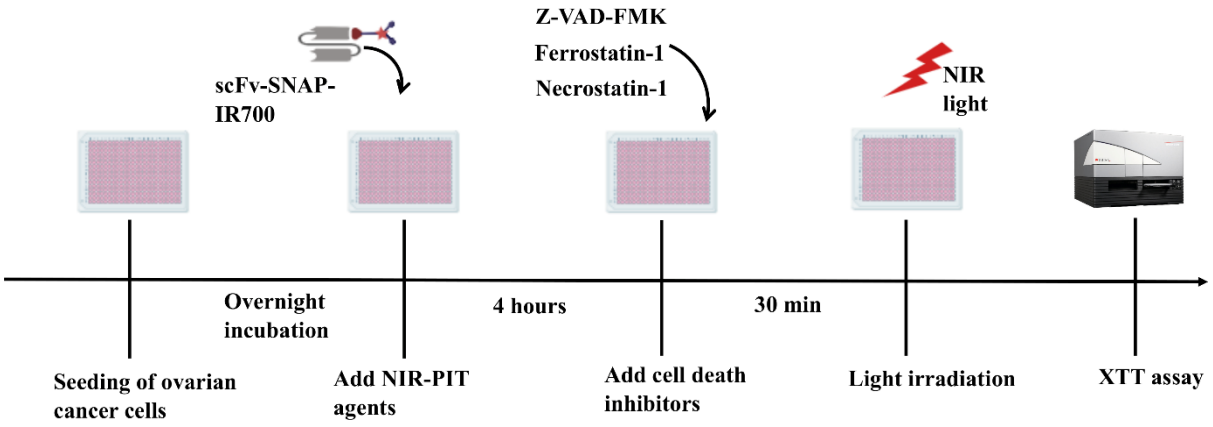

Figure 16: Schematic diagram of cell death pathway determination experiments.

2.8 Evaluating immunological responses triggered by NIR-PIT-killed tumor cells

The following methods were used for determining the cell surface expression of ICD marker (calreticulin, HSP70, HSP90) and extracellular release of ATP and HMGB1.

2.8.1 HSP70, HSP90 and calreticulin assay by flow cytometry

Cell surface expression of HSP70 after the treatment with NIR-PIT agents, was determined using flow cytometry. In this experiment, we used one positive cell lines for each NIR-PIT agent (OVCAR4 cells with scFv-Erbitux-SNAP-IR700, OVCAR3 with scFv-Herceptin-SNAP-IR700, IGROV1 with scFv-Farletuzumab-SNAP-IR700, Hey with scFv-Sacituzumab-SNAP-IR700, SKOV3 with scFv-Tisotumab-SNAP-IR700) and A2780 cell line for all five NIR-PIT agents as a control. SKOV3, OVCAR3, IGROV1, A2780, OVCAR4 and Hey cells were seeded in 24-well plates at a density of 50,000 cells/well in triplicates and incubated at 37°C overnight. The cells were washed with serum-free medium twice, followed by incubation with 1600 nM of IR700 conjugated antibodies (scFv-Erbitux-SNAP-IR700, scFv-Herceptin-SNAP-IR700, scFv-Farletuzumab-SNAP-IR700, scFv-Tisotumab-SNAP-IR700 and scFv-Sacituzumab-SNAP-IR700) and unconjugated antibodies (scFv-Erbitux-SNAP, scFv-Herceptin-SNAP, scFv-Farletuzumab-SNAP, scFv-Tisotumab-SNAP and scFv-Sacituzumab-SNAP) at 37°C for 4 h in the dark. Cells exposed to NIR-light irradiation without incubation with NIR-PIT agents were used as control. The cells were washed with serum-free medium three times. After NIR-light irradiation, the cells were cultured in complete medium for 24 h at 37°C and 5% CO_2 in the dark. After 24 h, floating cells were collected, and adherent cells were harvested by trypsinization. The cells were washed with 1 mL of PBS (600 g, 6 min) twice and incubated with 2 µL HSP70 antibody (FITC-Conjugated) (Miltenyi Biotech #130-105-548), 1 µg HSP90 antibody (APC conjugated, H9010, Invitrogen #MA5-45102) and 0.5

µg calreticulin antibody (488-conjugated, Clone 681233, R&D Systems #IC38981G-100UG) for 30 min at 4°C. After washing twice, the cells were resuspended in 200 µL of PBS and analyzed by CytoFLEX S Flow Cytometers (Figure 17). The number of the cells was expressed in percentages from the living gated cells and HSP70 and calreticulin, -specific MFI was calculated. The MFI are divided by 1000 and shown in bar graph and used for statistical analysis. The data from triplicate of two independent experiments were analyzed in FlowJo and GraphPad software.

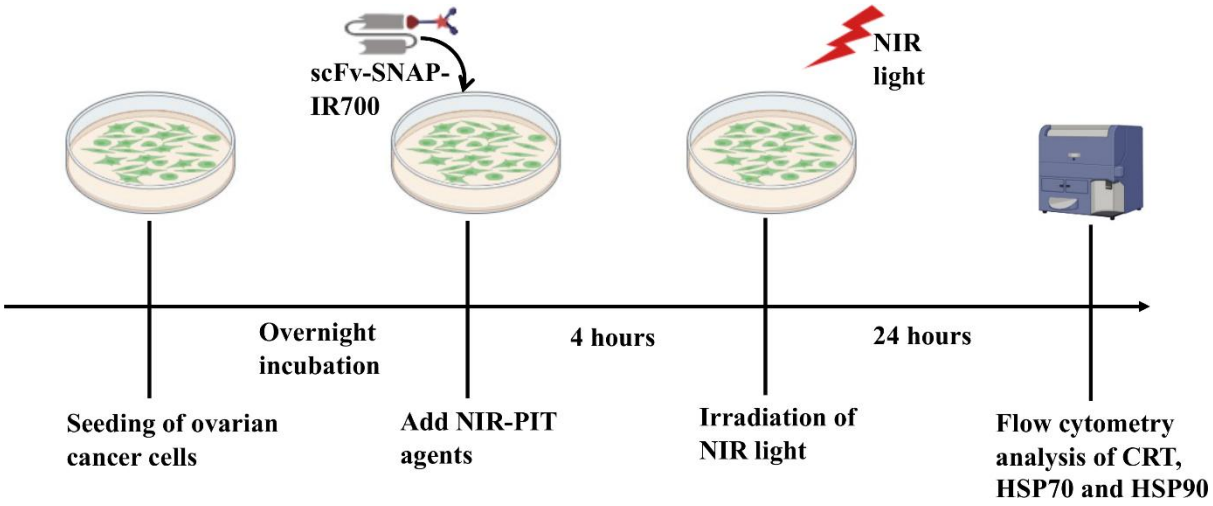

Figure 17: Schematic diagram of ICD hallmark (calreticulin, HSP70 and HSP90) determination experiments.

2.8.4 ATP assay

After the treatment, extracellular level of ATP was measured using ATP assay kit. In this experiment, one positive cell line was used for each NIR-PIT agent (OVCAR4 cells with scFv-Erbitux-SNAP-IR700, OVCAR3 with scFv-Herceptin-SNAP-IR700, IGROV1 with scFv-Farletuzumab-SNAP-IR700, Hey with scFv-Sacituzumab-SNAP-IR700, SKOV3 with scFv-Tisotumab-SNAP-IR700) and A28780 cell line for all five NIR-PIT agents as a control. SKOV3, OVCAR3, IGROV1, A2780, OVCAR4 and Hey cells were seeded in 24-well plates at a density of 50,000 cells/well in triplicates and incubated at 37°C overnight. The cells were washed with serum-free medium twice, followed by incubation with 1600 nM of IR700 conjugated antibodies (scFv-Erbitux-SNAP-IR700, scFv-Herceptin-SNAP-IR700, scFv-Farletuzumab-SNAP-IR700, scFv-Tisotumab-SNAP-IR700 and scFv-Sacituzumab-SNAP-IR700) and unconjugated antibodies (scFv-Erbitux-SNAP, scFv-Herceptin-SNAP, scFv-Farletuzumab-SNAP, scFv-Tisotumab-SNAP and scFv-Sacituzumab-SNAP) at 37°C for 4 h in the dark. The cells exposed to NIR-light irradiation without incubation with NIR-PIT agents were used as control. The cells were washed with serum-free medium media three times. After

NIR-light irradiation, the cells were cultured in complete medium for 24 h at 37°C and 5% CO_2 in the dark. After 24 h, the culture supernatants were collected and centrifuged. Extracellular ATP concentrations in the culture supernatants were evaluated by a luciferin-based ATP Assay kit (ENLITEN, Promega, Madison, WI, USA, LOT. 0000410249) according to the manufacturer's instructions (Figure 18). The amount of ATP level (pmol) was calculated by preparing standard curve. The data from triplicate of two independent experiments were analyzed in GraphPad software.

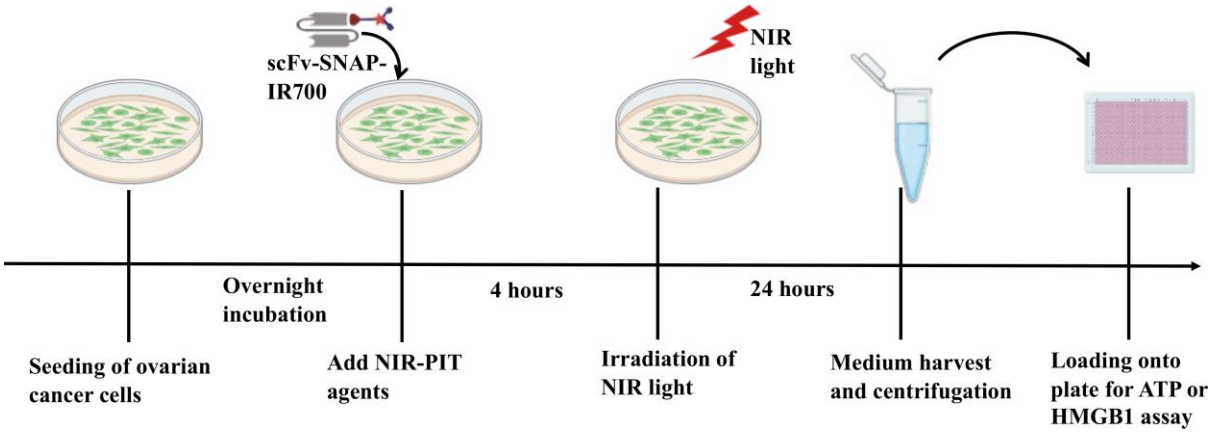

Figure 18: Schematic diagram of ATP and HMGB1 determination experiments.

2.8.5 HMGB1 assay

For analyzing extracellular release of HMGB1 level after the treatment, the same experimental set up was used as described in 2.8.4. After NIR-light irradiation, the cells were cultured in complete medium for 24 h at 37°C and 5% CO_2 in the dark. After 24 h, the culture supernatants were collected and centrifuged. The concentration of HMGB1 in the supernatant was measured using an HMGB1 ELISA kit (IBL International, Hamburg, Germany Lot. EHMG153) according to the manufacturer's instructions. The amount of HMGB1 level (ng/mL) was calculated by preparing standard curve. The data from triplicate of two independent experiments were analyzed in GraphPad software.

2.9 Determining DCs maturation induced by NIR-PIT-killed tumor cells

Peripheral blood mononuclear cells (PBMCs) were purchased from BPS Bioscience (#79059). $CD14^+$ monocytes cells were isolated from PBMCs by positive selection using CD14 microbeads (Miltenyi Biotec #130-097-052) and MACS column (LS column, Miltenyi Biotec #130-042-401) as described Ogawa *et al* 2017. The efficiency of $CD14^+$ monocytes cells isolation was investigated by staining with CD14 antibody (APC conjugated, clone REA599, Miltenyi Biotec #130-110-578). DCs were generated by culturing the $CD14^+$ monocytes cells

in the presence of 50 ng/mL granulocyte-macrophage colony-stimulating factor (GM-CSF) (PeproTech #300-03) and 10 ng/ mL interleukin-4 (IL-4) (Miltenyi Biotec #130-093-915). The generation of iDC cells were determined by staining them with DC marker (CD209 mAb, B515 conjugated, clone REA617, Miltenyi Biotec #130-132-023). SKOV3 cells were incubated with scFv-Tisotumab-SNAP and scFv-Tisotumab-SNAP-IR700 with NIR-light exposure and co-cultured for 48 h with immature DCs (day 5) at a DC/tumor cell ratio of 1:2. In addition, OVCAR4 cells were incubated with scFv-Erbitux-SNAP and scFv-Erbitux-SNAP-IR700 with NIR-light exposure and co-cultured for 24-48 h with immature DCs (day 5) at a DC/tumor cell ratio of 1:2. DCs stimulated with 100 ng/mL of lipopolysaccharide (LPS) (Invitrogen #00-4976-93) for 12 h were used as a positive control for DC maturation. After 48 h, all floating cells were collected and washed with PBS twice. Cells were incubated with 1.0 µg of CD80 (APC conjugated, clone B7-1, Invitrogen #17-0809-42) antibody, 2 µL of CD86 (PE conjugated, clone FM95, Miltenyi Biotec #130-094-877) antibody, 1.0 µg of CD40 (FITC conjugated, clone MH40-3, Invitrogen #11-0402-82) antibody and 2 µL of HLADR (APC conjugated, clone REA805, Miltenyi Biotec #130-111-943) antibody for 30 min on ice. After washing twice, the cells were resuspended in 200 µL of PBS and analyzed by CytoFLEX S Flow Cytometers (Figure 19). The number of the cells was expressed in percentages from the living DC gated cells and CD80, CD86, CD40 and HLADR-specific MFI was calculated. The MFI are divided by 1000 and shown in the graph. The data were analyzed in GraphPad software.

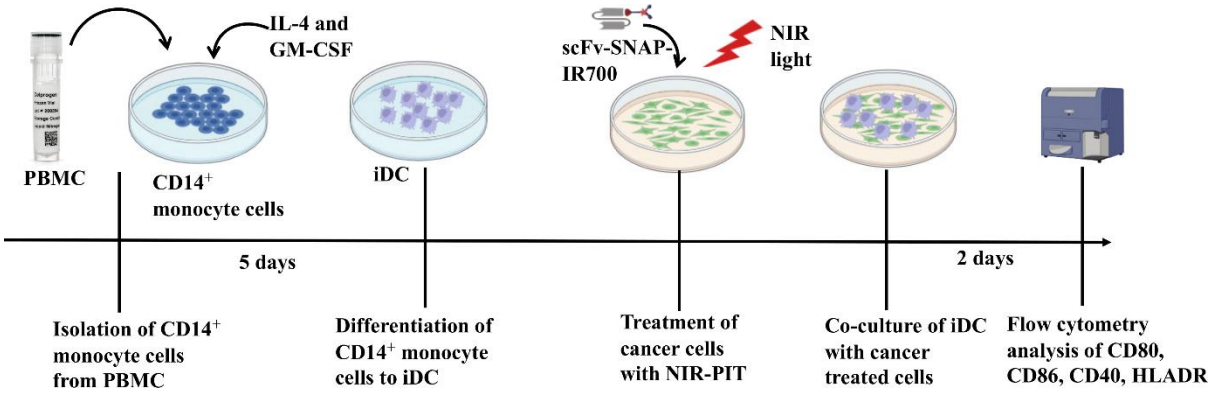

Figure 19: Schematic diagram of determining DCs maturation experiments.

2.10 Cell lines

OvCa cell lines SKOV3 (HTB-77), OVCAR3 (HTB-161), IGROV1 (SCC-203), A2780 (ECACC-93112519) and human embryonic kidney cell line HEK293T (CRL-11268) were purchased from American Type Culture Collection, European collection of Authenticated cell cultures and Sigma-Aldrich. OVCAR4 and Hey cell lines were kindly provided by Dr. Karen

Bräutigam (Department of Gynecology and Obstetrics, University Hospital Schleswig-Holstein, Campus Lübeck).

2.11 Medium

10% (v/v) fetal bovine serum (FBS) (Thermo Fisher Scientifc) and 1% (v/v) penicillin and streptomycin (Thermo Fisher Scientifc) was added with RPMI-1640 (Biowest) medium to prepare complete culture medium. Additional 0.1% (v/v) zeocin (InvivoGen) was added to RPMI 1640 complete culture medium to keep selecting transfected cells during the scFv-SNAP tag protein expression.

2.12 Designing the scFv genes

The V_H and V_L of Erbitux, Herceptin, Farletuzumab, Sacituzumab and Tisotumab amino acid sequences were determined from their full length mAbs from Global Substance Registration System. The constructs of scFv-Erbitux-SNAP, scFv-Herceptin-SNAP, scFv-Farletuzumab-SNAP, scFv-Sacituzumab-SNAP and scFv-Tisotumab-SNAP have been generated in Hussain Group (unpublished result).

2.13 Plasmids

Following table (Table 1) provides an overview of all used plasmids for conducted experiments described in chapter 3.1.

Table 1: Plasmids used in section 3.1.

Plasmids	Genotype	References
pMS-scFv-425-SNAP	ori ColE1, Amp^R, $P_{CMV,}$ IgG leader, scFv_425, SNAP tag, IRES, EGFP, f1 ori, and $Bleo^R$	Hussain *et al* 2019
pMS-scFv-Erbitux-SNAP	ori ColE1, Amp^R, $P_{CMV,}$ IgG leader, scFv_Erbitux, SNAP tag, IRES, EGFP, f1 ori, and $Bleo^R$	this study
pMS-scFv-Herceptin-SNAP	ori ColE1, Amp^R, $P_{CMV,}$ IgG leader, scFv_Herceptin, SNAP tag, IRES, EGFP, f1 ori, and $Bleo^R$	this study
pMS-scFv-Farletuzumab-SNAP	ori ColE1, Amp^R, $P_{CMV,}$ IgG leader, scFv_Farletuzumab, SNAP tag, IRES, EGFP, f1 ori, and $Bleo^R$	this study
pMS-scFv-Sacituzumab-SNAP	ori ColE1, Amp^R, $P_{CMV,}$ IgG leader, scFv_Sacituzumab, SNAP tag, IRES, EGFP, f1 ori, and $Bleo^R$	this study
pMS-scFv-Tisotumab-SNAP	ori ColE1, Amp^R, $P_{CMV,}$ IgG leader, scFv_Tisotumab, SNAP tag, IRES, EGFP, f1 ori, and $Bleo^R$	this study

2.14 Stains

Following table (Table 2) provides an overview of all used stains for conducted experiments described in chapter 3.1.

Table 2: Strains used in section 3.1.

Strain	Genotype	Reference
E. coli DH5α	-	Hussain *et al* 2019
E. coli DH5α pMS-scFv-Erbitux-SNAP	*E. coli* DH5α pMS-scFv-Erbitux-SNAP, Amp^R	this study
E. coli DH5α pMS-scFv-Herceptin-SNAP	*E. coli* DH5α pMS-scFv-Herceptin-SNAP, Amp^R	this study
E. coli DH5α pMS-scFv-Farletuzumab-SNAP	*E. coli* DH5α pMS-scFv-Farletuzumab-SNAP, Amp^R	this study
E. coli DH5α pMS-scFv-Sacituzumab-SNAP	*E. coli* DH5α pMS-scFv-Sacituzumab-SNAP, Amp^R	this study
E. coli DH5α pMS-scFv-Tisotumab-SNAP	*E. coli* DH5α pMS-scFv-Tisotumab-SNAP, Amp^R	this study

2.15 HEK293T cells containing SNAP tag fusion protein plasmid

Following table (Table 3) provides an overview of all used HEK293T cells containing SNAP tag fusion protein plasmid for conducted experiments described in chapter 3.1.

Table 3: HEK293T cells containing SNAP tag fusion protein plasmid used in section 3.1.

Strain	Genotype	Reference
HEK293T	-	Hussain *et al* 2019
HEK293T-pMS-scFv-Erbitux-SNAP	HEK293T-pMS-scFv-Erbitux-SNAP, $Bleo^R$	this study
HEK293T-pMS-scFv-Herceptin-SNAP	HEK293T-pMS-scFv-Herceptin-SNAP, $Bleo^R$	this study
HEK293T-pMS-scFv-Farletuzumab-SNAP	HEK293T-pMS-scFv-Farletuzumab-SNAP, $Bleo^R$	this study
HEK293T-pMS-scFv-Sacituzumab-SNAP	HEK293T-pMS-scFv-Sacituzumab-SNAP, $Bleo^R$	this study
HEK293T-pMS-scFv-Tisotumab-SNAP	HEK293T-pMS-scFv-Tisotumab-SNAP, $Bleo^R$	this study

2.16 Buffers

Following table (Table 4) provides an overview of all buffers used for conducting all the experiments.

Table 4: List of buffers

Buffer/Solution	Components	Concentration
10X PBS (pH 7.4)	Na_2HPO_4	76.8 mM
	$NaH_2PO_4 \cdot H_2O$	23.2 mM
	NaCl	1.54 M
10% SDS-PAGE (separation gel)	Milli-Q water	40.8% (v/v)
	Acrylamide/Bisacrylamide (30%, 37.5:1)	32.9% (v/v)
	Tris-HCl (pH 8.8)	373 mM
	SDS	0.1% (w/v)
	TEMED	0.1% (v/v)
	APS	0.032% (w/v)
4% SDS-PAGE gel (stacking gel)	Milli-Q water	60.3% (v/v)
	Acrylamide/Bisacrylamide (30%, 37.5:1)	12.9% (v/v)
	Tris-HCl (0.5 M, pH 6.8)	125 mM
	SDS	0.1% (w/v)
	TEMED	0.1% (v/v)
	APS	0.1% (w/v)
SDS running buffer	Tris	25 mM
	Glycine	0.192 mM
	SDS	0.1% (w/v)
4X Ni-NTA binding buffer (pH 8.0)	NaH_2PO_4	200 mM
	NaCl	1200 mM
	Imidazole	40 mM
1X Ni-NTA binding buffer (pH 8.0)	NaH_2PO_4	50 mM
	NaCl	300 mM
	Imidazole	10 mM
Ni-NTA washing buffer (pH 8.0)	NaH_2PO_4	50 mM
	NaCl	300 mM
	Imidazole	40 mM
Ni-NTA elution buffer (pH 8.0)	NaH_2PO_4	50 mM
	NaCl	300 mM
	Imidazole	250 mM

Stripping buffer (pH 7.4)	NaH_2PO_4	20 mM
	NaCl	500 mM
	EDTA	50 mM
Regeneration buffer	$NiCl_2$	100 mM
5X Protein loading buffer	Bromophenol blue	0.02% (v/v)
	Glycerol	30% (v/v)
	SDS	10% (v/v)
	Tris-HCl	250 mM
Coomassie brilliant blue gel staining solution	Brilliant blue R 250	1.21 mM
	Methanol	50% (v/v)
	Acetic acid	10% (v/v)
Coomassie brilliant blue gel destaining solution	Methanol	50% (v/v)
	Acetic acid	10% (v/v)
TAE buffer	Tris	40 mM
	Glacial acetic acid	5.71% (v/v)
	EDTA	1 mM
LB medium (pH 7.0)	LB-Medium (Luria/Miller)	25 g
	Milli-Q water	1000 mL
LB medium supplemented with ampicillin	LB medium	-
	Ampicillin	0.27 mM
LB-agar supplemented with ampicillin	LB medium	-
	Agar agar	0.015% (w/v)
	Ampicillin	0.27 mM
Annexin binding buffer (pH 8.0)	HEPES	10 mM
	NaCl	140 mM
	$CaCl_2$	2.5 mM

2.17 Antibodies

Following table (Table 5) provides an overview of all antibodies used for conducting experiments described in chapter 3.

Table 5: List of antibodies

Name	**Supplier**
Anti-Hsp70-FITC (#130-105-548)	Miltenyi Biotec
Anti-Hsp90-APC (clone H9010, #MA5-45102)	Invitrogen
Human Calreticulin antibody (Clone 681233, #IC38981G-100UG)	R&D Systems
CD80-APC (clone B7-1, #17-0809-42)	Invitrogen

HLADR-APC (clone REA805, #130-111-943)	Miltenyi Biotec
CD14 (clone REA599, #130-110-578)	Miltenyi Biotec
CD40-FITC (clone MH40-3, #11-0402-82)	Invitrogen
CD209 (clone REA617, #130-132-023)	Miltenyi Biotec
CD86-PE (clone FM95, #130-094-877)	Miltenyi Biotec
EGFR mAb (clone 111.6, #MA5-13269)	Invitrogen
Anti-Her2 (ErbB2 mAb, clone 3B5, # MA5-13675)	Invitrogen
FOLR1 mAb (clone 548908, #MA5-23917)	Invitrogen
Trop2 (EGP-1) mAb (clone MR54, #14-6024-82)	Invitrogen
CD142 Antibody (clone HTF-1) (130-098-741)	Miltenyi Biotec
Goat anti-Mouse IgG (H+L) Highly Cross-Adsorbed Secondary Antibody, Alexa Fluor™ Plus 647 (#A32728)	Invitrogen

2.18 Columns

Following table (Table 6) provides an overview of all columns used for conducting experiment described in chapter 3.

Table 6: List of columns

Name	**Application**	**Supplier**
40K MWCO Zeba ™ Spin Desalting Columns	Size exclusion	Thermo Fisher Scientific
7K MWCO Zeba ™ Spin Desalting Columns	Size exclusion	Thermo Fisher Scientific
HiTrap Desalting column	Buffer exchange	Cytiva
Ni-NTA superflow cartridge	Protein purification	Qiagen
MACS Column (LS column, #130-042-401)	MACS separation	Miltenyi Biotec
Eurospher II 100-5 C18 column	HPLC	Knauer

2.19 Kits and other reagents

Following table (Table 7) provides an overview of all kits and other reagents used for conducting the experiments described in chapter 3.

Table 7: List of kits and other reagents

Kit and other reagent name	**Supplier**
Cell Proliferation Kit II (#11465015001)	Roche
ATP assay kit (#FF200)	ENLITEN, Promega

HMGB1 ELISA kit (#ST51011)	IBL International
IL-4 (#130-093-915)	Miltenyi Biotec
GM-CSF (#300-03)	PEPROTECH
Z-VAD-FMK (#tlrl-vad)	Invivogen
Necrostatin-1 (#AG-CR1-2900-M005**)**	AdipoGen life Sciences
Ferrostatin-1 (#17729)	Cayman Chemical Company
IRdye700DX NHS (#92970010)	LI-COR Biosciences
BG-PEG-NH2 (#S9150S)	New England Biolabs
PBMC (#79059-1)	BPS bioscience

2.20 Equipment

Following table (Table 8) provides an overview of all equipment used for conducting the experiments described in chapter 3.

Table 8: List of equipment

Name	**Manufacturer**
Odyssey DLx Imager	LI-COR Biosciences
CytoFLEX S Flow Cytometers	Beckman Coulter
CytoFLEX Lx Flow Cytometers	Beckman Coulter
ÄKTA start system	GE Healthcare Bio-Sciences AB
Incubation shaker Multitron Standard	Infors
Infinite® Mplex microplate reader	Tecan
Balances	Kern & Sohn
Centrifuge Megafuge™ 16	Thermo Fisher Scientific
Centrifuge 5427 R	Eppendorf
ChemiDoc XRS+ System	BIORAD
DMi8 S Live-cell microscope	Leica Microsystems
ECLIPSE Ts2 inverted microscope	Nikon
Eppendorf ThermoMixer® F2.0	Eppendorf
Fisherbrand™ Multi-Platform Shaker	Fisher Scientific
NanoDrop™ One/OneC	Thermo Fisher Scientific
PEQLAB PCR Thermal Cycler (PEQLAB PEQSTAR)	PEQLAB Biotechnology
Schott CG 840 pH Meter	Schott
Trans-Blot® Turbo™ Transfer System	BIORAD
Vortex RS-VA 10	Phoenix Instrument
Water bath WB 7	Memmert

Incubator IN75	Memmert
Incubator Model CB 170	BINDER

2.21 Software for data analysis

Following table (Table 9) provides an overview of all software used for conducting the experiments described in chapter 3.

Table 9: List of software

Name	**Producer**	**Application**
FlowJo 10.7.1	Becton, Dickinson & Company	Image and Data analysis
GraphPad Prism 9.0.0	GraphPad Software	Data analysis
ImageJ	National Institutes of Health	Image analysis
Image Studio Lite Ver 5.2	LI-COR Biosciences	Image analysis
Image Lab software	Bio-Rad	Image analysis

3 Results

Since the discovery of NIR-PIT, extensive studies have been conducted to treat numerous cancer entities by targeting several cell surface antigens. To my knowledge, no study of NIR-PIT targeting FOLR1, TROP2 and TF has yet been reported for treating OvCa. This study aimed to develop NIR-PIT approaches for OvCa treatment. In this study, five tumor associated antigens (EGFR, Her2, FOLR1, TROP2 and TF) were chosen as they are expressed in different levels on OvCa cell lines. The results given in this chapter comprise four sections: the first section summarizes the generation and characterization of five scFv-SNAP based NIR-PIT agents and their binding properties on OvCa cell lines. The second section details the *in vitro* cytotoxicity and the type of cell death pathway of the generated NIR-PIT agents. The third section demonstrates the evaluation of immunogenic cell death hallmark after the treatment. Finally, the fourth section describes the measurements of DC maturation marker after NIR-PIT.

3.1 Expression, enrichment and functional analysis of scFv-SNAP-tag fusion proteins

The scFv-SNAP-tag fusion proteins were used to generate immunoconjugates. These fusion proteins can transiently be expressed in HEK293T cells using the pMS expression system to generate sufficient amount of targeted proteins with high purity (von Felbert *et al* 2016; Hussain *et al* 2011; Zhang *et al* 2022). The variable gene sequences encoding for scFv antibody fragments of anti-EGFR human-mouse chimeric mAb Erbitux (Bou-Assaly and Mukherji 2010), anti-Her2 humanized mAb Herceptin (Gemmete and Mukherji 2011), anti-FOLR1 mAb Farletuzumab (Konner *et al* 2010), anti-TROP2 humanized mAb Sacituzumab (Syed 2020) and anti-TF humanized mAb Tisotumab (Markham 2021) were obtained from publicly available resources (patents, journals, and antibody databases) and were fused to SNAP by *in-silico* expression plasmid design. The success of transforming the cells with the expression vectors was confirmed by monitoring the GFP signal (Figure 20a). The scFv-SNAP tag fusion proteins have been successfully produced in HEK293T cells with high yield (5-10 mg/L culture supernatant). The functional activity of SNAP-tag was evaluated by incubation with SNAP-Surface® Alexa Fluor® 488 followed by SDS gel separation. The fluorescence signal of 488 (Figure 20b) and Coomassie blue staining (Figure 20c) confirmed the SNAP-tag activity of scFv-Erbitux-SNAP and corresponding protein size (51.7 kDa). In addition, SNAP-tag activity of scFv-Herceptin-SNAP, scFv-Farletuzumab-SNAP, scFv-Sacituzumab-SNAP and scFv-Tisotumab-SNAP were confirmed by in-gel fluorescence scanning and each fusion proteins

were identified based on their molecular weights (51.2-51.7 kDa) (Figure S1). The final purity of scFv-SNAP-fusion proteins was ~90%.

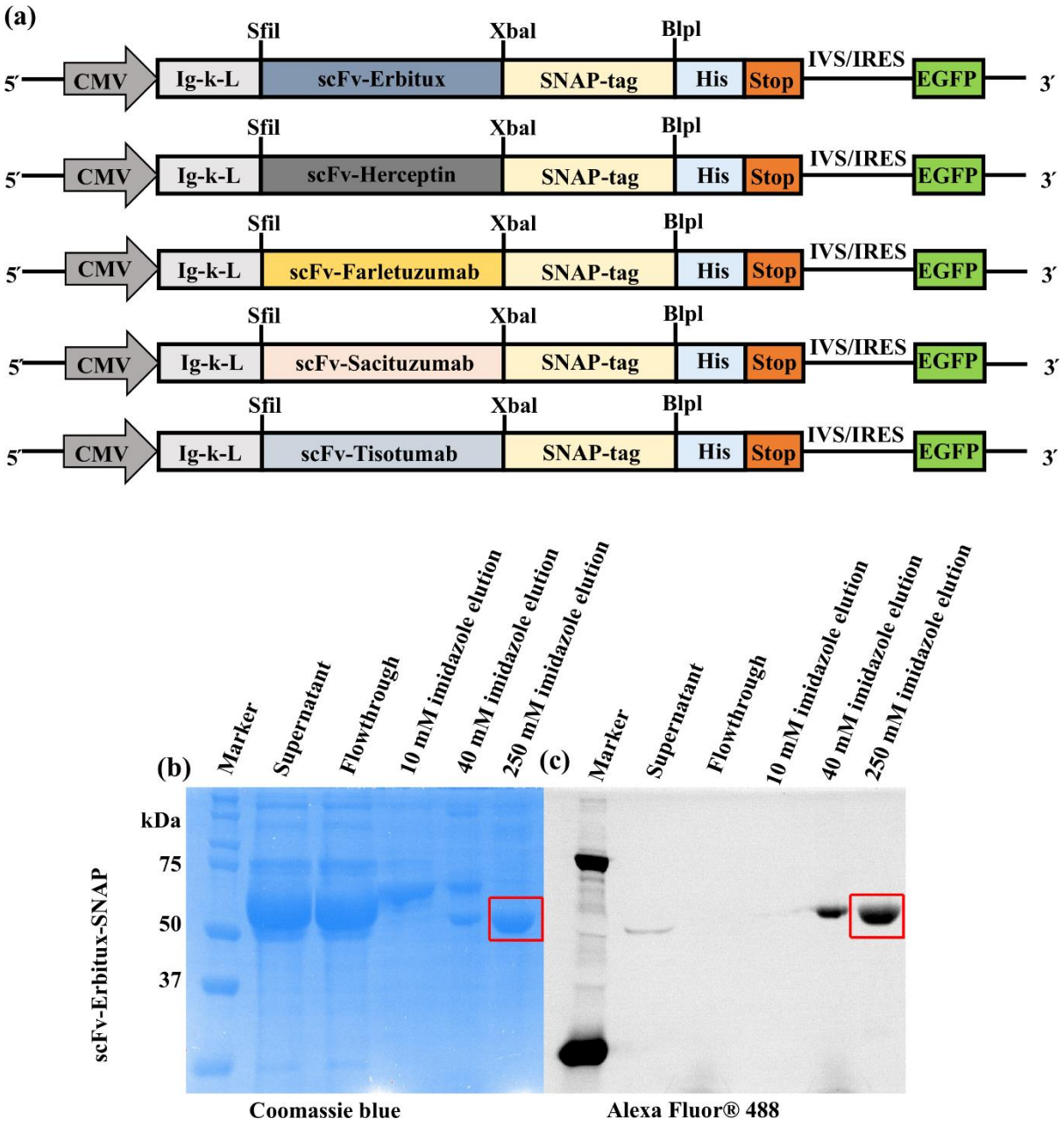

Figure 20: Construction and expression of the SNAP-tag fusion proteins. (a) Schematic diagram of the scFv-SNAP tag constructs. CMV: cytomegalovirus promoter; IgK leader: immunoglobulin kappa chain leader; His: poly-histidine tag; Stop: TGA stop codon, IRES: internal ribosome entry site, EGFP: enhanced fluorescent protein. (b) Enrichment of scFv-Erbitux-SNAP by nickel NTA using His-tagged and confirmed by SDS-PAGE by Coomassie blue staining and (c) SNAP-Surface® Alexa Fluor® 488 signal. The signal was visualized with ChemiDoc XRS^{+} System. Marker represent dual color protein standard broad range (10-250 kDa). The red box indicates the corresponding protein bands.

3.2 Labeling of SNAP-tag fusion proteins with BG-modified IR700

SNAP-tag provides robust site-specific conjugation of proteins to BG derivatives with a 1:1 stoichiometry and generates homogenous antibody drug molecules (Hussain *et al* 2011). To site specifically conjugate IR700 to scFv-SNAP tag fusion protein, IR700 molecules were modified with BG using BG-PEG-NH_2 linkers. The chemical coupling and purification of IR700 with BG-linkers was confirmed by HPLC and mass spectrometry analysis (Figure S2).

The labeling efficiency of scFv-SNAP tag fusion proteins was further determined by coupling them to BG-modified IR700 (BG-IR700). The BG-IR700 coupled efficiently to the fusion proteins, which was confirmed by visualizing the IR700 signal at 700 nm using an Odyssey DLx Imager (Figure 21). The conjugation was further confirmed by post-incubating them with SNAP-Surface® Alexa Fluor® 488. As shown in Figure 21b, the specific coupling site was blocked by BG-IR700 that inhibited the coupling with SNAP-Surface® Alexa Fluor® 488. This result suggests that BG-IR700 has been conjugated site specifically, irreversibly to SNAP-tag fusion proteins within 2 h at room temperature.

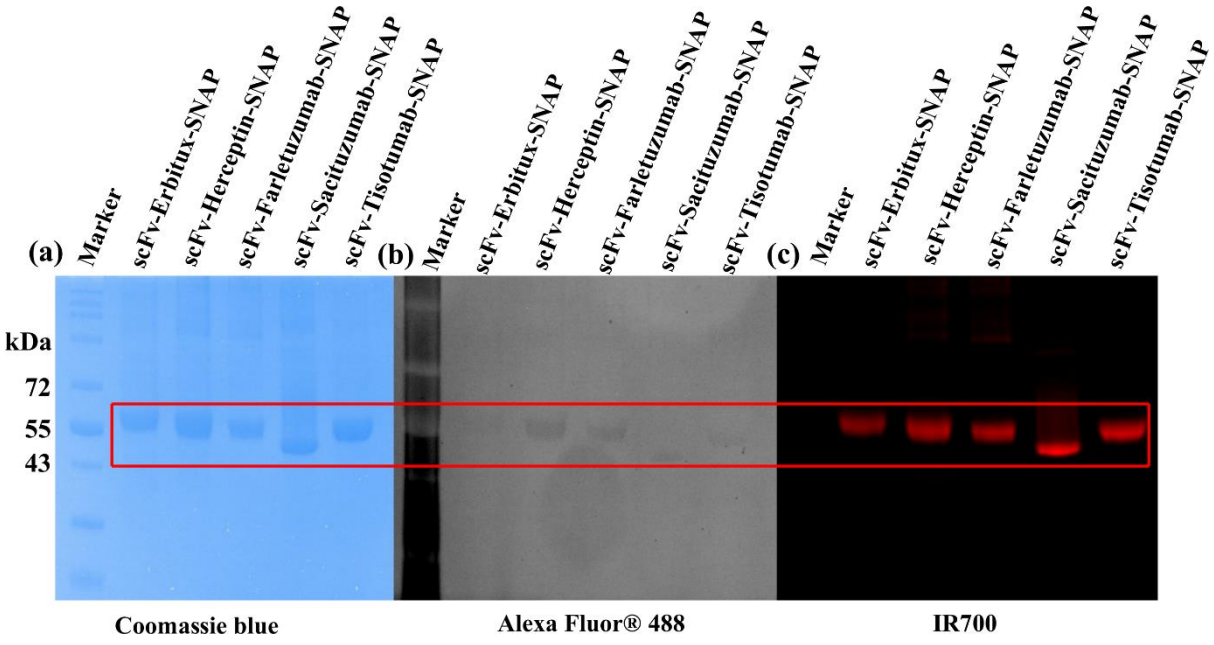

Figure 21: SNAP tag protein labeling with BG-IR700. (a) Coomassie blue staining represents IR700 conjugated scFv-Erbitux-SNAP, scFv-Herceptin-SNAP, scFv-Farletuzumab-SNAP, scFv-Sacituzumab-SNAP and scFv-Tisotumab-SNAP followed by post-incubation with SNAP-Surface® Alexa Fluor® 488. (b) Corresponding Alexa Fluor® 488 fluorescence and (c) IR700 signals are shown. Broad Range marker (11-250 kDa). The red box indicates the corresponding protein bands.

3.3 Expression levels of cell surface antigens in OvCa cells

The efficacy and applicability of NIR-PIT depend on the target antigens which overexpress on the cancer cells. Therefore, the overexpression of target antigens is important to design the NIR-PIT agent (Wei *et al* 2022). Here, the surface expressions of EGFR, Her2, FOLR1, TROP2 and TF in OvCa cells were analyzed by flow cytometry using commercial mAb.

The flow cytometric analysis showed strong binding signal of anti-EGFR-647 in SKOV3, OVCAR3, IGROV1, OVCAR4 and Hey cell lines. The average ΔMFI were ~484, ~723, ~266, ~399 and ~132 in SKOV3, OVCAR3, IGROV1, OVCAR4 and Hey cells, respectively, representing higher expression of EGFR. In contrast, A2780 cells showed low fluorescence signal and the ΔMFI was ~21, indicating A2780 cells express low level of EGFR (Figure 22). Similarly, SKOV3 and OVCAR3 cells showed high fluorescence signals when stained with anti-Her2-647. The ΔMFI were ~202 and ~448 in SKOV3 and OVCAR3 cells, respectively. Whereas IGROV1, A2780, OVCAR4 and Hey cell lines exhibited low fluorescence signals with the ΔMFI values of ~40, ~12, ~41 and ~20, respectively (Figure 22). As shown in Figure 23, the ΔMFI values of FOLR1 in OVCAR3 and IGROV1 cells were ~205 and ~1161, whereas the other four cell lines showed low to moderate fluorescence signals. The ΔMFI values of FOLR1 were ~57, ~18, ~5 and ~10 in SKOV3, A2780, OVCAR4 and Hey cells, respectively. These revealed that OVCAR3 and IGROV1 cells expressed high level of FOLR1. In addition, OVCAR3 (ΔMFI~208), OVCAR4 (ΔMFI~251) and Hey (ΔMFI~476) cells expressed high levels of TROP2 whereas SKOV3 (ΔMFI~50) cells expressed moderate level of TROP2. On the other hand, IGROV1 and A2780 cells showed low level of TROP2 and their ΔMFI value was ~12 for both cell lines (Figure 23). Moreover, the TF was highly expressed in SKOV3 cells and ΔMFI value was ~109. OVCAR3 (ΔMFI~52) and OVCAR4 (ΔMFI~55) cells exhibited moderate level of TF. On the contrary, IGROV1, A2780 and Hey cells showed low level of TF and their ΔMFI values were less than 14 (Figure 24) (Table 10).

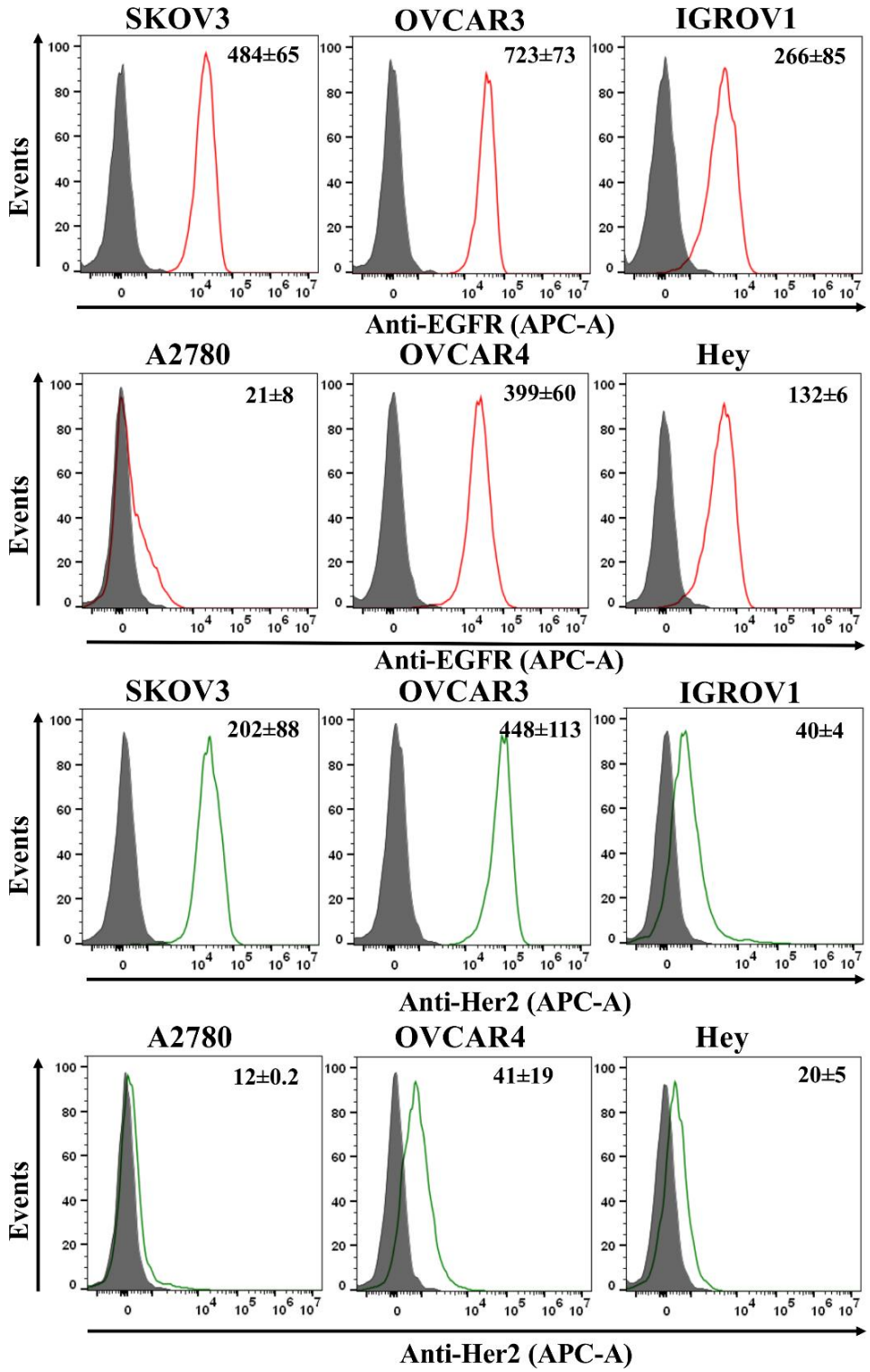

Figure 22: Expression patterns of EGFR and Her2 in OvCa cell lines. EGFR and Her2 expressions in OvCa cell lines were determined by flow cytometry. Cells were treated with anti-EGFR (EGFR mAb, H11) (red), anti-Her2 (ErbB2 mAb, 3B5) (green) antibodies, respectively, followed by incubation with the secondary antibody (Goat anti-Mouse IgG Highly Cross-Adsorbed Secondary Antibody, Alexa Fluor™ Plus 647). The ΔMFI values are shown in each histogram box (mean ± SE) from three independent experiments. The ΔMFI was calculated from the MFI of the cells expressing the marker of interest divided by the MFI of the unstained cells.

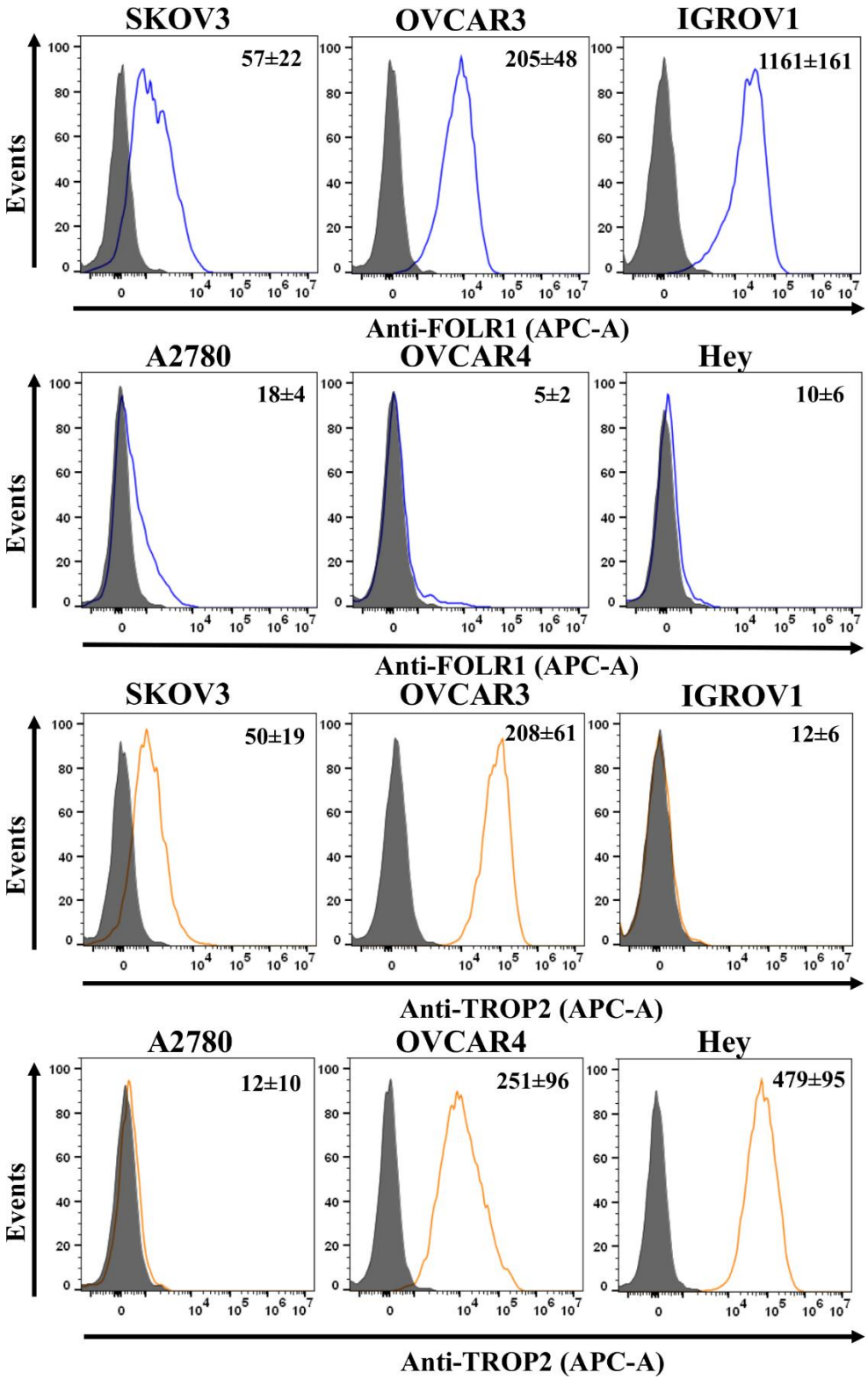

Figure 23: Expression patterns of FOLR1 and TROP2 in OvCa cell lines. FOLR1 and TROP2 expressions in OvCa cell lines were determined by flow cytometry. Cells were treated with anti FOLR1 (FOLR1 mAb, 548908) (blue) and anti-TROP2 (TROP2 mAb, MR54) (brown) antibodies, respectively followed by incubation with the secondary antibody (Goat anti-Mouse IgG Highly Cross-Adsorbed Secondary Antibody, Alexa Fluor™ Plus 647). The ΔMFI values are shown in each histogram box (mean ± SE) from three independent experiments.

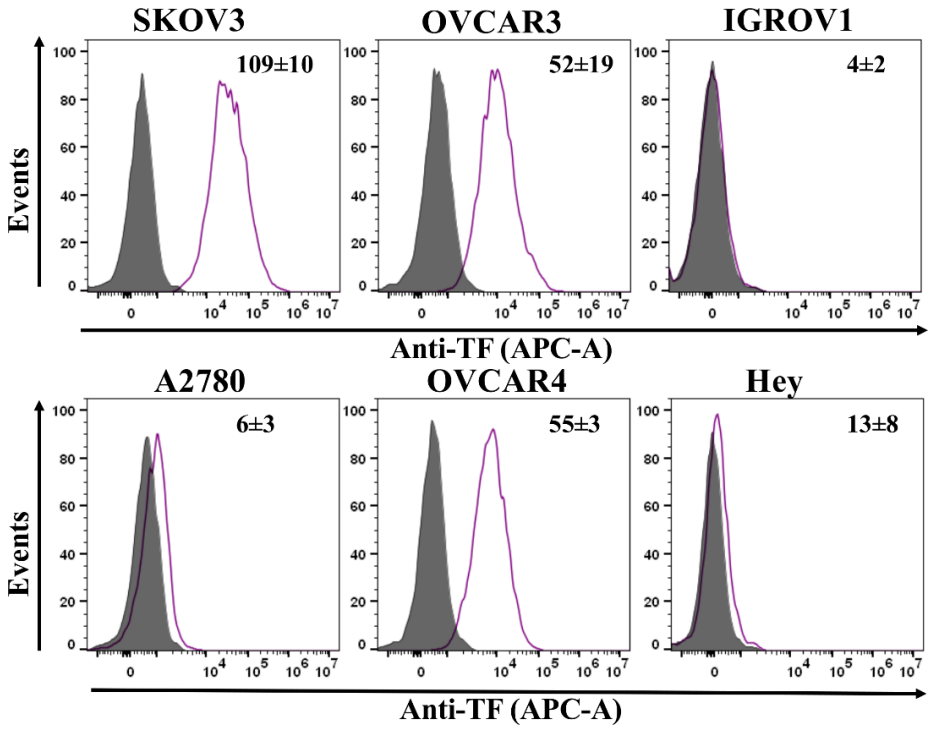

Figure 24: Expression pattern of TF in OvCa cell lines. TF expression in OvCa cell lines was determined by flow cytometry. The cells were treated with anti TF (CD142 mAb, HTF-1) (Magenta) antibodies, followed by incubation with the secondary antibody (Goat anti-Mouse IgG Highly Cross-Adsorbed Secondary Antibody, Alexa Fluor™ Plus 647). The ΔMFI values are shown in each histogram box (mean ± SE) from three independent experiments.

Table 10: Cell surface expression of EGFR, Her2, FOLR1, TROP2 and TF in ovarian cancer cell lines.

Cell surface antigens	SKOV3	OVCAR3	IGROV1	A2780	OVCAR4	Hey
EGFR	high	high	moderate	low	high	moderate
Her2	high	high	low	low	low	low
FOLR1	moderate	high	high	low	low	low
TROP2	moderate	high	low	low	high	high
TF	high	moderate	low	low	moderate	low

3.4 Specific binding of NIR-PIT agents on OvCa cells

One of the major challenges of the antibody-based therapeutics is their specificity to the targeted membrane proteins, which is essential for guiding on dosing, potency and efficacy (Wang *et al* 2021). The binding of NIR-PIT agents to targeted cancer cells is a crucial step in NIR-PIT. Antibodies or their fragments of NIR-PIT agents can specifically recognize and bind

to targeted molecules on the surface of cells. This precision in binding enhances therapeutic efficacy while minimizing off-target effects, making NIR-PIT a promising avenue for treating a variety of cancers (Biteghe *et al* 2020; Mitsunaga *et al* 2011; Shim 2020; Wei *et al* 2022).

Initially, the binding specificity of scFv-SNAP tag fusion proteins to OvCa cells was examined by labeling with SNAP-Surface® Alexa Fluor® 647 using flow cytometry. The flow cytometric analysis results revealed that the ΔMFI was high in SKOV3 (~173), OVCAR3 (~240), IGROV1 (~93) and OVCAR4 (~205) cells after incubation with 647 conjugated scFv-Erbitux-SNAP (Figure 25). Conversely, the ΔMFI values were ~5 and ~34 for low EGFR expressed A2780 and Hey cells, respectively. This confirms the specific binding properties of scFv-Erbitux-SNAP. The 647 labeled scFv-Herceptin-SNAP displayed the highest binding to the high Her2 expressed SKOV3 and OVCAR3 cells. In contrary, 647 fluorescence signal was low in low Her2 expressed IGROV1, A2780, OVCAR4 and Hey cells. The scFv-Farletuzumab-SNAP-647 incubated with IGROV1 cells showed high ΔMFI which was ~1499. In contrast, low FOLR1 expressed SKOV3, A2780, OVCAR4 and Hey cells exhibited low ΔMFI, representing the specific binding of scFv-Farletuzumab-SNAP. In addition, the specific binding was observed for scFv-Sacituzumab-SNAP-647 on SKOV3, OVCAR3, OVCAR4 and Hey cells. Moreover, high fluorescence signal was observed in SKOV3 (~70), OVCAR3 (~69) and OVCAR4 (~81) cells after incubation with 647 conjugated scFv-Tisotumab-SNAP, confirming their specific binding (Figure 25).

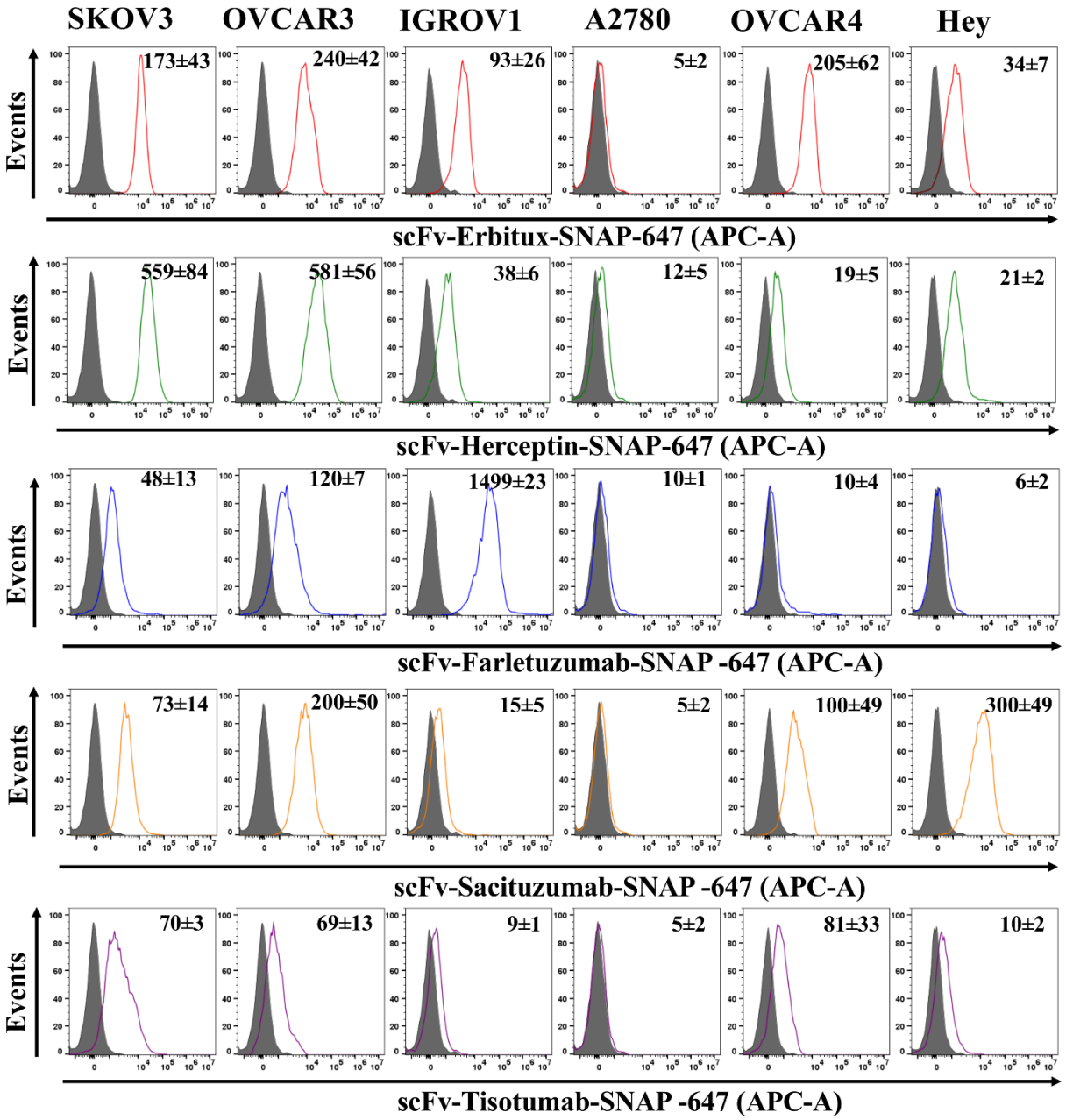

Figure 25: Specific binding of 647 conjugated scFv-SNAP tag to OvCa cells. The flow cytometric histogram represents the binding of scFv-SNAP-647 to OvCa cells. Filled gray curves represent untreated cells and red, green, blue, brown and magenta curves represent cells incubated with 0.5 µg/mL of the scFv-Erbitux-SNAP-647, scFv-Herceptin-SNAP-647, scFv-Farletuzumab-SNAP-647, scFv-Sacituzumab-SNAP-647 and scFv-Tisotumab-SNAP-647, respectively. The ΔMFI values are shown in each histogram box (mean ± SE) from three independent experiments.

To analyze the binding specificities of five scFv-SNAP tag proteins, BG-IR700 was conjugated with fusion protein and flow cytometry and fluorescence microscopy were carried out. The specific binding of the scFv-SNAP-IR700 correlated with the receptor expression level as measured by flow cytometry. The flow cytometry data revealed that scFv-Erbitux-SNAP-

IR700 specifically bound to the EGFR high-expressing SKOV3, OVCAR3 and OVCAR4 cells, while only a minimal fluorescence signal was observed on the EGFR low-expressing A2780 cells (Figure 26a). In fluorescence microscopy, intense membrane fluorescence was visualized in EGFR high-expressing SKOV3, OVCAR3 and OVCAR4 cells whereas no membrane-associated fluorescence was captured in EGFR low-expressing A2780 cells (Figure 26b) (Table 11). Similarly, the fluorescence signal was significantly higher in Her2-high expressing SKOV3 and OVCAR3 cell lines in the presence of scFv-Herceptin-SNAP-IR700 (Figure 27a). The membrane fluorescence signal was also strong in SKOV3 and OVCAR3 cells, indicating the scFv-Herceptin-SNAP-IR700 binding specificity (Figure 27b). After incubation of OvCa cells with scFv-Farletuzumab-SNAP-IR700, high-FOLR1 expressing IGROV1 cells exhibited detectable fluorescence signals and moderate-FOLR1 expressing OVCAR3 cells showed moderate fluorescence signal, whereas no fluorescence signal was detected in low-FOLR1 expressing cell lines (Figure 28) (Table 11). In addition, the flow cytometry and microscopic results showed enhanced binding of scFv-Sacituzumab-SNAP-IR700 to SKOV3, OVCAR3, OVCAR4 and Hey cells compared to IGROV1 and A2780 cells (Figure 29). Moreover, the scFv-Tisotumab-SNAP-IR700 showed enhanced binding to SKOV3, OVCAR3 and OVCAR4 cells relative to IGROV1, A2780 and Hey cells (Figure 30) (Table 11).

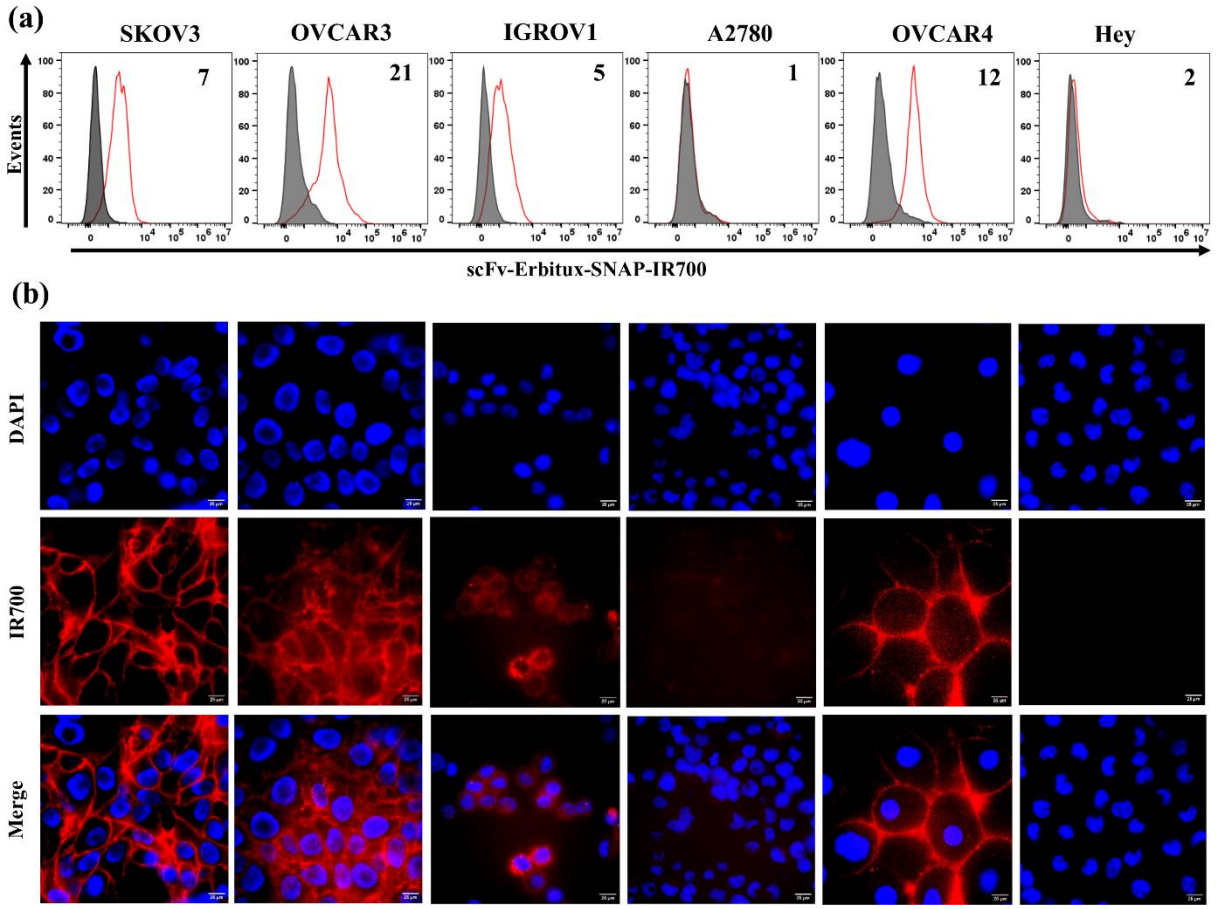

Figure 26: The scFv-Erbitux-SNAP-IR700 specifically binds to EGFR-expressing cells. (a) Specific binding of scFv-Erbitux-SNAP-IR700 to OvCa cell lines was analyzed by flow cytometry. The flow cytometric histograms represent the binding of scFv-Erbitux-SNAP-IR700 to OvCa cells. Filled gray curves represent untreated cells and red curves represent cells incubated with 0.5 µg/mL of the scFv-Erbitux-SNAP-IR700. The ΔMFI values are shown in each histogram box. (b) Specific binding was also analyzed using fluorescence microscopy. Fluorescence images were obtained for the $EGFR^{+}$ SKOV3, OVCAR3, IGROV1, OVCAR4 and Hey cells. The cells were incubated with scFv-Erbitux-SNAP-IR700 (red) and DAPI (blue).

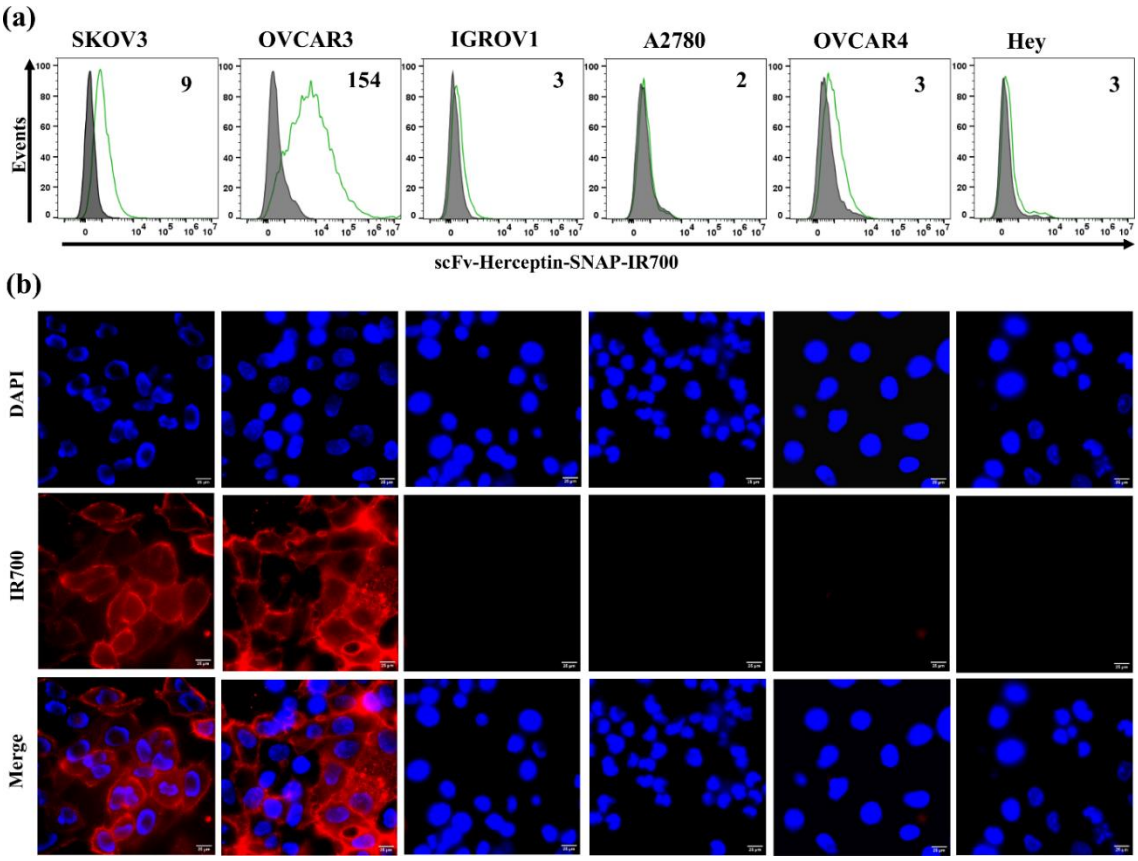

Figure 27: The scFv-Herceptin-SNAP-IR700 specifically binds to Her2-expressing cells. (a) Specific binding of scFv-Herceptin-SNAP-IR700 to OvCa cell lines was analyzed by flow cytometry. The flow cytometric histograms represent the binding of scFv-Herceptin-SNAP-IR700 to OvCa cells. Filled gray curves represent untreated cells and green curves represent cells incubated with 0.5 µg/mL of the scFv-Herceptin-SNAP-IR700. (b) Specific binding was also analyzed using fluorescence microscopy. Fluorescence images were obtained from the $Her2^{+}$ SKOV3 and OVCAR3 cells. The cells were incubated with scFv-Herceptin-SNAP-IR700 (red) and DAPI (blue).

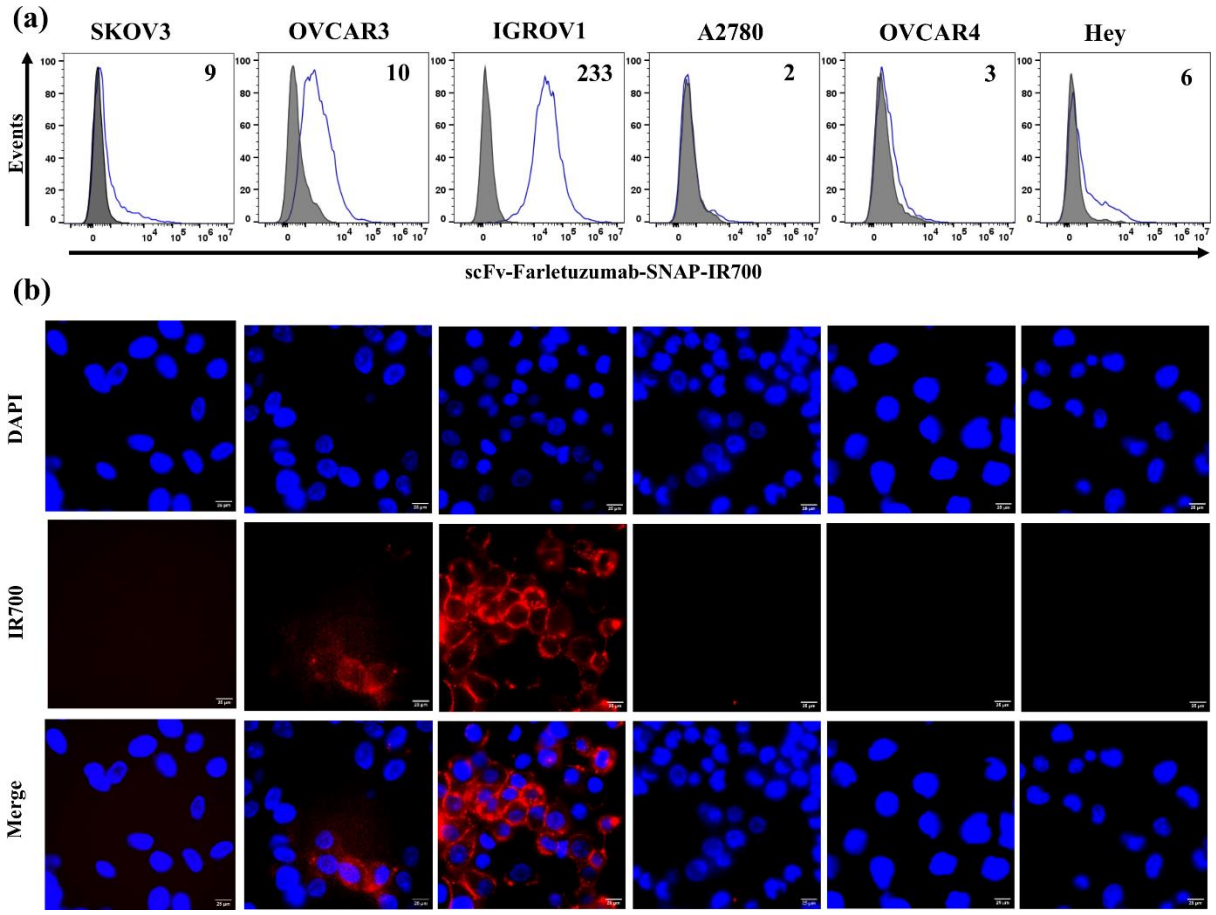

Figure 28: The scFv-Farletuzumab-SNAP-IR700 specifically binds to FOLR1-expressing cells. (a) Specific binding of scFv-Farletuzumab-SNAP-IR700 to OvCa cell lines was analyzed by flow cytometry. The flow cytometric histograms represent the binding of scFv-Farletuzumab-SNAP-IR700 to OvCa cells. Filled gray curves represent untreated cells and blue curves represent cells incubated with 0.5 µg/mL of the scFv-Farletuzumab-SNAP-IR700. (b) Specific binding was also analyzed using fluorescence microscopy. Fluorescence images were obtained from the FOLR1^{+} OVCAR3 and IGROV1 cells. The cells were incubated with scFv-Farletuzumab-SNAP-IR700 (red) and DAPI (blue).

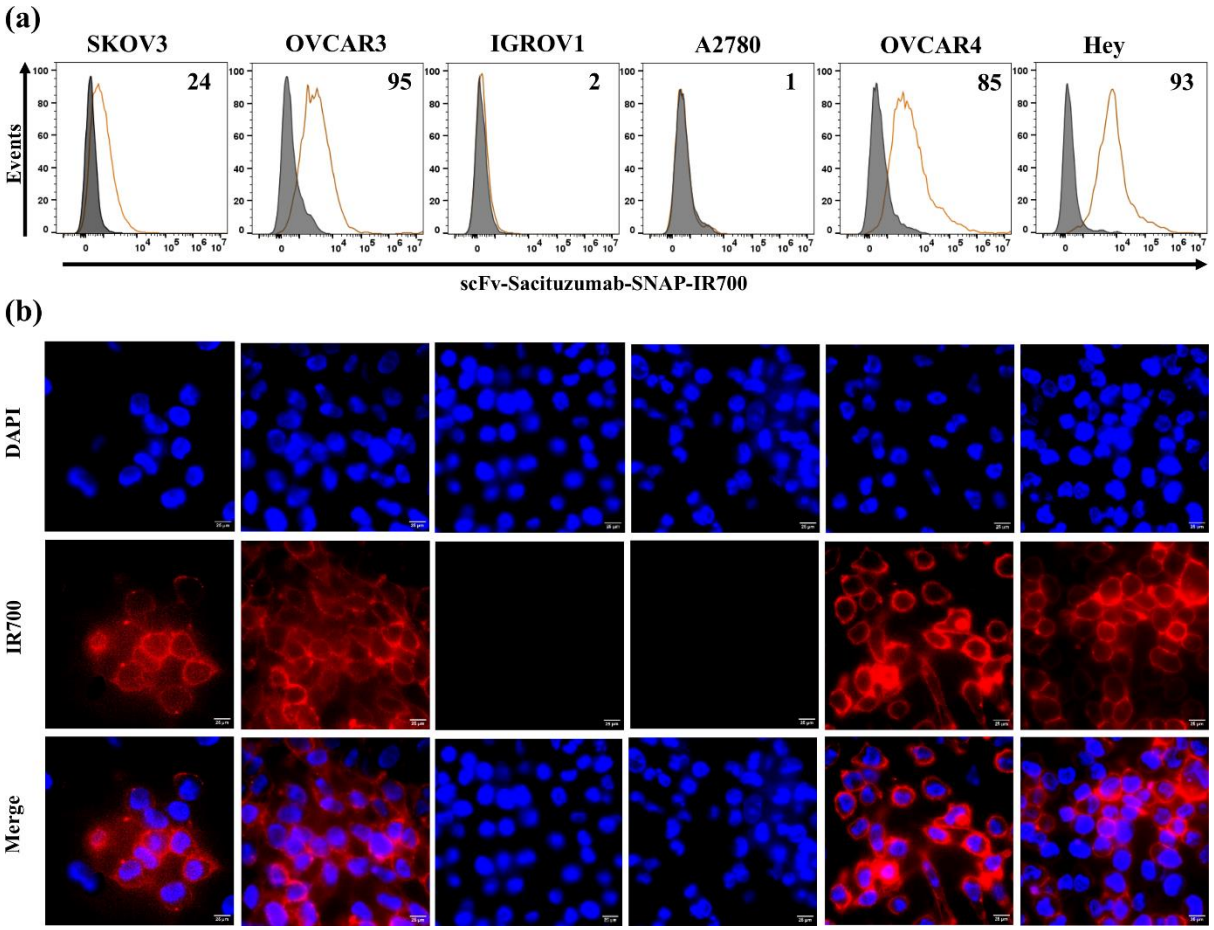

Figure 29: The scFv-Sacituzumab-SNAP-IR700 specifically binds to TROP2-expressing cells. (a) Specific binding of scFv-Sacituzumab-SNAP-IR700 to OvCa cell lines was analyzed by flow cytometry. The flow cytometric histograms represent the binding of scFv-Sacituzumab-SNAP-IR700 to OvCa cells. Filled gray curves represent untreated cells and brown curves represent cells incubated with 0.5 µg/mL of the scFv-Sacituzumab-SNAP-IR700. (b) Specific binding was also analyzed using fluorescence microscopy. Fluorescence images were obtained from the TROP2^{+} SKOV3, OVCAR3, OVCAR4 and Hey cells. The cells were incubated with scFv-Sacituzumab-SNAP-IR700 (red) and DAPI (blue).

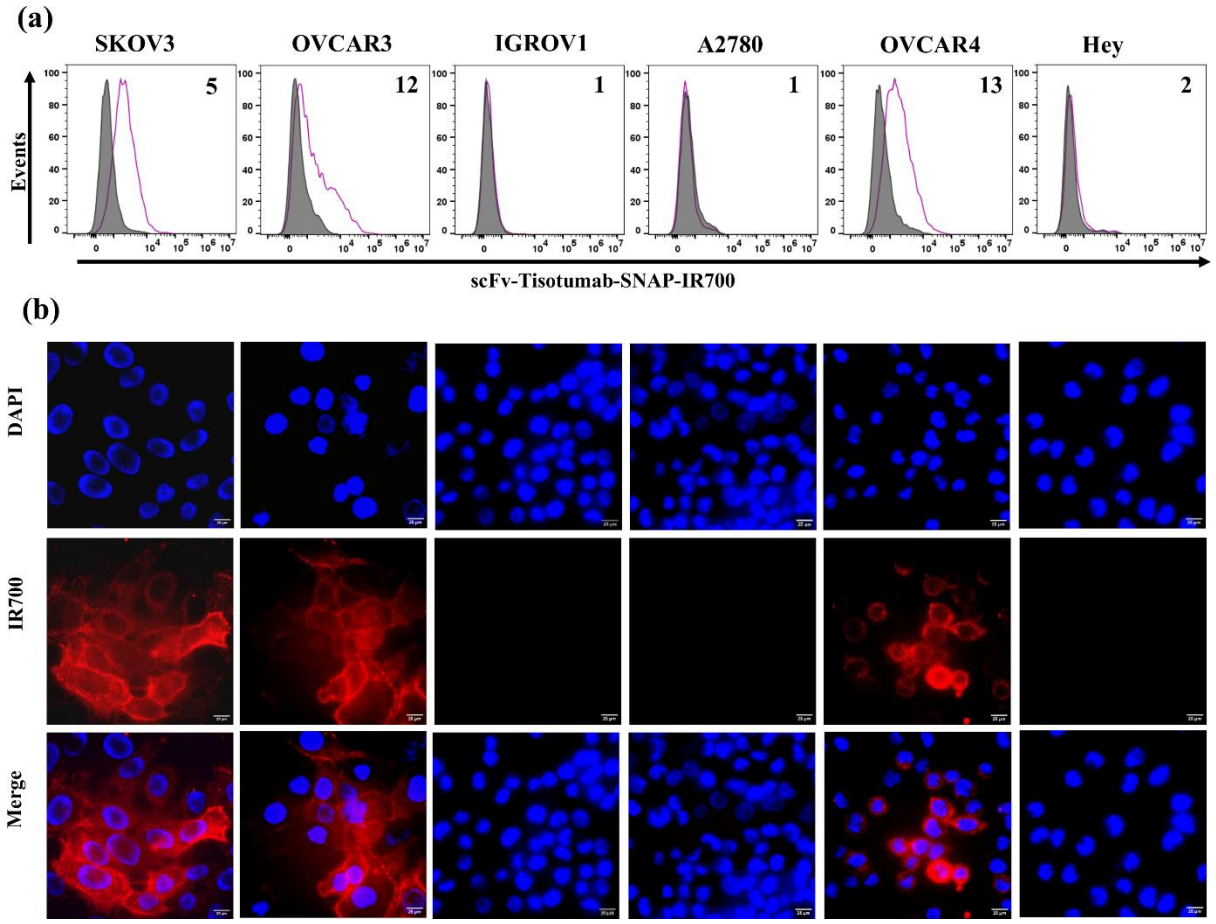

Figure 30: The scFv-Tisotumab-SNAP-IR700 specifically binds to TF-expressing cells. (a) Specific binding of scFv-Tisotumab-SNAP-IR700 to OvCa cell lines were analyzed by flow cytometry. The flow cytometric histograms represent the binding of scFv-Tisotumab-SNAP-IR700 to OvCa cells. Filled gray curves represent untreated cells and purple curves represent cells incubated with 0.5 µg/mL of the scFv-Tisotumab-SNAP-IR700. (b) Specific binding was also analyzed using fluorescence microscopy. Fluorescence images were obtained from the TF^+ SKOV3, OVCAR3 and OVCAR4 cells. The cells were incubated with scFv-Tisotumab-SNAP-IR700 (red) and DAPI (blue).

Table 11: Binding efficiency of five NIR-PIT agents in ovarian cancer cell lines**.**

NIR-PIT agents	SKOV3	OVCAR3	IGROV1	A2780	OVCAR4	Hey
scFv-Erbitux-SNAP-IR700	high	high	moderate	-	high	-
scFv-Herceptin-SNAP-IR700	high	high	-	-	-	-
scFv-Farletuzumab-SNAP-IR700	-	moderate	high	-	-	-
scFv-Sacituzumab-SNAP-IR700	moderate	high	-	-	high	high
scFv-Tisotumab-SNAP-IR700	moderate	moderate	-	-	moderate	-

3.5 *In vitro* photocytotoxicity of NIR-PIT agents

After NIR light irradiation, IR700 of the NIR-PIT agents-bound targeted cancer cell undergoes excitation, transitions to a triplet state, and leads to cleavage of the axial ligands. These water-soluble axial ligands separation from phthalocyanine core of IR700 changes its properties from hydrophilic to hydrophobic, such transition forms a water-insoluble aggregate on the targeted cancer cells, resulting in targeted cell swelling, bleb formation, and rupture of the vesicles representing cell death. The threshold for NIR light induced toxicity depends on the concentration of NIR-PIT agents and the light dose (Nakajima *et al* 2018; Nakajima *et al* 2023; Takakura *et al* 2021).

As all our investigated NIR-PIT agents showed specific binding properties, it was hypothesized that they exhibited specific photocytotoxicity. Therefore, the photocytotoxic effect of scFv-SNAP-IR700 mediated NIR-PIT was evaluated in six OvCa cell lines (SKOV3, OVCAR3, IGROV1, A2780, OVCAR4 and Hey). Cultured cells were incubated with scFv-Erbitux-SNAP-IR700, scFv-Herceptin-SNAP-IR700, scFv-Farletuzumab-SNAP-IR700, scFv-Tisotumab-SNAP-IR700 and scFv-Sacituzumab-SNAP-IR700 and then exposed to 690–710 nm LED (2 J/cm^2). The cytotoxicity mediated by NIR-PIT was determined using XTT-based colorimetric cell proliferation assay. Nonirradiated cells and unlabeled scFv-SNAP fusion proteins were used as controls. After 24 h of scFv-Erbitux-SNAP-IR700 treatment, high to moderate EGFR expressed cell lines SKOV3, OVCAR3, IGROV1 and OVCAR4 cells showed increased cell death in a concentration-dependent manner. The IC_{50} values of SKOV3, OVCAR3, IGROV1 and OVCAR4 cells were 1420 nM, 308 nM, 671 nM and 283 nM, respectively (Table 12). The scFv-Erbitux-SNAP-IR700 showed negligible effects on both A2780 and Hey cell lines. In contrast, nonirradiated and unconjugated scFv-Erbitux-SNAP demonstrated no toxicity to all the investigated cell lines (Figure 31). Similarly, for Her2 targeting NIR-PIT, scFv-Herceptin-SNAP-IR700 showed significant cell death in high Her-2 overexpressed SKOV3 (IC_{50}: 628 nM) and OVCAR3 cells (IC_{50}: 42 nM). There were very little effects on low expressed A2780, IGROV1, OVCAR4 and Hey cell lines (Figure 32) (Table 12). In addition, FOLR1-based NIR-PIT agent reduced the cell viability significantly in high FOLR1 expressing IGROV1 and moderate FOLR1 expressing OVCAR3 cells. The IC_{50} values were 1560 nM and 42 nM in OVCAR3 and IGROV1 cells, respectively (Figure 33) (Table 12). Moreover, scFv-Sacituzumab-SNAP-IR700 treatment was associated with decreased cell viability in high TROP2 expressing OVCAR3, OVCAR4 and Hey cells and moderate TROP2 expressing SKOV3 cells. The IC_{50} values were 59.9 nM, 96.2 nM, 45.9 nM and 956.1 nM in

OVCAR3, OVCAR4, Hey and SKOV3 cells, respectively (Figure 34) (Table 12). The scFv-Tisotumab-SNAP-IR700 agents killed high TF expressing SKOV3 (IC_{50}: 50.6 nM), OVCAR3 (IC_{50}: 125.7 nM) and OVCAR4 (IC_{50}: 161.7 nM) cells. Conversely, scFv-Tisotumab-SNAP-IR700 exhibited negligible effect on low expressed A2780, IGROV1 and Hey cell lines (Figure 35) (Table 12).

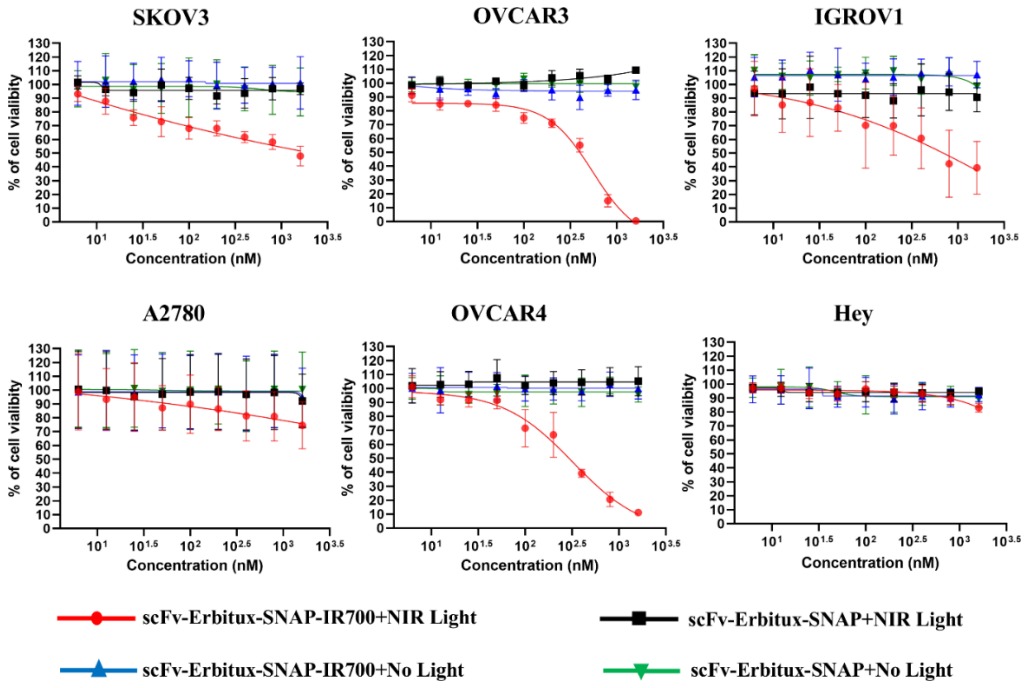

Figure 31: Evaluation of specific photocytotoxicity of scFv-Erbitux-SNAP-IR700 in OvCa cells. Cells were treated with increasing concentrations (6.25, 12.5, 25, 50, 100, 200, 400, 800 and 1600 nM) of scFv-Erbitux-SNAP-IR700 and scFv-Erbitux-SNAP with and without NIR light. Cell viability was determined by XTT Kit II after 24 h treatment. Data are shown in dose response curve from triplicates of two independent experiments with error bars (mean ± SD).

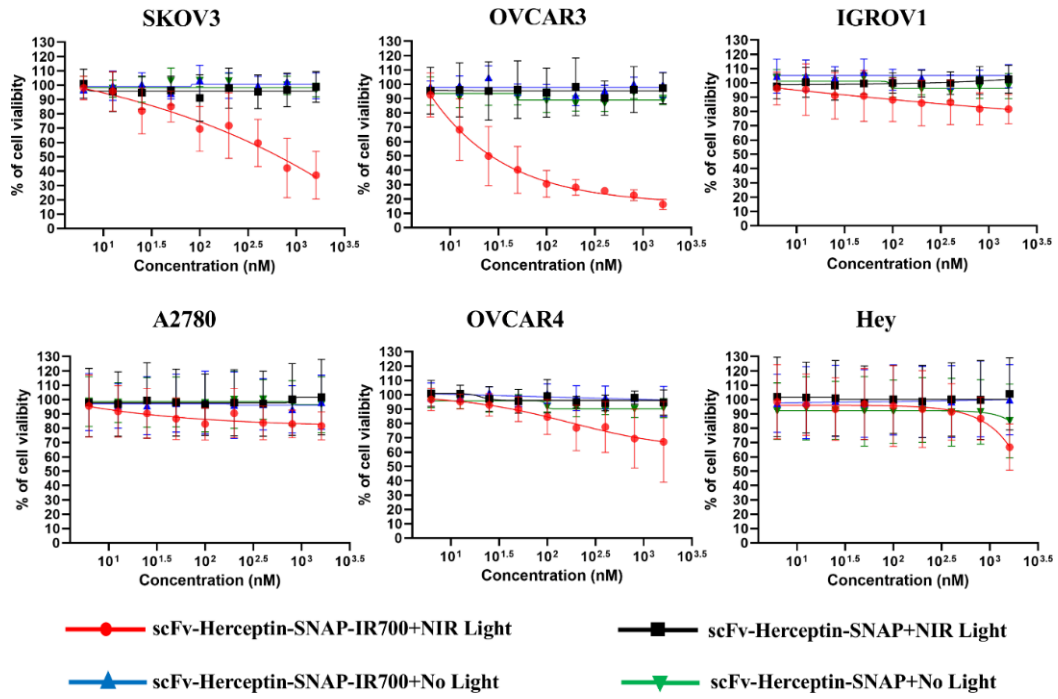

Figure 32: Evaluation of specific photocytotoxicity of scFv-Herceptin-SNAP-IR700 in OvCa cells. Cells were treated with increasing concentrations (6.25, 12.5, 25, 50, 100, 200, 400, 800 and 1600 nM) of scFv-Herceptin-SNAP-IR700 and scFv-Herceptin-SNAP with and without NIR light. Data are shown in dose response curve from triplicates of two independent experiments with error bars (mean ± SD).

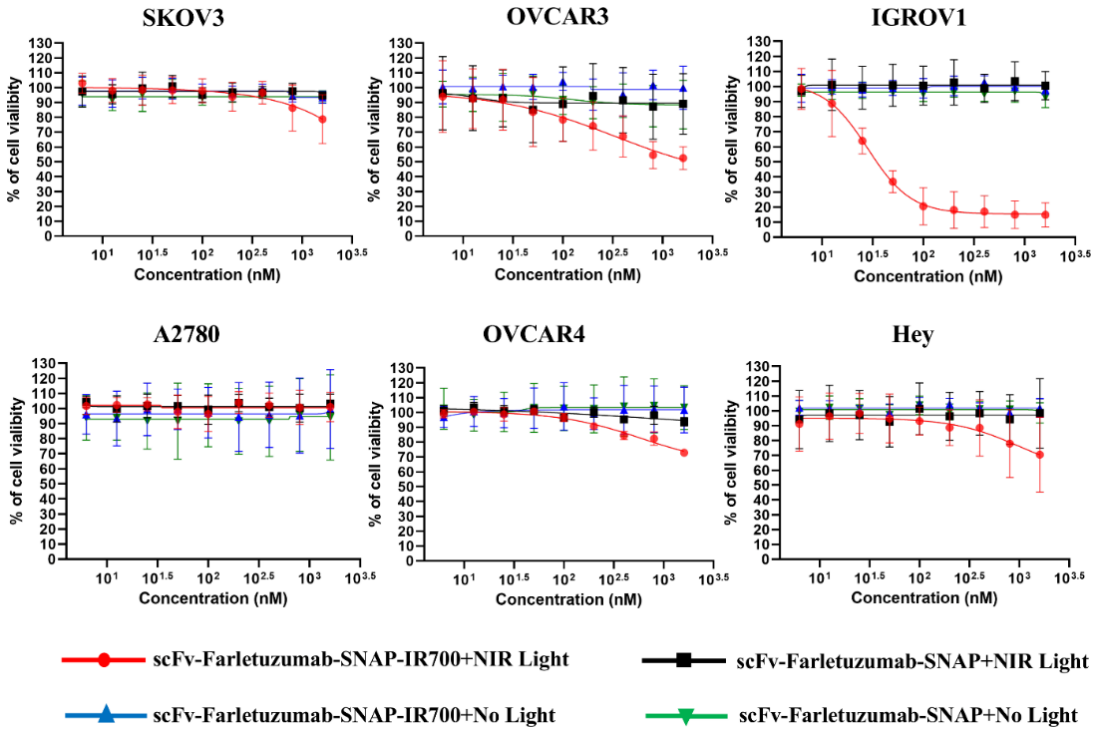

Figure 33: Evaluation of specific photocytotoxicity of scFv-Farletuzumab-SNAP-IR700 in OvCa cells. Cells were treated with increasing concentrations (6.25, 12.5, 25, 50, 100, 200, 400, 800 and 1600 nM) of scFv-Farletuzumab-SNAP-IR700 and scFv-Farletuzumab-SNAP with and without NIR light. Data are shown in dose response curve from triplicates of two independent experiments with error bars (mean ± SD).

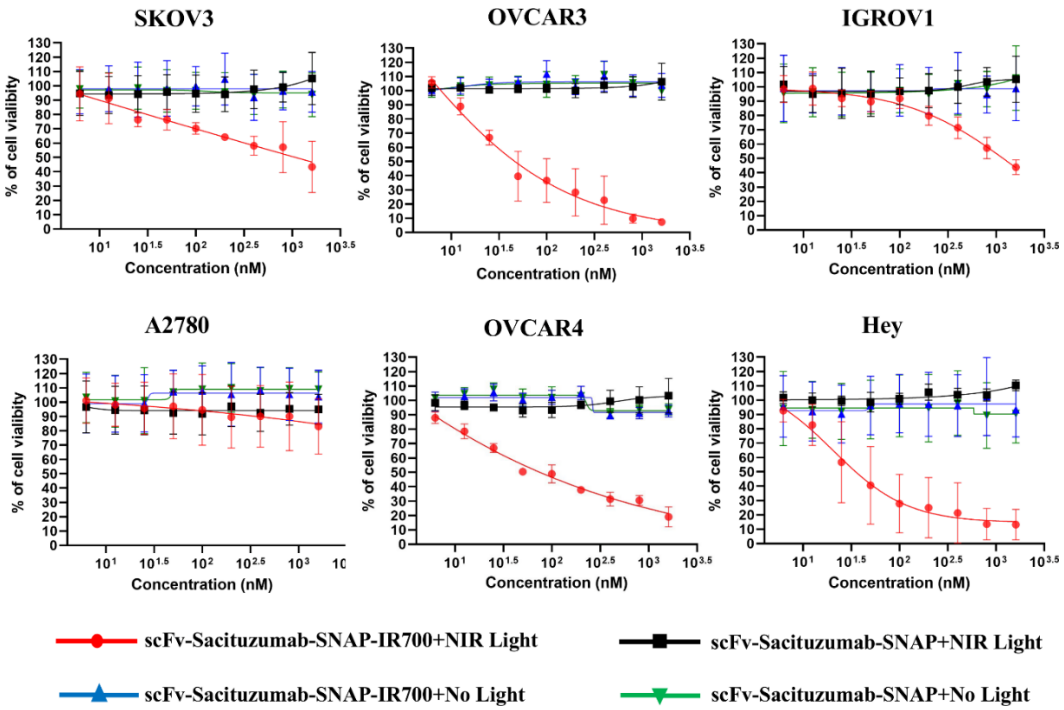

Figure 34: Evaluation of specific photocytotoxicity of scFv-Sacituzumab-SNAP-IR700 in OvCa cells. Cells were treated with increasing concentrations (6.25, 12.5, 25, 50, 100, 200, 400, 800 and 1600 nM) of scFv-Sacituzumab-SNAP-IR700 and scFv-Sacituzumab-SNAP with and without NIR light. Data are shown in dose response curve from triplicates of two independent experiments with error bars (mean ± SD).

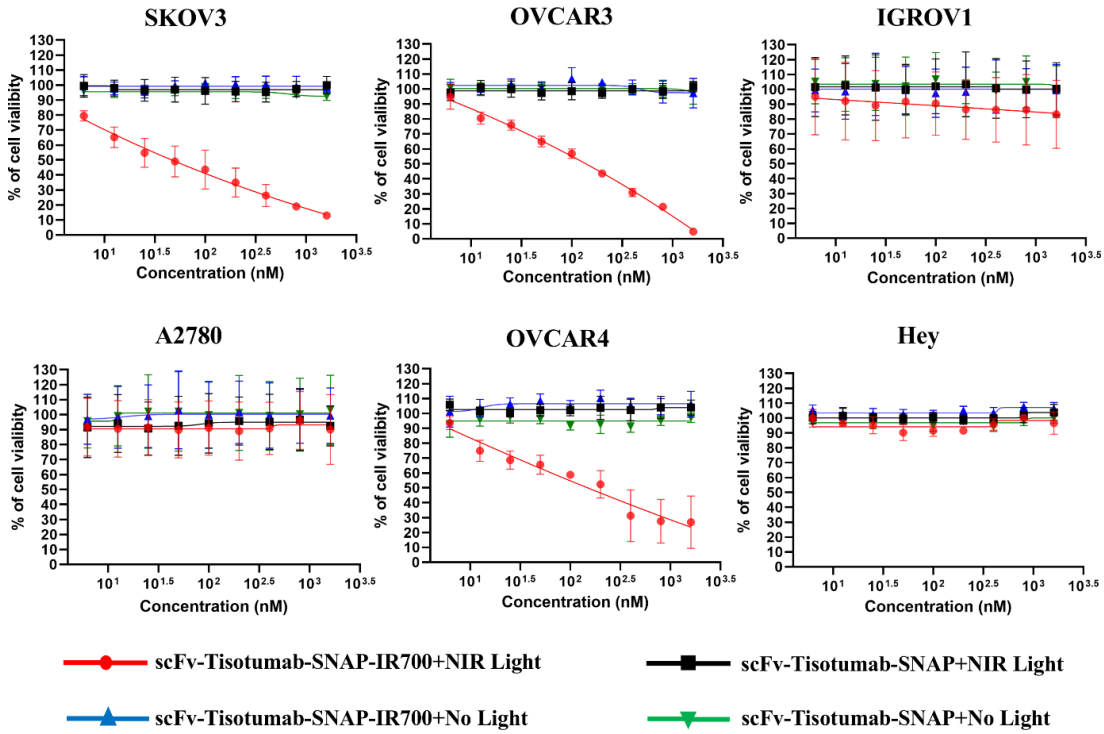

Figure 35: Evaluation of specific photocytotoxicity of scFv-Tisotumab-SNAP-IR700 in OvCa cells. Cells were treated with increasing concentrations (6.25, 12.5, 25, 50, 100, 200, 400, 800 and 1600 nM) of scFv-Tisotumab-SNAP-IR700 and scFv-Tisotumab-SNAP with and without NIR light. Data are shown in dose response curve from triplicates of two independent experiments with error bars (mean ± SD).

Table 12: IC_{50} values (nM) of NIT-PIT agents in six OvCa cell lines.

NIR-PIT agents	SKOV3	OVCAR3	IGROV1	A2780	OVCAR4	Hey
scFv-Erbitux-SNAP-IR700	1420.9±321.3	308.5±25.3	671.5±217.0	-	283.3±19.0*	-
scFv-Herceptin-SNAP-IR700	628.5±134.6	42.7±7.3*	-	-	-	-
scFv-Farletuzumab-SNAP-IR700	-	1560.0±596.6	42.3 ±4.7*	-	-	-
scFv-Sacituzumab-SNAP-IR700	956.1±263.4	59.9±7.1	-	-	96.2±7.0	45.9±8.3*
scFv-Tisotumab-SNAP-IR700	50.6±5.2*	125.7±6.3	-	-	161.7±22.4	-

*, highest cytotoxicity

3.6 Receptor mediated cell death induced by NIR-PIT agents

The photocytotoxicity mediated by NIR-PIT was further validated by Annexin assay following the protocol of Woitok *et al* (Woitok *et al* 2020). All six OvCa cell lines were treated with IR700 conjugated and unconjugated five scFv-SNAP tag fusion proteins. After 24 h of light irradiation, the percentage of cell death was measured. Negative and positive controls were set up by treating cells with PBS and zeocin, respectively. The flow cytometric dot plots depicted the living (Annexin V^-/PI^-, Q4), early apoptotic (Annexin V^+/PI^-, Q3), late apoptotic/necroptotic (Annexin V^+/PI^+, Q2) and necrotic (Annexin V^-/PI^+, Q1) cells.

The scFv-Erbitux-SNAP-IR700, scFv-Herceptin-SNAP-IR700, scFv-Sacituzumab-SNAP-IR700 and scFv-Tisotumab-SNAP-IR700 treated SKOV3 cells showed increase of cell death with ~75%, ~84%, ~80% and ~87%, respectively compared to untreated cells. In contrast, scFv-Farletuzumab-SNAP-IR700 treatment showed no or minimal increase of cell death. The unconjugated scFv-SNAP tag proteins showed no effect on this cell line. The percentage of cell death was high in zeocin treated cells (Figure 36). Similarly, all five NIR-PIT agents triggered significant level of cell death (~70-89%) in OVCAR3 cells in which scFv-Herceptin-SNAP-IR700 showed ~89% cell death (Figure 37). The scFv-Farletuzumab-SNAP-IR700 treated IGROV1 cells showed the highest toxicity (~90%) while the rest of the NIR-PIT agents (scFv-Erbitux-SNAP-IR700, scFv-Herceptin-SNAP-IR700, scFv-Tisotumab-SNAP-IR700 and scFv-Sacituzumab-SNAP-IR700) also showed cell death in IGROV1 cells (~32-67%)

(Figure 38). In contrast, the low expressed A2780 cells showed no effect after treating with scFv-Erbitux-SNAP-IR700 (~22%) and scFv-Farletuzumab-SNAP-IR700 (~16%) (Figure 39). Moreover, an increase (~92%) in cell death was observed in OVCAR4 cells post-treatment with scFv-Erbitux-SNAP-IR700. In addition, scFv-Sacituzumab-SNAP-IR700 and scFv-Tisotumab-SNAP-IR700 treated OVCAR4 cells showed ~92% and ~85% cell death, respectively (Figure 40). The cell death was increased approximately six-fold in Hey cells treated with scFv-Sacituzumab-SNAP-IR700 compared to the untreated cells. However, Hey cells treated with scFv-Erbitux-SNAP-IR700, scFv-Herceptin-SNAP-IR700, scFv-Farletuzumab-SNAP-IR700 and scFv-Tisotumab-SNAP-IR700 exhibited ~27% to ~33% cell death (Figure 41).

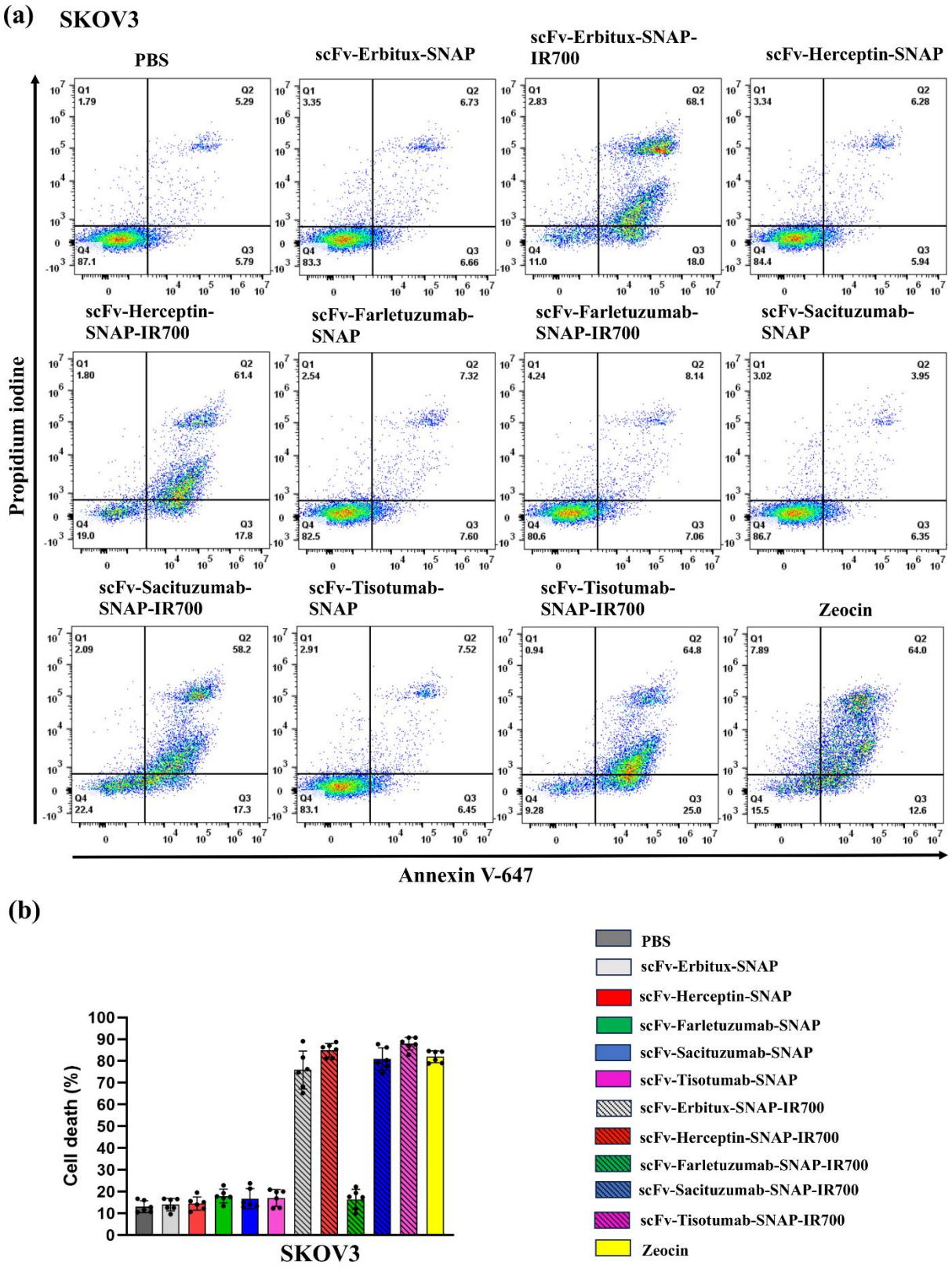

Figure 36: NIR-PIT agents induced cell death in SKOV3 cells. Cell death was measured by Annexin assay after 24 h treatment. (a) Flow cytometric data are shown in Scatter plot. (b) The cell death percentage are plotted in bar graph with mean ± SD.

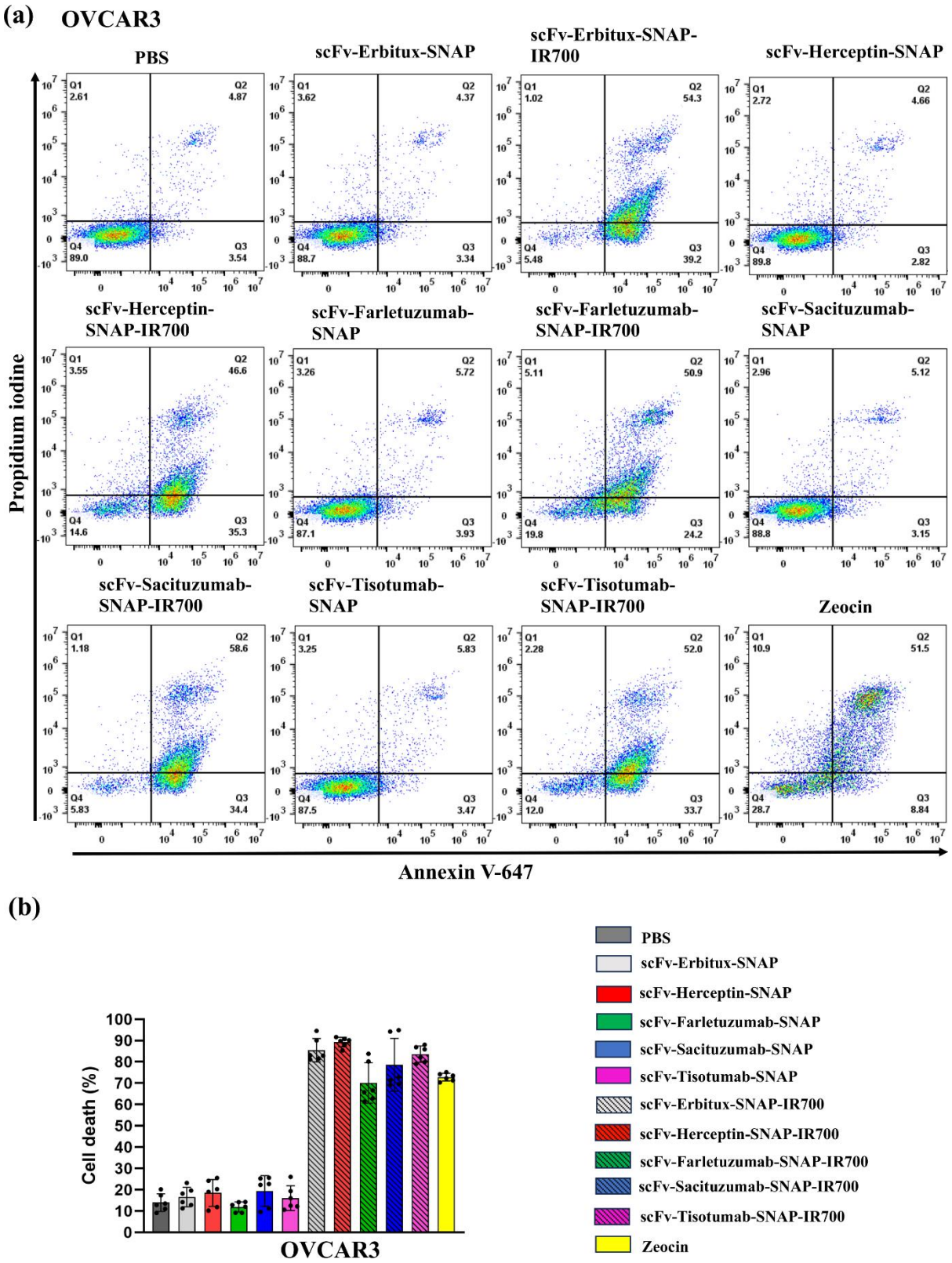

Figure 37: NIR-PIT agents induced cell death in OVCAR3 cells. Cell death was measured by Annexin assay after 24 h treatment. (a) Flow cytometric data are shown in Scatter plot. (b) The cell death percentage are plotted in bar graph with mean ± SD.

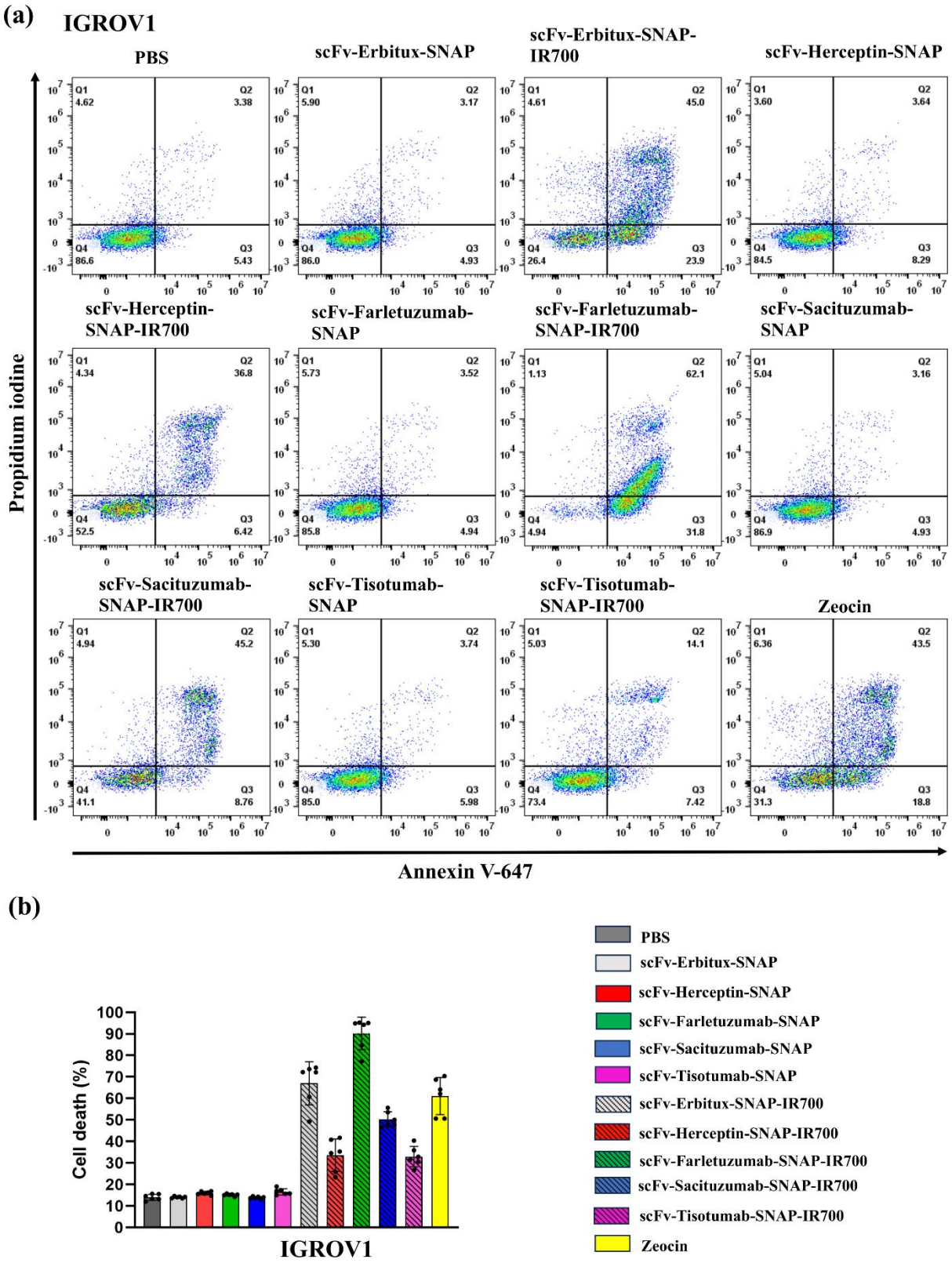

Figure 38: NIR-PIT agents induced cell death in IGROV1 cells. Cell death was measured by Annexin assay after 24 h treatment. (a) Flow cytometric data are shown in Scatter plot. (b) The cell death percentage are plotted in bar graph with mean ± SD.

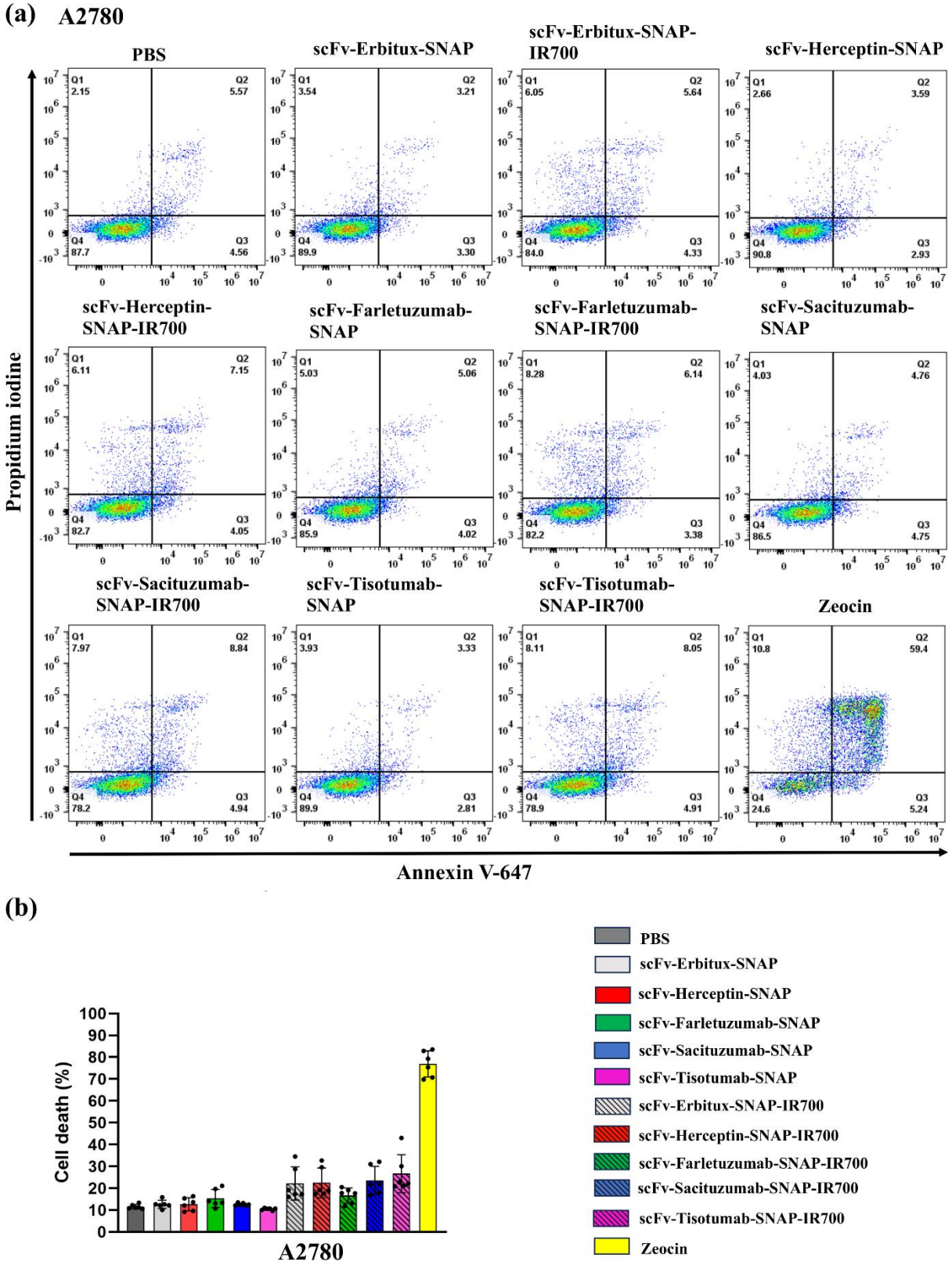

Figure 39: NIR-PIT agents induced cell death in A2780 cells. Cell death was measured by Annexin assay after 24 h treatment. (a) Flow cytometric data are shown in Scatter plot. (b) The cell death percentage are plotted in bar graph with mean ± SD.

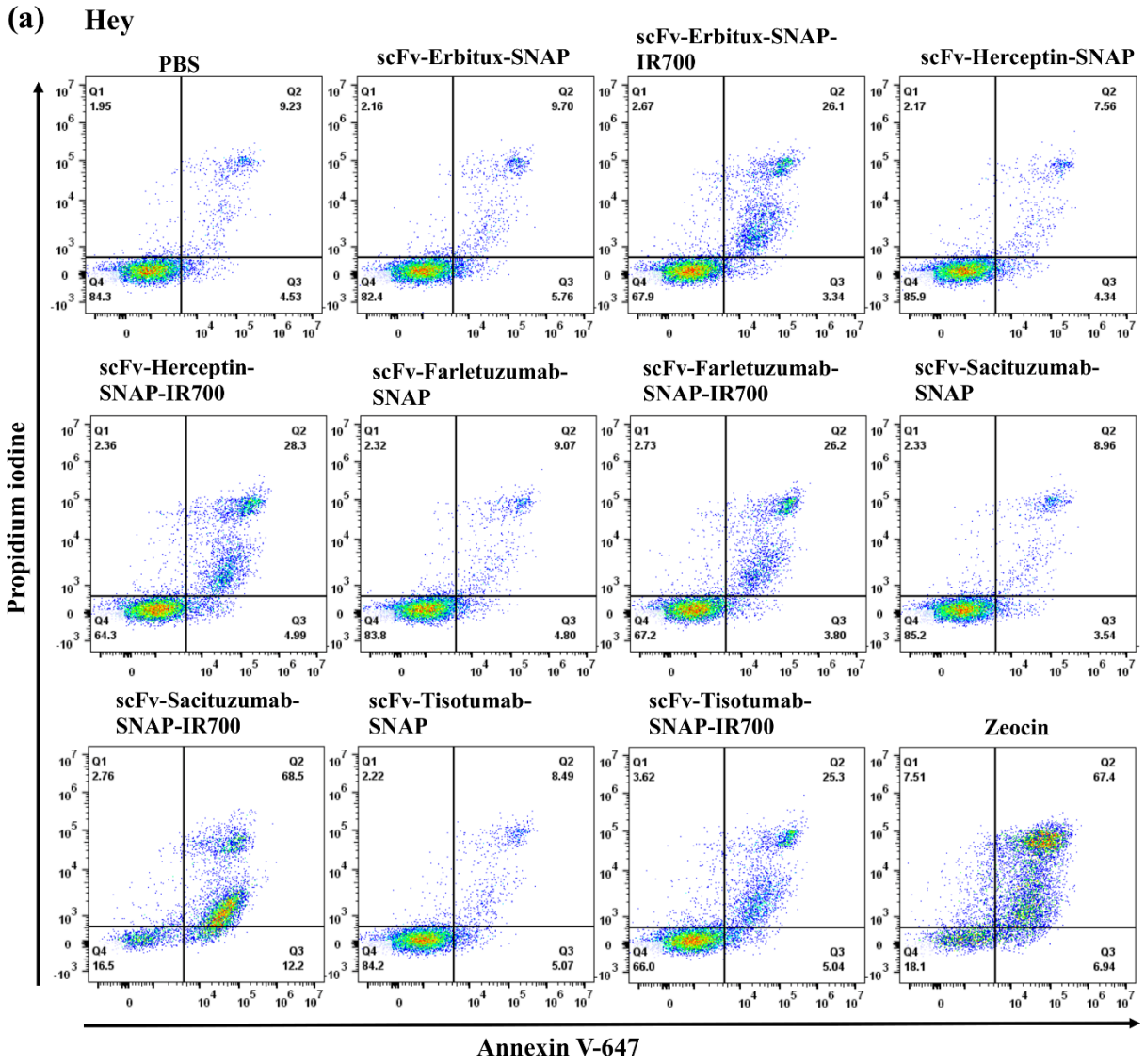

Figure 40: NIR-PIT agents induced cell death in OVCAR4 cells. Cell death was measured by Annexin assay after 24 h treatment. (a) Flow cytometric data are shown in Scatter plot. (b) The cell death percentage are plotted in bar graph with mean ± SD.

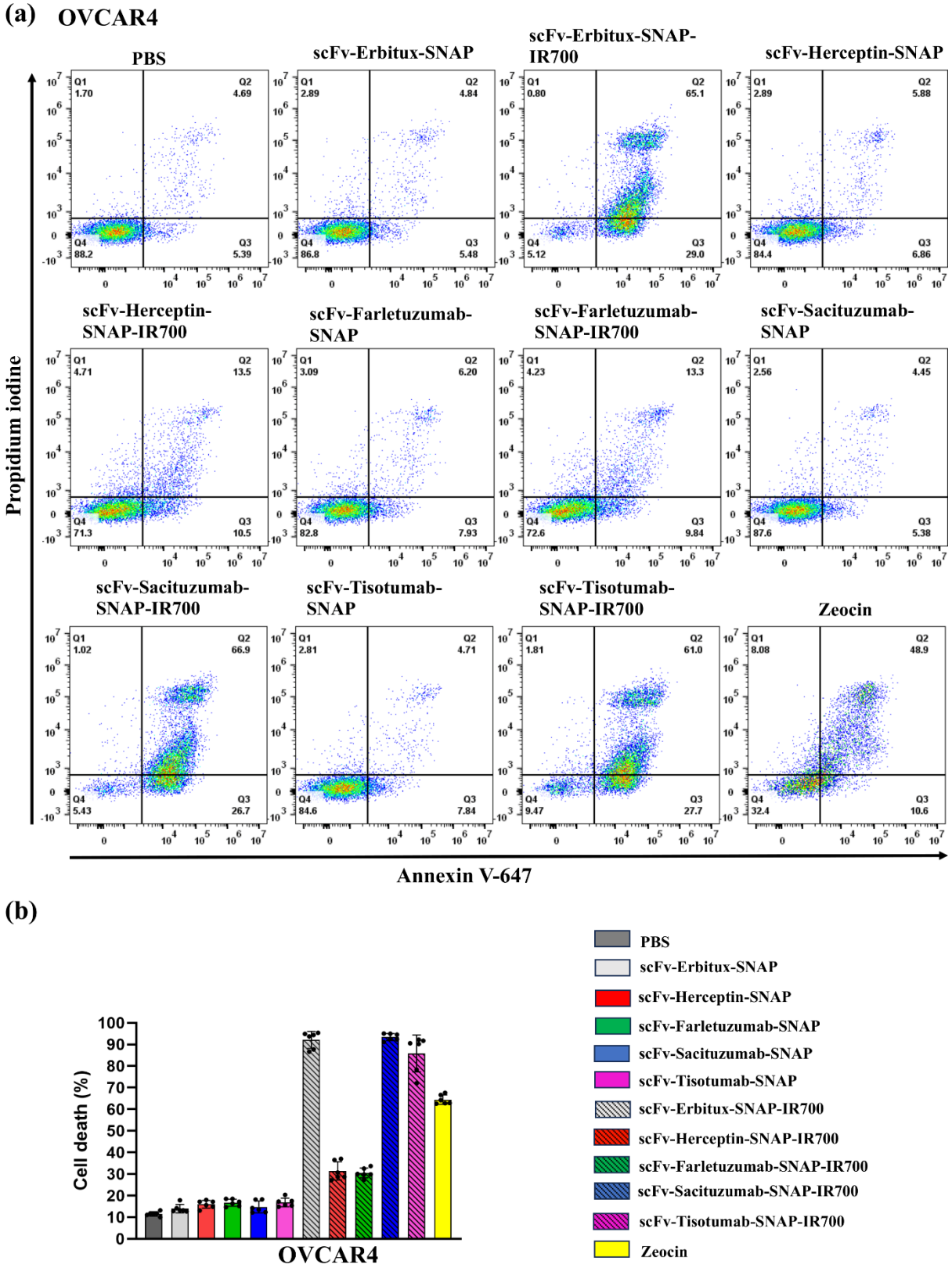

Figure 41: NIR-PIT agents induced cell death in Hey cells. Cell death was measured by Annexin assay after 24 h treatment. (a) Flow cytometric data are shown in Scatter plot. (b) The cell death percentage are plotted in bar graph with mean ± SD.

3.7 Determining the type of cell death pathway triggered by NIR-PIT

The molecular mechanism of NIR-PIT mediated cell death is still unclear. Several studies supported that the NIR-PIT rapidly induces necrotic cell death by rupturing the plasma membrane and dispersal of cellular contents (Ito *et al* 2016; Mitsunaga *et al* 2011; Nakajima *et al* 2018; Ogawa *et al* 2017; Shirasu *et al* 2014). To understand the cytotoxic mechanism of NIR-PIT, it is important to elucidate how cell death occur in NIR-PIT. Necroptotic cell death, apoptotic cell death and ferroptotic cell death are three major processes of cell death. Therefore, in this study, the cell death scavenging ability was investigated by using three different cell death inhibitors including z-VAD-FMK (apoptosis inhibitor), Necrostatin-1 (necroptosis inhibitor) and Ferrostatin-1 (ferroptosis inhibitor).

To determine the cell death pathway following NIR-PIT, XTT-based colorimetric cell proliferation assay was performed after 24 h post treatment. Cells without the cell death inhibitor were used as control. After treating OVCAR4 cells with scFv-Erbitux-SNAP-IR700, z-VAD-FMK, Necrostatin-1 and Ferrostatin-1 scavenged ~15%, ~26% and ~27% cell death, respectively (Figure 42a). In addition, ~26% cell death was scavenged after adding Ferrostatin-1 and ~18% cell death was inhibited after adding Necrostatin-1 in scFv-Herceptin-SNAP-IR700 treated OVCAR3 cells comparing to the control cells. Whereas there was 6% cell death scavenged after adding z-VAD-FMK in scFv-Herceptin-SNAP-IR700 treated OVCAR3 cells (Figure 42b). Moreover, Necrostatin-1 and Ferrostatin-1 scavenged 4% and 12%, respectively in scFv-Tisotumab-SNAP-IR700 treated SKOV3 cells (Figure 42e).

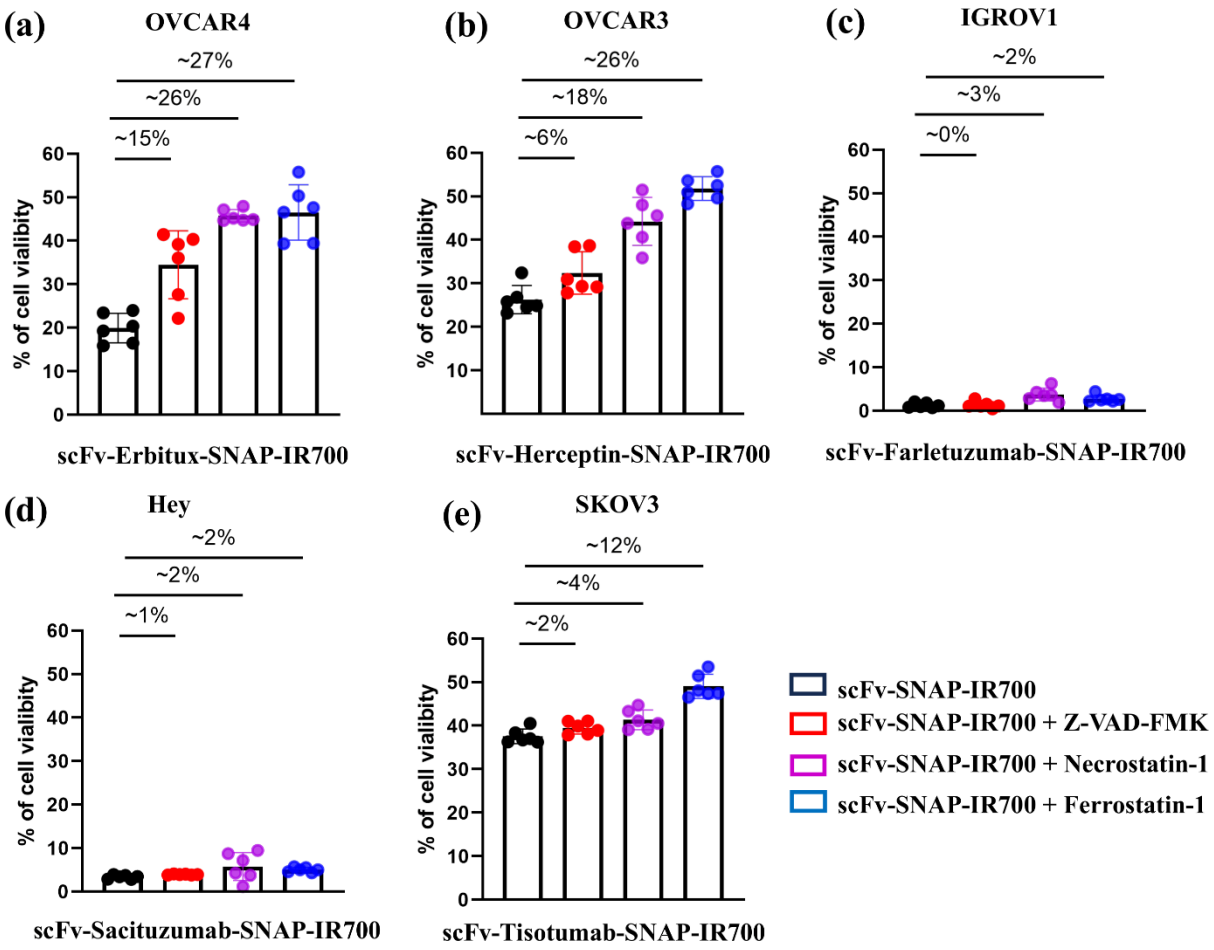

Figure 42: Determining the type of cell death pathway induced after NIR-PIT using cell death inhibitors. Cell death was measured by XTT assay after 24 h treatment. (a) OVCAR4, (b) OVCAR3, (c) IGROV1, (d) Hey and (e) SKOV3 were incubated with three different cell death inhibitors (z-VAD-FMK, Necrostatin-1 and Ferrostatin-1) followed by NIR-PIT. The cell viability is shown in bar graph with error bar (mean ± SE). The percentage of scavenging cell death are shown on the top of each bar and calculated by subtracting the percentage of cell viability of treatment with the control.

3.8 NIR-PIT triggered ICD

ICD has occurred by the exposure and release of several DAMPs that lead to the recruitment and activation of anti-cancer immune cells and the release of pro-inflammatory cytokines. Three DAMPs have been attributed a key role in the immunogenic potential of virtually all ICD inducers: calreticulin, ATP, and HMGB1 (Fucikova *et al* 2020; Keep *et al* 2014). Several studies reported that NIR-PIT induces ICD of targeted cancer cells. The relocation of ICD biomarkers such as calreticulin, HSP70, and HSP90 to the cell surface of the NIR-PIT-treated cancer cells can occur. In addition, NIR-PIT led to the release of HMGB1 and ATP that can activate adjacent immature DCs (Mączyńska *et al* 2020; Ogawa *et al* 2017).

3.8.1 Expressions of calreticulin, HSP70 and HSP 90 on the surface of dying cancer cells

Calreticulin, HSP70 and HSP90 are expressed on the plasma membrane of cells undergoing ICD and facilitates the DC maturation. In this study, HSP70, HSP90 and calreticulin were analyzed using flow cytometry after 24 h post irradiation. Irradiated cells without NIR-PIT agents were used as controls. OVCAR4 cells treated with scFv-Erbitux-SNAP-IR700 showed increased expressions of HSP70, HSP90 and calreticulin compared to the control and cells treated with scFv-Erbitux-SNAP (Figure 43). Conversely, there was no significant expression of HSP70, HSP90 and calreticulin in A2780 cells after the treatment (Figure 44). Similarly, scFv-Herceptin-SNAP-IR700 treated OVCAR3 cells expressed the elevated level of HSP70, HSP90 and calreticulin on the plasma membrane of dying cells compared to the controls (Figure 45, 46). In addition, the expressions of HSP70, HSP90 and calreticulin were upregulated in IGROV1 cells treated with scFv-Farletuzumab-SNAP-IR700 (Figure 47, 48). Moreover, scFv-Sacituzumab-SNAP-IR700 treated Hey cells showed augmentation of HSP70, HSP90 and calreticulin level HSP70 and HSP90 (Figure 49, 50). The SKOV3 cells treated with scFv-Tisotumab-SNAP-IR700 exhibited enhanced cell surface expressions of HSP70, HSP90 and calreticulin compared to the controls (Figure 51, 52).

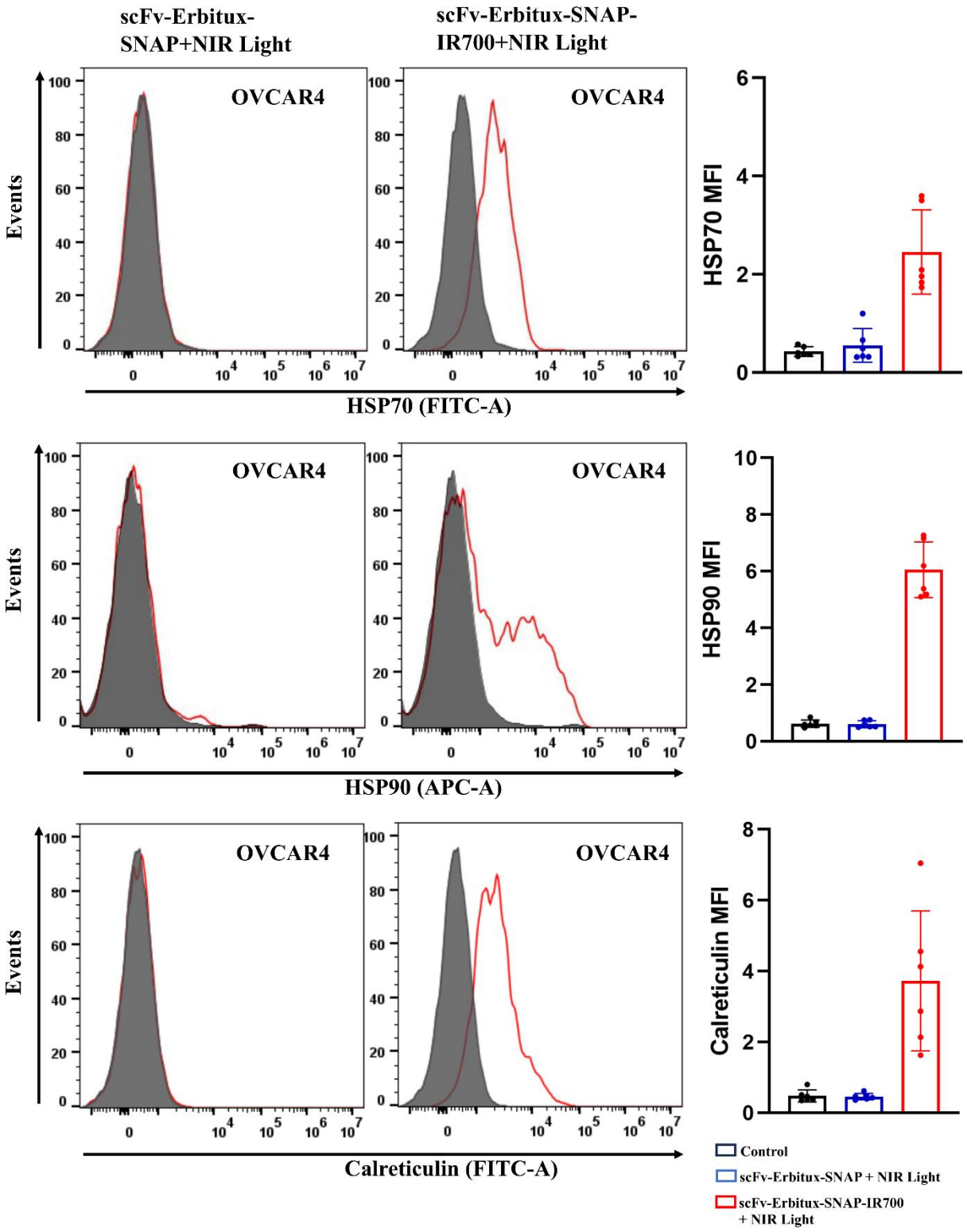

Figure 43: The scFv-Erbitux-SNAP-IR700 treatment triggers the release of ICD marker from OVCAR4. The flow cytometric histograms represent the cell surface expressions of HSP70, HSP90 and calreticulin in scFv-Erbitux-SNAP and scFv-Erbitux-SNAP-IR700 treated OVCAR4 cells. The MFI values of cell surface HSP70, HSP90 and calreticulin are shown in bar graph with error bar (mean ± SD).

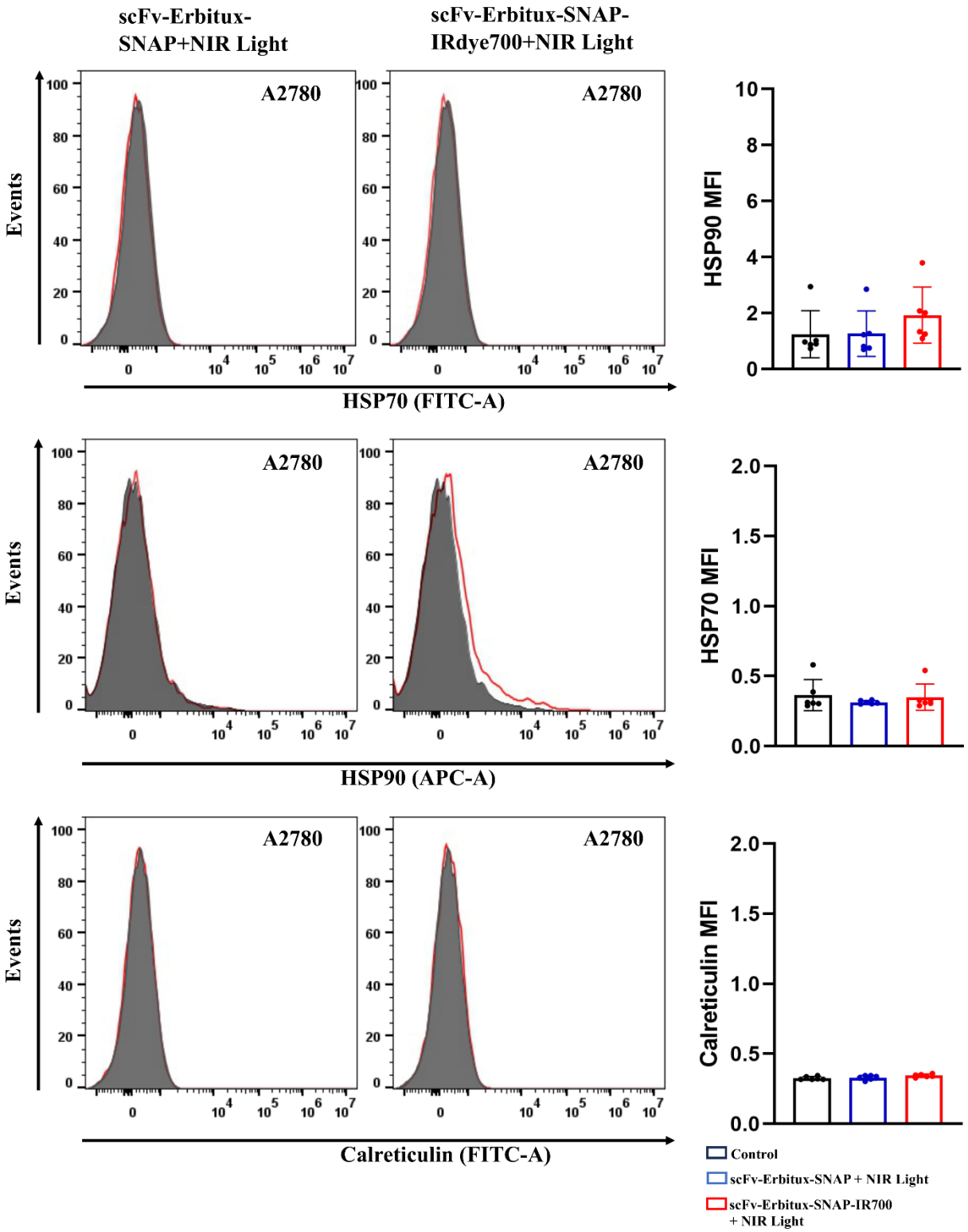

Figure 44: ICD marker analysis in A2780 cells after scFv-Erbitux-SNAP-IR700 treatment. The flow cytometric histograms represent the cell surface expressions of HSP70, HSP90 and calreticulin in scFv-Erbitux-SNAP and scFv-Erbitux-SNAP-IR700 treated A2780 cells. The MFI values of cell surface HSP70, HSP90 and calreticulin are shown in bar graph with error bar (mean ± SD).

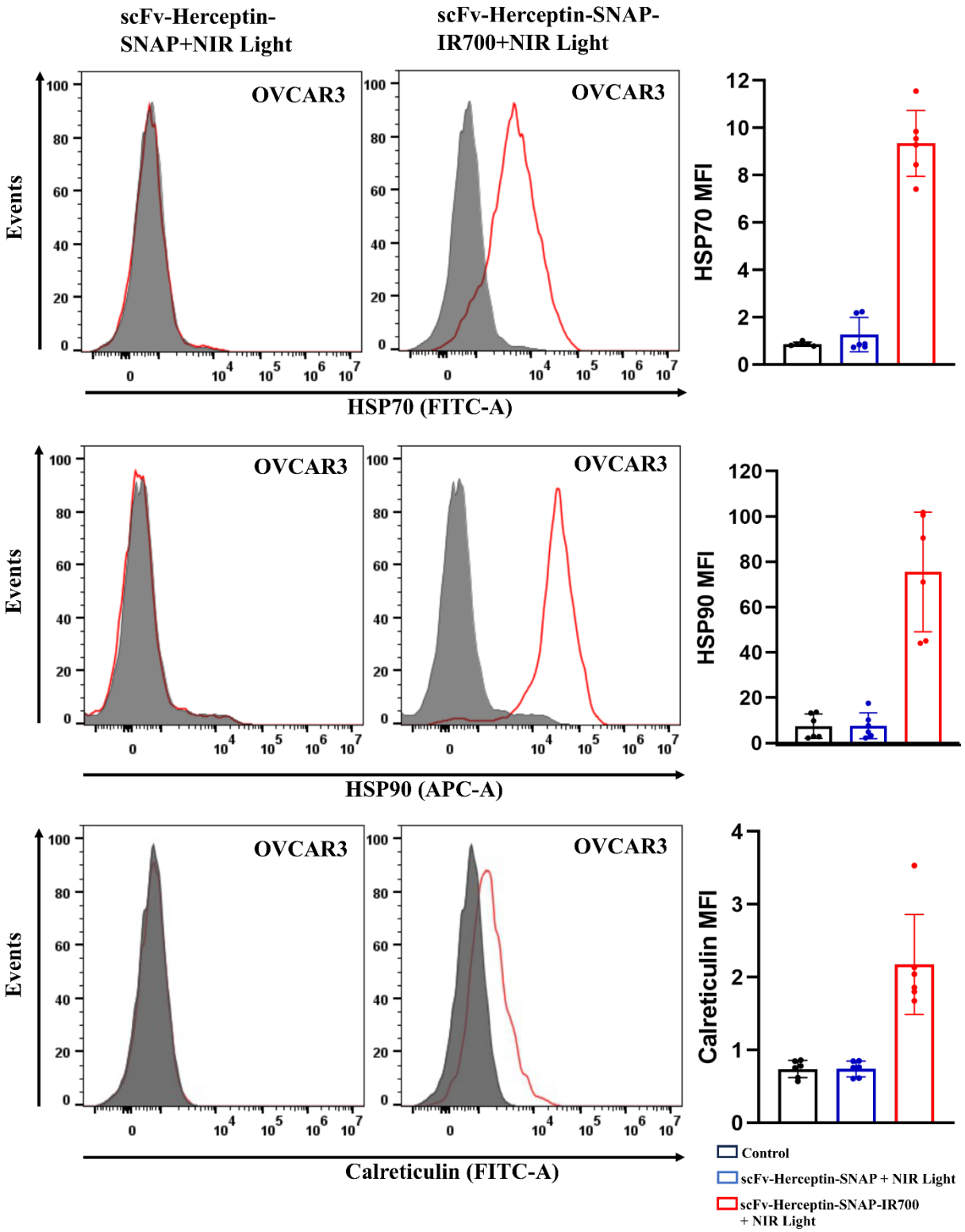

Figure 45: The scFv-Herceptin-SNAP-IR700 treatment triggers the release of ICD marker from OVCAR3 cells. The flow cytometric histograms represent the cell surface expressions of HSP70, HSP90 and calreticulin in scFv-Herceptin-SNAP and scFv-Herceptin-SNAP-IR700 treated OVCAR3 cells. The MFI values of cell surface HSP70, HSP90 and calreticulin are shown in bar graph with error bar (mean ± SD).

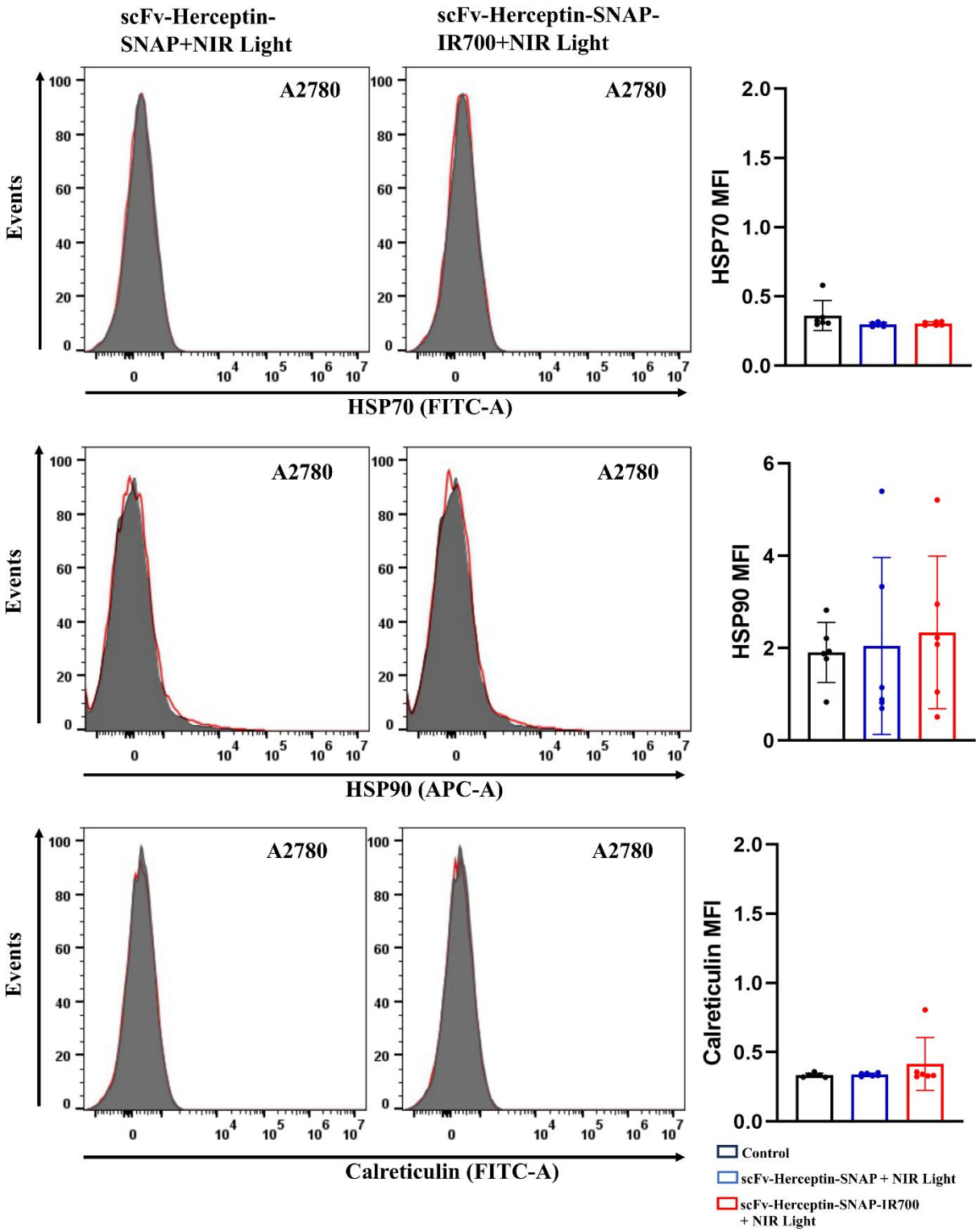

Figure 46: ICD marker analysis in A2780 cells after scFv-Herceptin-SNAP-IR700 treatment. The flow cytometric histograms represent the cell surface expressions of HSP70, HSP90 and calreticulin in scFv-Herceptin-SNAP and scFv-Herceptin-SNAP-IR700 treated A2780 cells. The MFI values of cell surface HSP70, HSP90 and calreticulin are shown in bar graph with error bar (mean ± SD).

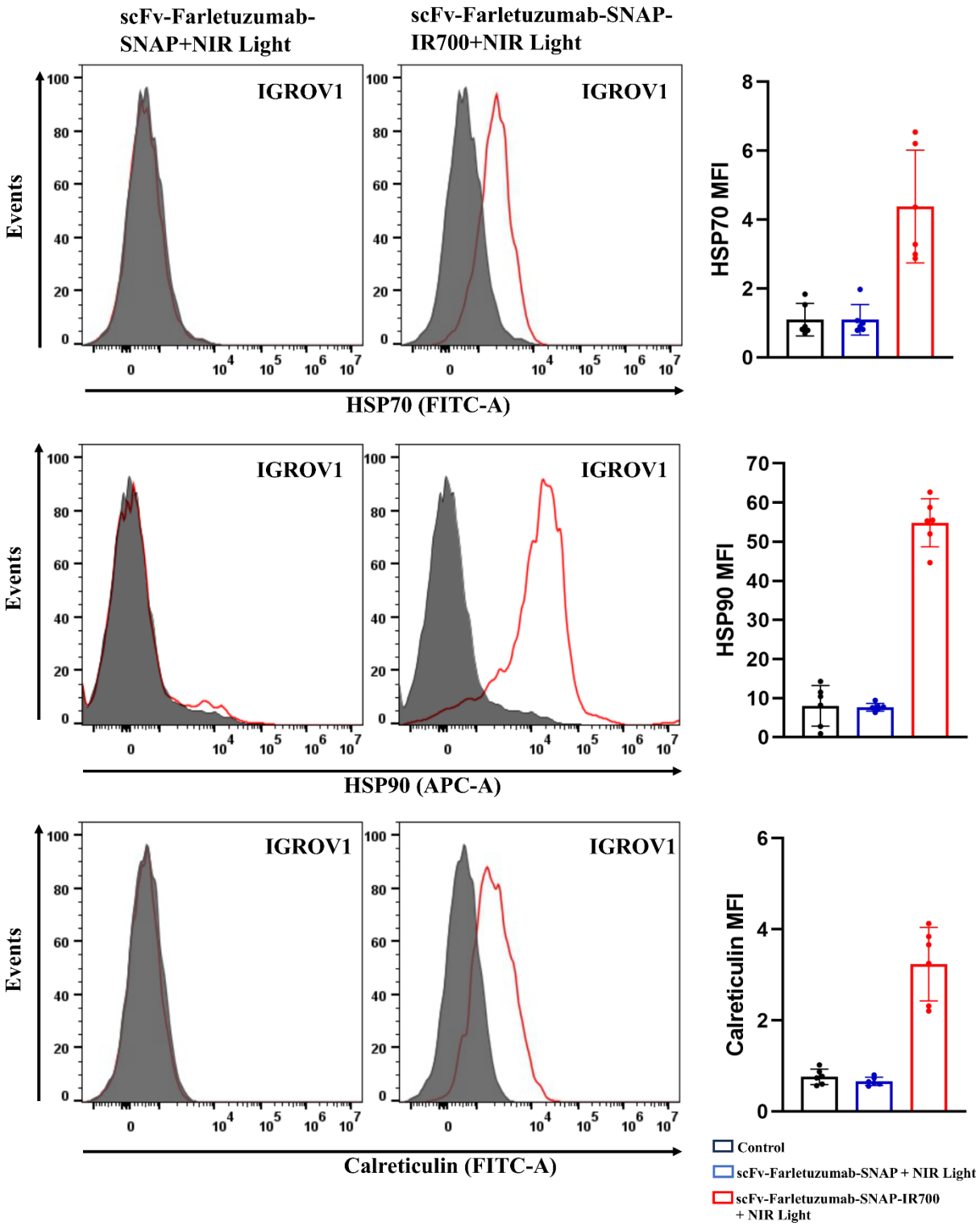

Figure 47: The scFv-Farletuzumab-SNAP-IR700 treatment triggers the release of ICD marker from IGROV1 cells. The flow cytometric histograms represent the cell surface expressions of HSP70, HSP90 and calreticulin in scFv-Farletuzumab-SNAP and scFv-Farletuzumab-SNAP-IR700 treated IGROV1 cells. The MFI values of cell surface HSP70, HSP90 and calreticulin are shown in bar graph with error bar (mean ± SD).

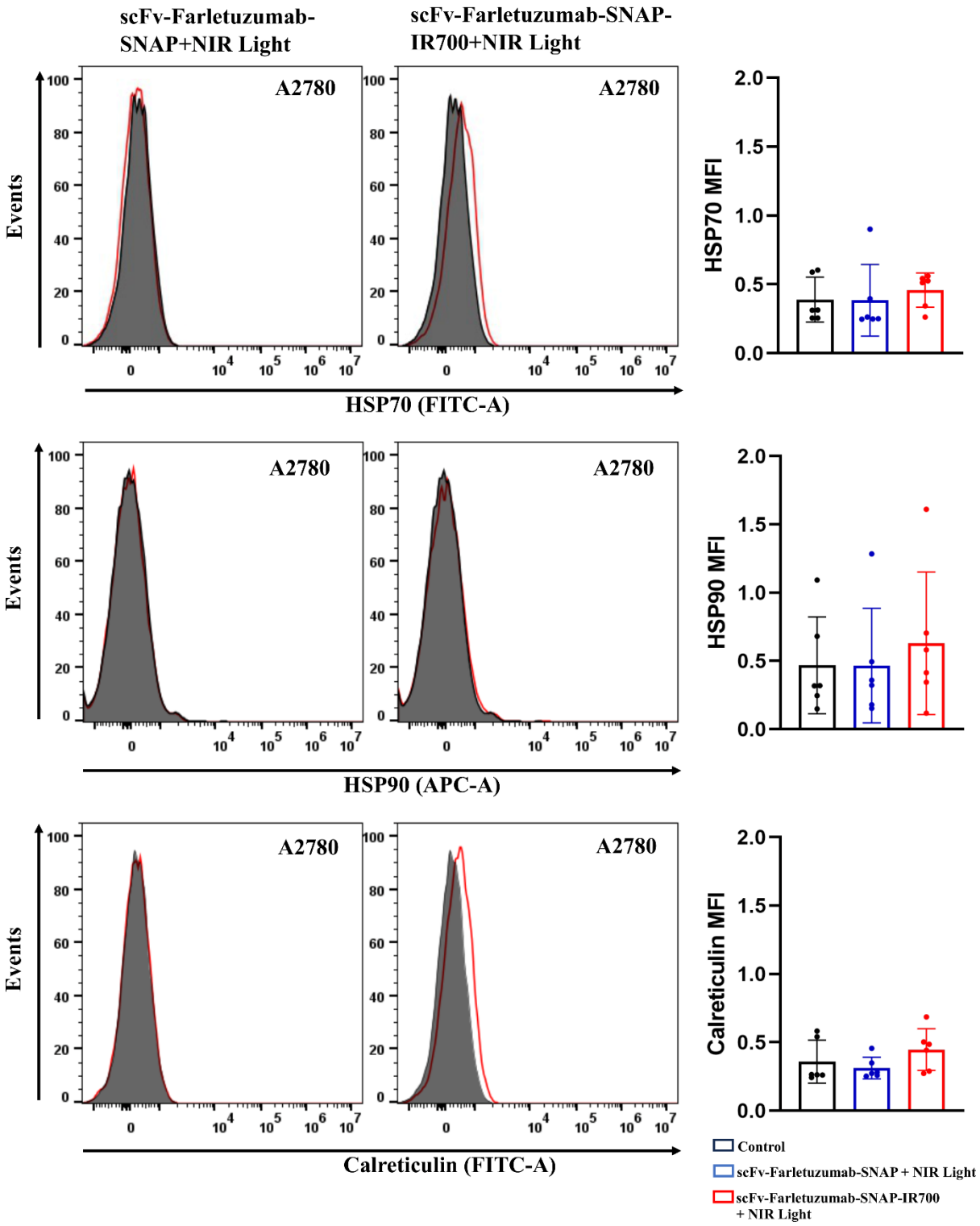

Figure 48: ICD marker analysis in A2780 cells after scFv-Farletuzumab-SNAP-IR700 treatment. The flow cytometric histograms represent the cell surface expressions of HSP70, HSP90 and calreticulin in scFv-Farletuzumab-SNAP and scFv-Farletuzumab-SNAP-IR700 treated A2780 cells. The MFI values of cell surface HSP70, HSP90 and calreticulin are shown in bar graph with error bar (mean ± SD).

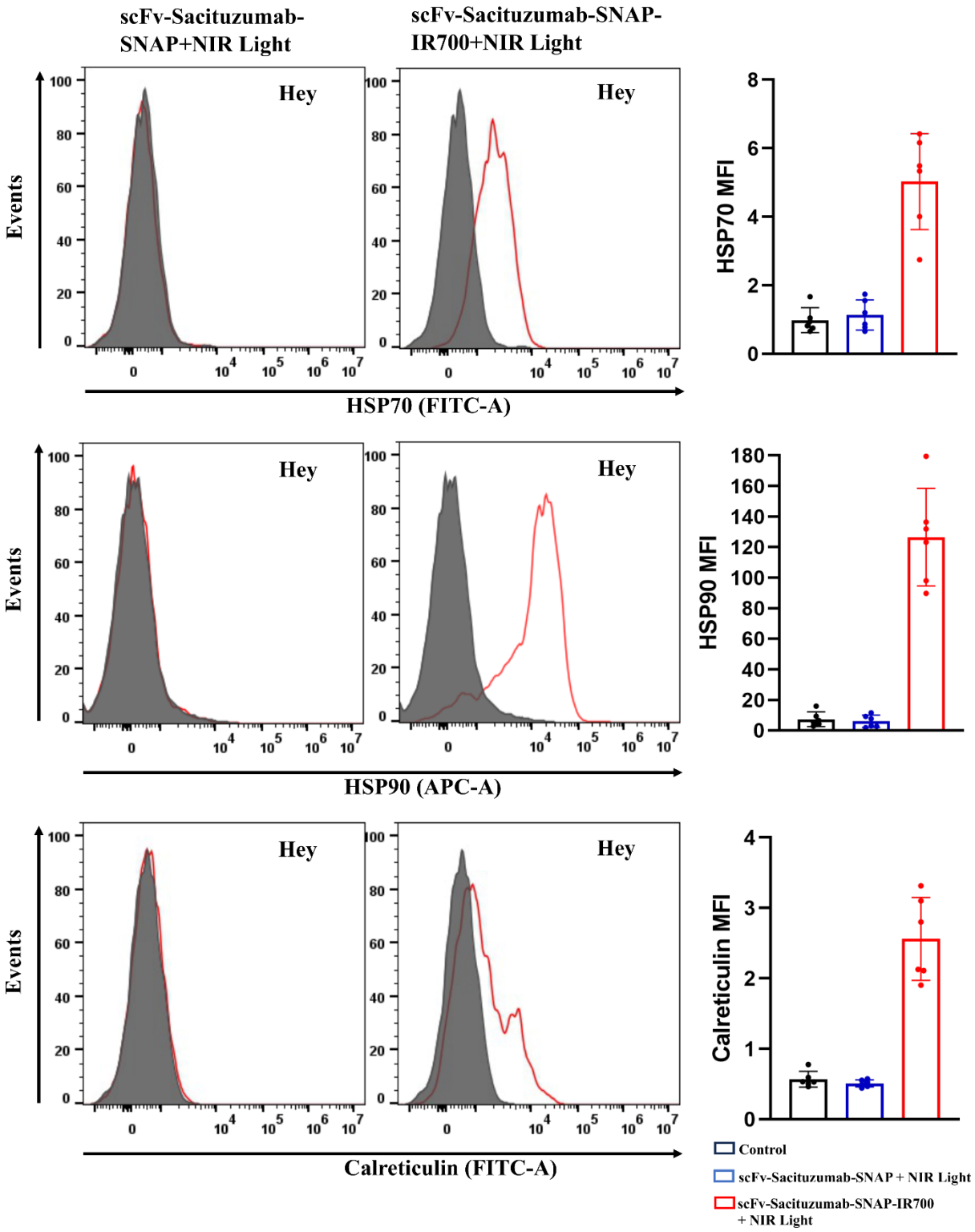

Figure 49: The scFv-Sacituzumab-SNAP-IR700 treatment triggers the release of ICD marker from Hey cells. The flow cytometric histograms represent the cell surface expressions of HSP70, HSP90 and calreticulin in scFv-Sacituzumab-SNAP and scFv-Sacituzumab-SNAP-IR700 treated Hey cells. The MFI values of cell surface HSP70, HSP90 and calreticulin are shown in bar graph with error bar (mean ± SD).

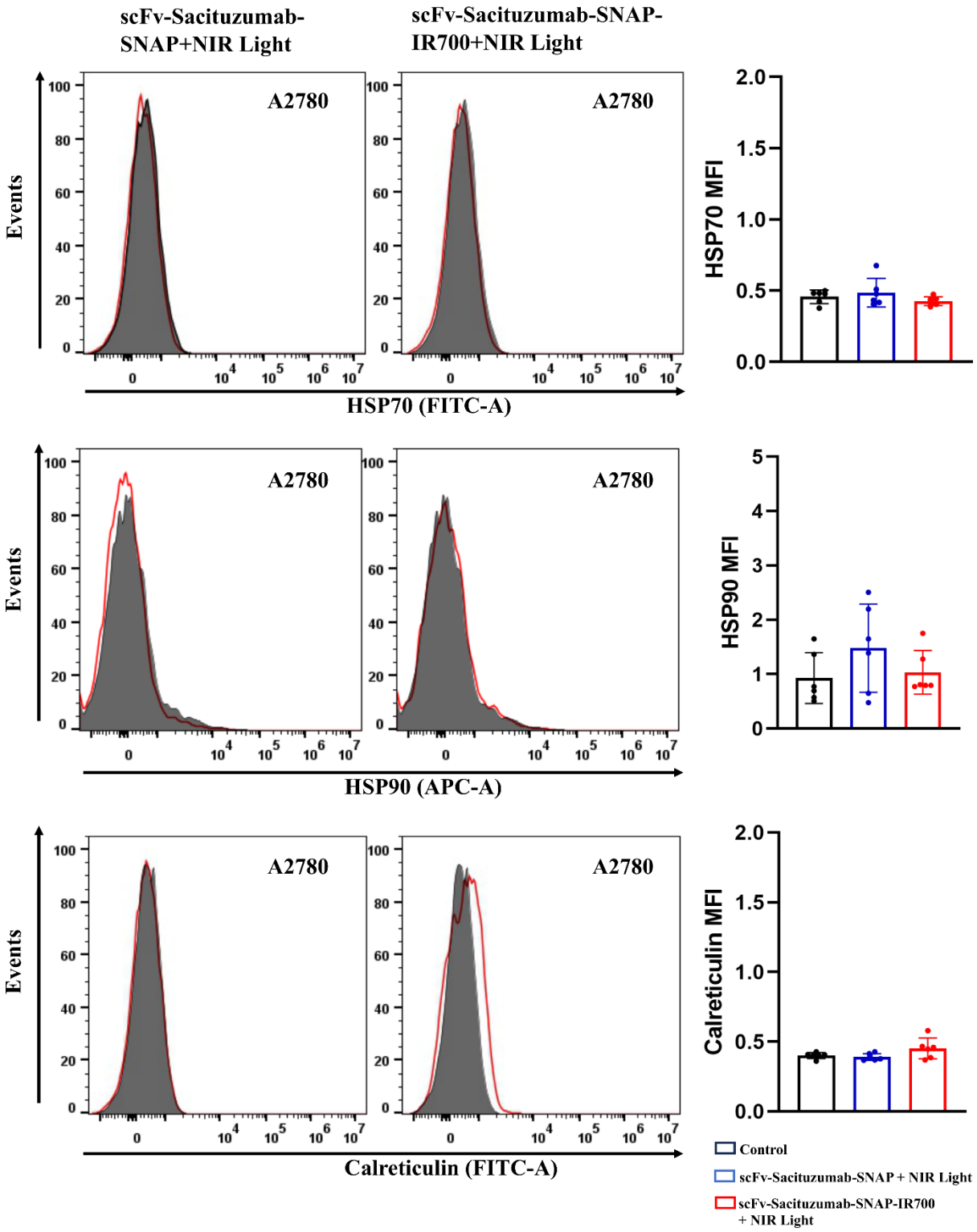

Figure 50: ICD marker analysis in A2780 cells after scFv-Sacituzumab-SNAP-IR700 treatment. The flow cytometric histograms represent the cell surface expressions of HSP70, HSP90 and calreticulin in scFv-Sacituzumab-SNAP and scFv-Sacituzumab-SNAP-IR700 treated A2780 cells. The MFI values of cell surface HSP70, HSP90 and calreticulin are shown in bar graph with error bar (mean ± SD).

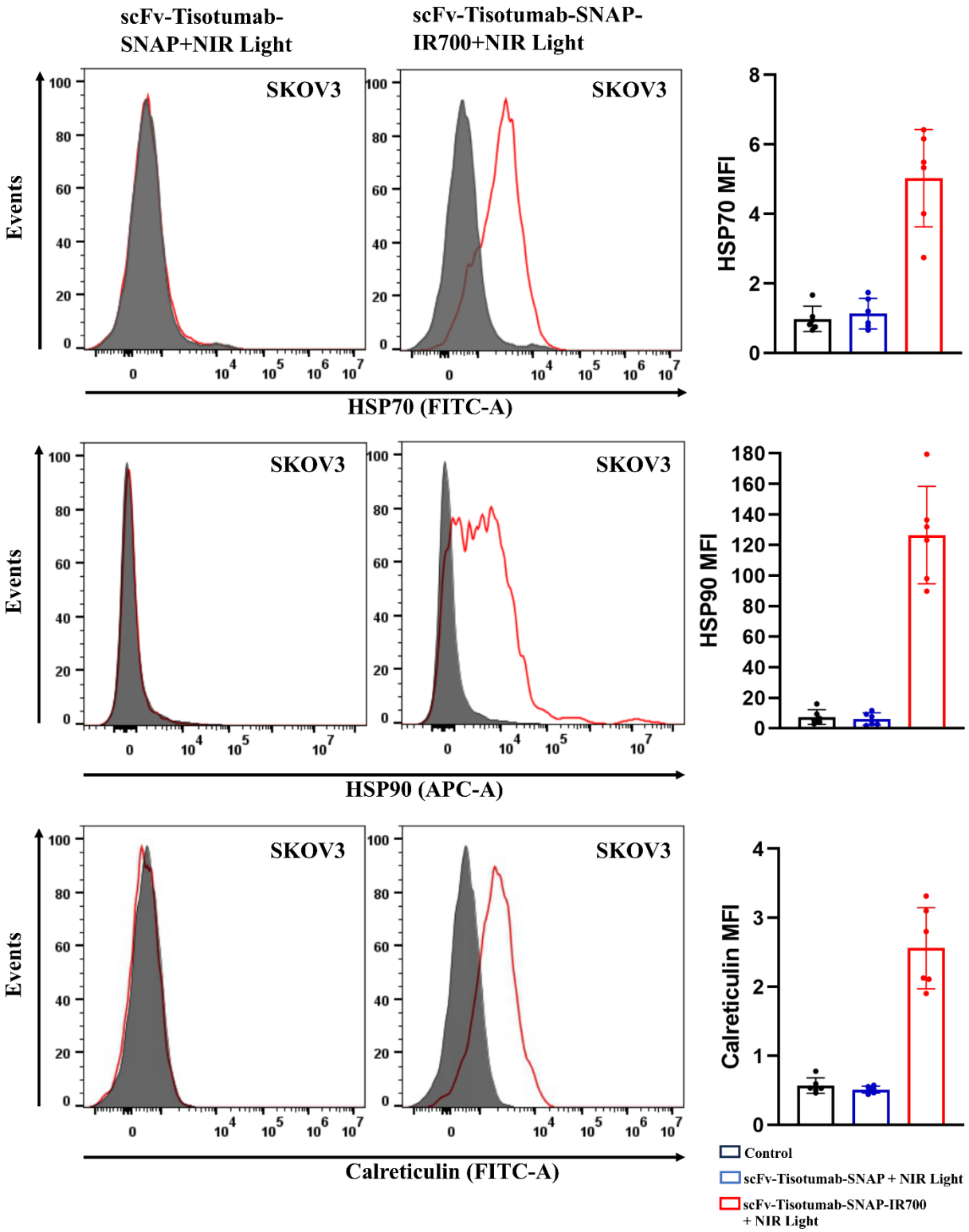

Figure 51: The scFv-Tisotumab-SNAP-IR700 treatment triggers the release of ICD marker from SKOV3 cells. The flow cytometric histograms represent the cell surface expressions of HSP70, HSP90 and calreticulin in scFv-Tisotumab-SNAP and scFv-Tisotumab-SNAP-IR700 treated SKOV3 cells. The MFI values of cell surface HSP70, HSP90 and calreticulin are shown in bar graph with error bar (mean ± SD).

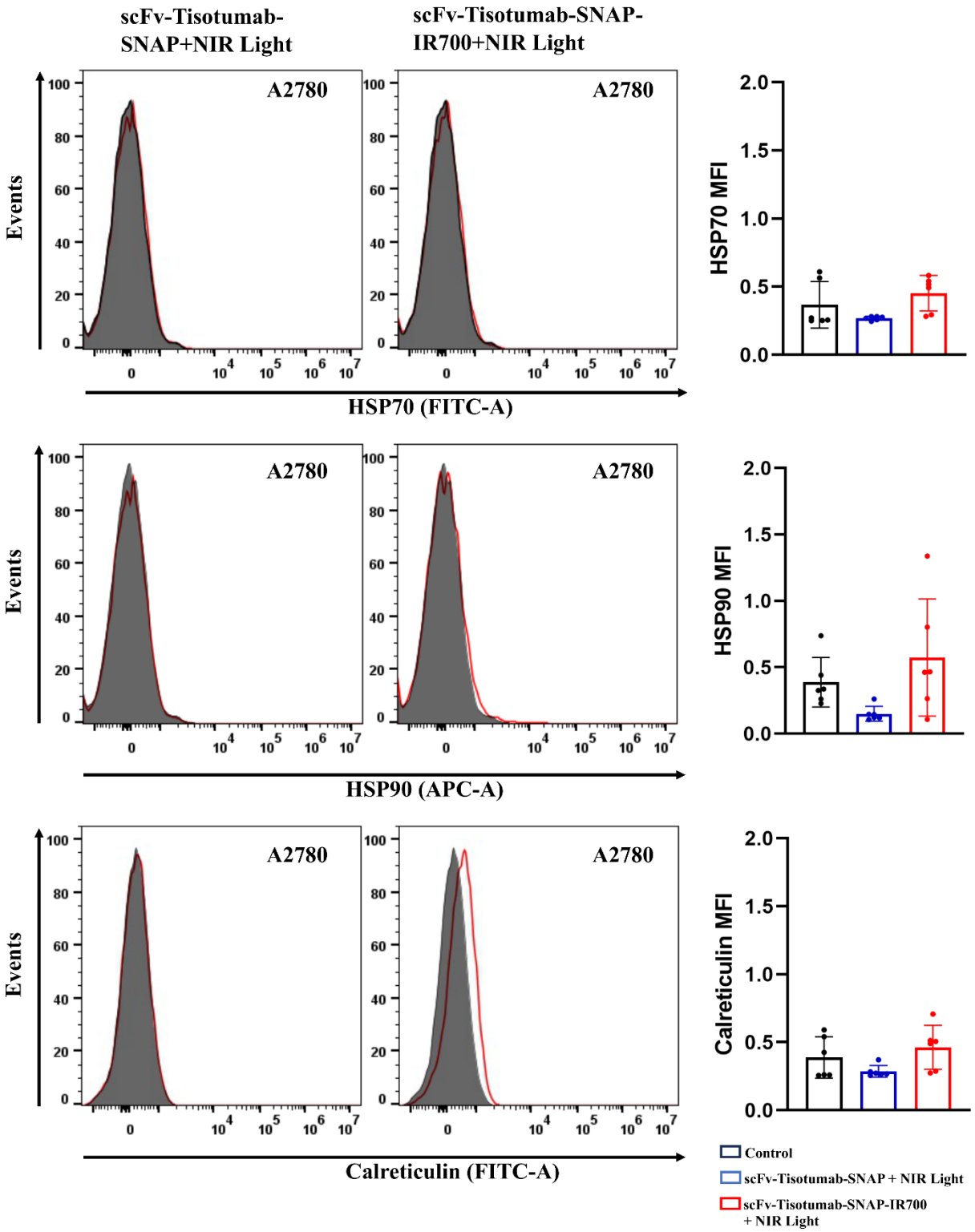

Figure 52: ICD marker analysis in A2780 cells after scFv-Tisotumab-SNAP-IR700 treatment. The flow cytometric histograms represent the cell surface expressions of calreticulin, HSP70, and HSP90 in scFv-Tisotumab-SNAP and scFv-Tisotumab-SNAP-IR700 treated A2780 cells. The MFI values of cell surface HSP70, HSP90 and calreticulin are shown in bar graph with error bar (mean ± SD).

3.8.2 Extracellular release of ATP and HMGB1 from dying cancer cells

During ICD, ATP-containing vesicles release ATP through the active exocytosis via pannexin channels that act as a “find-me” signal for DC precursors. This extracellular ATP binds to the purinergic receptor P2Y2 (P2RY2, a metabotropic receptor), promoting the recruitment of myeloid cells, mediating the secretion of pro-inflammatory molecule, thus culminating the activation of $CD8^+$ T cells (Elliott *et al* 2009; Fucikova *et al* 2020; Ghiringhelli *et al* 2009; Martins *et al* 2014). ICD of cancer cells also releases HMGB1 through translocation of the HMGB1 from the nucleus to the cytoplasm which is then released into the extracellular space. This HMGB1 can bind to the multiple pattern recognition receptors (PRRs) expressed by myeloid cells (Apetoh *et al* 2007; Fucikova *et al* 2020; Yang *et al* 2015).

The extracellular level of ATP and HMGB1 in the culture supernatants of treated OvCa cells were evaluated using ATP luminescence assay and HMGB1 ELISA assay, respectively. The extracellular level of ATP and HMGB1 released into the medium from OVCAR4 and A2780 cells were measured after treating with scFv-Erbitux-SNAP and scFv-Erbitux-SNAP-IR700. After 24 h of light exposure, the amount of ATP (~21 nmol) and HMGB1 (~23 ng/mL) were higher in scFv-Erbitux-SNAP-IR700 treated OVCAR4 cells compared to the controls. In contrast, there was no difference of ATP and HMGB1 level in A2780 cells after both treatments (Figure 53). Similarly, ~297 pmol extracellular ATP and ~18 ng/mL HMGB1 were released in scFv-Herceptin-SNAP-IR700 treated OVCAR3 cells (Figure 54). In addition, IGROV1 cells treated with scFv-Farletuzumab-SNAP-IR700 showed increases of ATP (~122 pmol) and HMGB1 (~47 ng/mL) amounts compared to the untreated cells (Figure 55). The extracellular ATP (~74 pmol) and HMGB1 (~14 ng/mL) levels in Hey cells were higher after scFv-Sacituzumab-SNAP-IR700 treatment whereas the A2780 cells showed no effect after the treatment (Figure 56). Finally, scFv-Tisotumab-SNAP-IR700 treated SKOV3 cells released ~910 pmol of ATP and ~21 ng/mL of HMGB1 (Figure 57).

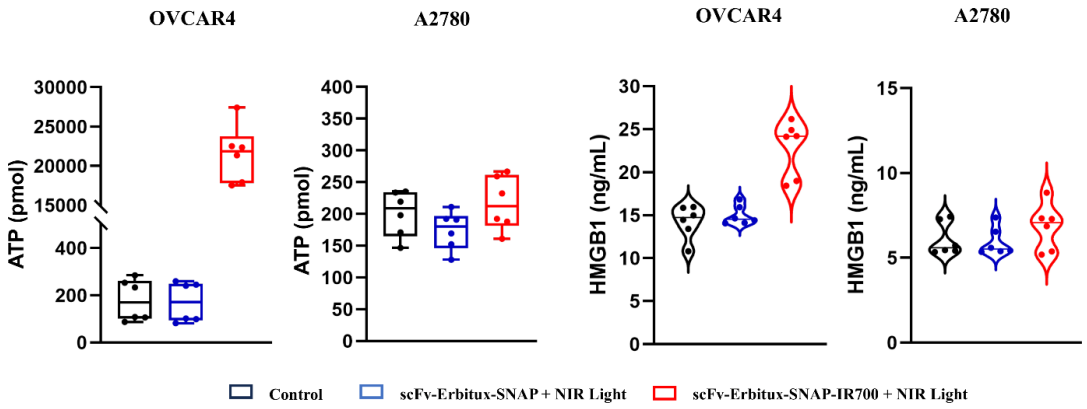

Figure 53: NIR-PIT induces rapid release of ATP and HMGB1 from scFv-Erbitux-SNAP-IR700 treated OVCAR4 and A2780 cells. After 24 h NIR-light irradiation, extracellular ATP was measured by ATP luminescence assay and extracellular HMGB1 was measured by ELISA assay. Data are presented from OVCAR4 and A2780 cells treated with NIR light, scFv-Erbitux-SNAP+NIR-light and scFv-Erbitux-SNAP-IR700+NIR-light in box plot (ATP release) and violin plot (HMGB1 release) as mean ± SD.

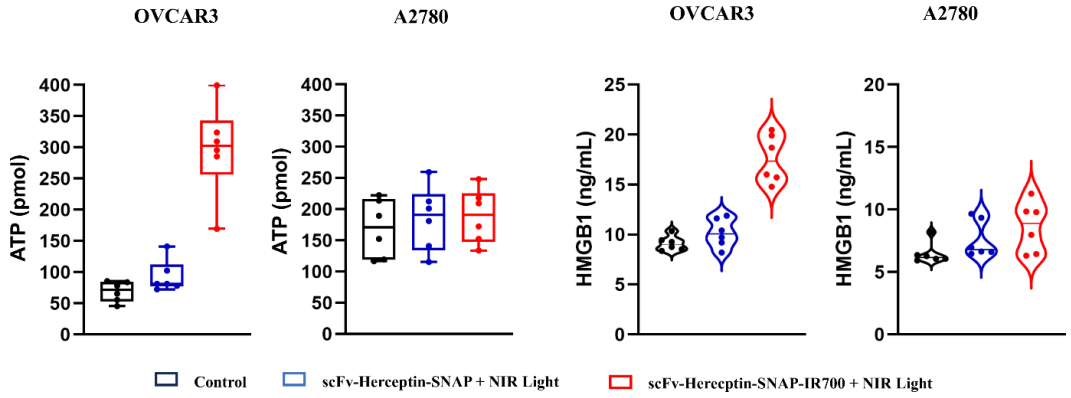

Figure 54: NIR-PIT induces rapid release of ATP and HMGB1 from scFv-Herceptin-SNAP-IR700 treated OVCAR3 and A2780 cells. Data are presented from OVCAR3 and A2780 cells in box plot (ATP release) and violin plot (HMGB1 release) as mean ± SD.

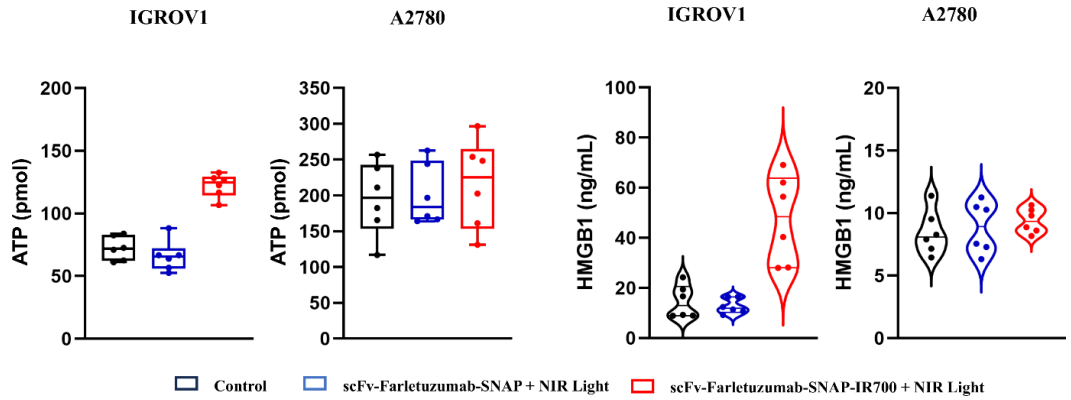

Figure 55: NIR-PIT induces rapid release of ATP and HMGB1 from scFv-Farletuzumab-SNAP-IR700 treated IGROV1 and A2780 cells. Data are presented from IGROV1 and A2780 cells in box plot (ATP release) and violin plot (HMGB1 release) as mean ± SD.

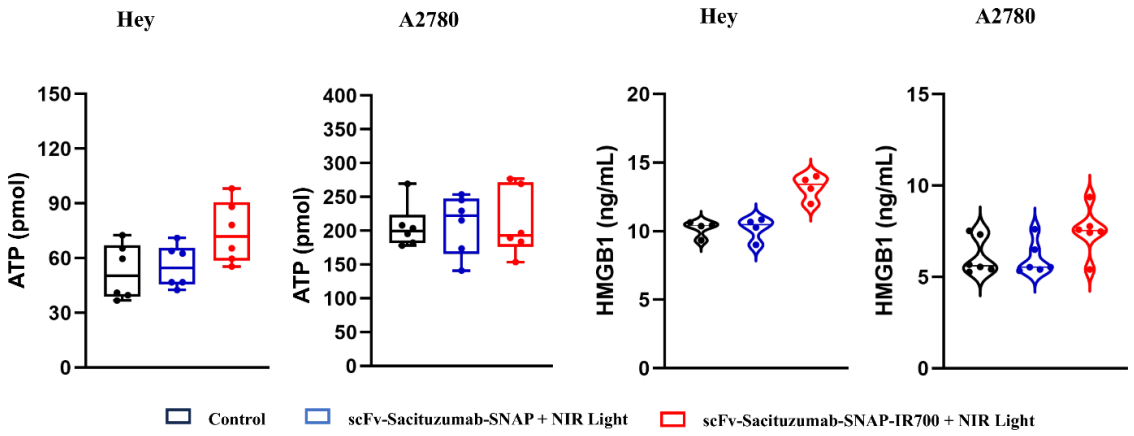

Figure 56: NIR-PIT induces rapid release of ATP and HMGB1 from scFv-Sacituzumab-SNAP-IR700 treated Hey and A2780 cells. Data are presented from Hey and A2780 cells in box plot (ATP release) and violin plot (HMGB1 release) as mean ± SD.

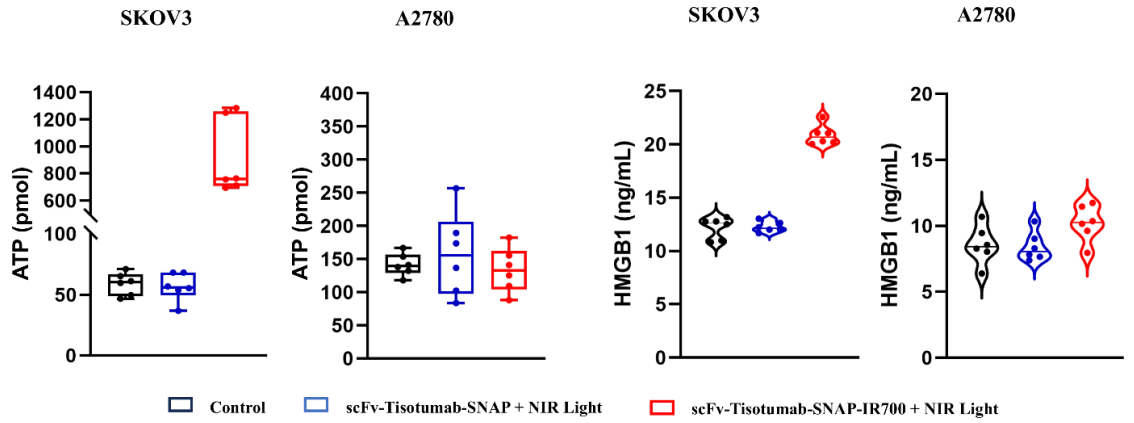

Figure 57: NIR-PIT induces a rapid release of ATP and HMGB1 from scFv-Tisotumab-SNAP-IR700 treated SKOV3 and A2780 cells. Data are presented from SKOV3 and A2780 cells in box plot (ATP release) and violin plot (HMGB1 release) as mean ± SD.

3.9 Maturation of DCs triggered by NIR-PIT-killed tumor cells

DCs have special antigen-presenting function and play an essential role in both innate and adaptive immune responses (Del Prete *et al* 2023). The maturation of DCs by uptaking antigens, processing them, and presenting the antigenic peptides on surface of MHC molecules is an essential process for initiating antigen-specific adaptive immunity (Cabeza-Cabrerizo *et al* 2021). A series of DAMPs released by the anticancer treatments through ICD can initiate the maturation of iDCs by upregulating costimulatory molecules including CD80, CD86, CD40 and HLADR (Lamberti *et al* 2020; Ogawa *et al* 2017).

The ability of the NIR-PIT approach to induce DC maturation *in vitro* was investigated by analyzing the expressions of DC maturation markers CD80, CD86, CD40 and HLADR. To conduct this experiment, $CD14^+$ monocytes were isolated from PBMC. Such isolation of

$CD14^+$ cells was confirmed by flow cytometry analysis (Figure S3). Then these $CD14^+$ monocytes undergo differentiate to iDCs in the presence of IL-4 and GM-CSF. The differentiation of iDCs was further confirmed by flow cytometric analysis of iDCs marker (CD209). To analyze the expressions of DC maturation markers CD80, CD86, CD40 and HLADR, iDCs were co-cultured with scFv-Tisotumab-SNAP-IR700 irradiated SKOV3 cells for 48 h. Flow cytometry analysis revealed that the expressions of CD80 and CD86 were enhanced on the DCs co-cultured with scFv-Tisotumab-SNAP-IR700 treated SKOV3 cells compared to the controls. In addition, the expressions of CD40 and HLADR were increased on the surface of DCs stimulated by scFv-Tisotumab-SNAP-IR700 treated SKOV3 cells or LPS (positive control) (Figure S4) compared to DCs co-cultured with scFv-Tisotumab-SNAP treated SKOV3 cells (Figure 58). Similarly, the DCs maturation was examined after 48 h co-culturing iDCs with scFv-Erbitux-SNAP-IR700 irradiated OVCAR4 cells to validate that the investigated NIR-PIT agents can trigger DCs maturation. The scFv-Erbitux-SNAP-IR700 irradiated OVCAR4 cells slightly increased the expressions of CD80 and CD86 on the surface of DCs whereas the expressions of CD40 and HLADR were upregulated in comparison to scFv-Erbitux-SNAP-irradiated OVCAR4 cells (Figure 59).

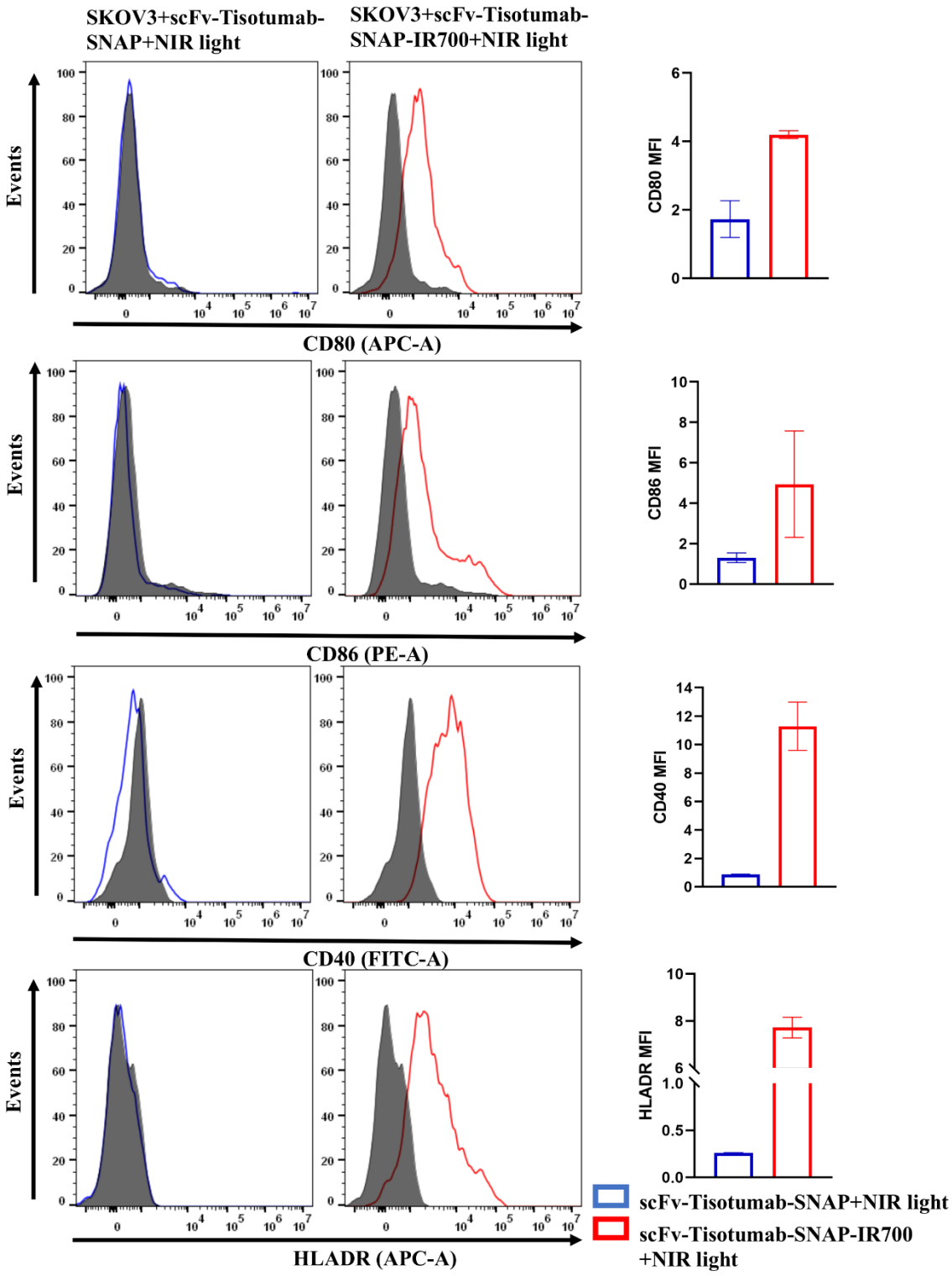

Figure 58: Co-culturing scFv-Tisotumab-SNAP-IR700 treated SKOV3 cells with iDCs promotes DCs maturation. Immature DCs were cultured with scFv-Tisotumab-SNAP-IR700 treated SKOV3 cells or cultured with scFv-Tisotumab-SNAP treated SKOV3 cells. After 48 h, the expressions of CD80, CD86, CD40 and HLADR on DCs were analyzed by flow cytometry. The gray curves represent iDCs without co-culture, the blue curves depict iDCs with scFv-Tisotumab-SNAP treated SKOV3 cells and the red curves indicate iDCs with scFv-Tisotumab-SNAP-IR700 treated SKOV3 cells. The MFI values of CD80, CD86, HLADR, and CD40 expressions on DCs are shown in bar graphs with error bar as mean ± SD.

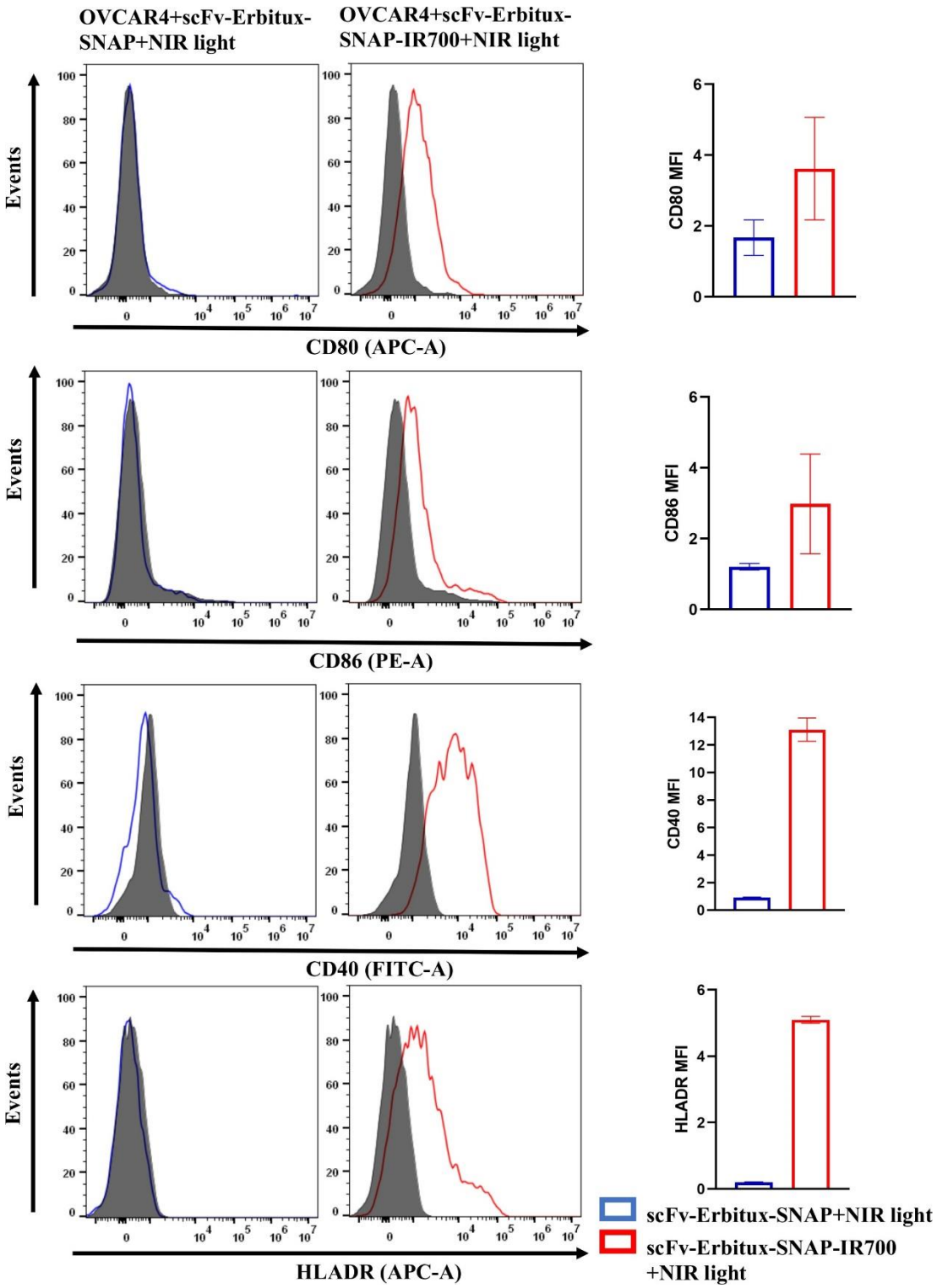

Figure 59: Co-culturing scFv-Erbitux-SNAP-IR700 treated OVCAR4 cells with iDCs promotes DCs maturation. Immature DCs were cultured with scFv-Erbitux-SNAP-IR700 treated OVCAR4 cells or cultured with scFv-Erbitux-SNAP treated OVCAR4 cells. After 48 h, the expressions of CD80, CD86, CD40 and HLADR on DCs were analyzed by flow cytometry. The gray curves represent iDCs without co-culture, the blue curves depict iDCs with scFv-Erbitux-SNAP treated OVCAR4 cells and the red curves indicate iDCs with scFv-Erbitux-SNAP-IR700 treated OVCAR4 cells. The MFI values of CD80, CD86, HLADR, and CD40 expressions on DCs are shown in bar graphs with error bar as mean ± SD.

4 Discussion

To date, only few studies are available describing the application of NIR-PIT for ovarian cancer treatment. Data presented in this study focused on developing NIT-PIT agents, using scFv-SNAP tag proteins, conjugating with IR700 photosensitizer, targeting OvCa cells expressing EGFR, Her2, FOLR1, TROP2 and TF antigens. This is the first report evaluating the potential therapeutic effects of FOLR1, TROP2 and TF targeted NIT-PIT in case of ovarian cancer treatment. The results generated in this study represent the development of NIR-PIT agents to selectively kill the OvCa cells and induce ICD, which will generate anticancer immunity to eliminate the residual OvCa cells.

4.1 The scFv-SNAP tag fusion proteins generated functional NIR-PIT agents

In particular, NIR-PIT agents are generated by conjugating mAb with IR700 through direct conjugation methods by binding amino group to NHS ester of IR700 (Akai *et al* 2024; Fukushima *et al* 2024; Inagaki *et al* 2023; Inagaki *et al* 2024; Mitsunaga *et al* 2011; Taki *et al* 2021). Antibody derivatives such as Fab, scFv, diabody, minibody, and affibody molecules are also used to generate NIR-PIT agents (Bauerschlag *et al* 2017; Mączyńska *et al* 2020; Sato *et al* 2016; Sioud *et al* 2021). In this study, scFv was introduced instead of full-length antibody to generate NIR-PIT agents. It was expected that scFv would retain the same binding specificity as full-length antibody, which was previously reported (Amoury *et al* 2016; Bauerschlag *et al* 2017; von Felbert *et al* 2016). Despite using direct conjugation, the SNAP tag technology can generate 1:1 antibody ratio which is important to get robust pharmacokinetic, efficacy and safety profile (Amoury *et al* 2016; Bauerschlag *et al* 2017; von Felbert *et al* 2016; Hussain *et al* 2019).

In this study, five scFv-SNAP tag fusion proteins were successfully expressed in HEK293T cells demonstrated rapid expression of proteins with relatively high yield. The expression vector contains an EGFP gene and bleomycin resistance gene that allow monitoring and selection of transfected cells. All scFv-SNAP tag fusion proteins retained self-labeling activity with the SNAP-tag substrate. Rapid conjugation with different BG-derivatives such as SNAP-Surface® Alexa Fluor® 647 or BG-IR700 was observed within 2 h. The site-specific conjugation was confirmed by blocking SNAP-fusion proteins through post-incubating with SNAP-Surface® Alexa Fluor® 488 (Figure 21). The SDS gel visualization showed that the conjugation site was blocked by BG-IR700. SNAP-Surface® Alexa Fluor® 488 was unable to bind with the scFv-SNAP-fusion proteins, ensuring the SNAP tag activity of the proteins. These

results suggest that the SNAP-tag technology allows the production of homogeneous NIR-PIT agents in a simple and rapid one-step conjugation reaction.

4.2 Expression of EGFR, Her2, FOLR1, TROP2 and TF on OvCa cells

After substantial literature survey, EGFR, Her2, FOLR1, TROP2 and TF were selected as potential cancer antigen targets for OvCa. EGFR is overexpressed in OvCa cells and plays crucial role in tumor growth, invasion, and metastasis. Immunobiological staining of EGFR in epithelial OvCa patients indicates that high expression of EGFR correlates with aggressive clinical features (Brustmann 2008; Normanno *et al* 2006; Wang *et al* 2016). EGFR is overexpressed in SKOV3, OVCAR3, IGROV1, OVCAR4 and Hey cells, whereas low expression was observed in A2780 cells (Figure 22). In line with these results, several studies reported that EGFR is expressed in SKOV3, Hey (Dickerson *et al* 2010), OVCAR4 (Parashar *et al* 2020), OVCAR3 and IGROV1 cells whereas A2780 cells expressed low levels of EGFR (Bauerschlag *et al* 2017).

Similarly, previous studies reported that Her2 is overexpressed in OvCa and plays an essential role in cell proliferation and tumor cell metastasis (Cai *et al* 2015; Luo *et al* 2018). In this study, Her2 overexpression was observed in SKOV3 and OVCAR3 cells. OVCAR3 cells expressed 2-fold Her2 higher than SKOV3 cells. Conversely, low level of expression was observed in IGROV1, A2780, OVCAR4 and Hey cells in which A2780 and Hey cells showed 3.3-fold and 2-fold lower expression than IGROV1 and OVCAR4 cells (Figure 22). In line with these results, Her2 is overexpressed in SKOV3 and OVCAR3 cells (Jiang *et al* 2017; Mączyńska *et al* 2020). Her2 targeting NIR-PIT (Trastuzumab-IR700) is widely used in different cancer types (Mitsunaga *et al* 2011; Sato *et al* 2015b; Takahashi *et al* 2021; Yamashita *et al* 2023). In addition, FOLR1 is overexpressed in OvCa (Bax *et al* 2022). In this study, FOLR1 was highly expressed in OVCAR3 and IGROV1 cells in which IGROV1 cells expressed 5.6-fold more FOLR1 than OVCAR3 cells and moderate expression was observed in SKOV3 cells which was 3-fold lower than OVCAR3 cells (Figure 23). There was no study targeting FOLR1 using NIR-PIT although PDT targeting FOLR1 was developed by conjugating a folate moiety to PS for the treatment of OvCa (Aung *et al* 2022; Baydoun *et al* 2023).

In addition, TROP2 overexpression correlates with poor prognosis in OvCa (Dum *et al* 2022; Wu *et al* 2017; Xu *et al* 2016). High expression of TROP2 was observed in OVCAR3, OVCAR4 and Hey cells. Hey cells expressed TROP2 1.9-fold and 2.3-fold more than OVCAR4 and OVCAR3 cells respectively. SKOV3 cells expressed moderate level of TROP2

which was 9.5-fold lower than Hey cells. Among six cell lines the highest expression was observed in Hey cells whereas A2780 and IGROV1 cells showed the lowest expression (Figure 23). Xu *et al* reported that the average relative expression of TROP2 mRNA is higher in SKOV3 than in A2780 (Xu *et al* 2016). Another study reported that the expression of Trop2 is higher in OVCAR4 cells as compared to SKOV3 cells which is in line with the results of this study (Kamble *et al* 2020). Nishimura *et al* used anti-TROP2-IR700 as a NIR-PIT agent for the first time targeting TROP2 for treating human pancreatic carcinoma and cholangiocarcinoma (Nishimura *et al* 2019). Moreover, the expression of TF is increased on the surface of tumor cells in OvCa (Cocco *et al* 2011). TF expression in SKOV3 cells was 2-fold higher than in OVCAR3 and OVCAR4 cells (Figure 24). Chanakira *et al* reported that modest TF antigen is expressed in SKOV3 and OVCAR3 cell lines which is consistent with the findings of this study (Chanakira *et al* 2017).

4.3 Specific binding of NIR-PIT agents to OvCa cells

In NIR-PIT, specific binding of NIR-PIT agents to the targeted tumor site is a pivotal step in achieving efficient therapeutic efficacy and limiting off-target effects (Mitsunaga *et al* 2011; Wei *et al* 2022). In this study, SNAP surface Alexa flour 647 was conjugated to the scFv-SNAP tag proteins. As the conjugation was efficient and site-specific, their specific binding to overexpressed cells was expected. Flow cytometry results revealed strong and specific binding of scFv-Erbitux-SNAP-647 to four moderates to high EGFR expressed cell lines including SKOV3, OVCAR3, IGROV1 and OVCAR4 (Figure 25). This finding was consistent with the expression pattern analysis using commercial antibody (Figure 22). However, Hey cells showed lower binding in compared with commercial antibodies. Bauerschlag *et al* reported that scFv-425-SNAP-647 specifically binds to $EGFR^{+}$ SKOV3, OVCAR3 and IGROV1 cell lines (Bauerschlag *et al* 2017). Similar to the expression of Her2 in OvCa cells (Figure 22), strong and specific binding of scFv-Herceptin-SNAP-647 was observed in high Her2 expressed cell lines (SKOV3 and OVCAR3 cells) and weak binding was observed in low expressed cell lines (IGROV1, OVCAR4 and Hey cells) (Figure 25). In addition, scFv-Farletuzumab-SNAP-647 showed specific binding to OVCAR3 and IGROV1. In line with the expression pattern analysis, scFv-Sacituzumab-SNAP-647 exhibited specific binding in moderate to high TROP2 expressed cell lines including SKOV3, OVCAR3, OVCAR4 and Hey. Moreover, SKOV3, OVCAR3 and OVCAR4 cells exhibited specific binding with scFv-Tisotumab-SNAP-647 which was similar to expression pattern analysis (Figure 24).

Furthermore, BG-IR700 was conjugated to the scFv-SNAP tag proteins, allowing the preparation of homogeneous scFv-Erbitux-SNAP-IR700, scFv-Herceptin-SNAP-IR700, scFv-Farletuzumab-SNAP-IR700, scFv-Sacituzumab-SNAP-IR700 and scFv-Tisotumab-SNAP-IR700. The binding specificity of five NIR-PIT agents was validated by flow cytometry and fluorescence microscopy. The flow cytometry results confirmed that scFv-Erbitux-SNAP-IR700 specifically binds to high EGFR expressed SKOV3, OVCAR3, IGROV1 and OVCAR4 (Figure 26 a). However, the low EGFR expressing cell lines showed no binding. The fluorescence microscopy analysis revealed intense membrane fluorescence to the high EGFR expressed cell lines which is in line to the flow cytometry results (Figure 26 b). Similar to these findings, Bauerschlag *et al* 2017 reported that EGFR targeting scFv-425-SNAP-647 is internalized in SKOV3, OVCAR3 and IGROV1 cells visualized by confocal microscopy (Bauerschlag *et al* 2017). Similarly, high Her2 expressed SKOV3 and OVCAR3 cells showed strong and specific binding to scFv-Herceptin-SNAP-IR700. By confocal microscopy, Mączyńska *et al* showed highly specific cell binding and uptake of Her2 targeting $Z_{HER2:2395}$-IR700 in SKOV3 cells (Mączyńska *et al* 2020). In addition, this is the very first study where strong, specific and homogeneous membrane IR700 fluorescence signal was observed in highly FOLR1 expressed IGROV1 cells when incubated with scFv-Farletuzumab-SNAP-IR700. Moreover, flow cytometry and fluorescence microscopy analysis revealed that the fluorescence shift of histogram and membrane fluorescence intensity were high in TROP2 expressed SKOV3, OVCAR3, OVCAR4 and Hey cells when using scFv-Sacituzumab-SNAP-IR700. The TF targeting scFv-Tisotumab-SNAP-IR700 showed specific membrane and internalized IR700 fluorescence signals in SKOV3, OVCAR3 and OVCAR4 cells. The reason could be scFv-Tisotumab-SNAP-IR700 was rapidly internalized into lysosomes. However, several studies demonstrated that internalization of NIR-PIT agents in cells is unnecessary for the cell-killing of targeted tumors (Kato *et al* 2023; Sioud *et al* 2021). The membrane binding of NIR-PIT agents is the most important factor for their biological efficacy (Mitsunaga *et al* 2011). Although, another study reported that Trastusumab-IR700 is located only at the plasma membrane immediately and internalize into lysosomes via the endocytic pathway after 6 h (Nakajima and Ogawa 2020).

The above-mentioned results indicate strong and specific binding of all the investigated NIR-PIT agents to target cancer cells, while no unspecific binding was observed for IR700 conjugated scFv-SNAP tag proteins. Using fluorescence microscopy, it was also validated that the investigated NIR-PIT agents were able to bind the membrane or internalize to target cancer

cells whereas no unspecific binding or internalization was detected in the low expressed cancer cell lines.

4.4 Target-specific, dose-dependent NIR-PIT induced photocytotoxicity of OvCa cells

NIR-PIT can be used as a local light irradiation that could reduce the adverse effect on other normal tissue. The therapeutic activity of NIR-PIT approach differs in the published reports due to different light doses, NIT-PIT agents, cell lines, conjugation methods and incubation time used. These resulted into a broad range (nanomolar to micromolar) of IC_{50} (Amoury *et al* 2016; Bauerschlag *et al* 2017; von Felbert *et al* 2016; Nagaya *et al* 2015; Nakajima *et al* 2018; Nakajima *et al* 2023; Takakura *et al* 2021; Yamashita *et al* 2023). As the NIR-PIT agents possessed specific and comparable binding that was confirmed in this study, specific photocytotoxicity was further evaluated. After light irradiation, the IR700 conjugated scFv-Erbitux-SNAP showed specific cytotoxicity in a concentration-dependent manner in EGFR expressing cell lines. The low expressed cell lines exhibited no effect in lower concentration, but mild toxicity was observed at higher concentration (Figure 31). The toxicity varies (Table 12) in different cell lines, which is in line with binding analysis (Figure 26). High EGFR expressed cell lines, SKOV3, OVCAR3, IGROV1 and OVCAR4 showed high toxicity. Several studies reported that high light doses caused edema (Furumoto *et al* 2022; Kato *et al* 2021a; Nakajima *et al* 2023). Therefore, a relatively low NIR light dose with higher concentration of NIR-PIT agents (1600 nM) was used in terms of optimizing the therapeutic efficacy and side effects. These results clearly indicate that the induction of cancer cell death occurs in a target-specific way that can reduce the side effect to normal cells. Nagaya *et al* reported that over 90% of MDA-MB-468 cells died when exposed to 1 J/cm^2 of EGFR targeting NIR-PIT and 85% cells of MDA-MB-231 died after applying 32 J of NIR-light irradiation (Nagaya *et al* 2015). Studies also reported that EGFR targeting (scFv-425-SNAP-IR700) NIR-PIT induces selective cell death of EGFR$^+$ cell lines in nM concentration at 25 J/cm^2 light dose (Amoury *et al* 2016; Bauerschlag *et al* 2017; von Felbert *et al* 2016).

Similarly, Her2 targeting scFv-Herceptin-SNAP-IR700 showed selective photocytotoxicity to high Her2$^+$ SKOV3 and OVCAR3 cells, which is in line with the fluorescence binding results (Figure 27, Figure 32). Similar effects were also found in previous studies when Her2 targeting affibody based NIR-PIT was applied in SKOV3 spheroids. The cell death was increased by ~85–97% in a concentration-dependent manner of $Z_{HER2:2395}$-IR700 within the SKOV3 spheroids after 96 h post irradiation (16 J/cm^2) (Mączyńska *et al* 2020). Although in this study,

IGROV1, A2780, OVCAR4 and Hey cells showed slight toxicity at high nM concentration because these cells also expressed low levels of Her2 (Figure 22 and Figure 25). Consistent with this result, Her2 targeting Trastuzumab-IR700 demonstrates promising therapeutic properties *in vitro* and *in vivo* against several types of cancers (Nagaya *et al* 2018; Siddiqui *et al* 2019; Takahashi *et al* 2021; Yamashita *et al* 2023). However, the photocytotoxicity level was different because these studies used approximately two to three molecules of IR700 for one single antibody and a higher light dose.

Among all five investigated NIT-PIT agents, FOLR1 targeting NIR-PIT agents exhibited IC_{50} at the lowest concentration (42.3 nM) in IGROV1 cells, which was the highly FOLR1 expressed cell line. OVCAR3 cells showed less toxicity although they expressed moderate levels of FOLR1. Similar to other NIR-PIT agents, negligible toxicity was detected at high concentration of scFv-Farletuzumab-SNAP-IR700 in low FOLR1 expressed SKOV3, OVCAR4 and Hey cells (Figure 33). Aung *et al* recently revealed that FOLR1 targeting NIR-PDT induces cell death in FR overexpressed KB cells by using folate-Si-rhodamine-1 and 50 J/cm^2 NIR-light irradiation (Aung *et al* 2022).

As most of the OvCa cells expressed high level of TROP2 and specific binding of scFv-Sacituzumab-SNAP-IR700 to this antigen, their specific photocytotoxicity was expected. The cells expressed high level of TROP2 (OVCAR3, OVCAR4 and Hey) showed very high toxicity and their IC_{50} was 45.9-96.2 nM. Nishimura *et al* demonstrated that anti-TROP2 mAb-IR700 conjugate shows target-specific cell killing in TROP2 overexpressed pancreatic carcinoma and cholangiocarcinoma cell lines (Nishimura *et al* 2019).

In this study, high level of cytotoxicity was detected in TF overexpressed SKOV3, OVCAR3 and OVCAR4 cell lines after treating with scFv-Tisotumab-SNAP-IR700 (Figure 35). Although the expression level of EGFR was higher than the expression level of TF in these cell lines, the cytotoxicity of scFv-Tisotumab-SNAP-IR700 was higher in these cell lines comparing to EGFR targeting NIR-PIT agent. Importantly, no alteration of cell death was observed in the TF low expressing IGROV1, A2780 and Hey after treating them under the same conditions. These results suggest that all the investigated NIR-PIT agents have specific cytotoxicity *in vitro*. Moreover, IR700 is a hydrophilic photoreactive dye with no phototoxic or cytotoxic properties of its own. The free unbound IR700 can easily excrete in the urine (Mitsunaga *et al* 2011). NIR light is a nonionizing form of radiation and can penetrate a few centimeters into the tissue without causing damage to DNA. In NIR-PIT, the antibody-IR700

binds predominantly to specific targeted cancer cells and is only activated in areas exposed to NIR light, thus targeted to the tumor without damaging adjacent normal cells. (Kobayashi and Choyke 2019; Kobayashi *et al* 2020). To further validate these results and measure the therapeutic efficacy, *in vivo* studies need to be performed.

4.5 Induction of NIR-PIT agents mediated cell death

In this study, the photocytotoxicity mediated by NIR-PIT was further confirmed by using Annexin assay. The scFv-Tisotumab-SNAP-IR700 induced the highest cell death in SKOV3 cells, which was in line of XTT photocytotoxicity result. The flow cytometry results showed 64% of cell death by necroptosis with 25% of early apoptotic cell death. Similarly, scFv-Erbitux-SNAP-IR700, scFv-Herceptin-SNAP-IR700 and scFv-Sacituzumab-SNAP-IR700 treatment induced 58-68% necroptotic cell death (Figure 36). High percentage of necroptotic cell death was also observed in cells treated with panitumumab-IR700 and trastuzumab-IR700 (Nakajima and Ogawa 2020; Railkar *et al* 2017). In a recent study, such distinct features of Annexin V^+/PI^+ sub-population were also observed in panitumumab-IR700 treated A431 cells (Yamashita *et al* 2023).

OVCAR3 is high grade serous OvCa cell line representative of HGSOC and has been extensively used as an OvCa model (Bradbury *et al* 2020). Elevated expression of EGFR, Her2, FOLR1, TROP2 and TF and their corresponding binding of NIR-PIT agents were detected in OVCAR3 cells. As expected, all the tested NIR-PIT agents caused high level of cell death in OVCAR3 cells which is in line with our XTT result. Besides 24-39% early apoptotic cell death, most of the cell death (46-58%) occurred by necroptosis (Figure 37). Consistent with these results, Her2 targeted affibody-IR700 treated SKOV3 cells shifted from viable to necrotic after 24 h irradiation and the percentage of necrotic cells (Annexin V^+/PI^+) was ~47% when 1 μM of the affibody-IR700 and 16 J/cm^2 light dose were applied (Mączyńska *et al* 2020).

In addition, 90% of cell death was observed when IGROV1 cells treated with scFv-Farletuzumab-SNAP-IR700 in which 62% and 31% cell death occurred by necroptosis and early apoptosis respectively (Figure 38). The second and third highest cell death occurred in IGROV1 cells treated with scFv-Erbitux-SNAP-IR700 and scFv-Sacituzumab-SNAP-IR700 which is similar to the findings of XTT assay. However, slight toxicity was observed after treating IGROV1 cells with scFv-Herceptin-SNAP-IR700 and scFv-Tisotumab-SNAP-IR700, although IGROV1 cells expressed low level of Her2 and TF. As 1600 nM of NIR-PIT agents were used for Annexin assay, this high concentration of NIR-PIT agents might cause cell death

in IGROV1 cells, which was also observed in XTT assay. In contrast, negligible cell death (16-26%) was observed in the low expressed A2780 cell lines in which 6-9% cell death occurred by necroptosis (Figure 39).

Consistent with the bindings and XTT assay, scFv-Erbitux-SNAP-IR700 and scFv-Sacituzumab-SNAP-IR700 were able to induce ~92% cell death in OVCAR4. In addition, a slight decrease in cell death (~85%) was observed in scFv-Tisotumab-SNAP-IR700 treated OVCAR4 (Figure 41). Previous study reported that the population of viable cells was 17.5% and 4% after treating the cells with EGFR targeting affibody-IR700, where most of the subpopulation was necrosis (Annexin V^+/PI^+) (Mączyńska *et al* 2022). In this study, scFv-Sacituzumab-SNAP-IR700 treatment caused the highest number of cell death in Hey cells in which ~69% subpopulation was Annexin V^+/PI^+ (Figure 40). Previous study reported that 79.9% cells were PI^+ after 24 h post irradiation with EGFR targeting affibody-IR700, demonstrating that cell death occurred by necrosis (Burley *et al* 2018). Besides TROP2 targeting NIR-PIT agents, the number of cell death was lower when treated with other four NIR-PIT agents. These results suggested that all the investigated NIR-PIT agents caused targeted cell death in which most representing cells in the necroptosis stage.

4.6 NIR-PIT mediated cell death occurred by irreversible and regulated necrosis

NIT-PIT causes rapid specific cell death through photochemical changes of antibody IR700 bound cell, thereby damaging the membrane of targeted cell. The pathway of cell death is not yet clear although many studies demonstrated that necrotic cell death occurred after NIR-PIT (Mączyńska *et al* 2022; Nakajima *et al* 2018; Nakajima and Ogawa 2020; Ogawa *et al* 2017). Previous studies demonstrated that necrosis could take place in well-regulated and genetically guided way. Regulated necrosis has different forms including necroptosis, ferroptosis, pyroptosis, and autophagic cell death (Galluzzi *et al* 2018). The exact pathway that induces cell death post-NIR light irradiation of scFv-SNAP-IR700 needs to be investigated. Therefore, we evaluated the cell death type by pre-treating the cells with apoptosis, necroptosis and ferroptosis inhibitors to understand the molecular mechanisms of scFv-SNAP-IR700 based NIR-PIT.

After treating OVCAR4 cells with scFv-Erbitux-SNAP-IR700, cell death inhibition was similar for necroptosis (26%) and ferroptosis inhibitors (27%). However, apoptotic inhibitor scavenged only 15% cell death (Figure 42). In this study, mixed types of cell death were detected in response to EGFR targeting scFv-SNAP based NIR-PIT. This indicated that most

of the cell death (53%) occurred in regulated necrosis (necroptosis, ferroptosis) and other major cell death might be due to the irreversible necrosis (Mitsunaga *et al* 2012; Sato *et al* 2015b) that could not be scavenged by the analyzed inhibitors. Previous studies demonstrated that NIR-PIT lead to irreversible cell death by immediate swelling, budding and rupture of the lysosome (Mitsunaga *et al* 2012; Sato *et al* 2015b). Similarly in this study, Her2 targeting scFv-SNAP based NIR-PIT induced cell death was suppressed by 26% when OVCAR3 cells were pretreated with ferroptosis inhibitor. In contrast, 18% and 6% cell death were inhibited respectively when necroptosis and apoptosis inhibitors were applied (Figure 42). These results also suggested that 46% cell death might occur in regulated necrosis pathway and the rest of the cell death could occur by irreversible necrosis.

However, contrasting results were observed in FOLR1 targeting NIR-PIT. Only 5% cell death was scavenged when IGROV1 cells were pretreated with necroptosis and ferroptosis inhibitors. Most of the cell death could not be scavenged as scFv- Farletuzumab-SNAP-IR700 was highly cytotoxic to IGROV1 cells as described in section 3.5 (Figure 33). Another reason could be IGROV1 cells expressed very high levels of FOLR1 after light irradiation, rapid irreversible cell damage might occur that could not be inhibited by the inhibitors. Similar to FOLR1 targeting scFv-SNAP based NIR-PIT, apoptosis, necroptosis and ferroptosis inhibitors scavenged 5% cell death after Hey cells were treated with scFv-Sacituzumab-SNAP-IR700 (Figure 42). Hey cells expressed very high level of TROP2 and their photocytotoxicity was also high, which led to their irreversible cell death. A previous study reported that the ROS scavenger suppressed intracellular ROS production and eventually resulted in an inhibition of PIT-induced cell death. The cell death inhibition is slightly reduced when high concentrations of NIR-PIT agents were applied at 16 J/cm^2 light dose (Mączyńska *et al* 2022). The scFv-SNAP based NIR-PIT agents could also localize in the lysosome and induce lysosomal membrane damage and leakage of the lysosomal contents into the cytosol. Similar findings were also reported when mAb-IR700 were applied (Nakajima and Ogawa 2020). Membrane bound or internalized scFv-SNAP based NIR-PIT agents might induce massive damage to membrane or lysosomes, leading to irreversible necrosis that could not be scavenged by the cell death inhibitors.

Moreover, after treating SKOV3 cells with TF targeting scFv-SNAP based NIR-PIT, 4% and 14% cell death were inhibited by necroptosis and ferroptosis inhibitors, respectively. In contrary, only 2% cell death was scavenged by apoptosis inhibitor. These results suggested that the most of the cell death occurred by either irreversible necrosis or regulated necrosis. The

above-mentioned results indicate that multiple coexistent cell death mechanisms occurr in scFv-SNAP based NIR-PIT, which is in line with previous studies where affibody based NIR-PIT was applied (Mączyńska *et al* 2020). These results also suggested that scFv-SNAP based NIR-PIT induced necrosis either in regulated necrosis (necroptosis or ferroptosis) or in irreversible necrosis. However, only apoptosis, necroptosis and ferroptosis inhibitors were studied in this experiment, while pyroptosis or entosis inhibitors might also have impact on cell death. The type of cell and target have influence on the subcellular localization of NIR-PIT agents. Different targeting molecules such as full-length antibodies or their fragments are internalized at different speeds (Glatt *et al* 2016; Mickler *et al* 2012; Opaliński *et al* 2018; Rafidi *et al* 2022). This might be the reason why universal results have not been obtained concerning the involvement of cell death scavenging by cell death inhibitors in NIR-PIT.

4.7 NIR-PIT triggered ICD by the release of DAMPs

In this study, we analyzed the major features of ICD after NIR-PIT treatment including cell surface exposure of CRT, HSP70, HSP90 and extracellular release of ATP and HMGB1.

Cancer cells undergoing ICD are expose calreticulin on the plasma membrane, serves as an "eat-me" signal (Kasikova *et al* 2019; Kielbik *et al* 2021). These surface-exposed calreticulin binds to CD91 of DCs (Gardai *et al* 2003). Besides initiating adaptive T-cell-mediated immunity, calreticulin can improve the innate immunity by *trans*-presenting IL-15 to natural killer cells (Truxova *et al* 2020). Therefore, the cell surface expression of calreticulin was analyzed after irradiated the cells with NIR-PIT agents. OVCAR4 cells treated with scFv-Erbitux-SNAP-IR700 showed 3.2-fold enhanced expression of calreticulin in comparison to the control. Similarly, the expression of calreticulin was enhanced up to 1.4-fold, 2.5-fold, 2.9-fold and 2.0-fold in OVCAR3, IGROV1, Hey and SKOV3 cells, respectively, after treating with Her2, FOLR1, TROP-2 and TF targeting NIT-PIT, respectively compared to the control. Previous studies demonstrated that enhanced surface expression of calreticulin was observed in cancer cells treated with Her2 and EGFR targeting affibody-IR700 (Burley *et al* 2018; Mączyńska *et al* 2020; Mączyńska *et al* 2022).

Other endoplasmic reticulum (ER) chaperones such as HSP70 and HSP90 can express on the plasma membrane of cells undergoing ICD and show immunostimulatory function (Joly *et al* 2010; Spisek and Dhodapkar 2007). They bind with several receptors like CD91, LOX1, and CD40 on APCs surface, induce the activation/maturation of DCs, thus activate the $CD8^+$ T-cells by cross-presenting tumor cells antigens to MHC class I molecule (Doody *et al* 2004;

Spisek and Dhodapkar 2007). Therefore, the cell surface expressions of HSP70 and HSP90 were analyzed after NIR-PIT. OVCAR4 cells treated with scFv-Erbitux-SNAP-IR700 expressed 2.0-fold and 5.4-fold higher HSP70 and HSP90, respectively in comparison to the controls. The expressions of HSP70 and HSP90 increased 8.5-fold and 68.1-fold after treating OVCAR3 cells with Her2 targeting NIR-PIT. Similarly, 3.3-fold (HSP70) and 46.8-fold (HSP90) enhanced expressions were observed in scFv-Farletuzumab-SNAP-IR700 treated IGROV1 cells. In addition, augmented expressions of HSP70 (3.2-fold) and HSP90 (24.8-fold) were monitored in scFv-Sacituzumab-SNAP-IR700 irradiated Hey cells. Moreover, HSP70 and HSP90 expressions were 4.0-fold and 119-fold higher in SKOV3 cells treated with scFv-Tisotumab-SNAP-IR700. These results indicated that all the investigated NIR-PIT treated cells augmented the expressions of cell surface HSP70 and HSP90. Particularly, all five NIR-PIT treated A2780 showed little to no change of HSP70 and HSP90 expressions in comparison to the control. The expression of HSP90 was higher than the HSP70 expression on all the NIR-PIT induced dying cells. This was in line with previously published studies demonstrating that the MFI of HSP70 and HSP90 is increased after NIR-PIT (Ogawa *et al* 2017; Sioud *et al* 2021).

During ICD of cancer cells, HMGB1 is released by translocating nucleus to the cytoplasm through permeabilizing nuclear lamina and the plasma membrane (Yang *et al* 2015). Moreover, ATP is released in an autophagy-dependent manner through ATP-containing vesicles (Anderson *et al* 2019; Martins *et al* 2014). These extracellular ATP and HMGB1 from ICD further bind to P2Y2 receptor and multiple PRRs of myeloid cells respectively and eventually activate the $CD8^+$ T cells (Apetoh *et al* 2007; Elliott *et al* 2009; Fucikova *et al* 2020). The extracellular levels of ATP and HMGB1 in the culture supernatants of treated OvCa cells were evaluated in this study. The released ATP level was 21.5 nmol when OVCAR4 cells treated with EGFR targeting NIR-PIT. In contrast, IGROV1 treated with scFv-Farletuzumab-SNAP-IR700 and Hey treated with scFv-Sacituzumab-SNAP-IR700 released low levels of ATP, which were 127.8 pmol and 74.2 pmol ATP, respectively. The morphological differences of different cell lines lead to the release of lower ATP levels. In addition, unconjugated scFv-SNAP treatment was unable to change the ATP levels in all the investigated cell lines with all five tested NIR-PIT agents compared to the control. Moreover, the extracellular HMGB1 level was 47.4 ng/mL in scFv-Farletuzumab-SNAP-IR700 treated IGROV1 cells. The scFv-Sacituzumab-SNAP-IR700 treated Hey cells released 13.8 ng/mL HMGB1, which was the lowest among all five treatments. Notably, there was no difference in HMGB1 level in the low expressed cell lines A2780. ATP and HMGB1 can be released passively by membrane rupture

if the cell death occurs by necrosis/necroptosis (Murao *et al* 2021). Some studies demonstrated that HMGB1 and ATP are released by ferroptotic cells (Efimova *et al* 2020; Wen *et al* 2019) and apoptotic cells (Elliott *et al* 2009; Jiang 2007; Murao *et al* 2021). Consistent with other reports, high levels of extracellular ATP and HMGB1 release were observed in this study after treatment (Mączyńska *et al* 2020; Mączyńska *et al* 2022; Ogawa *et al* 2017). A recent work reported that the serum concentration of HMGB1 increased after NIR-PIT in head and neck squamous cell carcinoma patients (Ishihara *et al* 2023). This study provided the proof of principle that scFv-SNAP-tag based NIR-PIT agents can induce immunogenic cell death. Further *in vivo* studies need to be conducted for analyzing their antitumor immunity.

4.8 Co-culturing iDCs with NIR-PIT agents treated cells led to DCs maturation

To generate immune response, a complex developmental program called DC maturation needs to occur by modifying the morphology and functions of DCs. Such modification includes enhanced expressions of co-stimulatory molecules, including CD80, CD86, CD40 and HLADR (Reis e Sousa 2006). As the investigated NIR-PIT agents induced ICD by exposing DMAPs, it was expected that these DMAPs would activate and mature DC and prime antitumor immunity (Mączyńska *et al* 2020; Ogawa *et al* 2017). Therefore, PBMC was differentiated into iDCs and subsequently co-cultured with scFv-Tisotumab-SNAP-IR700 treated SKOV3 cells. Enhanced expressions of DC maturation markers including CD80, CD86, CD40 and HLADR, were observed in co-cultured DCs with scFv-Tisotumab-SNAP-IR700 treated SKOV3 cells. The expression of CD80 was 2.4-fold higher in DCs co-cultured with scFv-Tisotumab-SNAP-IR700 treated SKOV3 cells than the scFv-Tisotumab-SNAP treated SKOV3 cells. Similarly, scFv-Tisotumab-SNAP-IR700 treated SKOV3 cells enhanced the expressions of CD86 3.6-fold higher and HLADR 7.7-fold higher than the controls. This was in line with previously published studies demonstrating that Her2 targeting affibody increased the expressions of CD86 and HLADR (Mączyńska *et al* 2020). In addition, the difference of CD40 expression was 10.4-fold higher on DCs. Notably, no changes of these markers were found when DCs were co-cultured with SKOV3 cells treated with unconjugated scFv-Tisotumab-SNAP. Ogawa *et al* demonstrated that the Her2 targeting NIR-PIT increases the expressions of CD80, CD86, HLADR and CD40 (Ogawa *et al* 2017). Markedly, this is the first study describing the potential therapeutic effects of TF targeting NIR-PIT to treat ovarian cancer and generate antitumor immune response by activating DC.

Moreover, the DC maturation was also examined after co-culturing DCs with OVCAR4 treated with EGFR targeting NIR-PIT agent (scFv-Erbitux-SNAP-IR700) to validate the activation of DCs by scFv-SNAP based NIR-PIT agents. The expressions of CD80, CD86, CD40 and HLADR were augmented in co-cultured DCs with scFv-Erbitux-SNAP-IR700 treated OVCAR4 cells. Moreover, 12.1-fold higher MFI of CD40 was observed than the control. The DCs maturation markers were highly expressed when co-cultured with scFv-Tisotumab-SNAP treated SKOV3 cells than scFv-Erbitux-SNAP treated OVCAR4 cells. These results suggest that the investigated NIR-PIT can lead to DCs maturation and generate antitumor immune response in OvCa patients. Taken together, these *in vitro* studies of DCs maturation suggest that the NIR-PIT agents can rapidly lead to induce ICD of targeted cancer cells and effectively activate DCs.

Although the results in this study present only *in vitro* findings, they provide the basis for future studies aimed to evaluate the efficacy of these agents in preclinical *in vivo* models. This work also provides an insight for using SNAP-tag technology to generate NIR-PIT, which can facilitate OvCa patients pre-screening, real-time treatment monitoring, as well as evaluating therapeutic efficacy.

5 References

Ahmad, Z. A., Yeap, S. K., Ali, A. M., Ho, W. Y., Alitheen, N. B., & Hamid, M. (2012). scFv antibody: principles and clinical application. Clinical & developmental immunology, 2012, 980250. https://doi.org/10.1155/2012/980250

Ahmadi, S. E., Shabannezhad, A., Kahrizi, A., Akbar, A., Safdari, S. M., Hoseinnezhad, T., Zahedi, M., Sadeghi, S., Mojarrad, M. G., & Safa, M. (2023). Tissue factor (coagulation factor III): a potential double-edge molecule to be targeted and re-targeted toward cancer. Biomarker research, 11(1), 60. https://doi.org/10.1186/s40364-023-00504-6

Akai, M., Noma, K., Kato, T., Nishimura, S., Matsumoto, H., Kawasaki, K., Kunitomo, T., Kobayashi, T., Nishiwaki, N., Kashima, H., Kikuchi, S., Ohara, T., Tazawa, H., Choyke, P. L., Kobayashi, H., & Fujiwara, T. (2024). Fibroblast activation protein-targeted near-infrared photoimmunotherapy depletes immunosuppressive cancer-associated fibroblasts and remodels local tumor immunity. British journal of cancer, 130(10), 1647–1658. https://doi.org/10.1038/s41416-024-02639-1

Amoury, M., Bauerschlag, D., Zeppernick, F., von Felbert, V., Berges, N., Di Fiore, S., Mintert, I., Bleilevens, A., Maass, N., Bräutigam, K., Meinhold-Heerlein, I., Stickeler, E., Barth, S., Fischer, R., & Hussain, A. F. (2016). Photoimmunotheranostic agents for triple-negative breast cancer diagnosis and therapy that can be activated on demand. Oncotarget, 7(34), 54925–54936. https://doi.org/10.18632/oncotarget.10705

Anderson, C. M., & Macleod, K. F. (2019). Autophagy and cancer cell metabolism. International review of cell and molecular biology, 347, 145–190. https://doi.org/10.1016/bs.ircmb.2019.06.002

Apetoh, L., Ghiringhelli, F., Tesniere, A., Obeid, M., Ortiz, C., Criollo, A., Mignot, G., Maiuri, M. C., Ullrich, E., Saulnier, P., Yang, H., Amigorena, S., Ryffel, B., Barrat, F. J., Saftig, P., Levi, F., Lidereau, R., Nogues, C., Mira, J. P., Chompret, A., … Zitvogel, L. (2007). Toll-like receptor 4-dependent contribution of the immune system to anticancer chemotherapy and radiotherapy. Nature medicine, 13(9), 1050–1059. https://doi.org/10.1038/nm1622

Armstrong, D. K., Alvarez, R. D., Backes, F. J., Bakkum-Gamez, J. N., Barroilhet, L., Behbakht, K., Berchuck, A., Chen, L. M., Chitiyo, V. C., Cristea, M., DeRosa, M., Eisenhauer, E. L., Gershenson, D. M., Gray, H. J., Grisham, R., Hakam, A., Jain, A., Karam, A., Konecny, G. E., Leath, C. A., III, … Hang, L. (2022). NCCN Guidelines® Insights: Ovarian Cancer, Version 3.2022. Journal of the National Comprehensive Cancer Network: JNCCN, 20(9), 972–980. https://doi.org/10.6004/jnccn.2022.0047

Aung, W., Tsuji, A. B., Hanaoka, K., & Higashi, T. (2022). Folate receptor-targeted near-infrared photodynamic therapy for folate receptor-overexpressing tumors. World journal of clinical oncology, 13(11), 880–895. https://doi.org/10.5306/wjco.v13.i11.880

Bardia, A., Mayer, I. A., Vahdat, L. T., Tolaney, S. M., Isakoff, S. J., Diamond, J. R., O'Shaughnessy, J., Moroose, R. L., Santin, A. D., Abramson, V. G., Shah, N. C., Rugo, H. S., Goldenberg, D. M., Sweidan, A. M., Iannone, R., Washkowitz, S., Sharkey, R. M., Wegener, W. A., & Kalinsky, K. (2019). Sacituzumab Govitecan-hziy in Refractory Metastatic Triple-Negative Breast Cancer. The New England journal of medicine, 380(8), 741–751. https://doi.org/10.1056/NEJMoa1814213

Barot, S., Patel, H., Yadav, A., & Ban, I. (2023). Recent advancement in targeted therapy and role of emerging technologies to treat cancer. Medical oncology (Northwood, London, England), 40(11), 324. https://doi.org/10.1007/s12032-023-02184-6

Bauerschlag, D., Meinhold-Heerlein, I., Maass, N., Bleilevens, A., Bräutigam, K., Al Rawashdeh, W., Di Fiore, S., Haugg, A. M., Gremse, F., Steitz, J., Fischer, R., Stickeler, E., Barth, S., & Hussain, A. F. (2017). Detection and Specific Elimination of EGFR+ Ovarian Cancer Cells Using a Near Infrared Photoimmunotheranostic Approach. Pharmaceutical research, 34(4), 696–703. https://doi.org/10.1007/s11095-017-2096-4

Bax, H. J., Chauhan, J., Stavraka, C., Santaolalla, A., Osborn, G., Khiabany, A., Grandits, M., López-Abente, J., Palhares, L. C. G. F., Chan Wah Hak, C., Robinson, A., Pope, A., Woodman, N., Naceur-Lombardelli, C., Malas, S., Coumbe, J. E. M., Nakamura, M., Laddach, R., Mele, S., Crescioli, S., … Josephs, D. H. (2023). Folate receptor alpha in ovarian cancer tissue and patient serum is associated with disease burden and treatment outcomes. British journal of cancer, 128(2), 342–353. https://doi.org/10.1038/s41416-022-02031-x

Baydoun, M., Boidin, L., Leroux, B., Vignion-Dewalle, A. S., Quilbe, A., Grolez, G. P., Azaïs, H., Frochot, C., Moralès, O., & Delhem, N. (2023). Folate Receptor Targeted Photodynamic Therapy: A Novel Way to Stimulate Anti-Tumor Immune Response in Intraperitoneal Ovarian Cancer. International journal of molecular sciences, 24(14), 11288. https://doi.org/10.3390/ijms241411288

Bedoui, S., Herold, M. J., & Strasser, A. (2020). Emerging connectivity of programmed cell death pathways and its physiological implications. Nature reviews. Molecular cell biology, 21(11), 678–695. https://doi.org/10.1038/s41580-020-0270-8

Bignotti, E., Ravaggi, A., Romani, C., Falchetti, M., Lonardi, S., Facchetti, F., Pecorelli, S., Varughese, J., Cocco, E., Bellone, S., Schwartz, P. E., Rutherford, T. J., & Santin, A. D. (2011). Trop-2 overexpression in poorly differentiated endometrial endometrioid carcinoma: implications for immunotherapy with hRS7, a humanized anti-trop-2 monoclonal antibody. International journal of gynecological cancer: official journal of the International Gynecological Cancer Society, 21(9), 1613–1621. https://doi.org/10.1097/IGC.0b013e318228f6da

Biteghe, F. A. N., Chalomie, N. E. T., Mungra, N., Vignaux, G., Gao, N., Vergeade, A., Okem, A., Naran, K., Ndong, J. C., & Barth, S. (2020). Antibody-Based Immunotherapy: Alternative Approaches for the Treatment of Metastatic Melanoma. Biomedicines, 8(9), 327. https://doi.org/10.3390/biomedicines8090327

Bou-Assaly, W., & Mukherji, S. (2010). Cetuximab (erbitux). AJNR. American journal of neuroradiology, 31(4), 626–627. https://doi.org/10.3174/ajnr.A2054

Bradbury, A., O'Donnell, R., Drew, Y., Curtin, N. J., & Sharma Saha, S. (2020). Characterisation of Ovarian Cancer Cell Line NIH-OVCAR3 and Implications of Genomic, Transcriptomic, Proteomic and Functional DNA Damage Response Biomarkers for Therapeutic Targeting. Cancers, 12(7), 1939. https://doi.org/10.3390/cancers12071939

Bray, F., Laversanne, M., Sung, H., Ferlay, J., Siegel, R. L., Soerjomataram, I., & Jemal, A. (2024). Global cancer statistics 2022: GLOBOCAN estimates of incidence and mortality worldwide for 36 cancers in 185 countries. CA: a cancer journal for clinicians, 74(3), 229–263. https://doi.org/10.3322/caac.21834

Bray, F., Laversanne, M., Weiderpass, E., & Soerjomataram, I. (2021). The ever-increasing importance of cancer as a leading cause of premature death worldwide. Cancer, 127(16), 3029–3030. https://doi.org/10.1002/cncr.33587

Brustmann H. (2008). Epidermal growth factor receptor expression in serous ovarian carcinoma: an immunohistochemical study with galectin-3 and cyclin D1 and outcome. International journal of gynecological pathology: official journal of the International Society of Gynecological Pathologists, 27(3), 380–389. https://doi.org/10.1097/PGP.0b013e31815d060d

Burgess, A. W., Cho, H. S., Eigenbrot, C., Ferguson, K. M., Garrett, T. P., Leahy, D. J., Lemmon, M. A., Sliwkowski, M. X., Ward, C. W., & Yokoyama, S. (2003). An open-and-shut case? Recent insights into the activation of EGF/ErbB receptors. Molecular cell, 12(3), 541–552. https://doi.org/10.1016/s1097-2765(03)00350-2

Burley, T. A., Mączyńska, J., Shah, A., Szopa, W., Harrington, K. J., Boult, J. K. R., Mrozek-Wilczkiewicz, A., Vinci, M., Bamber, J. C., Kaspera, W., & Kramer-Marek, G. (2018). Near-infrared photoimmunotherapy targeting EGFR-Shedding new light on glioblastoma treatment. International journal of cancer, 142(11), 2363–2374. https://doi.org/10.1002/ijc.31246

Butenas S. (2012). Tissue factor structure and function. Scientifica, 2012, 964862. https://doi.org/10.6064/2012/964862

Cabeza-Cabrerizo, M., Cardoso, A., Minutti, C. M., Pereira da Costa, M., & Reis e Sousa, C. (2021). Dendritic Cells Revisited. Annual review of immunology, 39, 131–166. https://doi.org/10.1146/annurev-immunol-061020-053707

Cai, W. Q., Zeng, L. S., Wang, L. F., Wang, Y. Y., Cheng, J. T., Zhang, Y., Han, Z. W., Zhou, Y., Huang, S. L., Wang, X. W., Peng, X. C., Xiang, Y., Ma, Z., Cui, S. Z., & Xin, H. W. (2020). The Latest Battles Between EGFR Monoclonal Antibodies and Resistant Tumor Cells. Frontiers in oncology, 10, 1249. https://doi.org/10.3389/fonc.2020.01249

Cai, Y., Wang, J., Zhang, L., Wu, D., Yu, D., Tian, X., Liu, J., Jiang, X., Shen, Y., Zhang, L., Ren, M., & Huang, P. (2015). Expressions of fatty acid synthase and HER2 are correlated with poor prognosis of ovarian cancer. Medical oncology (Northwood, London, England), 32(1), 391. https://doi.org/10.1007/s12032-014-0391-z

Calo, C. A., & O'Malley, D. M. (2021). Antibody-drug conjugates for the treatment of ovarian cancer. Expert opinion on biological therapy, 21(7), 875–887. https://doi.org/10.1080/14712598.2020.1776253

Cañueto, J., Cardeñoso, E., García, J. L., Santos-Briz, Á., Castellanos-Martín, A., Fernández-López, E., Blanco Gómez, A., Pérez-Losada, J., & Román-Curto, C. (2017). Epidermal growth factor receptor expression is associated with poor outcome in cutaneous squamous cell carcinoma. The British journal of dermatology, 176(5), 1279–1287. https://doi.org/10.1111/bjd.14936

Chanakira, A., Westmark, P. R., Ong, I. M., & Sheehan, J. P. (2017). Tissue factor-factor VIIa complex triggers protease activated receptor 2-dependent growth factor release and migration in ovarian cancer. Gynecologic oncology, 145(1), 167–175. https://doi.org/10.1016/j.ygyno.2017.01.022

Chau, C. H., Steeg, P. S., & Figg, W. D. (2019). Antibody-drug conjugates for cancer. Lancet (London, England), 394(10200), 793–804. https://doi.org/10.1016/S0140-6736(19)31774-X

Chen, Z., Wang, W., Abdul Razak, S. R., Han, T., Ahmad, N. H., & Li, X. (2023). Ferroptosis as a potential target for cancer therapy. Cell death & disease, 14(7), 460. https://doi.org/10.1038/s41419-023-05930-w

Cheng, J., Xu, J., Duanmu, J., Zhou, H., Booth, C. J., & Hu, Z. (2011). Effective treatment of human lung cancer by targeting tissue factor with a factor VII-targeted photodynamic therapy. Current cancer drug targets, 11(9), 1069–1081. https://doi.org/10.2174/156800911798073023

Chester, K., Pedley, B., Tolner, B., Violet, J., Mayer, A., Sharma, S., Boxer, G., Green, A., Nagl, S., & Begent, R. (2004). Engineering antibodies for clinical applications in cancer. Tumor biology: the journal of the International Society for Oncodevelopmental Biology and Medicine, 25(1-2), 91–98. https://doi.org/10.1159/000077727

Cheung, A., Bax, H. J., Josephs, D. H., Ilieva, K. M., Pellizzari, G., Opzoomer, J., Bloomfield, J., Fittall, M., Grigoriadis, A., Figini, M., Canevari, S., Spicer, J. F., Tutt, A. N., & Karagiannis, S. N. (2016). Targeting folate receptor alpha for cancer treatment. Oncotarget, 7(32), 52553–52574. https://doi.org/10.18632/oncotarget.9651

Chouman, K., Woitok, M., Mladenov, R., Kessler, C., Weinhold, E., Hanz, G., Fischer, R., Meinhold-Heerlein, I., Bleilevens, A., Gresch, G., Haugg, A. M., Zeppernick, F., Bauerschlag, D., Maass, N., Stickeler, E., Kolberg, K., & Hussain, A. F. (2017). Fine Tuning Antibody Conjugation Methods using SNAP-tag Technology. Anti-cancer agents in medicinal chemistry, 17(10), 1434–1440. https://doi.org/10.2174/1871520617666170213123737

Cocco, E., Varughese, J., Buza, N., Bellone, S., Lin, K. Y., Bellone, M., Todeschini, P., Silasi, D. A., Azodi, M., Schwartz, P. E., Rutherford, T. J., Carrara, L., Tassi, R., Pecorelli, S., Lockwood, C. J., & Santin, A. D. (2011). Tissue factor expression in ovarian cancer: implications for immunotherapy with hI-con1, a factor VII-IgGF(c) chimeric protein targeting tissue factor. Clinical & experimental metastasis, 28(7), 689–700. https://doi.org/10.1007/s10585-011-9401-0

Colcher, D., Pavlinkova, G., Beresford, G., Booth, B. J., Choudhury, A., & Batra, S. K. (1998). Pharmacokinetics and biodistribution of genetically-engineered antibodies. The quarterly journal of nuclear medicine: official publication of the Italian Association of Nuclear Medicine (AIMN) [and] the International Association of Radiopharmacology (IAR), 42(4), 225–241.

De Groof, T. W. M., Mashayekhi, V., Fan, T. S., Bergkamp, N. D., Sastre Toraño, J., van Senten, J. R., Heukers, R., Smit, M. J., & Oliveira, S. (2019). Nanobody-Targeted Photodynamic Therapy Selectively Kills Viral GPCR-Expressing Glioblastoma Cells. Molecular pharmaceutics, 16(7), 3145–3156. https://doi.org/10.1021/acs.molpharmaceut.9b00360

Del Prete, A., Salvi, V., Soriani, A., Laffranchi, M., Sozio, F., Bosisio, D., & Sozzani, S. (2023). Dendritic cell subsets in cancer immunity and tumor antigen sensing. Cellular & molecular immunology, 20(5), 432–447. https://doi.org/10.1038/s41423-023-00990-6

Del Prete, A., Salvi, V., Soriani, A., Laffranchi, M., Sozio, F., Bosisio, D., & Sozzani, S. (2023). Dendritic cell subsets in cancer immunity and tumor antigen sensing. Cellular & molecular immunology, 20(5), 432–447. https://doi.org/10.1038/s41423-023-00990-6

Di Lorenzo, G., Tortora, G., D'Armiento, F. P., De Rosa, G., Staibano, S., Autorino, R., D'Armiento, M., De Laurentiis, M., De Placido, S., Catalano, G., Bianco, A. R., & Ciardiello, F. (2002). Expression of epidermal growth factor receptor correlates with disease relapse and progression to androgen-independence in human prostate cancer. Clinical cancer research: an official journal of the American Association for Cancer Research, 8(11), 3438–3444.

Dickerson, E. B., Blackburn, W. H., Smith, M. H., Kapa, L. B., Lyon, L. A., & McDonald, J. F. (2010). Chemosensitization of cancer cells by siRNA using targeted nanogel delivery. BMC cancer, 10, 10. https://doi.org/10.1186/1471-2407-10-10

Dilawari, A., Shah, M., Ison, G., Gittleman, H., Fiero, M. H., Shah, A., Hamed, S. S., Qiu, J., Yu, J., Manheng, W., Ricks, T. K., Pragani, R., Arudchandran, A., Patel, P., Zaman, S., Roy, A., Kalavar, S., Ghosh, S., Pierce, W. F., Rahman, N. A., … Amiri-Kordestani, L. (2023). FDA Approval Summary: Mirvetuximab Soravtansine-Gynx for FOLR1-Positive, Platinum-Resistant Ovarian Cancer. Clinical cancer research: an official journal of the American Association for Cancer Research, 29(19), 3835–3840. https://doi.org/10.1158/1078-0432.CCR-23-0991

Dixon, S. J., Lemberg, K. M., Lamprecht, M. R., Skouta, R., Zaitsev, E. M., Gleason, C. E., Patel, D. N., Bauer, A. J., Cantley, A. M., Yang, W. S., Morrison, B., 3rd, & Stockwell, B. R. (2012). Ferroptosis: an iron-dependent form of nonapoptotic cell death. Cell, 149(5), 1060–1072. https://doi.org/10.1016/j.cell.2012.03.042

Doody, A. D., Kovalchin, J. T., Mihalyo, M. A., Hagymasi, A. T., Drake, C. G., & Adler, A. J. (2004). Glycoprotein 96 can chaperone both MHC class I- and class II-restricted epitopes for in vivo presentation, but selectively primes CD8+ T cell effector function. Journal of immunology (Baltimore, Md.: 1950), 172(10), 6087–6092. https://doi.org/10.4049/jimmunol.172.10.6087

Dou, X., Nomoto, T., Takemoto, H., Matsui, M., Tomoda, K., & Nishiyama, N. (2018). Effect of multiple cyclic RGD peptides on tumor accumulation and intratumoral distribution of IRDye 700DX-conjugated polymers. Scientific reports, 8(1), 8126. https://doi.org/10.1038/s41598-018-26593-0

Doubeni, C. A., Doubeni, A. R., & Myers, A. E. (2016). Diagnosis and Management of Ovarian Cancer. American family physician, 93(11), 937–944.

Dum, D., Taherpour, N., Menz, A., Höflmayer, D., Völkel, C., Hinsch, A., Gorbokon, N., Lennartz, M., Hube-Magg, C., Fraune, C., Bernreuther, C., Lebok, P., Clauditz, T. S., Jacobsen, F., Sauter, G., Uhlig, R., Wilczak, W., Steurer, S., Minner, S., Marx, A. H., … Luebke, A. M. (2022). Trophoblast Cell Surface Antigen 2 Expression in

Human Tumors: A Tissue Microarray Study on 18,563 Tumors. Pathobiology: journal of immunopathology, molecular and cellular biology, 89(4), 245–258. https://doi.org/10.1159/000522206

Efimova, I., Catanzaro, E., Van der Meeren, L., Turubanova, V. D., Hammad, H., Mishchenko, T. A., Vedunova, M. V., Fimognari, C., Bachert, C., Coppieters, F., Lefever, S., Skirtach, A. G., Krysko, O., & Krysko, D. V. (2020). Vaccination with early ferroptotic cancer cells induces efficient antitumor immunity. Journal for immunotherapy of cancer, 8(2), e001369. https://doi.org/10.1136/jitc-2020-001369

Elliott, M. R., Chekeni, F. B., Trampont, P. C., Lazarowski, E. R., Kadl, A., Walk, S. F., Park, D., Woodson, R. I., Ostankovich, M., Sharma, P., Lysiak, J. J., Harden, T. K., Leitinger, N., & Ravichandran, K. S. (2009). Nucleotides released by apoptotic cells act as a find-me signal to promote phagocytic clearance. Nature, 461(7261), 282–286. https://doi.org/10.1038/nature08296

Elmore S. (2007). Apoptosis: a review of programmed cell death. Toxicologic pathology, 35(4), 495–516. https://doi.org/10.1080/01926230701320337

Even-Desrumeaux, K., Baty, D., & Chames, P. (2011). State of the art in tumor antigen and biomarker discovery. Cancers, 3(2), 2554–2596. https://doi.org/10.3390/cancers3022554.

Fernandes, S. R. G., Fernandes, R., Sarmento, B., Pereira, P. M. R., & Tomé, J. P. C. (2019). Photoimmunoconjugates: novel synthetic strategies to target and treat cancer by photodynamic therapy. Organic & biomolecular chemistry, 17(10), 2579–2593. https://doi.org/10.1039/c8ob02902d

Frejd, F. Y., & Kim, K. T. (2017). Affibody molecules as engineered protein drugs. Experimental & molecular medicine, 49(3), e306. https://doi.org/10.1038/emm.2017.35

Fu, R., Carroll, L., Yahioglu, G., Aboagye, E. O., & Miller, P. W. (2018). Antibody Fragment and Affibody ImmunoPET Imaging Agents: Radiolabelling Strategies and Applications. ChemMedChem, 13(23), 2466–2478. https://doi.org/10.1002/cmdc.201800624

Fucikova, J., Kepp, O., Kasikova, L., Petroni, G., Yamazaki, T., Liu, P., Zhao, L., Spisek, R., Kroemer, G., & Galluzzi, L. (2020). Detection of immunogenic cell death and its relevance for cancer therapy. Cell death & disease, 11(11), 1013. https://doi.org/10.1038/s41419-020-03221-2

Fukushima, H., Takao, S., Furusawa, A., Valera Romero, V., Gurram, S., Kato, T., Okuyama, S., Kano, M., Choyke, P. L., & Kobayashi, H. (2024). Near-infrared photoimmunotherapy targeting Nectin-4 in a preclinical model of bladder cancer. Cancer letters, 585, 216606. https://doi.org/10.1016/j.canlet.2023.216606

Furumoto, H., Okada, R., Kato, T., Wakiyama, H., Inagaki, F., Fukushima, H., Okuyama, S., Furusawa, A., Choyke, P. L., & Kobayashi, H. (2022). Optimal Light Dose for hEGFR-Targeted Near-Infrared Photoimmunotherapy. Cancers, 14(16), 4042. https://doi.org/10.3390/cancers14164042

Galluzzi, L., Vitale, I., Aaronson, S. A., Abrams, J. M., Adam, D., Agostinis, P., Alnemri, E. S., Altucci, L., Amelio, I., Andrews, D. W., Annicchiarico-Petruzzelli, M., Antonov, A. V., Arama, E., Baehrecke, E. H., Barlev, N. A., Bazan, N. G., Bernassola, F., Bertrand, M. J. M., Bianchi, K., Blagosklonny, M. V., … Kroemer, G. (2018). Molecular mechanisms of cell death: recommendations of the Nomenclature Committee on Cell Death 2018. Cell death and differentiation, 25(3), 486–541. https://doi.org/10.1038/s41418-017-0012-4

Gardai, S. J., Xiao, Y. Q., Dickinson, M., Nick, J. A., Voelker, D. R., Greene, K. E., & Henson, P. M. (2003). By binding SIRPalpha or calreticulin/CD91, lung collectins act as dual function surveillance molecules to suppress or enhance inflammation. Cell, 115(1), 13–23. https://doi.org/10.1016/s0092-8674(03)00758-x

Garg, A. D., Nowis, D., Golab, J., Vandenabeele, P., Krysko, D. V., & Agostinis, P. (2010). Immunogenic cell death, DAMPs and anticancer therapeutics: an emerging amalgamation. Biochimica et biophysica acta, 1805(1), 53–71. https://doi.org/10.1016/j.bbcan.2009.08.003

Gautier, A., Juillerat, A., Heinis, C., Corrêa, I. R., Jr, Kindermann, M., Beaufils, F., & Johnsson, K. (2008). An engineered protein tag for multiprotein labeling in living cells. Chemistry & biology, 15(2), 128–136. https://doi.org/10.1016/j.chembiol.2008.01.007

Gemmete, J. J., & Mukherji, S. K. (2011). Trastuzumab (herceptin). AJNR. American journal of neuroradiology, 32(8), 1373–1374. https://doi.org/10.3174/ajnr.A2619

Gerotziafas, G. T., Galea, V., Mbemba, E., Khaterchi, A., Sassi, M., Baccouche, H., Prengel, C., van Dreden, P., Hatmi, M., Bernaudin, J. F., & Elalamy, I. (2012). Tissue factor over-expression by human pancreatic cancer cells BXPC3 is related to higher prothrombotic potential as compared to breast cancer cells MCF7. Thrombosis research, 129(6), 779–786. https://doi.org/10.1016/j.thromres.2011.07.049

Ghiringhelli, F., Apetoh, L., Tesniere, A., Aymeric, L., Ma, Y., Ortiz, C., Vermaelen, K., Panaretakis, T., Mignot, G., Ullrich, E., Perfettini, J. L., Schlemmer, F., Tasdemir, E., Uhl, M., Génin, P., Civas, A., Ryffel, B., Kanellopoulos, J., Tschopp, J., André, F., … Zitvogel, L. (2009). Activation of the NLRP3 inflammasome in dendritic cells induces IL-1beta-dependent adaptive immunity against tumors. Nature medicine, 15(10), 1170–1178. https://doi.org/10.1038/nm.2028

Glatt, D. M., Beckford Vera, D. R., Parrott, M. C., Luft, J. C., Benhabbour, S. R., & Mumper, R. J. (2016). The Interplay of Antigen Affinity, Internalization, and Pharmacokinetics on CD44-Positive Tumor Targeting of Monoclonal Antibodies. Molecular pharmaceutics, 13(6), 1894–1903. https://doi.org/10.1021/acs.molpharmaceut.6b00063

Goff, B. A., Blake, J., Bamberg, M. P., & Hasan, T. (1996). Treatment of ovarian cancer with photodynamic therapy and immunoconjugates in a murine ovarian cancer model. British journal of cancer, 74(8), 1194–1198. https://doi.org/10.1038/bjc.1996.516

Goldenberg, D. M., Stein, R., & Sharkey, R. M. (2018). The emergence of trophoblast cell-surface antigen 2 (TROP-2) as a novel cancer target. Oncotarget, 9(48), 28989–29006. https://doi.org/10.18632/oncotarget.25615

Goldin-Lang, P., Tran, Q. V., Fichtner, I., Eisenreich, A., Antoniak, S., Schulze, K., Coupland, S. E., Poller, W., Schultheiss, H. P., & Rauch, U. (2008). Tissue factor expression pattern in human non-small cell lung cancer tissues indicate increased blood thrombogenicity and tumor metastasis. Oncology reports, 20(1), 123–128.

Gong, H., Kovar, J. L., Baker, B., Zhang, A., Cheung, L., Draney, D. R., Corrêa, I. R., Jr, Xu, M. Q., & Olive, D. M. (2012). Near-infrared fluorescence imaging of mammalian cells and xenograft tumors with SNAP-tag. PloS one, 7(3), e34003. https://doi.org/10.1371/journal.pone.0034003

Gong, Y. N., Guy, C., Olauson, H., Becker, J. U., Yang, M., Fitzgerald, P., Linkermann, A., & Green, D. R. (2017). ESCRT-III Acts Downstream of MLKL to Regulate Necroptotic Cell Death and Its Consequences. Cell, 169(2), 286–300.e16. https://doi.org/10.1016/j.cell.2017.03.020

Grapa, C. M., Mocan, T., Gonciar, D., Zdrehus, C., Mosteanu, O., Pop, T., & Mocan, L. (2019). Epidermal Growth Factor Receptor and Its Role in Pancreatic Cancer Treatment Mediated by Nanoparticles. International journal of nanomedicine, 14, 9693–9706. https://doi.org/10.2147/IJN.S226628

Gronemeyer, T., Chidley, C., Juillerat, A., Heinis, C., & Johnsson, K. (2006). Directed evolution of O6-alkylguanine-DNA alkyltransferase for applications in protein labeling. Protein engineering, design & selection : PEDS, 19(7), 309–316. https://doi.org/10.1093/protein/gzl014

Guan, L. Y., & Lu, Y. (2018). New developments in molecular targeted therapy of ovarian cancer. Discovery medicine, 26(144), 219–229.

Gunaydin, G., Gedik, M. E., & Ayan, S. (2021). Photodynamic Therapy-Current Limitations and Novel Approaches. Frontiers in chemistry, 9, 691697. https://doi.org/10.3389/fchem.2021.691697

Han, S. H., Ryu, K. H., & Kwon, A. Y. (2021). The Prognostic Impact of HER2 Genetic and Protein Expression in Pancreatic Carcinoma-HER2 Protein and Gene in Pancreatic Cancer. Diagnostics (Basel, Switzerland), 11(4), 653. https://doi.org/10.3390/diagnostics11040653

Harter, P., Sehouli, J., Vergote, I., Ferron, G., Reuss, A., Meier, W., Greggi, S., Mosgaard, B. J., Selle, F., Guyon, F., Pomel, C., Lécuru, F., Zang, R., Avall-Lundqvist, E., Kim, J. W., Ponce, J., Raspagliesi, F., Kristensen, G., Classe, J. M., Hillemanns, P., … DESKTOP III Investigators (2021). Randomized Trial of Cytoreductive Surgery for Relapsed Ovarian Cancer. The New England journal of medicine, 385(23), 2123–2131. https://doi.org/10.1056/NEJMoa2103294

Haunschild, C. E., & Tewari, K. S. (2020). Bevacizumab use in the frontline, maintenance and recurrent settings for ovarian cancer. Future oncology (London, England), 16(7), 225–246. https://doi.org/10.2217/fon-2019-0042

Henderson, T. A., & Morries, L. D. (2015). Near-infrared photonic energy penetration: can infrared phototherapy effectively reach the human brain?. Neuropsychiatric disease and treatment, 11, 2191–2208. https://doi.org/10.2147/NDT.S78182

Heo Y. A. (2023). Mirvetuximab Soravtansine: First Approval. Drugs, 83(3), 265–273. https://doi.org/10.1007/s40265-023-01834-3

Hirata, H., Kuwatani, M., Nakajima, K., Kodama, Y., Yoshikawa, Y., Ogawa, M., & Sakamoto, N. (2021). Near-infrared photoimmunotherapy (NIR-PIT) on cholangiocarcinoma using a novel catheter device with light emitting diodes. Cancer science, 112(2), 828–838. https://doi.org/10.1111/cas.14780

Hisada, Y., & Mackman, N. (2019). Tissue Factor and Cancer: Regulation, Tumor Growth, and Metastasis. Seminars in thrombosis and hemostasis, 45(4), 385–395. https://doi.org/10.1055/s-0039-1687894

Hishida, T., Masai, K., Kaseda, K., Asakura, K., & Asamura, H. (2021). Debulking surgery for malignant tumors: the current status, evidence and future perspectives. Japanese journal of clinical oncology, 51(9), 1349–1362. https://doi.org/10.1093/jjco/hyab107

Hiss D. (2012). Optimizing molecular-targeted therapies in ovarian cancer: the renewed surge of interest in ovarian cancer biomarkers and cell signaling pathways. Journal of oncology, 2012, 737981. https://doi.org/10.1155/2012/737981

Hu, Z., Rao, B., Chen, S., & Duanmu, J. (2010). Targeting tissue factor on tumor cells and angiogenic vascular endothelial cells by factor VII-targeted verteporfin photodynamic therapy for breast cancer in vitro and in vivo in mice. BMC cancer, 10, 235. https://doi.org/10.1186/1471-2407-10-235

Hussain, A. F., Heppenstall, P. A., Kampmeier, F., Meinhold-Heerlein, I., & Barth, S. (2019). One-step site-specific antibody fragment auto-conjugation using SNAP-tag technology. Nature protocols, 14(11), 3101–3125. https://doi.org/10.1038/s41596-019-0214-y

Hussain, A. F., Kampmeier, F., von Felbert, V., Merk, H. F., Tur, M. K., & Barth, S. (2011). SNAP-tag technology mediates site specific conjugation of antibody fragments with a photosensitizer and improves target specific phototoxicity in tumor cells. Bioconjugate chemistry, 22(12), 2487–2495. https://doi.org/10.1021/bc200304k

Huysamen, A. M., Fadeyi, O. E., Mayuni, G., Dogbey, D. M., Mungra, N., Biteghe, F. A. N., Hardcastle, N., Ramamurthy, D., Akinrinmade, O. A., Naran, K., Cooper, S., Lang, D., Richter, W., Hunter, R., & Barth, S. (2023). Click Chemistry-Generated Auristatin F-Linker-Benzylguanine for a SNAP-Tag-Based Recombinant Antibody-Drug Conjugate Demonstrating Selective Cytotoxicity toward EGFR-Overexpressing Tumor Cells. ACS omega, 8(4), 4026–4037. https://doi.org/10.1021/acsomega.2c06844

Hwang, W. T., Adams, S. F., Tahirovic, E., Hagemann, I. S., & Coukos, G. (2012). Prognostic significance of tumor-infiltrating T cells in ovarian cancer: a meta-analysis. Gynecologic oncology, 124(2), 192–198. https://doi.org/10.1016/j.ygyno.2011.09.039

Hynes, N. E., & Lane, H. A. (2005). ERBB receptors and cancer: the complexity of targeted inhibitors. Nature reviews. Cancer, 5(5), 341–354. https://doi.org/10.1038/nrc1609

Inagaki, F. F., Fujimura, D., Furusawa, A., Okada, R., Wakiyama, H., Kato, T., Choyke, P. L., & Kobayashi, H. (2021). Diagnostic imaging in near-infrared photoimmunotherapy using a commercially available camera for indocyanine green. Cancer science, 112(3), 1326–1330. https://doi.org/10.1111/cas.14809

Inagaki, F. F., Kano, M., Furusawa, A., Kato, T., Okada, R., Fukushima, H., Takao, S., Okuyama, S., Choyke, P. L., & Kobayashi, H. (2024). Near-infrared photoimmunotherapy targeting PD-L1: Improved efficacy by preconditioning the tumor microenvironment. Cancer science, 115(7), 2396–2409. https://doi.org/10.1111/cas.16195

Inagaki, F. F., Wakiyama, H., Furusawa, A., Okada, R., Kato, T., Fujimura, D., Okuyama, S., Fukushima, H., Takao, S., Choyke, P. L., & Kobayashi, H. (2023). Near-infrared photoimmunotherapy (NIR-PIT) of bone metastases. Biomedicine & pharmacotherapy = Biomedecine & pharmacotherapie, 160, 114390. https://doi.org/10.1016/j.biopha.2023.114390

Inamura, K., Yokouchi, Y., Kobayashi, M., Ninomiya, H., Sakakibara, R., Subat, S., Nagano, H., Nomura, K., Okumura, S., Shibutani, T., & Ishikawa, Y. (2017). Association of tumor TROP2 expression with prognosis varies among lung cancer subtypes. Oncotarget, 8(17), 28725–28735. https://doi.org/10.18632/oncotarget.15647

Ishihara, H., Nishikawa, D., Muraoka, D., Masago, K., Beppu, S., Terada, H., Matsushita, H., & Hanai, N. (2023). Changes in serum DAMPs and cytokines/chemokines during near-infrared photoimmunotherapy for patients with head and neck cancer. Cancer medicine, 13(1), e6863. Advance online publication. https://doi.org/10.1002/cam4.6863

Isoda, Y., Piao, W., Taguchi, E., Iwano, J., Takaoka, S., Uchida, A., Yoshikawa, K., Enokizono, J., Arakawa, E., Tomizuka, K., Shiraishi, Y., & Masuda, K. (2018). Development and evaluation of a novel antibody-photon absorber conjugate reveals the possibility of photoimmunotherapy-induced vascular occlusion during treatment in vivo. Oncotarget, 9(59), 31422–31431. https://doi.org/10.18632/oncotarget.25831

Ito, K., Mitsunaga, M., Arihiro, S., Saruta, M., Matsuoka, M., Kobayashi, H., & Tajiri, H. (2016). Molecular targeted photoimmunotherapy for HER2-positive human gastric cancer in combination with chemotherapy results in improved treatment outcomes through different cytotoxic mechanisms. BMC cancer, 16, 37. https://doi.org/10.1186/s12885-016-2072-0

Jäger, V., Büssow, K., Wagner, A., Weber, S., Hust, M., Frenzel, A., & Schirrmann, T. (2013). High level transient production of recombinant antibodies and antibody fusion proteins in HEK293 cells. BMC biotechnology, 13, 52. https://doi.org/10.1186/1472-6750-13-52

Javadi, S., Ganeshan, D. M., Qayyum, A., Iyer, R. B., & Bhosale, P. (2016). Ovarian Cancer, the Revised FIGO Staging System, and the Role of Imaging. *AJR.* American journal of roentgenology, 206(6), 1351–1360. https://doi.org/10.2214/AJR.15.15199

Jiang, W., Bell, C. W., & Pisetsky, D. S. (2007). The relationship between apoptosis and high-mobility group protein 1 release from murine macrophages stimulated with lipopolysaccharide or polyinosinic-polycytidylic acid. Journal of immunology (Baltimore, Md.: 1950), 178(10), 6495–6503. https://doi.org/10.4049/jimmunol.178.10.6495

Jiang, D., Im, H. J., Sun, H., Valdovinos, H. F., England, C. G., Ehlerding, E. B., Nickles, R. J., Lee, D. S., Cho, S. Y., Huang, P., & Cai, W. (2017). Radiolabeled pertuzumab for imaging of human epidermal growth factor receptor 2 expression in ovarian cancer. European journal of nuclear medicine and molecular imaging, 44(8), 1296–1305. https://doi.org/10.1007/s00259-017-3663-y

Jin, S., Sun, Y., Liang, X., Gu, X., Ning, J., Xu, Y., Chen, S., & Pan, L. (2022). Emerging new therapeutic antibody derivatives for cancer treatment. Signal transduction and targeted therapy, 7(1), 39. https://doi.org/10.1038/s41392-021-00868-x

Joly, A. L., Wettstein, G., Mignot, G., Ghiringhelli, F., & Garrido, C. (2010). Dual role of heat shock proteins as regulators of apoptosis and innate immunity. Journal of innate immunity, 2(3), 238–247. https://doi.org/10.1159/000296508

Jovčevska, I., & Muyldermans, S. (2020). The Therapeutic Potential of Nanobodies. BioDrugs: clinical immunotherapeutics, biopharmaceuticals and gene therapy, 34(1), 11–26. https://doi.org/10.1007/s40259-019-00392-z

Kamble, P. R., Rane, S., Breed, A. A., Joseph, S., Mahale, S. D., & Pathak, B. R. (2020). Proteolytic cleavage of Trop2 at Arg87 is mediated by matriptase and regulated by Val194. FEBS letters, 594(19), 3156–3169. https://doi.org/10.1002/1873-3468.13899

Kampmeier, F., Niesen, J., Koers, A., Ribbert, M., Brecht, A., Fischer, R., Kiessling, F., Barth, S., & Thepen, T. (2010). Rapid optical imaging of EGF receptor expression with a single-chain antibody SNAP-tag fusion protein. European journal of nuclear medicine and molecular imaging, 37(10), 1926–1934. https://doi.org/10.1007/s00259-010-1482-5

Karpel, H. C., Powell, S. S., & Pothuri, B. (2023). Antibody-Drug Conjugates in Gynecologic Cancer. American Society of Clinical Oncology educational book. American Society of Clinical Oncology. Annual Meeting, 43, e390772. https://doi.org/10.1200/EDBK_390772

Kasi, P. M., Afable, M. G., Herting, C., Lukanowski, M., & Jin, Z. (2023). Anti-EGFR Antibodies in the Management of Advanced Colorectal Cancer. The oncologist, 28(12), 1034–1048. https://doi.org/10.1093/oncolo/oyad262

Kasikova, L., Hensler, M., Truxova, I., Skapa, P., Laco, J., Belicova, L., Praznovec, I., Vosahlikova, S., Halaska, M. J., Brtnicky, T., Rob, L., Presl, J., Kostun, J., Cremer, I., Ryska, A., Kroemer, G., Galluzzi, L., Spisek, R., & Fucikova, J. (2019). Calreticulin exposure correlates with robust adaptive antitumor immunity and favorable prognosis in ovarian carcinoma patients. Journal for immunotherapy of cancer, 7(1), 312. https://doi.org/10.1186/s40425-019-0781-z

Kato, T., Furusawa, A., Okada, R., Inagaki, F., Wakiyama, H., Furumoto, H., Fukushima, H., Okuyama, S., Choyke, P. L., & Kobayashi, H. (2023). Near-Infrared Photoimmunotherapy Targeting Podoplanin-Expressing Cancer Cells and Cancer-Associated Fibroblasts. Molecular cancer therapeutics, 22(1), 75–88. https://doi.org/10.1158/1535-7163.MCT-22-0313

Kato, T., Okada, R., Goto, Y., Furusawa, A., Inagaki, F., Wakiyama, H., Furumoto, H., Daar, D., Turkbey, B., Choyke, P. L., Takakura, H., Inanami, O., Ogawa, M., & Kobayashi, H. (2021a). Electron Donors Rather Than Reactive Oxygen Species Needed for Therapeutic Photochemical Reaction of Near-Infrared Photoimmunotherapy. ACS pharmacology & translational science, 4(5), 1689–1701. https://doi.org/10.1021/acsptsci.1c00184

Kato, T., Wakiyama, H., Furusawa, A., Choyke, P. L., & Kobayashi, H. (2021b). Near Infrared Photoimmunotherapy; A Review of Targets for Cancer Therapy. Cancers, 13(11), 2535. https://doi.org/10.3390/cancers13112535

Keam S. J. (2020). Trastuzumab Deruxtecan: First Approval. Drugs, 80(5), 501–508. https://doi.org/10.1007/s40265-020-01281-4

Keppler, A., Gendreizig, S., Gronemeyer, T., Pick, H., Vogel, H., & Johnsson, K. (2003). A general method for the covalent labeling of fusion proteins with small molecules in vivo. Nature biotechnology, 21(1), 86–89. https://doi.org/10.1038/nbt765

Keppler, A., Pick, H., Arrivoli, C., Vogel, H., & Johnsson, K. (2004). Labeling of fusion proteins with synthetic fluorophores in live cells. Proceedings of the National Academy of Sciences of the United States of America, 101(27), 9955–9959. https://doi.org/10.1073/pnas.0401923101

Khan, N., Lawlor, K. E., Murphy, J. M., & Vince, J. E. (2014). More to life than death: molecular determinants of necroptotic and non-necroptotic RIP3 kinase signaling. Current opinion in immunology, 26, 76–89. https://doi.org/10.1016/j.coi.2013.10.017

Khongorzul, P., Ling, C. J., Khan, F. U., Ihsan, A. U., & Zhang, J. (2020). Antibody-Drug Conjugates: A Comprehensive Review. Molecular cancer research: MCR, 18(1), 3–19. https://doi.org/10.1158/1541-7786.MCR-19-0582

Kielbik, M., Szulc-Kielbik, I., & Klink, M. (2021). Calreticulin-Multifunctional Chaperone in Immunogenic Cell Death: Potential Significance as a Prognostic Biomarker in Ovarian Cancer Patients. Cells, 10(1), 130. https://doi.org/10.3390/cells10010130

Kishimoto, S., Oshima, N., Yamamoto, K., Munasinghe, J., Ardenkjaer-Larsen, J. H., Mitchell, J. B., Choyke, P. L., & Krishna, M. C. (2018). Molecular imaging of tumor photoimmunotherapy: Evidence of photosensitized tumor necrosis and hemodynamic changes. Free radical biology &

Kiss, B., van den Berg, N. S., Ertsey, R., McKenna, K., Mach, K. E., Zhang, C. A., Volkmer, J. P., Weissman, I. L., Rosenthal, E. L., & Liao, J. C. (2019). CD47-Targeted Near-Infrared Photoimmunotherapy for Human Bladder Cancer. Clinical cancer research: an official journal of the American Association for Cancer Research, 25(12), 3561–3571. https://doi.org/10.1158/1078-0432.CCR-18-3267

Kobayashi, H., & Choyke, P. L. (2019). Near-Infrared Photoimmunotherapy of Cancer. Accounts of chemical research, 52(8), 2332–2339. https://doi.org/10.1021/acs.accounts.9b00273

Kobayashi, H., Furusawa, A., Rosenberg, A., & Choyke, P. L. (2021). Near-infrared photoimmunotherapy of cancer: a new approach that kills cancer cells and enhances anti-cancer host immunity. International immunology, 33(1), 7–15. https://doi.org/10.1093/intimm/dxaa037

Kobayashi, H., Griffiths, G. L., & Choyke, P. L. (2020). Near-Infrared Photoimmunotherapy: Photoactivatable Antibody-Drug Conjugates (ADCs). Bioconjugate chemistry, 31(1), 28–36. https://doi.org/10.1021/acs.bioconjchem.9b00546

Konner, J. A., Bell-McGuinn, K. M., Sabbatini, P., Hensley, M. L., Tew, W. P., Pandit-Taskar, N., Vander Els, N., Phillips, M. D., Schweizer, C., Weil, S. C., Larson, S. M., & Old, L. J. (2010). Farletuzumab, a humanized monoclonal antibody against folate receptor alpha, in epithelial ovarian cancer: a phase I study. Clinical cancer research: an official journal of the American Association for Cancer Research, 16(21), 5288–5295. https://doi.org/10.1158/1078-0432.CCR-10-0700

Konstantinopoulos, P. A., & Matulonis, U. A. (2023). Clinical and translational advances in ovarian cancer therapy. Nature cancer, 4(9), 1239–1257. https://doi.org/10.1038/s43018-023-00617-9

Kumar, S., Dorstyn, L., & Lim, Y. (2022). The role of caspases as executioners of apoptosis. Biochemical Society transactions, 50(1), 33–45. https://doi.org/10.1042/BST20210751

Lamberti, M. J., Nigro, A., Mentucci, F. M., Rumie Vittar, N. B., Casolaro, V., & Dal Col, J. (2020). Dendritic Cells and Immunogenic Cancer Cell Death: A Combination for Improving Antitumor Immunity. Pharmaceutics, 12(3), 256. https://doi.org/10.3390/pharmaceutics12030256

Lee, N. Y., Hazlett, T. L., & Koland, J. G. (2006). Structure and dynamics of the epidermal growth factor receptor C-terminal phosphorylation domain. Protein science: a publication of the Protein Society, 15(5), 1142–1152. https://doi.org/10.1110/ps.052045306

Lee, Y. T., Tan, Y. J., & Oon, C. E. (2018). Molecular targeted therapy: Treating cancer with specificity. European journal of pharmacology, 834, 188–196. https://doi.org/10.1016/j.ejphar.2018.07.034

Lenárt, S., Lenárt, P., Šmarda, J., Remšík, J., Souček, K., & Beneš, P. (2020). Trop2: Jack of All Trades, Master of None. Cancers, 12(11), 3328. https://doi.org/10.3390/cancers12113328

Lheureux, S., Braunstein, M., & Oza, A. M. (2019). Epithelial ovarian cancer: Evolution of management in the era of precision medicine. CA: a cancer journal for clinicians, 69(4), 280–304. https://doi.org/10.3322/caac.21559

Li, F., Zhao, Y., Mao, C., Kong, Y., & Ming, X. (2017). RGD-Modified Albumin Nanoconjugates for Targeted Delivery of a Porphyrin Photosensitizer. Molecular pharmaceutics, 14(8), 2793–2804. https://doi.org/10.1021/acs.molpharmaceut.7b00321

Li, X., Lovell, J. F., Yoon, J., & Chen, X. (2020). Clinical development and potential of photothermal and photodynamic therapies for cancer. Nature reviews. Clinical oncology, 17(11), 657–674. https://doi.org/10.1038/s41571-020-0410-2

Li, Z., Yin, Y., Jin, W., Zhang, B., Yan, H., Mei, H., Wang, H., Guo, T., Shi, W., & Hu, Y. (2020). Tissue Factor-Targeted "O2-Evolving" Nanoparticles for Photodynamic Therapy in Malignant Lymphoma. Frontiers in oncology, 10, 524712. https://doi.org/10.3389/fonc.2020.524712

Liang, C. P., Nakajima, T., Watanabe, R., Sato, K., Choyke, P. L., Chen, Y., & Kobayashi, H. (2014). Real-time monitoring of hemodynamic changes in tumor vessels during photoimmunotherapy using optical coherence tomography. Journal of biomedical optics, 19(9), 98004. https://doi.org/10.1117/1.JBO.19.9.098004

Liberto, J. M., Chen, S. Y., Shih, I. M., Wang, T. H., Wang, T. L., & Pisanic, T. R., 2nd (2022). Current and Emerging Methods for Ovarian Cancer Screening and Diagnostics: A Comprehensive Review. Cancers, 14(12), 2885. https://doi.org/10.3390/cancers14122885

Liu, H., Zhao, Z., Zhang, L., Li, Y., Jain, A., Barve, A., Jin, W., Liu, Y., Fetse, J., & Cheng, K. (2019). Discovery of low-molecular weight anti-PD-L1 peptides for cancer immunotherapy. Journal for immunotherapy of cancer, 7(1), 270. https://doi.org/10.1186/s40425-019-0705-y

Liu, T., Liu, Y., Bao, X., Tian, J., Liu, Y., & Yang, X. (2013). Overexpression of TROP2 predicts poor prognosis of patients with cervical cancer and promotes the proliferation and invasion of cervical cancer cells by regulating ERK signaling pathway. PloS one, 8(9), e75864. https://doi.org/10.1371/journal.pone.0075864

Liu, Z., Xie, Z., Li, W., Wu, X., Jiang, X., Li, G., Cao, L., Zhang, D., Wang, Q., Xue, P., & Zhang, H. (2021). Photodynamic immunotherapy of cancers based on nanotechnology: recent advances and future challenges. Journal of nanobiotechnology, 19(1), 160. https://doi.org/10.1186/s12951-021-00903-7

Lo, L., Valentine, H., Harrison, J., Hayes, S., Welch, I., Pritchard, S., West, C., & Ang, Y. (2012). Tissue factor expression in the metaplasia-adenoma-carcinoma sequence of gastric cancer in a European population. British journal of cancer, 107(7), 1125–1130. https://doi.org/10.1038/bjc.2012.363

Luhrs, C. A., & Slomiany, B. L. (1989). A human membrane-associated folate binding protein is anchored by a glycosyl-phosphatidylinositol tail. The Journal of biological chemistry, 264(36), 21446–21449.

Luo, H., Xu, X., Ye, M., Sheng, B., & Zhu, X. (2018). The prognostic value of HER2 in ovarian cancer: A meta-analysis of observational studies. PloS one, 13(1), e0191972. https://doi.org/10.1371/journal.pone.0191972

Mączyńska, J., Da Pieve, C., Burley, T. A., Raes, F., Shah, A., Saczko, J., Harrington, K. J., & Kramer-Marek, G. (2020). Immunomodulatory activity of IR700-labelled affibody targeting HER2. Cell death & disease, 11(10), 886. https://doi.org/10.1038/s41419-020-03077-6

Mączyńska, J., Raes, F., Da Pieve, C., Turnock, S., Boult, J. K. R., Hoebart, J., Niedbala, M., Robinson, S. P., Harrington, K. J., Kaspera, W., & Kramer-Marek, G. (2022). Triggering anti-GBM immune response with EGFR-mediated photoimmunotherapy. BMC medicine, 20(1), 16. https://doi.org/10.1186/s12916-021-02213-z

Maennling, A. E., Tur, M. K., Niebert, M., Klockenbring, T., Zeppernick, F., Gattenlöhner, S., Meinhold-Heerlein, I., & Hussain, A. F. (2019). Molecular Targeting Therapy against EGFR Family in Breast Cancer: Progress and Future Potentials. Cancers, 11(12), 1826. https://doi.org/10.3390/cancers11121826

Mahner, S., Heitz, F., Burges, A., Reuss, A., Kraemer, B., Schmalfeldt, B., Jalid Sehouli, J., Lampe, B., Schnelzer, A., Wimberger, P., Fotopoulou, C., Guyon, F., Lecuru, F., Querleu, D., Greggi, S., Colombo, N., Aletti, G. D., Harter, P., Bois, A. D. (2017). TRUST: Trial of radical upfront surgical therapy in advanced ovarian cancer (ENGOT ov33/AGO-OVAR OP7). Journal of Clinical Oncology 35:15. https://doi.org/10.1200/JCO.2017.35.15_suppl.TPS56

Manzano, A., & Ocaña, A. (2020). Antibody-Drug Conjugates: A Promising Novel Therapy for the Treatment of Ovarian Cancer. Cancers, 12(8), 2223. https://doi.org/10.3390/cancers12082223

Markham A. (2021). Tisotumab Vedotin: First Approval. Drugs, 81(18), 2141–2147. https://doi.org/10.1007/s40265-021-01633-8

Marmé F. (2022). Antibody-Drug Conjugates for Breast Cancer. Oncology research and treatment, 45(1-2), 26–36. https://doi.org/10.1159/000521499

Martins, I., Wang, Y., Michaud, M., Ma, Y., Sukkurwala, A. Q., Shen, S., Kepp, O., Métivier, D., Galluzzi, L., Perfettini, J. L., Zitvogel, L., & Kroemer, G. (2014). Molecular mechanisms of ATP secretion during immunogenic cell death. Cell death and differentiation, 21(1), 79–91. https://doi.org/10.1038/cdd.2013.75

Maruoka, Y., Furusawa, A., Okada, R., Inagaki, F., Fujimura, D., Wakiyama, H., Kato, T., Nagaya, T., Choyke, P. L., & Kobayashi, H. (2020). Combined CD44- and CD25-Targeted Near-Infrared Photoimmunotherapy Selectively Kills Cancer and Regulatory T Cells in Syngeneic Mouse Cancer Models. Cancer immunology research, 8(3), 345–355. https://doi.org/10.1158/2326-6066.CIR-19-0517

Maruoka, Y., Wakiyama, H., Choyke, P. L., & Kobayashi, H. (2021). Near infrared photoimmunotherapy for cancers: A translational perspective. EBioMedicine, 70, 103501. https://doi.org/10.1016/j.ebiom.2021.103501

Mas, L., Cros, J., Svrcek, M., Van Laethem, J. L., Emile, J. F., Rebours, V., Nicolle, R., & Bachet, J. B. (2023). Trop-2 is a ubiquitous and promising target in pancreatic adenocarcinoma. Clinics and research in hepatology and gastroenterology, 47(4), 102108. https://doi.org/10.1016/j.clinre.2023.102108

Matulonis, U. A., Sood, A. K., Fallowfield, L., Howitt, B. E., Sehouli, J., & Karlan, B. Y. (2016). Ovarian cancer. Nature reviews. Disease primers, 2, 16061. https://doi.org/10.1038/nrdp.2016.61

McCord, E., Pawar, S., Koneru, T., Tatiparti, K., Sau, S., & Iyer, A. K. (2021). Folate Receptors' Expression in Gliomas May Possess Potential Nanoparticle-Based Drug Delivery Opportunities. ACS omega, 6(6), 4111–4118. https://doi.org/10.1021/acsomega.0c05500

Meinhold-Heerlein, I., Fotopoulou, C., Harter, P., Kurzeder, C., Mustea, A., Wimberger, P., Hauptmann, S., Sehouli, J., & Kommission Ovar of the AGO (2015). Statement by the Kommission Ovar of the AGO: The New FIGO and WHO Classifications of Ovarian, Fallopian Tube and Primary Peritoneal Cancer. Geburtshilfe und Frauenheilkunde, 75(10), 1021–1027. https://doi.org/10.1055/s-0035-1558079

Ménard, S., Tagliabue, E., Campiglio, M., & Pupa, S. M. (2000). Role of HER2 gene overexpression in breast carcinoma. Journal of cellular physiology, 182(2), 150–162. https://doi.org/10.1002/(SICI)1097-4652(200002)182:2<150::AID-JCP3>3.0.CO;2-E

Mickler, F. M., Möckl, L., Ruthardt, N., Ogris, M., Wagner, E., & Bräuchle, C. (2012). Tuning nanoparticle uptake: live-cell imaging reveals two distinct endocytosis mechanisms mediated by natural and artificial EGFR targeting ligand. Nano letters, 12(7), 3417–3423. https://doi.org/10.1021/nl300395q

Min, H. Y., & Lee, H. Y. (2022). Molecular targeted therapy for anticancer treatment. Experimental & molecular medicine, 54(10), 1670–1694. https://doi.org/10.1038/s12276-022-00864-3

Minner, S., Rump, D., Tennstedt, P., Simon, R., Burandt, E., Terracciano, L., Moch, H., Wilczak, W., Bokemeyer, C., Fisch, M., Sauter, G., & Eichelberg, C. (2012). Epidermal growth factor receptor protein expression and genomic alterations in renal cell carcinoma. Cancer, 118(5), 1268–1275. https://doi.org/10.1002/cncr.26436

Mitsunaga, M., Nakajima, T., Sano, K., Choyke, P. L., & Kobayashi, H. (2012). Near-infrared theranostic photoimmunotherapy (PIT): repeated exposure of light enhances the effect of immunoconjugate. Bioconjugate chemistry, 23(3), 604–609. https://doi.org/10.1021/bc200648m

Mitsunaga, M., Ogawa, M., Kosaka, N., Rosenblum, L. T., Choyke, P. L., & Kobayashi, H. (2011). Cancer cell-selective in vivo near infrared photoimmunotherapy targeting specific membrane molecules. Nature medicine, 17(12), 1685–1691. https://doi.org/10.1038/nm.2554

Mohiuddin, T. M., Zhang, C., Sheng, W., Al-Rawe, M., Zeppernick, F., Meinhold-Heerlein, I., & Hussain, A. F. (2023). Near Infrared Photoimmunotherapy: A Review of Recent Progress and Their Target Molecules for Cancer Therapy. International journal of molecular sciences, 24(3), 2655. https://doi.org/10.3390/ijms24032655

Momenimovahed, Z., Tiznobaik, A., Taheri, S., & Salehiniya, H. (2019). Ovarian cancer in the world: epidemiology and risk factors. International journal of women's health, 11, 287–299. https://doi.org/10.2147/IJWH.S197604

Monaco, H., Yokomizo, S., Choi, H. S., & Kashiwagi, S. (2022). Quickly evolving near-infrared photoimmunotherapy provides multifaceted approach to modern cancer treatment. View (Beijing, China), 3(3), 20200110. https://doi.org/10.1002/VIW.20200110

Mungra, N., Biteghe, F. A. N., Malindi, Z., Huysamen, A. M., Karaan, M., Hardcastle, N. S., Bunjun, R., Chetty, S., Naran, K., Lang, D., Richter, W., Hunter, R., & Barth, S. (2023). CSPG4 as a target for the specific killing of triple-negative breast cancer cells by a recombinant SNAP-tag-based antibody-auristatin F drug conjugate. Journal of cancer research and clinical oncology, 149(13), 12203–12225. https://doi.org/10.1007/s00432-023-05031-3

Murao, A., Aziz, M., Wang, H., Brenner, M., & Wang, P. (2021). Release mechanisms of major DAMPs. Apoptosis: an international journal on programmed cell death, 26(3-4), 152–162. https://doi.org/10.1007/s10495-021-01663-3

Mussini, A., Uriati, E., Bianchini, P., Diaspro, A., Cavanna, L., Abbruzzetti, S., & Viappiani, C. (2022). Targeted photoimmunotherapy for cancer. Biomolecular concepts, 13(1), 126–147. https://doi.org/10.1515/bmc-2022-0010

Nagaya, T., Sato, K., Harada, T., Nakamura, Y., Choyke, P. L., & Kobayashi, H. (2015). Near Infrared Photoimmunotherapy Targeting EGFR Positive Triple Negative Breast Cancer: Optimizing the Conjugate-Light Regimen. *PloS one*, *10*(8), e0136829. https://doi.org/10.1371/journal.pone.0136829

Nagaya, T., Friedman, J., Maruoka, Y., Ogata, F., Okuyama, S., Clavijo, P. E., Choyke, P. L., Allen, C., & Kobayashi, H. (2019a). Host Immunity Following Near-Infrared Photoimmunotherapy Is Enhanced with PD-1 Checkpoint Blockade to Eradicate Established Antigenic Tumors. Cancer immunology research, 7(3), 401–413. https://doi.org/10.1158/2326-6066.CIR-18-0546

Nagaya, T., Nakamura, Y., Okuyama, S., Ogata, F., Maruoka, Y., Choyke, P. L., & Kobayashi, H. (2017). Near-Infrared Photoimmunotherapy Targeting Prostate Cancer with Prostate-Specific Membrane Antigen (PSMA) Antibody. Molecular cancer research: MCR, 15(9), 1153–1162. https://doi.org/10.1158/1541-7786.MCR-17-0164

Nagaya, T., Okuyama, S., Ogata, F., Maruoka, Y., Choyke, P. L., & Kobayashi, H. (2018). Endoscopic near infrared photoimmunotherapy using a fiber optic diffuser for peritoneal dissemination of gastric cancer. Cancer science, 109(6), 1902–1908. https://doi.org/10.1111/cas.13621

Nagaya, T., Okuyama, S., Ogata, F., Maruoka, Y., Choyke, P. L., & Kobayashi, H. (2019b). Near infrared photoimmunotherapy using a fiber optic diffuser for treating peritoneal gastric cancer dissemination. Gastric cancer: official journal of the International Gastric Cancer Association and the Japanese Gastric Cancer Association, 22(3), 463–472. https://doi.org/10.1007/s10120-018-0871-5

Nakajima, K., & Ogawa, M. (2020). Phototoxicity in near-infrared photoimmunotherapy is influenced by the subcellular localization of antibody-IR700. Photodiagnosis and photodynamic therapy, 31, 101926. https://doi.org/10.1016/j.pdpdt.2020.101926

Nakajima, K., & Ogawa, M. (2024). Near-infrared photoimmunotherapy and anti-cancer immunity. International immunology, 36(2), 57–64. https://doi.org/10.1093/intimm/dxad042

Nakajima, K., Miyazaki, F., Terada, K., Takakura, H., Suzuki, M., & Ogawa, M. (2021). Comparison of low-molecular-weight ligand and whole antibody in prostate-specific membrane antigen targeted near-infrared photoimmunotherapy. International journal of pharmaceutics, 609, 121135. https://doi.org/10.1016/j.ijpharm.2021.121135

Nakajima, K., Sugikawa, A., Yasui, H., Higashikawa, K., Suzuki, C., Natsume, T., Suzuki, M., Takakura, H., Tomita, M., Takahashi, S., Hirata, K., Magata, Y., Kuge, Y., & Ogawa, M. (2023). In vivo imaging of acute physiological responses after treatment of cancer with near-infrared photoimmunotherapy. Molecular imaging and biology, 25(4), 648–658. https://doi.org/10.1007/s11307-023-01822-9

Nakajima, K., Takakura, H., Shimizu, Y., & Ogawa, M. (2018). Changes in plasma membrane damage inducing cell death after treatment with near-infrared photoimmunotherapy. Cancer science, 109(9), 2889–2896. https://doi.org/10.1111/cas.13713

Nakajima, T., Sato, K., Hanaoka, H., Watanabe, R., Harada, T., Choyke, P. L., & Kobayashi, H. (2014). The effects of conjugate and light dose on photo-immunotherapy induced cytotoxicity. BMC cancer, 14, 389. https://doi.org/10.1186/1471-2407-14-389

Narayan, P., Dilawari, A., Osgood, C., Feng, Z., Bloomquist, E., Pierce, W. F., Jafri, S., Kalavar, S., Kondratovich, M., Jha, P., Ghosh, S., Tang, S., Pazdur, R., Beaver, J. A., & Amiri-Kordestani, L. (2023). US Food and Drug Administration Approval Summary: Fam-Trastuzumab Deruxtecan-nxki for Human Epidermal Growth Factor Receptor 2-Low Unresectable or Metastatic Breast Cancer. Journal of clinical oncology: official journal of the American Society of Clinical Oncology, 41(11), 2108–2116. https://doi.org/10.1200/JCO.22.02447

Neitemeier, S., Jelinek, A., Laino, V., Hoffmann, L., Eisenbach, I., Eying, R., Ganjam, G. K., Dolga, A. M., Oppermann, S., & Culmsee, C. (2017). BID links ferroptosis to mitochondrial cell death pathways. Redox biology, 12, 558–570. https://doi.org/10.1016/j.redox.2017.03.007

Newton K. (2015). RIPK1 and RIPK3: critical regulators of inflammation and cell death. Trends in cell biology, 25(6), 347–353. https://doi.org/10.1016/j.tcb.2015.01.001

Nguyen, Q. D., Das, A., Do, D. V., Dugel, P. U., Gomes, A., Holz, F. G., Koh, A., Pan, C. K., Sepah, Y. J., Patel, N., MacLeod, H., & Maurer, P. (2020). Brolucizumab: Evolution through Preclinical and Clinical Studies and the Implications for the Management of Neovascular Age-Related Macular Degeneration. Ophthalmology, 127(7), 963–976. https://doi.org/10.1016/j.ophtha.2019.12.031

Nishimura, T., Mitsunaga, M., Ito, K., Kobayashi, H., & Saruta, M. (2020). Cancer neovasculature-targeted near-infrared photoimmunotherapy (NIR-PIT) for gastric cancer: different mechanisms of phototoxicity compared to cell membrane-targeted NIR-PIT. Gastric cancer: official journal of the International Gastric Cancer Association and the Japanese Gastric Cancer Association, 23(1), 82–94. https://doi.org/10.1007/s10120-019-00988-y

Nishimura, T., Mitsunaga, M., Sawada, R., Saruta, M., Kobayashi, H., Matsumoto, N., Kanke, T., Yanai, H., & Nakamura, K. (2019). Photoimmunotherapy targeting biliary-pancreatic cancer with humanized anti-TROP2 antibody. Cancer medicine, 8(18), 7781–7792. https://doi.org/10.1002/cam4.2658

Nitori, N., Ino, Y., Nakanishi, Y., Yamada, T., Honda, K., Yanagihara, K., Kosuge, T., Kanai, Y., Kitajima, M., & Hirohashi, S. (2005). Prognostic significance of tissue factor in pancreatic ductal adenocarcinoma. Clinical cancer research: an official journal of the American Association for Cancer Research, 11(7), 2531–2539. https://doi.org/10.1158/1078-0432.CCR-04-0866

Normanno, N., De Luca, A., Bianco, C., Strizzi, L., Mancino, M., Maiello, M. R., Carotenuto, A., De Feo, G., Caponigro, F., & Salomon, D. S. (2006). Epidermal growth factor receptor (EGFR) signaling in cancer. Gene, 366(1), 2–16. https://doi.org/10.1016/j.gene.2005.10.018

Norquist, B. M., Harrell, M. I., Brady, M. F., Walsh, T., Lee, M. K., Gulsuner, S., Bernards, S. S., Casadei, S., Yi, Q., Burger, R. A., Chan, J. K., Davidson, S. A., Mannel, R. S., DiSilvestro, P. A., Lankes, H. A., Ramirez, N. C., King, M. C., Swisher, E. M., & Birrer, M. J. (2016). Inherited Mutations in Women With Ovarian Carcinoma. JAMA oncology, 2(4), 482–490. https://doi.org/10.1001/jamaoncol.2015.5495

Norton, N., Youssef, B., Hillman, D. W., Nassar, A., Geiger, X. J., Necela, B. M., Liu, H., Ruddy, K. J., Polley, M. C., Ingle, J. N., Couch, F. J., Perez, E. A., Liu, M. C., Carter, J. M., Leon-Ferre, R. A., Boughey, J. C., Somers, E. B., Kalari, K. R., Visscher, D. W., Goetz, M. P., … Knutson, K. L. (2020). Folate receptor alpha expression associates with improved disease-free survival in triple negative breast cancer patients. NPJ breast cancer, 6, 4. https://doi.org/10.1038/s41523-020-0147-1

Nurgül, K., Jagoe, R. T., & Abalo, R. (2018). Editorial: Adverse Effects of Cancer Chemotherapy: Anything New to Improve Tolerance and Reduce Sequelae?. Frontiers in pharmacology, 9, 245. https://doi.org/10.3389/fphar.2018.00245

Ogawa, M., Tomita, Y., Nakamura, Y., Lee, M. J., Lee, S., Tomita, S., Nagaya, T., Sato, K., Yamauchi, T., Iwai, H., Kumar, A., Haystead, T., Shroff, H., Choyke, P. L., Trepel, J. B., & Kobayashi, H. (2017). Immunogenic cancer cell death selectively induced by near infrared photoimmunotherapy initiates host tumor immunity. Oncotarget, 8(6), 10425–10436. https://doi.org/10.18632/oncotarget.14425

Ohmachi, T., Tanaka, F., Mimori, K., Inoue, H., Yanaga, K., & Mori, M. (2006). Clinical significance of TROP2 expression in colorectal cancer. Clinical cancer research: an official journal of the American Association for Cancer Research, 12(10), 3057–3063. https://doi.org/10.1158/1078-0432.CCR-05-1961

Okada, R., Furusawa, A., Vermeer, D. W., Inagaki, F., Wakiyama, H., Kato, T., Nagaya, T., Choyke, P. L., Spanos, W. C., Allen, C. T., & Kobayashi, H. (2021). Near-infrared photoimmunotherapy targeting human-EGFR in a mouse tumor model simulating current and future clinical trials. EBioMedicine, 67, 103345. https://doi.org/10.1016/j.ebiom.2021.103345

Okada, R., Kato, T., Furusawa, A., Inagaki, F., Wakiyama, H., Fujimura, D., Okuyama, S., Furumoto, H., Fukushima, H., Choyke, P. L., & Kobayashi, H. (2022). Selection of antibody and light exposure regimens alters therapeutic effects of EGFR-targeted near-infrared photoimmunotherapy. Cancer immunology, immunotherapy: CII, 71(8), 1877–1887. https://doi.org/10.1007/s00262-021-03124-x

Oliveira, L. R. L. B., Horvat, N., Andrieu, P. I. C., Panizza, P. S. B., Cerri, G. G., & Viana, P. C. C. (2021). Ovarian cancer staging: What the surgeon needs to know. The British journal of radiology, 94(1125), 20210091. https://doi.org/10.1259/bjr.20210091

Ono, M., & Kuwano, M. (2006). Molecular mechanisms of epidermal growth factor receptor (EGFR) activation and response to gefitinib and other EGFR-targeting drugs. Clinical cancer research: an official journal of the American Association for Cancer Research, 12(24), 7242–7251. https://doi.org/10.1158/1078-0432.CCR-06-0646

Opaliński, Ł., Szymczyk, J., Szczepara, M., Kucińska, M., Krowarsch, D., Zakrzewska, M., & Otlewski, J. (2018). High Affinity Promotes Internalization of Engineered Antibodies Targeting FGFR1. International journal of molecular sciences, 19(5), 1435. https://doi.org/10.3390/ijms19051435

O'Shannessy, D. J., Yu, G., Smale, R., Fu, Y. S., Singhal, S., Thiel, R. P., Somers, E. B., & Vachani, A. (2012). Folate receptor alpha expression in lung cancer: diagnostic and prognostic significance. Oncotarget, 3(4), 414–425. https://doi.org/10.18632/oncotarget.519

Oza, A. M., Cook, A. D., Pfisterer, J., Embleton, A., Ledermann, J. A., Pujade-Lauraine, E., Kristensen, G., Carey, M. S., Beale, P., Cervantes, A., Park-Simon, T. W., Rustin, G., Joly, F., Mirza, M. R., Plante, M., Quinn, M., Poveda, A., Jayson, G. C., Stark, D., Swart, A. M., … ICON7 trial investigators (2015). Standard chemotherapy with or without bevacizumab for women with newly diagnosed ovarian cancer (ICON7): overall survival results of a phase 3 randomised trial. *The Lancet. Oncology*, *16*(8), 928–936. https://doi.org/10.1016/S1470-2045(15)00086-8

Pabla, B., Bissonnette, M., & Konda, V. J. (2015). Colon cancer and the epidermal growth factor receptor: Current treatment paradigms, the importance of diet, and the role of chemoprevention. World journal of clinical oncology, 6(5), 133–141. https://doi.org/10.5306/wjco.v6.i5.133

Paraboschi, I., Turnock, S., Kramer-Marek, G., Musleh, L., Barisa, M., Anderson, J., & Giuliani, S. (2021). Near-InfraRed PhotoImmunoTherapy (NIR-PIT) for the local control of solid cancers: Challenges and potentials for human applications. Critical reviews in oncology/hematology, 161, 103325. https://doi.org/10.1016/j.critrevonc.2021.103325

Parashar, D., Nair, B., Geethadevi, A., George, J., Nair, A., Tsaih, S. W., Kadamberi, I. P., Gopinadhan Nair, G. K., Lu, Y., Ramchandran, R., Uyar, D. S., Rader, J. S., Ram, P. T., Mills, G. B., Pradeep, S., & Chaluvally-Raghavan, P. (2020). Peritoneal Spread of Ovarian Cancer Harbors Therapeutic Vulnerabilities Regulated by FOXM1 and EGFR/ERBB2 Signaling. Cancer research, 80(24), 5554–5568. https://doi.org/10.1158/0008-5472.CAN-19-3717

Peng, F., Liao, M., Qin, R., Zhu, S., Peng, C., Fu, L., Chen, Y., & Han, B. (2022). Regulated cell death (RCD) in cancer: key pathways and targeted therapies. Signal transduction and targeted therapy, 7(1), 286. https://doi.org/10.1038/s41392-022-01110-y

Peng, Z., Lv, X., & Huang, S. (2022). Photoimmunotherapy: A New Paradigm in Solid Tumor Immunotherapy. Cancer Control: Journal of the Moffitt Cancer Center, 29, 10732748221088825. https://doi.org/10.1177/10732748221088825

Pfisterer, J., Weber, B., Reuss, A., Kimmig, R., du Bois, A., Wagner, U., Bourgeois, H., Meier, W., Costa, S., Blohmer, J. U., Lortholary, A., Olbricht, S., Stähle, A., Jackisch, C., Hardy-Bessard, A. C., Möbus, V., Quaas, J., Richter, B., Schröder, W., Geay, J. F., … GINECO (2006). Randomized phase III trial of topotecan following carboplatin and paclitaxel in first-line treatment of advanced ovarian cancer: a gynecologic cancer intergroup trial of the AGO-OVAR and GINECO. Journal of the National Cancer Institute, 98(15), 1036–1045. https://doi.org/10.1093/jnci/djj296

Phi, L. T. H., Sari, I. N., Yang, Y. G., Lee, S. H., Jun, N., Kim, K. S., Lee, Y. K., & Kwon, H. Y. (2018). Cancer Stem Cells (CSCs) in Drug Resistance and their Therapeutic Implications in Cancer Treatment. Stem cells international, 2018, 5416923. https://doi.org/10.1155/2018/5416923

Pirkalkhoran, S., Grabowska, W. R., Kashkoli, H. H., Mirhassani, R., Guiliano, D., Dolphin, C., & Khalili, H. (2023). Bioengineering of Antibody Fragments: Challenges and Opportunities. Bioengineering (Basel, Switzerland), 10(2), 122. https://doi.org/10.3390/bioengineering10020122

Potti, A., Willardson, J., Forseen, C., Kishor Ganti, A., Koch, M., Hebert, B., Levitt, R., & Mehdi, S. A. (2002). Predictive role of HER-2/neu overexpression and clinical features at initial presentation in patients with extensive stage small cell lung carcinoma. Lung cancer (Amsterdam, Netherlands), 36(3), 257–261. https://doi.org/10.1016/s0169-5002(01)00488-3

Rafidi, H., Rajan, S., Urban, K., Shatz-Binder, W., Hui, K., Ferl, G. Z., Kamath, A. V., & Boswell, C. A. (2022). Effect of molecular size on interstitial pharmacokinetics and tissue catabolism of antibodies. mAbs, 14(1), 2085535. https://doi.org/10.1080/19420862.2022.2085535

Railkar, R., Krane, L. S., Li, Q. Q., Sanford, T., Siddiqui, M. R., Haines, D., Vourganti, S., Brancato, S. J., Choyke, P. L., Kobayashi, H., & Agarwal, P. K. (2017). Epidermal Growth Factor Receptor (EGFR)-targeted Photoimmunotherapy (PIT) for the Treatment of EGFR-expressing Bladder Cancer. Molecular cancer therapeutics, 16(10), 2201–2214. https://doi.org/10.1158/1535-7163.MCT-16-0924

Reis e Sousa C. (2006). Dendritic cells in a mature age. Nature reviews. Immunology, 6(6), 476–483. https://doi.org/10.1038/nri1845

Reuss, A., du Bois, A., Harter, P., Fotopoulou, C., Sehouli, J., Aletti, G., Guyon, F., Greggi, S., Mosgaard, B. J., Reinthaller, A., Hilpert, F., Schade-Brittinger, C., Chi, D. S., & Mahner, S. (2019). TRUST: Trial of Radical Upfront Surgical Therapy in advanced ovarian cancer (ENGOT ov33/AGO-OVAR OP7). International journal of gynecological cancer : official journal of the International Gynecological Cancer Society, *29*(8), 1327–1331. https://doi.org/10.1136/ijgc-2019-000682

Rolitsky, C. D., Theil, K. S., McGaughy, V. R., Copeland, L. J., & Niemann, T. H. (1999). HER-2/neu amplification and overexpression in endometrial carcinoma. International journal of gynecological pathology: official journal of the International Society of Gynecological Pathologists, 18(2), 138–143. https://doi.org/10.1097/00004347-199904000-00007

Sai, D. L., Lee, J., Nguyen, D. L., & Kim, Y. P. (2021). Tailoring photosensitive ROS for advanced photodynamic therapy. Experimental & molecular medicine, 53(4), 495–504. https://doi.org/10.1038/s12276-021-00599-7

Sambasivan S. (2022). Epithelial ovarian cancer: Review article. Cancer treatment and research communications, 33, 100629. https://doi.org/10.1016/j.ctarc.2022.100629

Sano, K., Mitsunaga, M., Nakajima, T., Choyke, P. L., & Kobayashi, H. (2013). Acute cytotoxic effects of photoimmunotherapy assessed by 18F-FDG PET. Journal of nuclear medicine: official publication, Society of Nuclear Medicine, 54(5), 770–775. https://doi.org/10.2967/jnumed.112.112110

Saraste, A., & Pulkki, K. (2000). Morphologic and biochemical hallmarks of apoptosis. Cardiovascular research, 45(3), 528–537. https://doi.org/10.1016/s0008-6363(99)00384-3

Sasikumar, P. G., & Ramachandra, M. (2017). Small-molecule antagonists of the immune checkpoint pathways: concept to clinic. Future medicinal chemistry, 9(12), 1305–1308. https://doi.org/10.4155/fmc-2017-0107

Sato, K., Ando, K., Okuyama, S., Moriguchi, S., Ogura, T., Totoki, S., Hanaoka, H., Nagaya, T., Kokawa, R., Takakura, H., Nishimura, M., Hasegawa, Y., Choyke, P. L., Ogawa, M., & Kobayashi, H. (2018). Photoinduced Ligand Release from a Silicon Phthalocyanine Dye Conjugated with Monoclonal Antibodies: A Mechanism of Cancer Cell Cytotoxicity after Near-Infrared Photoimmunotherapy. ACS central science, 4(11), 1559–1569. https://doi.org/10.1021/acscentsci.8b00565

Sato, K., Nagaya, T., Mitsunaga, M., Choyke, P. L., & Kobayashi, H. (2015b). Near infrared photoimmunotherapy for lung metastases. Cancer letters, 365(1), 112–121. https://doi.org/10.1016/j.canlet.2015.05.018

Sato, K., Nakajima, T., Choyke, P. L., & Kobayashi, H. (2015a). Selective cell elimination in vitro and in vivo from tissues and tumors using antibodies conjugated with a near infrared phthalocyanine. RSC advances, 5(32), 25105–25114. https://doi.org/10.1039/C4RA13835J

Sato, K., Sato, N., Xu, B., Nakamura, Y., Nagaya, T., Choyke, P. L., Hasegawa, Y., & Kobayashi, H. (2016). Spatially selective depletion of tumor-associated regulatory T cells with near-infrared photoimmunotherapy. *Science translational medicine*, *8*(352), 352ra110. https://doi.org/10.1126/scitranslmed.aaf6843

Schlessinger J. (2002). Ligand-induced, receptor-mediated dimerization and activation of EGF receptor. Cell, 110(6), 669–672. https://doi.org/10.1016/s0092-8674(02)00966-2

Schröfelbauer, B., Kimes, P. K., Hauke, P., Reid, C. E., Shao, K., Hill, S. J., Irizarry, R., & Hahn, W. C. (2023). Discovery of antibodies and cognate surface targets for ovarian cancer by surface profiling. Proceedings of the National Academy of Sciences of the United States of America, 120(1), e2206751120. https://doi.org/10.1073/pnas.2206751120

Senol, S., Ceyran, A. B., Aydin, A., Zemheri, E., Ozkanli, S., Kösemetin, D., Sehitoglu, I., & Akalin, I. (2015). Folate receptor α expression and significance in endometrioid endometrium carcinoma and endometrial hyperplasia. International journal of clinical and experimental pathology, 8(5), 5633–5641.

Shafirstein, G., Bellnier, D., Oakley, E., Hamilton, S., Potasek, M., Beeson, K., & Parilov, E. (2017). Interstitial Photodynamic Therapy-A Focused Review. Cancers, 9(2), 12. https://doi.org/10.3390/cancers9020012

Shen, L., Zhou T., Fan, Y., Chang, X., Wang, Y., Sun, J., Xing, L., Jiang, H. (2020). Recent progress in tumor photodynamic immunotherapy. Chinese Chemical Letters, 31(7), 1709-1716. https://doi.org/10.1016/j.cclet.2020.02.007

Shi, Q., Tao, Z., Yang, H., Fan, Q., Wei, D., Wan, L., & Lu, X. (2017). PDGFRβ-specific affibody-directed delivery of a photosensitizer, IR700, is efficient for vascular-targeted photodynamic therapy of colorectal cancer. Drug delivery, 24(1), 1818–1830. https://doi.org/10.1080/10717544.2017.1407011

Shigetomi, H., Higashiura, Y., Kajihara, H., & Kobayashi, H. (2012). Targeted molecular therapies for ovarian cancer: an update and future perspectives (Review). Oncology reports, 28(2), 395–408. https://doi.org/10.3892/or.2012.1833

Shim H. (2020). Bispecific Antibodies and Antibody-Drug Conjugates for Cancer Therapy: Technological Considerations. Biomolecules, 10(3), 360. https://doi.org/10.3390/biom10030360

Shirasu, N., Yamada, H., Shibaguchi, H., Kuroki, M., & Kuroki, M. (2014). Potent and specific antitumor effect of CEA-targeted photoimmunotherapy. International journal of cancer, 135(11), 2697–2710. https://doi.org/10.1002/ijc.28907

Siddiqui, M. R., Railkar, R., Sanford, T., Crooks, D. R., Eckhaus, M. A., Haines, D., Choyke, P. L., Kobayashi, H., & Agarwal, P. K. (2019). Targeting Epidermal Growth Factor Receptor (EGFR) and Human Epidermal Growth Factor Receptor 2 (HER2) Expressing Bladder Cancer Using Combination Photoimmunotherapy (PIT). Scientific reports, 9(1), 2084. https://doi.org/10.1038/s41598-019-38575-x

Siegel, R. L., Giaquinto, A. N., & Jemal, A. (2024). Cancer statistics, 2024. CA: a cancer journal for clinicians, 74(1), 12–49. https://doi.org/10.3322/caac.21820.

Siegel, R. L., Miller, K. D., & Jemal, A. (2019). Cancer statistics, 2019. CA: a cancer journal for clinicians, 69(1), 7–34. https://doi.org/10.3322/caac.21551

Siegel, R. L., Miller, K. D., Wagle, N. S., & Jemal, A. (2023). Cancer statistics, 2023. CA: a cancer journal for clinicians, 73(1), 17–48. https://doi.org/10.3322/caac.21763

Sigismund, S., Avanzato, D., & Lanzetti, L. (2018). Emerging functions of the EGFR in cancer. Molecular oncology, 12(1), 3–20. https://doi.org/10.1002/1878-0261.12155

Sioud, M., Juzenas, P., Zhang, Q., Kleinauskas, A., & Peng, Q. (2021). Evaluation of In Vitro Phototoxicity of a Minibody-IR700 Conjugate Using Cell Monolayer and Multicellular Tumor Spheroid Models. Cancers, 13(13), 3356. https://doi.org/10.3390/cancers13133356

Spisek, R., & Dhodapkar, M. V. (2007). Towards a better way to die with chemotherapy: role of heat shock protein exposure on dying tumor cells. Cell cycle (Georgetown, Tex.), 6(16), 1962–1965. https://doi.org/10.4161/cc.6.16.4601

Ståhl, S., Gräslund, T., Eriksson Karlström, A., Frejd, F. Y., Nygren, P. Å., & Löfblom, J. (2017). Affibody Molecules in Biotechnological and Medical Applications. Trends in biotechnology, 35(8), 691–712. https://doi.org/10.1016/j.tibtech.2017.04.007

Stewart, C., Ralyea, C., & Lockwood, S. (2019). Ovarian Cancer: An Integrated Review. Seminars in oncology nursing, 35(2), 151–156. https://doi.org/10.1016/j.soncn.2019.02.001

Stewart, C., Ralyea, C., & Lockwood, S. (2019). Ovarian Cancer: An Integrated Review. Seminars in oncology nursing, 35(2), 151–156. https://doi.org/10.1016/j.soncn.2019.02.001

Stockwell, B. R., Friedmann Angeli, J. P., Bayir, H., Bush, A. I., Conrad, M., Dixon, S. J., Fulda, S., Gascón, S., Hatzios, S. K., Kagan, V. E., Noel, K., Jiang, X., Linkermann, A., Murphy, M. E., Overholtzer, M., Oyagi, A., Pagnussat, G. C., Park, J., Ran, Q., Rosenfeld, C. S., … Zhang, D. D. (2017). Ferroptosis: A Regulated Cell Death Nexus Linking Metabolism, Redox Biology, and Disease. Cell, 171(2), 273–285. https://doi.org/10.1016/j.cell.2017.09.021

Syed Y. Y. (2020). Sacituzumab Govitecan: First Approval. Drugs, 80(10), 1019–1025. https://doi.org/10.1007/s40265-020-01337-5

Takahashi, K., Taki, S., Yasui, H., Nishinaga, Y., Isobe, Y., Matsui, T., Shimizu, M., Koike, C., & Sato, K. (2021). HER2 targeting near-infrared photoimmunotherapy for a CDDP-resistant small-cell lung cancer. Cancer medicine, 10(24), 8808–8819. https://doi.org/10.1002/cam4.4381

Takakura, H., Goto, Y., Kitamura, A., Yoshihara, T., Tobita, S., Kinjo, M., Ogawa, M. (2021). Analysis of the triplet-state kinetics of a photosensitizer for photoimmunotherapy by fluorescence correlation spectroscopy. Journal of Photochemistry and Photobiology A: Chemistry, 408:113094. https://doi.org/10.1016/j.jphotochem.2020.113094

Taki, S., Matsuoka, K., Nishinaga, Y., Takahashi, K., Yasui, H., Koike, C., Shimizu, M., Sato, M., & Sato, K. (2021). Spatiotemporal depletion of tumor-associated immune checkpoint PD-L1 with near-infrared photoimmunotherapy promotes antitumor immunity. Journal for immunotherapy of cancer, 9(11), e003036. https://doi.org/10.1136/jitc-2021-003036

Tang, D., Kang, R., Berghe, T. V., Vandenabeele, P., & Kroemer, G. (2019). The molecular machinery of regulated cell death. Cell research, 29(5), 347–364. https://doi.org/10.1038/s41422-019-0164-5

Tang, Q., Nagaya, T., Liu, Y., Lin, J., Sato, K., Kobayashi, H., & Chen, Y. (2017). Real-time monitoring of microdistribution of antibody-photon absorber conjugates during photoimmunotherapy in vivo. Journal of controlled release: official journal of the Controlled Release Society, 260, 154–163. https://doi.org/10.1016/j.jconrel.2017.06.004

Tewari, K. S., Burger, R. A., Enserro, D., Norquist, B. M., Swisher, E. M., Brady, M. F., Bookman, M. A., Fleming, G. F., Huang, H., Homesley, H. D., Fowler, J. M., Greer, B. E., Boente, M., Liang, S. X., Ye, C., Bais, C., Randall, L. M., Chan, J. K., Ferriss, J. S., Coleman, R. L., … Monk, B. J. (2019). Final Overall Survival of a Randomized

Trial of Bevacizumab for Primary Treatment of Ovarian Cancer. Journal of clinical oncology : official journal of the American Society of Clinical Oncology, *37*(26), 2317–2328. https://doi.org/10.1200/JCO.19.01009

Tolmachev, V., Orlova, A., Nilsson, F. Y., Feldwisch, J., Wennborg, A., & Abrahmsén, L. (2007). Affibody molecules: potential for in vivo imaging of molecular targets for cancer therapy. Expert opinion on biological therapy, 7(4), 555–568. https://doi.org/10.1517/14712598.7.4.555

Tong, J. T. W., Harris, P. W. R., Brimble, M. A., & Kavianinia, I. (2021). An Insight into FDA Approved Antibody-Drug Conjugates for Cancer Therapy. Molecules (Basel, Switzerland), 26(19), 5847. https://doi.org/10.3390/molecules26195847

Torre, L. A., Trabert, B., DeSantis, C. E., Miller, K. D., Samimi, G., Runowicz, C. D., Gaudet, M. M., Jemal, A., & Siegel, R. L. (2018). Ovarian cancer statistics, 2018. CA: a cancer journal for clinicians, 68(4), 284–296. https://doi.org/10.3322/caac.21456

Trerotola, M., Cantanelli, P., Guerra, E., Tripaldi, R., Aloisi, A. L., Bonasera, V., Lattanzio, R., de Lange, R., Weidle, U. H., Piantelli, M., & Alberti, S. (2013). Upregulation of Trop-2 quantitatively stimulates human cancer growth. Oncogene, 32(2), 222–233. https://doi.org/10.1038/onc.2012.36

Truxova, I., Kasikova, L., Salek, C., Hensler, M., Lysak, D., Holicek, P., Bilkova, P., Holubova, M., Chen, X., Mikyskova, R., Reinis, M., Kovar, M., Tomalova, B., Kline, J. P., Galluzzi, L., Spisek, R., & Fucikova, J. (2020). Calreticulin exposure on malignant blasts correlates with improved natural killer cell-mediated cytotoxicity in acute myeloid leukemia patients. Haematologica, 105(7), 1868–1878. https://doi.org/10.3324/haematol.2019.223933

Tsukamoto, T., Fujita, Y., Shimogami, M., Kaneda, K., Seto, T., Mizukami, K., Takei, M., Isobe, Y., Yasui, H., & Sato, K. (2022). Inside-the-body light delivery system using endovascular therapy-based light illumination technology. EBioMedicine, 85, 104289. https://doi.org/10.1016/j.ebiom.2022.104289

Ueno, T., Toi, M., Koike, M., Nakamura, S., & Tominaga, T. (2000). Tissue factor expression in breast cancer tissues: its correlation with prognosis and plasma concentration. British journal of cancer, 83(2), 164–170. https://doi.org/10.1054/bjoc.2000.1272

Vendel, M. C., Favis, M., Snyder, W. B., Huang, F., Capili, A. D., Dong, J., Glaser, S. M., Miller, B. R., & Demarest, S. J. (2012). Secretion from bacterial versus mammalian cells yields a recombinant scFv with variable folding properties. Archives of biochemistry and biophysics, 526(2), 188–193. https://doi.org/10.1016/j.abb.2011.12.018

Vitale, I., Pietrocola, F., Guilbaud, E., Aaronson, S. A., Abrams, J. M., Adam, D., Agostini, M., Agostinis, P., Alnemri, E. S., Altucci, L., Amelio, I., Andrews, D. W., Aqeilan, R. I., Arama, E., Baehrecke, E. H., Balachandran, S., Bano, D., Barlev, N. A., Bartek, J., Bazan, N. G., … Galluzzi, L. (2023). Apoptotic cell death in disease-Current understanding of the NCCD 2023. Cell death and differentiation, 30(5), 1097–1154. https://doi.org/10.1038/s41418-023-01153-w

von Felbert, V., Bauerschlag, D., Maass, N., Bräutigam, K., Meinhold-Heerlein, I., Woitok, M., Barth, S., & Hussain, A. F. (2016). A specific photoimmunotheranostics agent to detect and eliminate skin cancer cells expressing EGFR. Journal of cancer research and clinical oncology, 142(5), 1003–1011. https://doi.org/10.1007/s00432-016-2122-7

Walsh, T., Casadei, S., Lee, M. K., Pennil, C. C., Nord, A. S., Thornton, A. M., Roeb, W., Agnew, K. J., Stray, S. M., Wickramanayake, A., Norquist, B., Pennington, K. P., Garcia, R. L., King, M. C., & Swisher, E. M. (2011). Mutations in 12 genes for inherited ovarian, fallopian tube, and peritoneal carcinoma identified by massively parallel sequencing. Proceedings of the National Academy of Sciences of the United States of America, 108(44), 18032–18037. https://doi.org/10.1073/pnas.1115052108

Wan Y. Y. (2010). Regulatory T cells: immune suppression and beyond. Cellular & molecular immunology, 7(3), 204–210. https://doi.org/10.1038/cmi.2010.20

Wang, B., Gallolu Kankanamalage, S., Dong, J., & Liu, Y. (2021). Optimization of therapeutic antibodies. Antibody therapeutics, 4(1), 45–54. https://doi.org/10.1093/abt/tbab003

Wang, J. L., Fang, C. L., Tzeng, Y. T., Hsu, H. L., Lin, S. E., Yu, M. C., Bai, K. J., Wang, L. S., & Liu, H. E. (2018). Prognostic value of localization of epidermal growth factor receptor in lung adenocarcinoma. Journal of biomedical science, 25(1), 53. https://doi.org/10.1186/s12929-018-0451-3

Wang, K., Li, D., & Sun, L. (2016). High levels of EGFR expression in tumor stroma are associated with aggressive clinical features in epithelial ovarian cancer. OncoTargets and therapy, 9, 377–386. https://doi.org/10.2147/OTT.S96309

Wang, M., Rao, J., Wang, M., Li, X., Liu, K., Naylor, M. F., Nordquist, R. E., Chen, W. R., & Zhou, F. (2021). Cancer photo-immunotherapy: from bench to bedside. Theranostics, 11(5), 2218–2231. https://doi.org/10.7150/thno.53056

Wang, Q., Peng, H., Qi, X., Wu, M., & Zhao, X. (2020). Targeted therapies in gynecological cancers: a comprehensive review of clinical evidence. Signal transduction and targeted therapy, 5(1), 137. https://doi.org/10.1038/s41392-020-0199-6

Watanabe, R., Hanaoka, H., Sato, K., Nagaya, T., Harada, T., Mitsunaga, M., Kim, I., Paik, C. H., Wu, A. M., Choyke, P. L., & Kobayashi, H. (2015). Photoimmunotherapy targeting prostate-specific membrane antigen: are antibody fragments as effective as antibodies?. Journal of nuclear medicine: official publication, Society of Nuclear Medicine, 56(1), 140–144. https://doi.org/10.2967/jnumed.114.149526

Wei, D., Qi, J., Hamblin, M. R., Wen, X., Jiang, X., & Yang, H. (2022). Near-infrared photoimmunotherapy: design and potential applications for cancer treatment and beyond. Theranostics, 12(16), 7108–7131. https://doi.org/10.7150/thno.74820

Wen, Q., Liu, J., Kang, R., Zhou, B., & Tang, D. (2019). The release and activity of HMGB1 in ferroptosis. Biochemical and biophysical research communications, 510(2), 278–283. https://doi.org/10.1016/j.bbrc.2019.01.090

Wen, Y., Ouyang, D., Zou, Q., Chen, Q., Luo, N., He, H., Anwar, M., & Yi, W. (2022). A literature review of the promising future of TROP2: a potential drug therapy target. Annals of translational medicine, 10(24), 1403. https://doi.org/10.21037/atm-22-5976

Woitok, M., Grieger, E., Akinrinmade, O. A., Bethke, S., Pham, A. T., Stein, C., Fendel, R., Fischer, R., Barth, S., & Niesen, J. (2020). Using the SNAP-Tag technology to easily measure and demonstrate apoptotic changes in cancer and blood cells with different dyes. PloS one, 15(12), e0243286. https://doi.org/10.1371/journal.pone.0243286

Wollschlaeger, C., Meinhold-Heerlein, I., Cong, X., Bräutigam, K., Di Fiore, S., Zeppernick, F., Klockenbring, T., Stickeler, E., Barth, S., & Hussain, A. F. (2018). Simultaneous and Independent Dual Site-Specific Self-Labeling of Recombinant Antibodies. Bioconjugate chemistry, 29(11), 3586–3594. https://doi.org/10.1021/acs.bioconjchem.8b00545

Wong R. S. (2011). Apoptosis in cancer: from pathogenesis to treatment. Journal of experimental & clinical cancer research: CR, 30(1), 87. https://doi.org/10.1186/1756-9966-30-87

Wu, B., Yu, C., Zhou, B., Huang, T., Gao, L., Liu, T., & Yang, X. (2017). Overexpression of TROP2 promotes proliferation and invasion of ovarian cancer cells. Experimental and therapeutic medicine, 14(3), 1947–1952. https://doi.org/10.3892/etm.2017.4788

Xu, N., Zhang, Z., Zhu, J., Xu, L., Li, Y., Duan, L., Mao, Y., & Li, H. (2016). Overexpression of trophoblast cell surface antigen 2 as an independent marker for a poor prognosis and as a potential therapeutic target in epithelial ovarian carcinoma. International journal of experimental pathology, 97(2), 150–158. https://doi.org/10.1111/iep.12174

Xu, X., Lu, H., & Lee, R. (2020). Near Infrared Light Triggered Photo/Immuno-Therapy Toward Cancers. Frontiers in bioengineering and biotechnology, 8, 488. https://doi.org/10.3389/fbioe.2020.00488

Yamaguchi, H., On, J., Morita, T., Suzuki, T., Okada, Y., Ono, J., & Evdokiou, A. (2021). Combination of Near-Infrared Photoimmunotherapy Using Trastuzumab and Small Protein Mimetic for HER2-Positive Breast Cancer. International journal of molecular sciences, 22(22), 12213. https://doi.org/10.3390/ijms222212213

Yamashita, S., Kojima, M., Onda, N., Yoshida, T., & Shibutani, M. (2023). Trastuzumab-based near-infrared photoimmunotherapy in xenograft mouse of breast cancer. Cancer medicine, 12(4), 4579–4589. https://doi.org/10.1002/cam4.5302

Yang, H., Wang, H., Chavan, S. S., & Andersson, U. (2015). High Mobility Group Box Protein 1 (HMGB1): The Prototypical Endogenous Danger Molecule. Molecular medicine (Cambridge, Mass.), 21 Suppl 1(Suppl 1), S6–S12. https://doi.org/10.2119/molmed.2015.00087

Yang, L., Xie, H. J., Li, Y. Y., Wang, X., Liu, X. X., & Mai, J. (2022). Molecular mechanisms of platinum based chemotherapy resistance in ovarian cancer (Review). Oncology reports, 47(4), 82. https://doi.org/10.3892/or.2022.8293

Yang, W. S., SriRamaratnam, R., Welsch, M. E., Shimada, K., Skouta, R., Viswanathan, V. S., Cheah, J. H., Clemons, P. A., Shamji, A. F., Clish, C. B., Brown, L. M., Girotti, A. W., Cornish, V. W., Schreiber, S. L., & Stockwell, B. R. (2014). Regulation of ferroptotic cancer cell death by GPX4. Cell, 156(1-2), 317–331. https://doi.org/10.1016/j.cell.2013.12.010

Yang, Y., Yan, X., Li, J., Liu, C., & Yang, X. (2022). CD47-targeted optical molecular imaging and near-infrared photoimmunotherapy in the detection and treatment of bladder cancer. Molecular therapy oncolytics, 24, 319–330. https://doi.org/10.1016/j.omto.2021.12.020

Yatim, N., Jusforgues-Saklani, H., Orozco, S., Schulz, O., Barreira da Silva, R., Reis e Sousa, C., Green, D. R., Oberst, A., & Albert, M. L. (2015). RIPK1 and NF-κB signaling in dying cells determines cross-priming of $CD8^+$ T cells. Science (New York, N.Y.), 350(6258), 328–334. https://doi.org/10.1126/science.aad0395

Yazaki, S., Kojima, Y., Yoshida, H., Takamizawa, S., Kitadai, R., Nishikawa, T., Shimoi, T., Sudo, K., Saito, A., Okuma, H. S., Tanioka, M., Noguchi, E., Uno, M., Ishikawa, M., Kato, T., Fujiwara, Y., Ohe, Y., & Yonemori, K. (2022). High expression of folate receptor alpha is associated with poor prognosis in patients with cervical cancer. Journal of gynecologic oncology, 33(6), e82. https://doi.org/10.3802/jgo.2022.33.e82

Yokota, T., Milenic, D. E., Whitlow, M., & Schlom, J. (1992). Rapid tumor penetration of a single-chain Fv and comparison with other immunoglobulin forms. Cancer research, 52(12), 3402–3408.

Zeng, P., Chen, M. B., Zhou, L. N., Tang, M., Liu, C. Y., & Lu, P. H. (2016). Impact of TROP2 expression on prognosis in solid tumors: A Systematic Review and Meta-analysis. Scientific reports, 6, 33658. https://doi.org/10.1038/srep33658

Zeppernick, F., & Meinhold-Heerlein, I. (2014). The new FIGO staging system for ovarian, fallopian tube, and primary peritoneal cancer. Archives of gynaecology and obstetrics, *290*(5), 839–842. https://doi.org/10.1007/s00404-014-3364-8

Zhang, B., Gao, S., Li, R., Li, Y., Cao, R., Cheng, J., Guo, Y., Wang, E., Huang, Y., & Zhang, K. (2020). Tissue mechanics and expression of TROP2 in oral squamous cell carcinoma with varying differentiation. BMC cancer, 20(1), 815. https://doi.org/10.1186/s12885-020-07257-7

Zhang, C., Sheng, W., Al-Rawe, M., Mohiuddin, T. M., Niebert, M., Zeppernick, F., Meihold-Heerlein, I., & Hussain, A. F. (2022). EpCAM- and EGFR-Specific Antibody Drug Conjugates for Triple-Negative Breast Cancer Treatment. International journal of molecular sciences, 23(11), 6122. https://doi.org/10.3390/ijms23116122

Zhang, L., Conejo-Garcia, J. R., Katsaros, D., Gimotty, P. A., Massobrio, M., Regnani, G., Makrigiannakis, A., Gray, H., Schlienger, K., Liebman, M. N., Rubin, S. C., & Coukos, G. (2003). Intratumoral T cells, recurrence, and survival in epithelial ovarian cancer. The New England journal of medicine, 348(3), 203–213. https://doi.org/10.1056/NEJMoa020177

Zhang, S., Royer, R., Li, S., McLaughlin, J. R., Rosen, B., Risch, H. A., Fan, I., Bradley, L., Shaw, P. A., & Narod, S. A. (2011). Frequencies of BRCA1 and BRCA2 mutations among 1,342 unselected patients with invasive ovarian cancer. Gynecologic oncology, 121(2), 353–357. https://doi.org/10.1016/j.ygyno.2011.01.020

Zhang, X., Nakajima, T., Mizoi, K., Tsushima, Y., & Ogihara, T. (2022). Imaging modalities for monitoring acute therapeutic effects after near-infrared photoimmunotherapy in vivo. Journal of biophotonics, 15(1), e202100266. https://doi.org/10.1002/jbio.202100266

Zhao, W., Zhu, H., Zhang, S., Yong, H., Wang, W., Zhou, Y., Wang, B., Wen, J., Qiu, Z., Ding, G., Feng, Z., & Zhu, J. (2016). Trop2 is overexpressed in gastric cancer and predicts poor prognosis. Oncotarget, 7(5), 6136–6145. https://doi.org/10.18632/oncotarget.6733

Zhao, X., Cheng, C., Gou, J., Yi, T., Qian, Y., Du, X., & Zhao, X. (2018). Expression of tissue factor in human cervical carcinoma tissue. Experimental and therapeutic medicine, 16(5), 4075–4081. https://doi.org/10.3892/etm.2018.6723

Zhong, L., Li, Y., Xiong, L., Wang, W., Wu, M., Yuan, T., Yang, W., Tian, C., Miao, Z., Wang, T., & Yang, S. (2021). Small molecules in targeted cancer therapy: advances, challenges, and future perspectives. Signal transduction and targeted therapy, 6(1), 201. https://doi.org/10.1038/s41392-021-00572-w

Zou, J., Li, L., Yang, Z. & Chen, X. (2021). Phototherapy meets immunotherapy: a win–win strategy to fight against cancer. Nanophotonics, 10(12), 3229-3245. https://doi.org/10.1515/nanoph-2021-0209

Zubair, T., & Bandyopadhyay, D. (2023). Small Molecule EGFR Inhibitors as Anti-Cancer Agents: Discovery, Mechanisms of Action, and Opportunities. International journal of molecular sciences, 24(3), 2651. https://doi.org/10.3390/ijms24032651

6 Supplementary materials

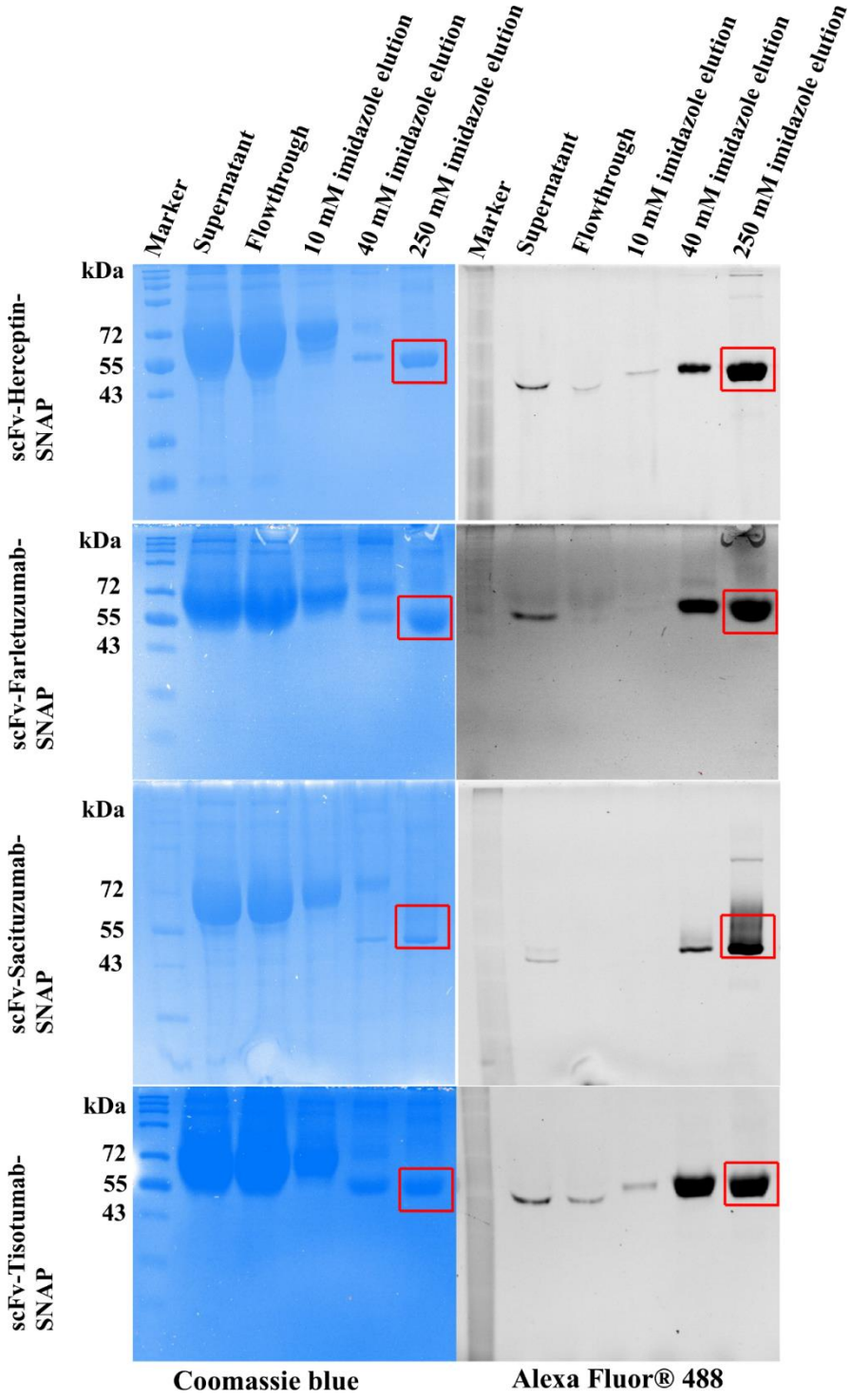

Figure S1: Enrichment of scFv-Herceptin-SNAP, scFv-Farletuzumab-SNAP, scFv-Sacituzumab-SNAP and scFv-Tisotumab-SNAP by nickel NTA using His-tagged and confirmed by SDS-PAGE by Coomassie blue staining (left panel) and SNAP-Surface® Alexa Fluor® 488 signal (right panel). The signal was visualized with ChemiDoc XRS^{+} System. Protein standard broad range (11-250 kDa) was used as marker. The red box indicates the corresponding protein bands.

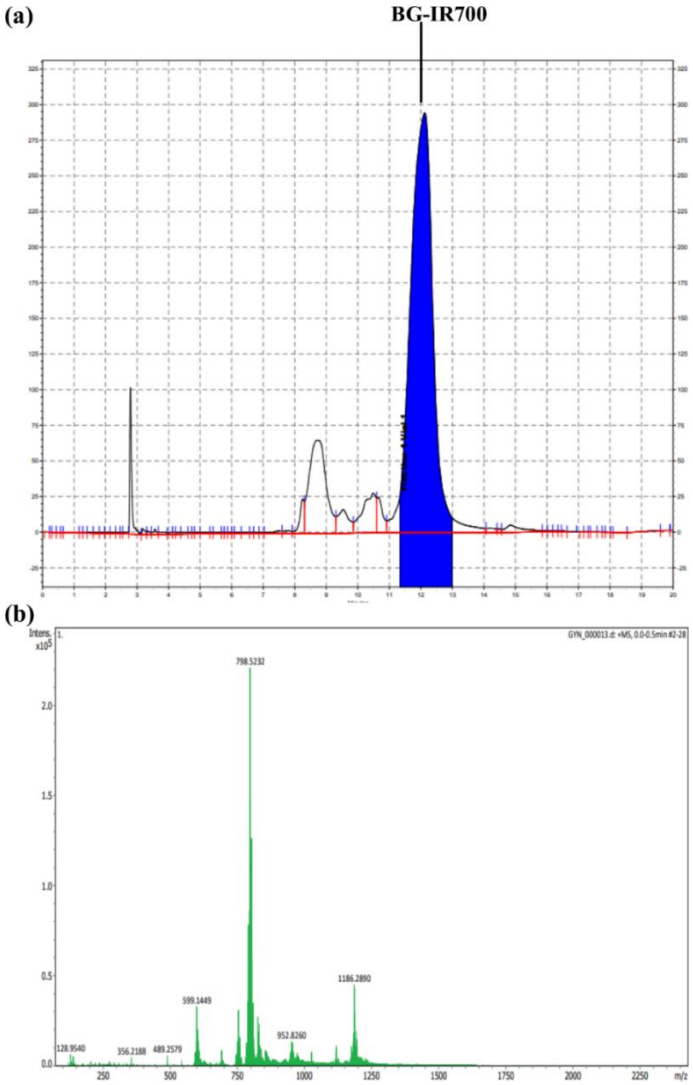

Figure S2: Purification of BG-IR700. (a) HPLC analysis of BG-IR700. The arrow indicates the peak of purified BG-IR700. (b) Mass spectra of BG-IR700.

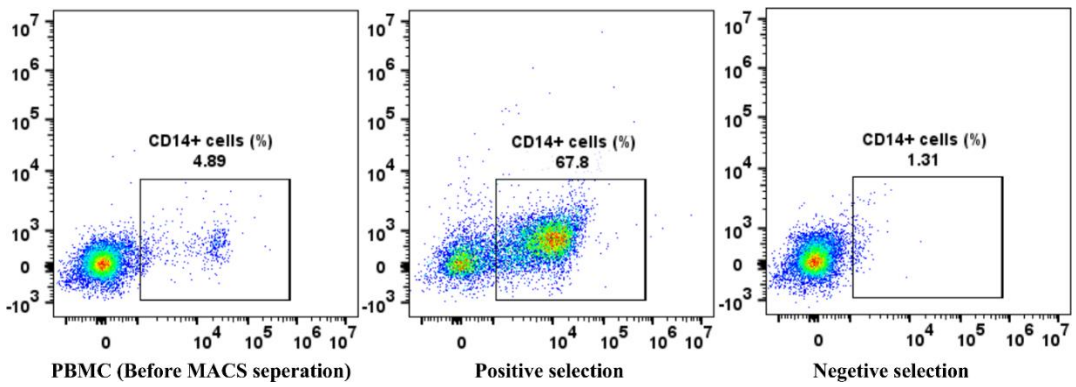

Figure S3: Isolation of $CD14^+$ monocytes cells from PBMC using by positive selection using CD14 microbeads and MACS LS column. The efficiency of $CD14^+$ monocytes cells isolation was investigated by staining with CD14 antibody using flow cytometry. The gated dot plot represents the percentage of $CD14^+$ cells before the MACS separation (left dot plot), positive (middle dot plot) and negative (middle dot plot) selected cells after MACS separation.

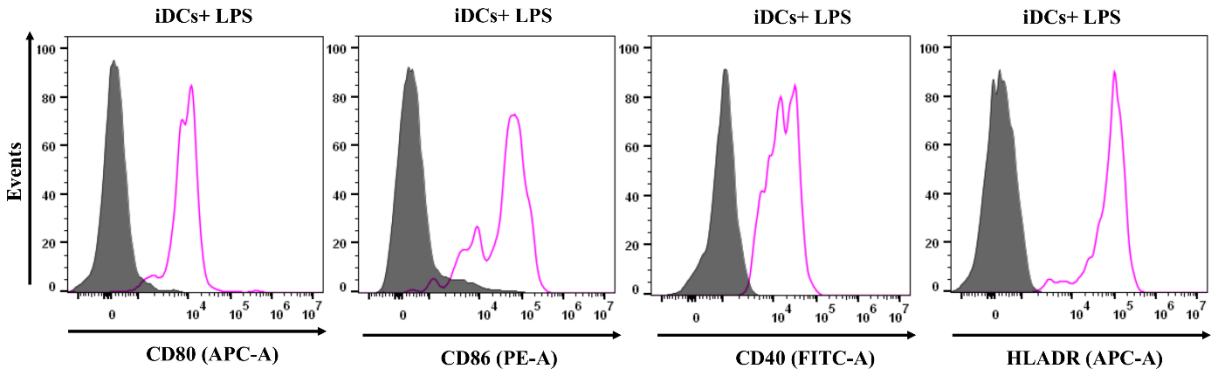

Figure S4: LPS treated iDCs promotes DCs maturation. Immature DCs were cultured with LPS. After 12h, the expressions of CD80, CD86, CD40 and HLADR on DCs were analyzed by flow cytometry. Immature DCs without co-culture are shown as a control. The expressions of CD80, CD86, HLADR, and CD40 on DCs are presented as flow cytometric histograms. The grey lines represent iDCs without LPS, the purple lines depict iDCs with LPS.

Abbreviation

mAb	Monoclonal antibody
FDA	Food and Drug Administration
scFv	Single-chain variable fragment
BG-IR700	BG modified IR700
ΔMFI	Δ mean fluorescence intensity
ADC	Antibody drug conjugate
CD	cluster of differentiation
PSMA	Prostate-specific membrane antigen
NIR-PIT	Near-infrared photoimmunotherapy
IR700	IRDye700DX
ICD	Immunogenic cell death
DAMPs	damage associated molecular patterns
HSP70	Heat shock protein 70
HSP90	Heat shock protein 90
ATP	Adenosine triphosphate
HMGB1	high-mobility group box 1
PBMC	Peripheral blood mononuclear cell
DC	Dendritic cell
iDC	Immature dendritic cell
EpCAM	Epithelial cell adhesion molecule
DAR	Drug-to-antibody ratio
TF	Tissue factor
TROP2	Trophoblast cell-surface antigen 2
FOLR1	Folate receptor alpha
Her2	Human epidermal growth factor receptor 2
PD-1	Programmed death receptor-1
PD-L1	Programmed death-ligand 1
Fab	Fragment antigen-binding region
IC_{50}	Half maximal inhibitory concentration
BG	Benzylguanine
EGFR	Epidermal growth factor receptor
EpCAM	Epithelial cell adhesion molecule

SDS-PAGE	Sodium dodecyl-sulfate polyacrylamide gel electrophoresis
BSA	Bovine serum albumin
HPLC	High-performance liquid chromatography
PI	propidium iodide
IgK leader	Murine immunoglobulin kappa chain leader
CMV	Cytomegalovirus enhancer and promoter
GS	Glycine-serine
LPS	Lipopolysaccharide

Acknowledgements

I feel immense pleasure to express my gratitude and appreciation to my supervisor Prof. Dr. med. Ivo Meinhold-Heerlein, for his guidance, inspiration, and all the necessary facilities to attain this research work.

I would like to express my special thanks to my supervisor Prof. Dr. Andreas Krueger, for accepting me as a PhD student, cooperation, guidance and reviewing this manuscript. I would like to express my deepest sense of gratitude and indebtedness to Dr. Ahmad Fawzi Hussain for his constant support, constructive guidance, cooperation during the period of research work and preparation of this manuscript.

I specially thank Chauyo and Wenjie and all the colleagues, technical and administrative staffs for giving necessary support and an excellent working environment.

Finally, I would like to express my special thanks to my parents for their blessings and continuous inspiration throughout this study.